Conformational Dynamics and Solvent Interactions of Amyloidogenic Peptides in Biologically Relevant Environments: Insights with Molecular Dynamics Simulations

Thesis Submitted to AcSIR for the Award of the Degree of Doctor of Philosophy in Chemical Sciences

By

Ms. Jaya C. Jose

Registration Number: 10CC11J26036

Under the Guidance of

Dr. Neelanjana Sengupta

Physical and Materials Chemistry Division

CSIR - National Chemical Laboratory

Pune - 411008, India

August 2015

Dedicated to

My most beloved family

Acknowledgements

"I can no other answer make but thanks,
and thanks, and ever thanks"

-William Shakespeare

It is a great opportunity for me to express my heartfelt thanks to all those who inspired me, supported me and cared for me during the period of my thesis work. For all those who made my life more meaningful and enjoyable throughout this journey, thanks, and thanks, and ever thanks.

First and foremost, I would like to express my sincere gratitude to my research advisor Dr. Neelanjana Sengupta for introducing me to such a fascinating area of research. I am deeply thankful for her unconditional support, continuous encouragement, sincere cooperation and personal understanding throughout my research tenure without which it was impossible for me to accomplish my work in time. I was highly inspired by her positive energy, immense patience and hard working nature, especially during the hard times.

I am deeply indebted to our collaborators Dr. Sanjoy Bandyopadhyay (IIT, Kharagpur) and Dr. Sudipta Maiti (TIFR, Mumbai). The experiences with them gave me great exposure to different experimental and theoretical aspects of my research problem. My sincere thanks to all research scholars involved in the collaborative projects especially to Mr. Prabir Khatua (IIT, Kharagpur) for providing great support to complete the essential analyses and publish the findings successfully.

All in my CSIR-upgradation panel and doctoral advisory committee - Dr. C. G. Suresh, Dr. Arun Vekatnathan (IISER, Pune), Dr. Sarika Maitra Bhattacharyya, Dr. Anu Reghunathan and Dr. Sudip Roy - encouraged me with their valuable suggestions and constructive criticism during my work presentations. I am extremely grateful to all for making me a better research student.

I got a wonderful chance to enjoy the supreme art of teaching by Dr. Sourav Pal during my time in NCL. I was greatly amazed by his extraordinary knowledge and teaching style. I would like to express my honest gratitude to Dr. Pal for being a wonderful teacher. I also acknowledge Dr. Nayana Vaval, Dr. T. Ajithkumar and all those who taught me during my course work in NCL.

I am thankfully remembering all my teachers who laid a strong base for my personal development from the beginning of my formal education. Words are not enough

to express my thanks to Prof. George Francis and Dr. Sunny Kuriakose (St. Thomas College, Pala, Kerala) for their sincere encouragements and the most appropriate directions during the difficult times in my life. With great respect, I remember my most beloved teachers during my graduation and post-graduation.

I am very happy to thank Dr. Kumar Vanka for all his selfless efforts to conduct reviews on insightful books and world classic movies. I was greatly influenced by all these programs and it helped me to expand the boundaries of my world in multiple directions with improved skills and positive attitude. The enjoyable trips with his group helped me to reduce the stress and strain during my research life.

I am thankfully remembering all my seniors, especially Deepti, Achintya, Chandan, Mudit and Shantanu for providing all the required technical help when I was in need. I got a wonderful friend with a beautiful mind as my group mate who supported me from my first day in the lab, thank you Prathit for all the help. My most beloved juniors Nupur and Sneha were always by my side with immense love. I extremely enjoyed the time we were together; thank you Nupur and Sneha for all the help. Thank you Dhanashree, Asis, Xavier, Manoj, Amrita, Nisha, Jugal, Sayali, Anagha, Kamalika, Debarati, Swagatha, Manzoor, Susanto, Anju, Atreyi, Deepak, Guptajee, and all my juniors and friends in NCL for all memorable moments together.

My heartfelt thanks to Dr. Nandini Devi for her care and support when I was new in NCL. I had great time with my friends from Kerala during Onam, Vishu and Christmas, thank you for those sweet memories. I would like extend my special thanks to Bindhu, Jima, Aany, Leena, Shoy, Anish, Deepa, Kumari Nisha and Rajesh for all help provided when I joined in NCL and thereafter.

My life in Pune was extremely beautiful when I was with my ever dearest roommates Anshu, Roshna and Pushpa in SA-55. We were strongly united with one heart, supported each other, enjoyed all joys and faced all problems together; it was really wonderful. The sweet memories of our journeys, celebrations, cooking experiments and all other adventures are really precious and close to my heart. Special thanks to our special guest Saumya.

Finally, with immense pleasure I would like to thank everyone in my family. Their unconditional love, prayers and blessings fueled me each and every day to move ahead in life to achieve my dreams. The constant moral support and timely advice of my Appan, Amma, Dalichechi, Priyachechi and Ribuchettan helped me to face all difficult challenges

during my research work. The innocent prayers and sweet comedies of Johan and Jewel made my days pleasant and energetic.

I thank almighty god for arranging everyone and everything for my good.

Jaya C. Jose

Table of Contents

Abstract

The misfolding and amyloidogenic aggregation of Intrinsically Disordered Proteins (IDPs) were found to be an important cause of many incurable neurodegenerative diseases like Alzheimer's disease (AD), Parkinson's disease (PD), Lewy Body Disorder (LBD) etc[1, 2]. This class of proteins does not possess stable secondary structure in its monomeric state under physiological conditions[3, 4]. Molecular level understanding of the conformational dynamics and interactions of IDPs in its monomeric state is highly challenging using existing experimental techniques because of its complexity and rapid inter-conversion between different heterogeneous structural states. Enhanced aggregation propensity of IDPs in fully aqueous environment also makes it difficult to study the early conformational evolution as well as the microscopic hydration properties of these proteins. Hence different computational techniques are required to generate more understanding about the particularities of this class of peptides. Molecular dynamics simulation technique is one of the most appropriate tools to discern the intra- and inter-molecular interactions and dynamics of different IDPs and such information is essential for designing suitable drug molecules to prevent the toxic transformations of this class of peptides.

Statement of Problem

Amyloid beta peptide (Aβ), which is strongly associated with the onset of Alzheimer's disease, has been considered as a representative IDP system[5]. Molecular level characterization of the conformational dynamics and interactions of A$\beta_{1\text{-}42}$ with the surrounding solvent molecules, biologically relevant surfaces and also with other IDPs are of high demand to provide better understanding about the toxic aggregation mechanism of this amyloid peptide. Hence, it is the specific aim of the work presented in this thesis.

Specific Objectives of the Thesis

1) To understand the role of hydrophobicity of the central hydrophobic core (CHC) in the early observed structural collapse of the peptide by mutating the central residue of the CHC i.e. F_{19} with Tyrosine and Isoleucine.

2) To understand the effect of a model hydrophilic nano surface TiO_2 (rutile) on the early conformational pathway of Aβ_{42}

3) To investigate the microscopic dynamic properties of water molecules present in the hydration layer of heterogeneous conformations of A$\beta_{1\text{-}42}$ and a natively folded protein ubiquitin (UBQ).

4) To probe the molecular level details of heterogeneous cross dimerization pathways of A$\beta_{1\text{-}42}$ and αSynuclein (αSyn$_{1\text{-}95}$) in aqueous environment.

Methodology Used

Atomistic molecular dynamics simulation techniques are used for the generation of the peptide ensemble for the analysis required for this work.

Arrangement of the Thesis

Chapter 1

The basic understandings about protein folding, misfolding and aggregation are reviewed in the first part of this chapter. The general characteristic properties of intrinsically disordered proteins along with the structural details of two representative IDPs Amyloid-β and α- synuclein are introduced. The pathological and statistical details regarding AD, PD and the synergic occurrence of these disease conditions are briefly discussed. The important strategic approaches in drug designing for such disease conditions are also covered in this chapter. This chapter is concluded with an overview of the scope of this thesis.

Chapter 2

The second chapter of this thesis provides an outline of different computational methods. Theoretical basics as well as the practical aspects of molecular dynamics (MD) simulation techniques are described in detail. Some of the analytical methods are also overviewed in this chapter and this chapter is concluded with an overview of existing complementary experiental techniques for IDP studies.

Chapter 3

This chapter includes the description of the effect of hydrophobicity of the CHC on the early observed dynamics of A$\beta_{1\text{-}42}$ peptide monomer[6]. The observed distance dependent variation in the secondary structural propensity and other dynamic changes at the proximity of the model hydrophilic TiO_2 surface[7] are also discussed in this chapter. These results have implications in the self assembly of Aβ on hydrophilic biological surface.

Chapter 4

A comparative study of the microscopic hydration properties of an IDP (A$\beta_{1\text{-}42}$) and a globular protein (UBQ) is included in this chapter. The significance of various A$\beta_{1\text{-}42}$

monomeric conformations selected for this study and the corresponding methodological strategies adopted for its generation are described in detail. Using systematic analytical techniques, we have provided mechanistic insights about the observed dynamic heterogeneity of hydration shell water molecules around the IDP conformations[8]. The findings are of biological significance in studies of Aβ self-assembly, where hydration water has been shown to play crucial roles in early oligomeric assembly and in protofibrillar stability.

Chapter 5

We have probed the molecular details of heterogeneous cross dimerization pathways of A$\beta_{1\text{-}42}$ and αSynuclein ($\alpha Syn_{1\text{-}95}$) in aqueous environment and the results are explained in this chapter. The characteristics of different interaction modes shows the significance of repeating Lys residues, mainly in the imperfect repeats 'KTKEGV' and the non-amyloid component (NAC) region present in $\alpha Syn_{1\text{-}95}$[9]. The details of the interactions and hydration characteristics of the heterogeneous interfaces formed during the cross dimerisation of these IDPs are also described. The existence of such hetero complexes and therefore hetero assembly pathways may lead to polymorphic aggregates with variations in pathological attributes.

Chapter 6

This chapter summarizes major conclusions and future directions evolved from the studies presented in the previous chapters.

References

1. Hardy, J.; Selkoe, D. J., The Amyloid Hypothesis of Alzheimer's Disease: Progress and Problems on the Road to Therapeutics. *Science* **2002,** 297, 353-356.

2. Spillantini, M. G.; Schmidt, M. L.; Lee, V. M.-Y.; Trojanowski, J. Q.; Jakes, R.; Goedert, M., α-Synuclein in Lewy Bodies. *Nature* **1997,** 388, 839-840.

3. Dyson, H. J.; Wright, P. E., Intrinsically Unstructured Proteins and their Functions. *Nat. Rev. Mol. Cell Biol.* **2005,** 6, 197-208.

4. Tompa, P., Intrinsically Disordered Proteins: a 10-year Recap. *Trends Biochem. Sci.* **2012,** 37, 509-516.

5. Ball, K. A.; Phillips, A. H.; Nerenberg, P. S.; Fawzi, N. L.; Wemmer, D. E.; Head-Gordon, T., Homogeneous and Heterogeneous Tertiary Structure Ensembles of Amyloid-β Peptides. *Biochemistry* **2011,** 50, 7612-7628.

6. Jana, A. K.; Jose, J. C.; Sengupta, N., Critical Roles of Key Domains in Complete Adsorption of Aβ Peptide on Single-Walled Carbon Nanotubes: Insights with Point Mutations and MD Simulations. *Phys.Chem. Chem. Phys.* **2013,** 15, 837-844.

7. Jose, J. C.; Sengupta, N., Molecular Dynamics Simulation Studies of the Structural Response of an Isolated Aβ_{42} Monomer Localized in the Vicinity of the Hydrophilic TiO_2 Surface. *Euro. Biophys. J.* **2013,** 42, 487-494.

8. Jose, J. C.; Khatua, P.; Bansal, N.; Sengupta, N.; Bandyopadhyay, S., Microscopic Hydration Properties of the A$\beta_{1–42}$ Peptide Monomer and the Globular Protein Ubiquitin: A Comparative Molecular Dynamics Study. *J. Phys. Chem. B* **2014,** 118, 11591-11604.

9. Jose, J. C.; Chatterjee, P.; Sengupta, N., Cross Dimerization of Amyloid-β and αSynuclein Proteins in Aqueous Environment: A Molecular Dynamics Simulations Study. *PLOS ONE* **2014,** 9, e106883.

List of Tables

corresponding data averaged over the Aβ monomers (AB-avg) and that for pure bulk water are listed for comparison.

Table 4.8. The Values of α Obtained From Fits of the Water Density Distribution $P(n^*)$ to Eq. 11 for the Aβ Peptide Conformations and UBQ.

Table 5.1. The inter-protein center of mass distances (in Å) at the start of the unbiased simulations is denoted as d_0, at 10 ns is denoted as d_{10}, and at 50 ns is denoted as d_{50}. The relative orientations of the proteins are specified by the angle (in degrees) between the vectors joining the N- and C- terminii of each protein, at 10 ns (θ_{10}) and at 50 ns (θ_{50}). E_{int} denotes the total inter-protein interaction at 50 ns (in kcal mol^{-1}).

Table 5.2. The number of inter-protein contacts (N_{cont}), radius of gyration of the dimer complex (R_g), total interaction strength (E_{tot}), and the electrostatic (E_{coul}) and the van der Waals components (E_{vdW}) of the total interaction. The units for distances and energies are Å and kcal mol^{-1}, respectively.

Table 5.3. Mean values of the total number of internal contacts formed in the Aβ ($N_{int}^{A\beta}$) and αSyn ($N_{int}^{\boldsymbol{\alpha S}}$) proteins in the five clusters. The corresponding radii of gyration (in Å) have been denoted as $R_g^{A\beta}$ and $R_g^{\boldsymbol{\alpha}S}$.

Table 5.4. Configurational entropy per heavy atoms (in J K^{-1} mol^{-1}) for Aβ (S_1) and the αSyn (S_2) proteins in the unbound states and in the clusters C1, C2, C3, C4 and C5. The entropy differences between the unbound and bound states, as well as the difference between the entropies of Aβ and αSyn are also provided.

Table AII-1. Structural persistence, *Q*, averaged over the 2 ns analysis run for each Aβ conformation. Standard deviations are provided in the parentheses.

Table AII-2. Average relaxation times as obtained from the continuous WW ($<\tau_s^{WW}>$) hydrogen bond TCFs (calculated using the energy-based criterion) for the water molecules present in the first hydration layers around different Aβ peptide conformations and UBQ. The corresponding data averaged over the Aβ monomers (AB-avg) and that for pure bulk water are listed for comparison.

Table AIII-1. Mean value of the inter-residue sidechain distances (d^{SB}, in Å) between the residues that form salt bridges in the clusters a) C1, b) C2, c) C3, d) C5. Standard deviations are provided in braces. The first residue belongs to αSyn; the second residue belongs to Aβ.

List of Figures

conformations and UBQ. As a reference, the corresponding functions for pure bulk water are included.

Figure 4.5. Mean square displacement (MSD) of water molecules present in the first hydration layers of different Aβ peptide conformations and UBQ. The MSD of water in pure bulk state is shown for comparison. The results for UBQ, pure bulk water, and that averaged over the Aβ monomers are also included in the inset.

Figure 4.6. Reorientational time correlation function, $C_{\mu}(t)$, of water molecules present in the first hydration layers of different Aβ peptide conformations and UBQ. The corresponding function for water in pure bulk state is shown for comparison. The results for UBQ, pure bulk water, and that averaged over the Aβ monomers are also included in the inset.

Figure 4.7. Comparison of (a) distributions of the total protein-water interaction strength, $E_{tot\text{-}PW}$, and (b) the mean square displacement (MSD) of the hydration layer water molecules, between the restrained and the flexible Aβ conformations AB1 and AB4, and those of UBQ. The MSD of water in pure bulk state is shown for comparison.

Figure 4.8. (a) Intermittent time correlation function, $C_{PW}(t)$, for the PW hydrogen bonds formed between water molecules and the residues of different Aβ peptide conformations and UBQ. (b) The corresponding function, $C_{WW}(t)$, for the WW hydrogen bonds formed by the first hydration layer water molecules around different Aβ peptide conformations and UBQ. The function $C_{WW}(t)$ for water in pure bulk state is shown for comparison. The results for UBQ, pure bulk water, and that averaged over the Aβ monomers are also included in the insets.

Figure 4.9. (a) Continuous time correlation function, $S_{PW}(t)$, for the PW hydrogen bonds formed between water molecules and the residues of different Aβ peptide conformations and UBQ. (b) The corresponding function, $S_{WW}(t)$, for the WW hydrogen bonds formed by the first hydration layer water molecules around different Aβ peptide conformations and UBQ. The function $S_{WW}(t)$ for water in pure bulk state is shown for comparison. The results for UBQ, pure bulk water, and that averaged over the Aβ monomers are also included in the insets.

Figure 4.10. Probability distributions of water densities near the surfaces of different Aβ peptide conformations and UBQ fitted to the Gaussian form.

Figure 5.1. Snapshots of starting monomeric structures of a) Aβ and b) αSyn used in the unbiased simulations in the study. Correlation of average theoretical ^{15}N chemical shifts

with experimentally determined ^{15}N chemical shifts for c) Aβ and d) αSyn. The linear regressions (straight lines) and the corresponding Pearson Correlation Coefficients (R) are provided.

Figure 5.2. Evolution of the a) total inter-peptide interaction strength, and b) inter peptide distance over the first 50 ns of the unbiased simulation. Data for the dimerising trajectories are shown in *gray*, and averages shown in *green*; the data for non-dimerising trajectories are in *brown* and the averages shown in *maroon.*

Figure 5.3. The backbone mean square fluctuation (MSF) for the a) N-terminal residues, b) middle regions, and c) C-terminal residues of A$\beta_{1\text{-}42,}$ and the d) N-terminal residues, e) middle regions, and f) C-terminal residues of αSyn$_{1\text{-}95}$. The data for the last 50 ns of the dimerising trajectories are shown in *gray*, with the averages in *green* (solid line). Corresponding average data for the same systems for the initial 50 ns is provided in green (broken line). Average data for the non-dimerising systems is shown in *maroon* (broken line) for comparison.

Figure 5.4. Non bonded interaction energies in kcal mol^{-1}. Residue wise: average interaction energy of A$\beta_{1\text{-}42}$ with αSyn$_{1\text{-}95}$ (a), maximum interaction energy of A$\beta_{1\text{-}42}$ with αSyn$_{1\text{-}95}$ (b), average interaction of αSyn$_{1\text{-}95}$ with A$\beta_{1\text{-}42}$ (c), and maximum interaction energy of αSyn$_{1\text{-}95}$ with A$\beta_{1\text{-}42}$ (D). The residues with strong interactions are labeled with one letter code of the respective amino acids.

Figure 5.5. The clusters evolved during Cartesian principal component analysis (PCA) of A$\beta_{1\text{-}42}$ and αSyn$_{1\text{-}95}$ cross dimer system. The two dimentional representation of the distribution of density function ΔG, corresponding to the fluctuations of the Cα atoms on the plane of the top two principal components, pc1 and pc2 is shown. The ΔG values spread in the range of 0 to 4.2 kcal mol $^{-1}$. The representative structures from five distinct clusters are shown.

Figure 5.6. Residue specific side chain contact probability of αSyn$_{1\text{-}95}$ with A$\beta_{1\text{-}42}$ in different interaction sub modes.

Figure 5.7. Residue wise maximum electrostatic (left column) and van der Waal (right column) interaction energies (in kcal mol^{-1}) of αSyn$_{1\text{-}95}$ with A$\beta_{1\text{-}42}$ for clusters C1, C2, C3, C4 and C5.

Figure 5.8. Distributions of the inter-residue distances between the residues that form inter-protein salt bridges, in clusters a) C1, b) C2, c) C3, d) C5. Distributions corresponding to the stable and the transient salt bridges are indicated in solid and broken

Abbreviations

AMD	Accelerated Molecular Dynamics
ATP	Adenosine triphosphate
αSyn	Alpha-Synuclein
AD	Alzheimer's Disease
Aβ	Amyloid beta
APP	Amyloid Precursor Protein
CHC	Central Hydrophobic Core
CHARMM	Chemistry at HARvard Macromolecular Mechanics
DNA	Deoxyribonucleic acid
DMPC	Dimyristoylphosphatidylcholine
DOPS	Dioleoylphosphatidylserine
DPPC	Dipalmitoylphoshatidylcholine
FCS	Fluorescence Correlation Spectroscopy
GBIS	Generalised Born Implicit Solvent
HFIP	Hexafluoroisopropanol
HS-AFM	High Speed Atomic Force Microscopy
H-bond	Hydrogen bond
IDP	Intrinsically Disordered Proteins
LJ	Lennard-Jones
LBD	Lewy Body Disorder
MSD	Mean Square Displacements
mRNA	Messenger RNA
MD	Molecular Dynamics
MM	Molecular Mechanics
MC	Monte Carlo
NAMD	NAnoscale Molecular Dynamics
ND	Neurodegenerative Disease
NAC	Non-Amyloid Component
NMR	Nuclear Magnetic Resonance
NOE	Nuclear Overhauser Effect
POPE	Palmitoyloleoylphosphatidylethanolamine

PRE	Paramagnetic Relaxation Enhancement
PD	Parkinson's Disease
PME	Particle Mesh Ewald
PCs	Principal Components
PCA	Principal Component Analysis
PDB	Protein Data Bank
PW	Protein-Water
QM	Quantum Mechanics
RDFs	Radial Distribution Functions
R_g	Radius of Gyration
REMD	Replica Exchange Molecular Dynamics
RDC	Residual Dipolar Coupling
RNA	Ribonucleic acid
RMSD	Root Mean Square Deviation
RMSF	Root Mean Squared Fluctuation
smFRET	Single molecule Förster Resonance Energy Transfer
SWCN	Single Walled Carbon Nanotube
SAXS	Small Angle X-ray Scattering
SASA	Solvent Accessible Surface Area
TCF	Time Correlation Functions
tRNA	Transfer RNA
UBQ	Ubiquitin
VMD	Visual Molecular Dynamics
WW	Water-Water

Chapter 1

Introduction

"If I have seen further it is by standing on the shoulders of Giants."

-Isaac Newton

Proteins are nanomachines present in all living organisms for carrying out diverse and complex cellular processes. These macromolecules are synthesized on ribosome as linear polycondensate of amino acid units connected together by peptide bonds. The specific order of amino acids in a protein is encoded in DNA sequences. Messenger RNAs (mRNA), produced by transcription from DNA are translated to an aminoacid chain by a ribosome with the help of complementary transfer RNAs (tRNAs). The specific sequence of such polypeptide chains, known as the primary structure of the protein, is embedded with the information essential to attain particular three-dimensional structure to perform its unique functions in the body. Among different classes of proteins, globular proteins constitute the majority and these proteins fold to a compact arrangement with well defined secondary and tertiary structures. While, other important classes like Intrinsically Disordered Proteins (IDPs), membrane proteins etc. do not posses such characteristic secondary or tertiary structure. Hence, its propensity for mifolding and aggregation is very high and this leads to different fatal diseases like Alzheimers disease (AD), Parkinson's Disease (PD), Lewybody disorder (LBD), etc. Folding correctly into a functional native form with specific seconday and tertiary structure is considered as one of the most important fundamental phenomena in the nature. Thus, studies on protein misfolding diseases are necessitated to start with the understanding of protein folding mechanism.

1.1 Protein Folding

The spontaneous process by which a newly synthesized protein transforms from its intial random disordered structure to a native functional form under physiological condition is known as 'protein folding'[1]. Because of the favorable internal interactions, proteins attain compact globular structure with hydrophobic interior and hydrophilic exterior in the correctly folded state[1]. The specific structural arrangement of proteins evolves during the folding process gives them long term stability in the crowded cellular environment[1]. The protein folding process is also coupled to many cellular processes like growth, trafficking of molecules to specific locations, translocation, cellular cycle regulation, etc[1]., the failure of proteins to fold correctly leads to several pathological conditions. The earliest experimental studies conducted by Anfinsen and co-workers on unfolded ribonuclease A, provided significant contribution towards the preliminary understanding of protein folding problem[2]. Their studies mainly showed that folding is a spontaneous, reversible process and can occur even in the absence of any catalytic biomolecules by using only the

information stored in the protein's amino acid sequence[2]. These facts lead to an assumption that the completely folded proteins exist in its global free energy minimum. However, Levinthal discerned the conceptual difficulty of a protein to systematically search the particular minimized structure from its cosmologically large number of possible conformations, in a biologically reasonable time period[3]. This suggested that the protein folding process occurs through a directed, rather than a random search, on the conformational landscape. The diversity in the set of conformational states a protein can access during the folding procedure has been further demonstrated using atomistic level computer simulations[4, 5]. These studies ruled out the hypothesis of mandatory pathways of folding and suggested the possibility of stochastic search of many conformations accessible to a polypeptide chain. A very exciting view point known as 'energy landscape' theory emerged thereafter, which gave satisfactory explanation for the folding process[5-7].

1.1.1 Protein Folding Energy Landscape

According to the theory, during the folding process a protein passes through an ensemble of partially folded structures, instead of a series of discrete intermediates, to reach the thermodynamically stable and kinetically accessible unique native conformations[1, 5, 6, 8]. This concept projected the form of free energy and its variation with different protein conformation as a rugged funnel with local energy minima where the protein can transiently reside[1, 5, 6, 8]. The bottom of the funnel corresponds to the folded structure with lowest free energy [1, 5, 6, 8]. Figure 1.1 depicts the energy landscape of protein folding. The surface of this folding funnel for a specific protein under a given set of conditions is determined by its thermodynamic and kinetic properties and this will be unique for that particular polypeptide chain[1, 5, 6, 8].

It has been observed from numerous experimental studies that mild mutations cannot block the protein folding process but it can only alter the folding routes to the stable folded structure[7]. If one set of route to the native structure completely blocked by a strong mutation the system will follow another possible route to the stable conformation[7]. To limit the space for protein to search for a proper folding path, there must be an ensemble of transition states through which the system must pass through[7]. This transition state ensemble 'funnels' the large number of molten globule conformations to the unique native globular structure[1, 5, 7, 8]. The high energy transition state conformations usually possess some of the native like interactions and hence, attain more stability than the

disordered structures[5, 9]. All the unfolded conformations have to cross a critical energy barrier to achieve the natively folded conformation[5, 9].

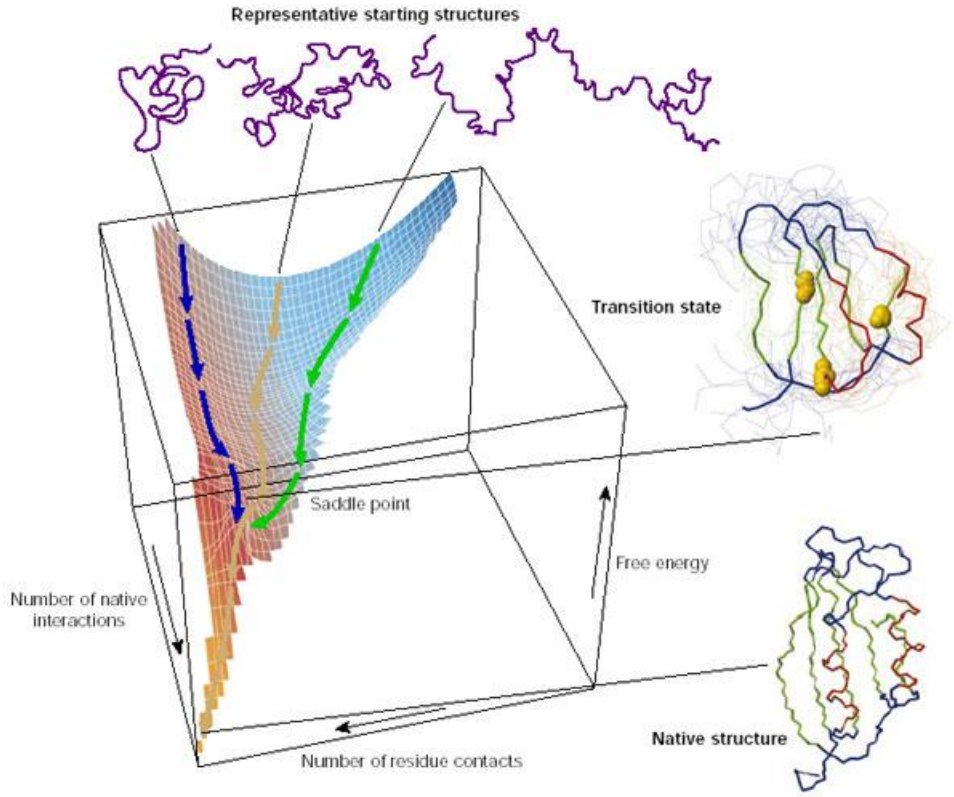

Figure 1.1: Schematic representation of a protein energy landscape. Reproduced from Ref. 1 with permission from Nature publishing group.

A range of theoretical studies investigated the dynamics of the folding process to get more understanding about this mechanism[1, 9, 10]. The intrinsic random fluctuations of the disordered polypeptide chain allow different regions of the system to come close and interact with each other[1, 9, 10]. Native interactions between residues are assumed to be more stable than non native contacts[1, 9, 10]. Hence, the interactions of key residues reduce the number of available conformations. Such native interactions lead to the formation of a folding nucleus and about which the rest of the structure organize rapidly to establish the native-like fold. The side-chains of each residue attain its unique close packed arrangement during the final folding step[9]. The characterization of the native fold is based on the local secondary structure. Most of the native compact structures contain regions in helical and sheet conformations, which are stabilized mainly by hydrogen bonding and hydrophobic interactions[1, 7, 9]. Because of these interactions, the enthalpy change during the folding process will be favorable for the thermodynamically stable folded state and

the enthalpy gain will help to overcome the conformational entropy loss during the folding process[1, 7]. The energy landscape theory explains the kinetics and thermodynamics of the folding process in an acceptable manner.

1.1.2 Protein Misfolding and Aggregation

In certain conditions protein molecules fail to fold into its native structure and undergo misfolding[1, 9, 11]. Because of misfolding, protein loses its functional properties and self assembles into aggregates[1, 9, 11]. It has been reported that aggregation is promoted by longer lived intermediates and the conditions which favor the formation of these intermediates[9]. In the incompletely folded intermediate states, different hydrophobic regions of the protein get more exposure to the solvent environment and hence, are more prone to make inappropriate interactions with other molecules in the crowded cellular environment[1, 11].

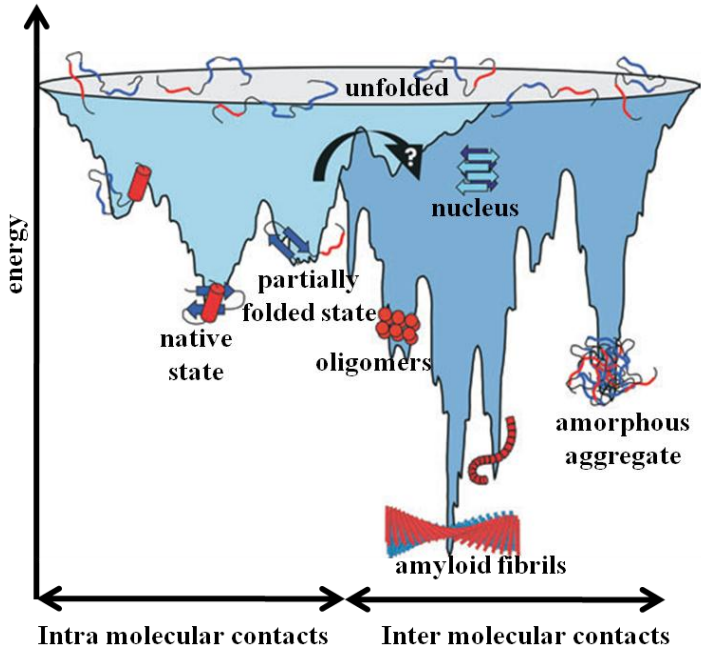

Figure 1.2. Schematic representation of the free energy landscape of protein folding vs aggregation. Reproduced from Ref. 11 with permission from John Wiley and Sons publishing group.

Because of enhanced inter molecular interactions, there will be considerable decrease in the number of native contacts and thus, the evolution of secondary and tertiary structure of the protein get altered[1, 9, 11]. Such non-native intermolecular interactions propagate three dimensionally and form larger aggregates[1, 9, 11]. Protein folding and aggregation are two kinetically competitive processes[11]. At low concentrations, protein folding is favored,

while aggregation is favored at higher concentrations[11]. The free energy landscape of protein folding and its aggregation to more energetically favorable amyloid fibril is represented in Figure 1.2.

The aggregation of a polypeptide chain is triggered by critical mutations; interactions of metal ions and lipid molecules; alteration in the cellular conditions like elevated temperature, variation in the pH, decreased ATP level, oxidative stress etc[1, 9, 11]. In the crowded cellular milieu, the assistance of chaperones is an essential requirement for most of the large poly peptide chain to fold correctly hence, any abnormal behavior of chaperone can also affect the native folding procedure and enhance the aggregation process[1, 9, 11].

The solvent exposed hydrophobic surface area of the aggregates increases with size, consequently its solubility decreases; the lower aggregates are water soluble. The insoluble aggregate formation under physiological conditions is very often irreversible[9, 11]. The aggregation process further leads to the formation of amorphous precipitates or highly structured fibrils[11]. Very often cellular machineries detect and dispose the amorphous aggregates before their precipitation[11]. On the contrary, an ordered assembling mechanism leads to the formation of very stable deposits known as 'amyloid fibrils'[12]. A large number of diseases are related to such protein misfolding as well as aggregation[13]. Hence, the detailed mechanism of misfolding and amyloid formation is essential in developing strategies to prevent these diseases.

1.1.3 Metastability of Native Proteins

Irrespective of substantial differences in the primary structural sequence, many polypeptide chains have shown the tendency to form amyloid fibrils of identical structural characteristics *in vitro*[12]. Recent experimental studies conducted by Dobson et al to determine the thermodynamic stability of various amyloid fibrils revealed that this structural form is the most stable one, a polypeptide chain adopts even under physiological conditions[14]. This finding questioned the already accepted concept that the functional forms of proteins correspond to the global minima in their free energy surface. Hence, recent studies suggested that the native form is almost universally stable with respect to unfolding; it is only metastable with respect to amyloid formation[10, 14].

1.1.4 Amyloid Aggregation Mechanism

Amyloid is an unbranched protein fiber, composed of monomers predominantly in β-sheet conformation[12]. Despite of dissimilarity in the primary sequence, structure and functions various peptides and proteins form amyloid fibrils with similar architecture[13].

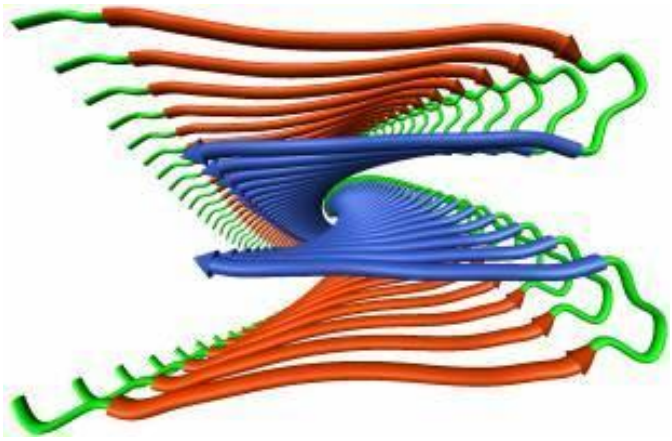

Figure 1.3. Cartoon representation of amyloid fibril. Reproduced with the permission of Elsevier.

Eventhough the soluble oligomeric forms are identified with heterogeneous morphology for most of these amyloidogenic proteins, their fibrils are insoluble and characterized by identical organized core structure[13]. As shown in Figure1.3, the β-strands of the individual monomeric units run perpendicular to the fiber axis, resulting in the formation of a cross-β sheet structure[15]. It has been also found that hydrophobic interaction of the sidechains and backbone hydrogen bonding are two major forces that stabilize most of these fibrilar structures[13, 15, 16]. To optimize these nonbonded interactions and to stabilize the fibrilar state, β-sheets very often adopt a twisted structure[13, 17]. All amyloid fibrils show specific optical behavior on binding dye molecules such as Congo red[18]. The observed commonalities in the structure of the final stable amyloids of a variety of proteins suggest the possibility of a common aggregation pathway[19].

Amyloid fibril formation appears to be a multistep process, but the full mechanism is still unclear. It has been observed that a number of intermediate aggregates appear along the amyloid fibril formation pathway[20-23]. Kinetic studies demonstrated that the rate law of amyloid formation follows a sigmoid function as shown in Figure1.4 with three distinct phases; an initial lag phase, a fast growth phase and a final equilibrium phase[23, 24]. During the lag phase, the misfolded soluble peptide associate and form a 'nucleus'[11, 23]. This nucleus with critical size and shape interacts with monomers or oligomers and form protofilaments[11, 23]. During the growth phase the protofilaments further aggregate rapidly to form the stable fibrils[11, 23].

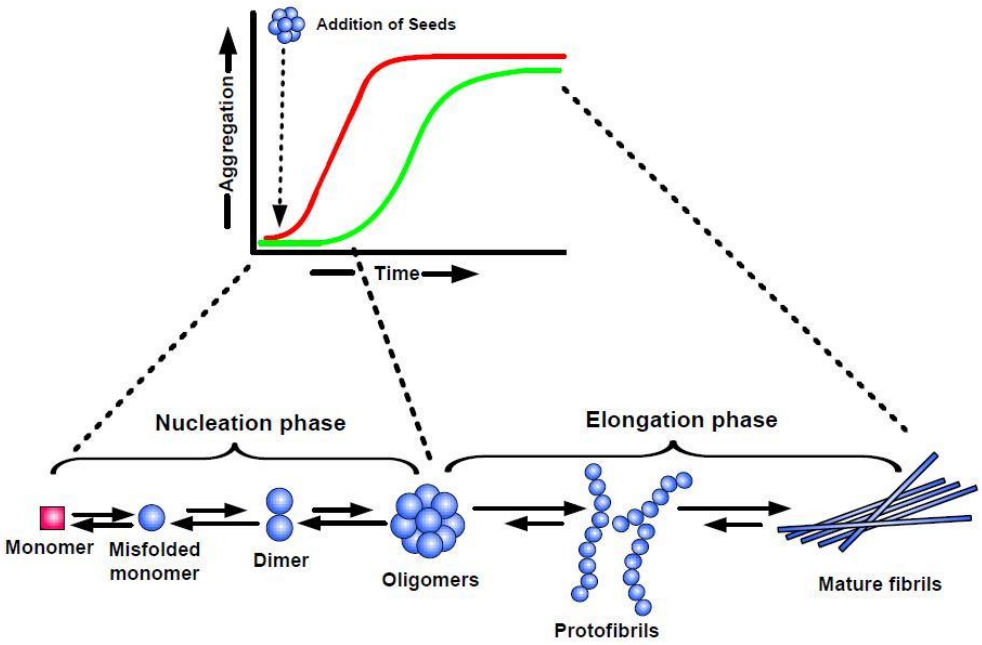

Figure 1. 4. The nucleation and growth mechanism of amyloid fibril formation Reproduced from Ref.26.

The initial nucleation phase is found to be kinetically driven while, the latter elongation phase is thermodynamically driven[11, 23]. The addition of preformed aggregates during the lag phase enhances the rate of fibril formation because of 'seeding effect' as in case of crystallization[23, 25, 26]. In the final equilibrium state, the concentration of the insoluble fibrilar form and the soluble monomeric form of the peptide come into equilibrium[17, 23].

1.1.5 Role of Water in the Amyloid Aggregation

Protein folding, misfolding and aggregation are highly influenced by the cellular environment. It is a well known fact that 65-90% of the cell is constituted by water. Hence, large number of studies is focused on the role of water in the mechanism of these biologically relevant processes using different peptides and proteins[27-34]. Self-assembly kinetics, structural properties and conformational characteristics of proteins were found to be getting affected by the modifications in the solvent environment[35-39]. The dynamic correlation of biomolecules with their first hydration shell, or 'biological waters', is considered very significant in biology[27-34]. Water mediated intra and inter molecular interactions stabilize various conformations of biological macromolecules during its functional and structural evolution[40].

The role of water in the aggregation kinetics of proteins is diverse and depends on the chemical nature of the surface. Recently, Thirumalai *et al* proposed a mechanism for

these controversial roles of water using two model peptides[41]. They have reported that water accelerates fibril formation in case of predominantly hydrophobic proteins, but the fibril formation is retarded by water molecule in case of hydrophilic sequences[41]. The release of structured water molecules around the protein into the bulk resulted in an increase in entropy change hence, considered as one of the thermodynamic driving force for protein aggregation[41]. On the approach of two hydrophobic peptide monomers, water molecules get expelled from its contact region and this promote the formation of aggregation prone structure (N*) and further fibril formation through stable intermediate structures[41]. Whereas, in case hydrophilic peptides, water wires form in between two peptide monomers on its approach and retard the further aggregation[41]. This mechanism is depicted in Figure 1.5. It has been also reported that water stabilizes various intermediate oligomers and various polymorphic structures of amyloids[41]. As amyloidogenic peptides and proteins are amphiphilic in nature, understanding of local and global dynamics of hydration layer water molecules is challenging, but highly demanding.

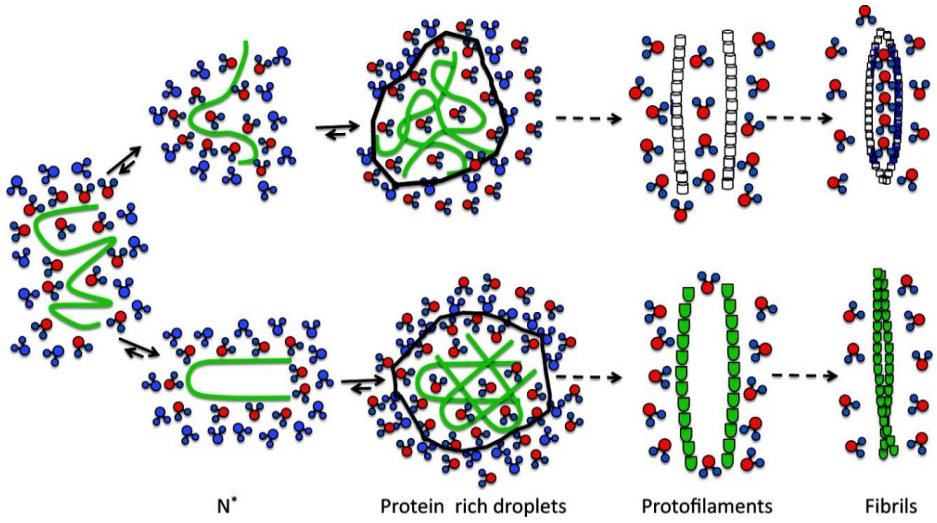

Figure 1.5. Schematic representation of water guided amyloid aggregation. Reproduced from Ref. 41 with the permission of American Chemical Soceity.

1.2 Intrinsically Disordered Proteins

Recent studies discovered that large number of proteins performs various cellular functions without having perfectly folded compact three-dimensional structure[42-44]. Instead of a single stable equilibrium structure, these proteins exist in an ensemble of disordered structures and rapidly interconvert its conformations under physiological conditions[42-44]. Besides this, several proteins are identified with intrinsically disordered

regions (IDRs) with specific biological functions[42-44]. These wide groups of proteins are known as intrinsically disordered proteins (IDPs)[42-44]. The functions of IDPs include signaling, molecular recognition, assistance of folding and unfolding, molecular assembly, etc[42-44].

It has been assumed that, the absence of rigid structure and the internal disorder are encoded in the primary structure of IDPs, similar to that of a normal globular protein in which the primary sequence guides the protein to reach its rigid 3D structure[42-45]. The presence of numerous uncompensated charged groups, low overall hydrophobicity, presence of polar and disorder-promoting amino acid residues: Ala, Gly, Arg, Gln, Lys, Ser, Glu, are few commonly observed characteristics of IDPs and IDRs[43]. Therefore, these exceptional features are some of the suspected reasons for the intrinsic disorder of these proteins[43]. High net charge of the protein sequence leads to charge-charge repulsion and the inter residue repulsion affects the compactification during the folding process [43].

Detailed NMR studies showed that the active functional sites of IDPs have significant local structure in the form of transient structural motifs[46]. IDPs possess structural flexibility either in the entire sequence or having shorter and longer regions with high conformational dynamics. The functionality of many of these proteins derived from its intrinsic flexibility[42, 43, 46]. The intrinsic disorder affects the speed of interactions of the IDPs and also allows to adapt distinct conformations, so this gives specificity for the function of different conformations[42, 43, 46]. Hence, we can say the kinetics and thermodynamics of this particular class of proteins are greatly influenced by the extent of its flexibility.

The functional characteristics of this group of proteins ruled out the structure-function paradigm which projected the idea that protein must fold into 3D structure to carry out its functions. A more comprehensive view 'The protein Trinity hypothesis',[44] connects the sequence- structure- function of the IDPs. This model suggested that native proteins can be in an ordered solid-like state or in a collapsed-disordered liquid-like state or in a gas-like extended disordered state. Further, this concept extended to include pre-molten globule state and transitions between all these four states[44].

1.2.1 Diseases Associated with IDPs

Disorder is an important and essential structural element, an IDP possesses at various levels of its functional and structural evolution. Because of this characteristic disorder and flexibility, IDPs are very prone to misfolding and amyloid formation[44, 45]. The formation of such non-native protein aggregates leads to functional failure and resulted in the

generation of toxic intermediates. This leads to the formulation of disorder in disorders concept (D^2 concept)[44]. There are now around 50 disorders which are associated with the misfolding of normally soluble functional proteins and their later transition into aggregates. Some of these diseases and the corresponding IDPs are listed in Table1.1.

Diseases	**IDPs associated with**
Alzheimer‟s disease	Aβ peptides , tau protein
Parkinson's disease	α-Synuclein
Type II diabetes	Amylin
Spongiform encephalopathies	Prion proteins
Glaucoma	Aβ peptides
Lewy Body Dimentia	α-Synuclein
Secondary systemic amyloidosis	Serum amyloid A
Fronto-temporal dementias	Tau
cancer	P53
cancer	α-Fetoprotein
Huntington's disease	Huntingtin

Table1.1. List of diseases and the associated IDPs.

The work presented in this thesis includes the dynamics and interactions of two broadly studied IDPs, amyloid beta and alpha-synuclein. These are mainly associated with neurodegenerative diseases Alzheimer's disease, Parkinson's disease and Lewy body disorder.

1.2.2 Alzheimer's Disease and Amyloid Hypothesis

Alzheimer's disease (AD) is a progressive neurodegenerative disease (ND) that affects brain's functions like memory, thinking, behavior and personality of the diseased individual and eventually leads to their death[47]. It is the most common form of dementia and accounts for 50 to 75% of all cases. It has been estimated that there will be over 80 million new cases during the next 40 years worldwide. As it is one of the major causes of death in many developed nations, it has been labeled the 'twenty-first century plague'[13].

The research on AD started in 1907 after Alois Alzheimer found the abnormal shrinkage of brain in an AD patient compared to that of a normal individual[48]. On detailed examination of the diseased brain it has been noticed that many of the cells were damaged and disappeared and also found deposits of a tangles and plaques in the brain[48].

Afterwards, vast research has been undertaken on different aspects of AD but scientific world has not yet succeeded in finding the exact cause or remedy for this disease. Recently, it has been identified that the commonly found plaque in the AD brain is constituted by a peptide known as amyloid beta (Aβ)[47]. This leads to 'Amyloid hypothesis', which claimed that AD arises from deposition of insoluble fibrilar plaques of Aβ in the neuronal synapsis of the brain and thereby interrupting normal neurotransmission[47].

Amyloid Beta is a well studied group of ID peptides having 39 to 43 residues, which originates from a transmembrane glycoprotein named Amyloid Precursor Protein (APP)[49]. The most toxic A$\beta_{1\text{-}42}$ and the most abundant A$\beta_{1\text{-}40}$ species are the major components of the insoluble fibrilar aggregates in the extracellular senile plaque of diseased brain and are found to be in a stacked beta sheet structure. Aβ is formed through sequential proteolytic cleavage of APP, catalysed by β- and γ-secretase[50]. The N-terminal region of Aβ derives from the extracellular region of APP by the action of β- secretase and the C-terminus derives by the action of γ-secretase from the transmembrane region[50]. The peptide dynamics and the vital interactions which lead to the aggregation are highly related to the primary structural characteristics. The N-terminal central hydrophobic core (CHC), $L_{17}VFFA_{21}$, has significant involvement in the intra- and inter- molecular interactions[51].

The pathogenic aggregation of Aβ is influenced by several factors like concentration, pH, interaction with different surfaces in the crowded intra and extra cellular space[52-55]. It has been believed that the interaction of the peptide with metal ions mainly of zinc, copper, aluminium and macromolecules namely proteins, cholesterol, lipids etc. can be conceivable reasons for the fibril formation at lower concentrations of the peptide[54, 56-59]. Various crowding agents are also capable to influence the amyloid aggregation kinetics *in vitro*[60].

The presence of amyloid aggregates, even in normal individuals, signifies the importance to distinguish this peptide's pathological aggregates and the pathways leading to its formation[61]. The detailed investigation of the dynamics of monomeric and lower oligomeric forms of Aβ peptide is required for the understanding of early toxic transformation of the peptide. The presence of neuro-fibrillary tangles and meshes of the microtubule-associated protein, tau within the nerve cells are also identified as characteristics of AD[62]. But, because of the appearance of Aβ aggregates in very early stages of the progression of this disease, vibrant research using different *in vivo, in vitro,*

and *in silico* techniques are targeted to reveal the toxic transformations of Aβ peptide during the progression of AD.

Recent structural studies of Aβ oligomer formation gave evidences for the existence of toxic soluble oligomers, which are more toxic than the fibrils[49, 63, 64]. The interaction of these oligomers with the cell membrane is a suspecting cause for the cellular degeneration[65]. Various amyloid oligomers have been demonstrated to form pore-like structures in biological membranes[66]. This channel formation will alter the membrane structure and leads to unfavorable ion leakage, which cause cell death [67, 68]. Hence, recent research is highly focused on the mechanism and characteristics of early oligomer formation pathway from its monomeric state and the interactions of monomers as well as small oligomers with biologically relevant surfaces[69-72].

1.2.3 Strategies of Drug Development

One of the major targets of the present AD drug research is Aβ peptide[73]. Eventhough, the cerebral plaque is composed of both Aβ and tau protein, it is evidenced that toxic transformation of Aβ is the prime pathological cause of this disease[74, 75]. The identity of the toxic species of Aβ involved in AD is not yet discovered hence, the development of suitable drug molecules or preventive measures is highly challenging. The existing therapeutic strategies are mainly targeted to reduce symptoms of the disease like dementia and cognitive impairment[76]. Aβ targeted AD drug research primarily adopts four different approaches to develop potential methods to reduce the production and neurotoxic transformations of this IDP. The first approach focuses on the proteolysis of APP to reduce the production of Aβ, the second approach focuses on the prevention of the amyloid aggregation, the third method is to stabilize the nontoxic native monomeric species to prevent the aggregation and the fourth method is to facilitate the destabilization of the toxic aggregates.

A group of drug candidates modulate the function of enzymes involved in the cleavage of APP. β- and γ-secretases enhance the cleavage Aβ fragment from APP while, α-secretase catalyses the cleavage of other harmless fragments[76]. The production of Aβ can be reduced either by inhibiting the action of β- and γ- secretases or by enhancing the action of α-secretase[76]. Various anti -β- amyloid aggregation agents, metal complexing agents and immunization agents are believed to be efficient in the prevention of aggregation, stabilization of the non toxic species and in the destabilization of toxic aggregates[76]. Many research groups developed potential drugs with different peptide fragments that inhibit the association of the Aβ peptide. Because of the greater

aggregation propensity, various hydrophobic fragments of Aβ and their slight variants are accepted as effective β-sheet blockers[77-79]. A recent study reported that the fragment Aβ_{16-22} is the best amongst different Aβ fragments to act as effective part of a beta sheet mimic which could antagonize the aggregation and reduce the toxicity *in vitro* as well as *in vivo* significantly[78].

In the quest of the cure for AD and similar NDs, research world has to bring out solution for many unanswered questions. The exact structure of the amyloid fibrils, the characteristics of intermediate aggregates, the identity of the toxic species, the typical reason for the toxic transformations of this peptide in diseased individuals, the toxic cellular interaction mechanism of the peptide aggregates etc. are still unclear. Identity, dynamic properties and inter/intra molecular interactions of the monomeric conformations especially the aggregation prone structure of peptide are essential for designing of suitable preventive measures.

1.2.4 Parkinson's disease and Alpha-Synuclein

Parkinson's disease is the second most common neurodegenerative disease, after AD[80, 81]. It is the most common movement disorder and first described by James Parkinson's in 1817[81]. It has been estimated that approximately 2% of the people above the age of 65 are affected by this disorder. This disease is clinically characterized by muscle rigidity, resting tremor, postural instability etc. and in most of the cases cognitive impairment observed at an advanced stage of PD[80, 81].

The prominent pathological hallmark of PD are the loss of dopaminergic neurons in the substantia nigra, region of the brain that controls movement, and the presence of intracellular inclusions called Lewy bodies and Lewy neuritis[82]. Lewy bodies are amyloid like fibrils mainly composed of oligomerised form of an IDP, αSynuclein (αS)[83]. There are sporadic and familial forms of PD[84]. In 1997, it has been discovered that the missence mutations in the gene for αS is the cause of the familial form[85]. Thereafter, numerous studies were attempted to understand the structural and dynamical characteristics of wild type and the mutated αS protein intermediates on its toxic transformation pathway[62, 86]. Oxidative stress and mitochondrial dysfunction are other causative factors for PD[86].

αS is a well studied representative member of the IDP family[87]; misfolding and aggregation of this protein is associated not only with PD but with other neuro degenerative diseases like AD and Lewy Body Dementia (LBD)[82, 88]. It is 14.46 kilodalton protein contains 140 amino acids. As in case of Aβ peptide, the primary sequence of αS also has some significant features. A continuous hydrophobic segment

present in this protein which is the non amyloid component (NAC) of the amyloid plaques found in AD[89]. The N-terminal region of the protein contains six imperfect repeat sequence motifs 'KTKEGV', but the role of these repeats in the toxicity of the protein has not yet been understood. The C-terminal region is highly acidic in nature.

*α*S is natively unstructured with little ordered secondary structure. This protein has an enhanced tendency to bind with different lipid molecules and these interactions induce alpha helicity in the protein[90, 91]. The hydrophobic segment -NAC- has significant role in the oligomerisation of the protein[92]. It has been evident from different *in vitro* studies that the acidic C-terminal region inhibits the assembly of this protein[93-95]. The aggregation propensity of three familial αS variants A30P, E46K and A53T is controversial; enhanced fibrilisation is observer in E46K and A53T while, soluble oligomer formation is enhanced in A30P variant[80]. The soluble oligomeric forms of all these variants are found to be more toxic than the mature fibrils *in vitro*[96]. The interaction of these oligomers with lipid bilayer is found to be disruptive and this can be the plausible cause of cell death[86, 91].

1.2.5 Cross-interactions of Amyloid Peptides

Recent epidemiological studies revealed strong correlation between different amyloidogenic diseases[97-99]. The bidirectional relationship between AD and PD, AD and LBD, AD and type II diabetes, etc are some of the noted examples of this mixed pathology[98, 99]. The observed similarity in the structure and toxic interactions of the pathological intermediates of different IDPs involved in each of these diseases suggested the possibility of cross-interaction between these proteins[100]. It has been confirmed clinically that the aggregates of various IDPs coexist in patients with amyloidogenic diseases[98-100].

The investigation to understand the molecular level mechanism of cross interaction between A*β* and *α*S started by the identification NAC region of *α*S in the amyloid plaque of AD[92]. According to recent statistics, about 50% of AD patients are detected with the presence of *α*S aggregates along with that of A*β*[101]. The direct interaction of A*β* with *α*S is evidenced from recent *in vivo* as well as *in vitro* studies[102-104]. These interactions stabilize the *α*S homologous oligomers and also enhance the formation of toxic cross oligomers[102, 103]. The amyloid aggregation kinetics also get influenced by the cross interaction of different IDPs. Recent kinetics studies on the aggregation of A*β* and *α*S showed that each of these IDPs acted as seeds and reduce the time lag in the initial

nucleation process during the aggregation of the other peptide[104]. The molecular level investigation of the cross interaction is essential for the mechanistic understanding of the kinetics and toxic transformations of these IDPs.

1.2.6 Challenges for the Studies of IDPs

Structural and functional characterization of IDP using existing experimental and theoretical methods is highly challenging mainly because of its inherent properties. In case of amyloid peptides like Aβ, αS etc. the topology of the toxic species in not yet confirmed or even not identified correctly. The structure and toxic interactions of this class of peptides under physiological conditions in the upstream of its aggregation pathway needs to be indentified for further studies on the preventive measures.

Nuclear Magnetic Resonance (NMR) techniques and X-ray diffraction techniques are generally used to determine the ensemble average structure of natively folded proteins[105-108]. It has been considered that the ensemble average structure for an IDP, obtained using classic experimental techniques cannot be representative of any structure in its wide ensemble because of its rapid conformational exchange between non native conformations[108, 109]. Another challenge to perform different experimental techniques is its higher propensity to precipitate *in vitro*. Hence, these methods only provide information about the possible boundaries of the structural ensemble[43, 108]. It should be mentioned here that most of these classic experimental techniques required non biological conditions but, the structure of IDPs is highly sensitive to its environmental conditions.

1.3 Scope of this Thesis

The objective of this thesis is to provide a molecular level understanding of the conformational dynamics of A$\beta_{1\text{-}42}$ monomer and its interactions with the surrounding solvent molecules, biologically relevant model hydrophilic surface and with another disease associated IDP αSynuclein$_{1\text{-}95}$ (αSyn) with which it has coevolving pathologies. Aβ is widely considered a representative peptide to study the general dynamics and exceptional properties of amyloidogenic proteins as well as IDPs[110]. Existing experimental methods are insufficient to provide molecular lever details of interactions of Aβ because of the ambiguity about the secondary structure of the nontoxic monomeric state and its rapid inter-conversion between different conformational states. This requires the use of appropriate computational techniques to probe the intrinsic structural and functional details. Molecular dynamic (MD) simulation is widely accepted as an appropriate computational method to understand the atomistic details of the dynamics of

biological macromolecules. We have used fully atomistic MD simulations with appropriate statistical analyses, to achieve the stated objectives.

The very early intra and inter molecular interactions of the peptide needs to be monitored to identify the characteristics aggregation prone structure and various conditions favoring its formation. We found that the early dynamics of the solvated peptide is characterized by a structural collapse initiated by nonlocal interactions between the CHC of the peptide with the C-terminal hydrophobic region. Earlier experimental and theoretical studies observed similar early dynamics and consider the compactification of monomeric peptide as a prerequisite for the aggregation[111, 112]. Our investigation showed that the change in hydrophobicity of the CHC causes significant change in the observed internal interaction pattern of the peptide. These results provide proper directions to develop strategies to alter the toxic dynamics of the Aβ peptide monomer.

Recent research focuses on the possibility of using different nanomaterials as therapeutics in amyloidogenic diseases[113, 114]. Hence, it is very important to monitor the influence of different surfaces on the peptide's characteristics. To understand the effect of hydrophilic nano surface on the early conformational pathway of Aβ, we have studied the dynamics of the peptide on a model hydrophilic surface, the TiO_2 (rutile) surface. Enhanced beta sheet propensity was observed at the proximity of the surface, with major disruption to the intrinsic collapse propesities. On the hydrophilic surface, the early observed intrinsic collapse of the peptide gets disrupted. The observed structural alteration of Aβ on the inorganic model surface has implications in the self assembly of Aβ on hydrophilic biological surface.

Since Aβ is an IDP, it can sample a wide ensemble of conformations in aqueous media at physiological conditions. We have investigated the dynamics of water around heterogeneous conformations of Aβ and compared the results with that of a natively folded protein Ubiquitin (UBQ). Our study shows that the conformational heterogeneity of the Aβ monomers affects the translational and rotational motions of hydration water molecules in a non-uniform manner. Relatively faster dynamics of hydration layer water molecules around Aβ conformations is evidenced compared to that of UBQ. We have attempted to understand the mechanistic details of these observations. The findings are of biological significance in studies of Aβ self-assembly, where hydration water has been shown to play profound roles in early oligomeric assembly and in protofibrillar stability.

We have probed the molecular details of heterogeneous cross dimerization pathways of Aβ and αSyn in fully aqueous environment. Principal Component Analysis (PCA) of simulation data on the μs timescales yielded heterogeneous interaction modes. The imperfect repeats 'KTKEGV' and the NAC region present in αSyn were found to be significant in the heterologous early oligomerisation. We elicited introspected into the chemical characteristics of interfacial regions of the distinct hetro dimers. The results give new insights about the hetero assembly pathways, which lead to polymorphic aggregates with variations in pathological attributes.

The work presented in this thesis gives clarification about various characteristic aspects of Aβ peptide monomer in biologically relevant environments. As Aβ is generally considered as a representative IDP, it is possible to extrapolate atleast some of the results to this particular class of proteins after appropriate extensions of these work. The details of the early dynamics and interactions of this peptide provided in this thesis have the potential to provide insights into the early onset toxic transitions, and hence help in the design of suitable preventive strategies for the homologous and heterologous IDP assembly and aggregation.

1.4 References

1. Dobson, C. M., Protein Folding and Misfolding. *Nature* **2003,** 426, 884-890.
2. Anfinsen, C. B.; Haber, E.; Sela, M.; White, F. H., The Kinetics of Formation of Native Ribonuclease During Oxidation of The Reduced Polypeptide Cain. *Proc. Natl. Acad. Sci. U.S.A.* **1961,** 47, 1309-1314.
3. Levinthal, C., Are there Pathways for Protein Folding. *J. Chim. phys* **1968,** 65, 44-45.
4. Kim, P. S.; Baldwin, R. L., Specific Intermediates in the Folding Reactions of Small Proteins and the Mechanism of Protein Folding. *Annu. Rev. Biochem.* **1982,** 51, 459-489.
5. Dill, K. A.; Chan, H. S., From Levinthal to Pathways to Funnels. *Nat. struct. biol.* **1997,** 4, 10-19.
6. Onuchic, J. N.; Luthey-Schulten, Z.; Wolynes, P. G., Theory of Protein Folding: the Energy Landscape Perspective. *Annu. Rev. Phys. Chem.* **1997,** 48, 545-600.
7. Bryngelson, J. D.; Onuchic, J. N.; Socci, N. D.; Wolynes, P. G., Funnels, Pathways, and the Energy Landscape of Protein Folding: A Synthesis. *Proteins: Struct., Funct., Bioinf.* **1995,** 21, 167-195.

8. Leopold, P. E.; Montal, M.; Onuchic, J. N., Protein Folding Funnels: a Kinetic Approach to the Sequence-Structure Relationship. *Proc. Natl. Acad. Sci. U.S.A.* **1992,** 89, 8721-8725.
9. Dobson, C. M., Protein Misfolding, Evolution and Disease. *Trends Biochem. Sci.* **1999,** 24, 329-332.
10. Thirumalai, D.; Reddy, G., Protein Thermodynamics: Are Native Proteins Metastable? *Nat. Chem.* **2011,** 3, 910-911.
11. Jahn, T. R.; Radford, S. E., The Yin and Yang of Protein Folding. *FEBS J.* **2005,** 272, 5962-5970.
12. Sipe, J. D.; Cohen, A. S., Review: History of the Amyloid Fibril. *J. Struct. Biol.* **2000,** 130, 88-98.
13. Knowles, T. P. J.; Vendruscolo, M.; Dobson, C. M., The Amyloid State and its Association with Protein Misfolding Diseases. *Nat. Rev. Mol. Cell Biol.* **2014,** 15, 384-396.
14. Baldwin, A. J.; Knowles, T. P. J.; Tartaglia, G. G.; Fitzpatrick, A. W.; Devlin, G. L.; Shammas, S. L.; Waudby, C. A.; Mossuto, M. F.; Meehan, S.; Gras, S. L.; Christodoulou, J.; Anthony-Cahill, S. J.; Barker, P. D.; Vendruscolo, M.; Dobson, C. M., Metastability of Native Proteins and the Phenomenon of Amyloid Formation. *J. Am. Chem. Soc.* **2011,** 133, 14160-14163.
15. Tycko, R., Solid State NMR Studies of Amyloid Fibril Structure. *Annu. Rev. Phys. Chem.* **2011,** 62, 279-299.
16. Marchut, A. J.; Hall, C. K., Side-Chain Interactions Determine Amyloid Formation by Model Polyglutamine Peptides in Molecular Dynamics Simulations. *Biophys. J.* **2006,** 90, 4574-4584.
17. Hall, C. K., Thermodynamic and Kinetic Origins of Alzheimer's and Related Diseases: A Chemical Engineer's Perspective. *AIChE J.* **2008,** 54, 1956-1962.
18. Puchtler, H.; Sweat, F.; Levine, M., On the Binding of Congo Red by Amyloid. *J. Histochem. Cytochem.* **1962,** 10, 355-364.
19. Kayed, R.; Head, E.; Thompson, J. L.; McIntire, T. M.; Milton, S. C.; Cotman, C. W.; Glabe, C. G., Common Structure of Soluble Amyloid Oligomers Implies Common Mechanism of Pathogenesis. *Science* **2003,** 300, 486.
20. Pallitto, M. M.; Murphy, R. M., A Mathematical Model of the Kinetics of β-Amyloid Fibril Growth from the Denatured State. *Biophys. J.* **2001,** 81, 1805-1822.

21. Pellarin, R.; Caflisch, A., Interpreting the Aggregation Kinetics of Amyloid Peptides. *J. Mol. Biol.* **2006,** 360, 882-892.
22. Teplow, D. B., Structural and Kinetic Features of Amyloid *β*-protein Fibrillogenesis. *Amyloid* **1998,** 5, 121-142.
23. Harper, J. D.; Lansbury, P. T., Models of Amyloid Seeding in Alzheimer's Disease and Scrape: Mechanistic Truths and Physiological Consequences of the Time-Dependent Solubility of Amyloid Proteins. *Annu. Rev. Biochem.* **1997,** 66, 385-407.
24. Burgold, S.; Filser, S.; Dorostkar, M. M.; Schmidt, B.; Herms, J., In vivo Imaging Reveals Sigmoidal Growth Kinetic of β-amyloid Plaques. *Acta Neuropathol. Commun.* **2014,** 2, 30-41.
25. Morozova-Roche, L. A.; Zurdo, J. s.; Spencer, A.; Noppe, W.; Receveur, V.; Archer, D. B.; Joniau, M.; Dobson, C. M., Amyloid Fibril Formation and Seeding by Wild-Type Human Lysozyme and Its Disease-Related Mutational Variants. *J. Struct. Biol.* **2000,** 130, 339-351.
26. Kumar, S.; Walter, J., Phosphorylation of Amyloid beta (Aβ) Peptides - A Trigger for Formation of Toxic Aggregates in Alzheimer's disease. *Aging* **2011,** 3, 803-812.
27. Sengupta, N.; Jaud, S.; Tobias, D. J., Hydration Dynamics in a Partially Denatured Ensemble of the Globular Protein Human α-Lactalbumin Investigated with Molecular Dynamics Simulations. *Biophys. J.* **2008,** 95, 5257-5267.
28. Bagchi, B., Water Dynamics in the Hydration Layer around Proteins and Micelles. *Chem. Rev.* **2005,** 105, 3197-3219.
29. Bandyopadhyay, S.; Chakraborty, S.; Bagchi, B., Exploration of the Secondary Structure Specific Differential Solvation Dynamics between the Native and Molten Globule States of the Protein HP-36. *J. Phys. Chem. B* **2006,** 110, 20629-20634.
30. Pal, S. K.; Peon, J.; Bagchi, B.; Zewail, A. H., Biological Water: Femtosecond Dynamics of Macromolecular Hydration. *J. Phys. Chem. B* **2002,** 106, 12376-12395.
31. Ebbinghaus, S.; Kim, S. J.; Heyden, M.; Yu, X.; Heugen, U.; Gruebele, M.; Leitner, D. M.; Havenith, M., An Extended Dynamical Hydration Shell around Proteins. *Proc. Natl. Acad. Sci. U.S.A.* **2007,** 104, 20749-20752.
32. Halle, B., Protein Hydration Dynamics in Solution: a Critical Survey. *Philos. Trans. R. Soc. B* **2004,** 359, 1207-1224.
33. Frauenfelder, H.; Fenimore, P. W.; Chen, G.; McMahon, B. H., Protein Folding is Slaved to Solvent Motions. *Proc. Natl. Acad. Sci. U.S.A.* **2006,** 103, 15469-15472.

34. Fenimore, P. W.; Frauenfelder, H.; McMahon, B. H.; Parak, F. G., Slaving: Solvent Fluctuations Dominate Protein Dynamics and Functions. *Proc. Natl. Acad. Sci. U.S.A.* **2002,** 99, 16047-16051.
35. Tomaselli, S.; Esposito, V.; Vangone, P.; van Nuland, N. A.; Bonvin, A. M.; Guerrini, R.; Tancredi, T.; Temussi, P. A.; Picone, D., The Alpha-to-Beta Conformational Transition of Alzheimer's Abeta-(1-42) Peptide in Aqueous Media is Reversible: A Step by Step Conformational Analysis Suggests the Location of Beta Conformation Seeding. *ChemBioChem* **2006,** 7, 257-267.
36. Crescenzi, O.; Tomaselli, S.; Guerrini, R.; Salvadori, S.; D'Ursi, A. M.; Temussi, P. A.; Picone, D., Solution Structure of the Alzheimer Amyloid *β*-Peptide (1–42) in an Apolar Microenvironment. *Eur. J. Biochem.* **2002,** 269, 5642-5648.
37. van der Wel, P. C. A.; Lewandowski, J. z. R.; Griffin, R. G., Solid-State NMR Study of Amyloid Nanocrystals and Fibrils Formed by the Peptide GNNQQNY from Yeast Prion Protein Sup35p. *J. Am. Chem. Soc.* **2007,** 129, 5117-5130.
38. Shen, C. L.; Murphy, R. M., Solvent Effects on Self-assembly of Beta-Amyloid Peptide. *Biophys. J.* **1995,** 69, 640-651.
39. Tran, H. T.; Mao, A.; Pappu, R. V., Role of Backbone-Solvent Interactions in Determining Conformational Equilibria of Intrinsically Disordered Proteins. *J. Am. Chem. Soc.* **2008,** 130, 7380-7392.
40. Vaiana, S. M.; Manno, M.; Emanuele, A.; Palma-Vittorelli, M. B.; Palma, M. U., The Role of Solvent in Protein Folding and in Aggregation. *J. Biol. Phys.* **2001,** 27, 133-145.
41. Thirumalai, D.; Reddy, G.; Straub, J. E., Role of Water in Protein Aggregation and Amyloid Polymorphism. *Acc. Chem. Res.* **2012,** 45, 83-92.
42. Dunker, A. K.; Lawson, J. D.; Brown, C. J.; Williams, R. M.; Romero, P.; Oh, J. S.; Oldfield, C. J.; Campen, A. M.; Ratliff, C. M.; Hipps, K. W.; Ausio, J.; Nissen, M. S.; Reeves, R.; Kang, C.; Kissinger, C. R.; Bailey, R. W.; Griswold, M. D.; Chiu, W.; Garner, E. C.; Obradovic, Z., Intrinsically Disordered Protein. *J. Mol. Graph. Model.* **2001,** 19, 26-59.
43. Tompa, P., Intrinsically Disordered Proteins: A 10-Year Recap. *Trends Biochem. Sci.* **2012,** 37, 509-516.
44. Uversky, V. N.; Oldfield, C. J.; Dunker, A. K., Intrinsically Disordered Proteins in Human Diseases: Introducing the D2 Concept. *Annu. Rev. Biophys.* **2008,** 37, 215-246.

45. Eliezer, D., Biophysical Characterization of Intrinsically Disordered Proteins. *Curr. Opin. Struct. Biol.* **2009,** 19, 23-30.
46. Dyson, H. J.; Wright, P. E., Intrinsically Unstructured Proteins and their Functions. *Nat. Rev. Mol. Cell Biol.* **2005,** 6, 197-208.
47. Hardy, J.; Selkoe, D. J., The Amyloid Hypothesis of Alzheimer's Disease: Progress and Problems on the Road to Therapeutics. *Science* **2002,** 297, 353-356.
48. Graeber, M. B.; Kösel, S.; Egensperger, R.; Banati, R. B.; Müller, U.; Bise, K.; Hoff, P.; Möller, H. J.; Fujisawa, K.; Mehraein, P., Rediscovery of the Case Described by Alois Alzheimer in 1911: Historical, Histological and Molecular Genetic Analysis. *Neurogenetics* **1997,** 1, 73-80.
49. Haass, C.; Selkoe, D. J., Soluble Protein Oligomers in Neurodegeneration: Lessons from the Alzheimer's Amyloid *β*-Peptide. *Nat. Rev. Mol. Cell Biol.* **2007,** 8, 101-112.
50. Gralle, M.; Ferreira, S. T., Structure and Functions of the Human Amyloid Precursor Protein: The Whole is More than the Sum of its Parts. *Prog. Neurobiol.* **2007,** 82, 11-32.
51. Petkova, A. T.; Ishii, Y.; Balbach, J. J.; Antzutkin, O. N.; Leapman, R. D.; Delaglio, F.; Tycko, R., A Structural Model for Alzheimer's *β*-Amyloid Fibrils Based on Experimental Constraints from Solid State NMR. *Proc Natl Acad Sci USA* **2002,** 99, 16742-16747.
52. Giacomelli, C. E.; Norde, W., Conformational Changes of the Amyloid β-Peptide (1–40) Adsorbed on Solid Surfaces. *Macromol. Biosci.* **2005,** 5, 401-407.
53. Wood, S. J.; Maleeff, B.; Hart, T.; Wetzel, R., Physical, Morphological and Functional Differences between pH 5.8 and 7.4 Aggregates of the Alzheimer's Amyloid Peptide A*β*. *J. Mol. Biol.* **1996,** 256, 870-877.
54. Tofoleanu, F.; Buchete, N.-V., Alzheimer A*β* Peptide Interactions with Lipid Membranes: Fibrils, Oligomers and Polymorphic Amyloid Channels. *Prion* **2012,** 6, 339-345.
55. Utesch, T.; Daminelli, G.; Mroginski, M. A., Molecular Dynamics Simulations of the Adsorption of Bone Morphogenetic Protein-2 on Surfaces with Medical Relevance. *Langmuir* **2011,** 27, 13144-13153.
56. Hane, F.; Leonenko, Z., Effect of Metals on Kinetic Pathways of Amyloid-β Aggregation. *Biomolecules* **2014,** 4, 101-116.
57. Chen, W.-T.; Liao, Y.-H.; Yu, H.-M.; Cheng, I. H.; Chen, Y.-R., Distinct Effects of Zn^{2+}, Cu^{2+}, Fe^{3+}, and Al^{3+} on Amyloid-β Stability, Oligomerization, and

Aggregation: Amyloid-β Destabilization Promotes Annular Protofibril Formation. *J. Biol. Chem.* **2011,** 286, 9646-9656.

58. Miller, Y.; Ma, B.; Nussinov, R., Zinc Ions Promote Alzheimer Aβ Aggregation via Population Shift of Polymorphic States. *Proc. Natl. Acad. Sci. U.S.A.* **2010,** 107, 9490-9495.
59. Wong, B. X.; Hung, Y. H.; Bush, A. I.; Duce, J. A., Metals and Cholesterol: Two Sides of the Same Coin in Alzheimer's Disease Pathology. *Front. Aging Neurosci.* **2014,** 6, 91.
60. Latshaw, D. C.; Cheon, M.; Hall, C. K., Effects of Macromolecular Crowding on Amyloid Beta (16-22) Aggregation Using Coarse-Grained Simulations. *J. Phys. Chem. B* **2014,** 118, 13513-13526.
61. Pimplikar, S. W., Reassessing the Amyloid Cascade Hypothesis of Alzheimer's Disease. *Int. J. Biochem. Cell Biol.* **2009,** 41, 1261-1268.
62. Goedert, M.; Spillantini, M. G.; Jakes, R.; Rutherford, D.; Crowther, R. A., Multiple Isoforms of Human Microtubule-Associated Protein Tau: Sequences and Localization in Neurofibrillary Tangles of Alzheimer's Disease. *Neuron* **1989,** 3, 519-526.
63. Liao, M. Q.; Tzeng, Y. J.; Chang, L. Y. X.; Huang, H. B.; Lin, T. H.; Chyan, C. L.; Chen, Y. C., The Correlation between Neurotoxicity, Aggregative Ability and Secondary Structure Studied by Sequence Truncated Aβ Peptides. *FEBS lett.* **2007,** 581, 1161-1165.
64. Cappai, R.; Barnham, K., Delineating the Mechanism of Alzheimer's Disease Aβ Peptide Neurotoxicity. *Neurochem. Res.* **2008,** 33, 526-532.
65. Williams, T. L.; Serpell, L. C., Membrane and Surface Interactions of Alzheimer's Aβ Peptide Insights into the Mechanism of Cytotoxicity. *FEBS J.* **2011,** 278, 3905-3917.
66. Lashuel, H. A.; Hartley, D.; Petre, B. M.; Walz, T.; Lansbury, P. T., Neurodegenerative Disease: Amyloid Pores from Pathogenic Mutations. *Nature* **2002,** 418, 291-291.
67. Pollard, H. B.; Arispe, N.; Rojas, E., Ion Channel Hypothesis for Alzheimer Amyloid Peptide Neurotoxicity. *Cell Mol. Neurobiol.* **1995,** 15, 513-526.
68. Quist, A.; Doudevski, I.; Lin, H.; Azimova, R.; Ng, D.; Frangione, B.; Kagan, B.; Ghiso, J.; Lal, R., Amyloid Ion Channels: A Common Structural Link for Protein-Misfolding Disease. *Proc. Natl. Acad. Sci. U.S.A.* **2005,** 102, 10427-10432.

69. Chong, S.-H.; Ham, S., Distinct Role of Hydration Water in Protein Misfolding and Aggregation Revealed by Fluctuating Thermodynamics Analysis. *Acc. Chem. Res.* **2015,** 48, 956-965.
70. Jana, A. K.; Jose, J. C.; Sengupta, N., Critical Roles of Key Domains in Complete Adsorption of Aβ Peptide on Single-Walled Carbon Nanotubes: Insights with Point Mutations and MD Simulations. *Phys. Chem. Chem. Phys.* **2012,** 15, 837-844.
71. Jana, A. K.; Sengupta, N., Adsorption Mechanism and Collapse Propensities of the Full-Length, Monomeric Aβ1-42 on the Surface of a Single-Walled Carbon Nanotube: A Molecular Dynamics Simulation Study. *Biophys. J.* **2012,** 102, 1889-1896.
72. Jana, A. K.; Sengupta, N., A*β* self-Association and Adsorption on a Hydrophobic Nanosurface: Competitive Effects and the Detection of Small Oligomers via Electrical Response. *Soft Matter* **2015,** 11, 269-279.
73. Eleuteri, S.; Di Giovanni, S.; Rockenstein, E.; Mante, M.; Adame, A.; Trejo, M.; Wrasidlo, W.; Wu, F.; Fraering, P. C.; Masliah, E.; Lashuel, H. A., Novel Therapeutic Strategy for Neurodegeneration by Blocking Aβ Seeding Mediated Aggregation in Models of Alzheimer's Disease. *Neurobiol. Dis.* **2015,** 74, 144-157.
74. Wolfe, M. S., Therapeutic Strategies for Alzheimer's Disease. *Nat. Rev. Drug Discov.* **2002,** 1, 859-866.
75. Hampel, H.; Schneider, L. S.; Giacobini, E.; Kivipelto, M.; Sindi, S.; Dubois, B.; Broich, K.; Nisticò, R.; Aisen, P. S.; Lista, S., Advances in the Therapy of Alzheimer's Disease: Targeting Amyloid Beta and Tau and Perspectives for the Future. *Expert Rev. Neurother.* **2015,** 15, 83-105.
76. Jia, Q.; Deng, Y.; Qing, H., Potential Therapeutic Strategies for Alzheimer's Disease Targeting or Beyond *β*-Amyloid: Insights from Clinical Trials. *BioMed Res. Int.* **2014,** 2014, 837157-837179.
77. Viet, M. H.; Ngo, S. T.; Lam, N. S.; Li, M. S., Inhibition of Aggregation of Amyloid Peptides by Beta-Sheet Breaker Peptides and their Binding Affinity. *J. Phys. Chem. B* **2011,** 115, 7433-7446.
78. Cheng, P.-N.; Liu, C.; Zhao, M.; Eisenberg, D.; Nowick, J. S., Amyloid β-Sheet Mimics that Antagonize Protein Aggregation and Reduce Amyloid Toxicity. *Nat. Chem.* **2012**, 927-933.

79. Chini, M. G.; Scrima, M.; D'Ursi, A. M.; Bifulco, G., Fibril Aggregation Inhibitory Activity of the β-sheet Breaker Peptides: a Molecular Docking Approach. *J. Pept. Sci.* **2009,** 15, 229-234.
80. Goedert, M., Alpha-Synuclein and Neurodegenerative Diseases. *Nat. Rev. Neurosci.* **2001,** 2, 492-501.
81. Ellis, H., James Parkinson: Parkinson's Disease. *J. Perioper. Pract.* **2013,** 23, 262-263.
82. Spillantini, M. G.; Schmidt, M. L.; Lee, V. M.-Y.; Trojanowski, J. Q.; Jakes, R.; Goedert, M., α-Synuclein in Lewy Bodies. *Nature* **1997,** 388, 839-840.
83. Uversky, V. N., α-Synuclein Misfolding and Neurodegenerative Diseases. *Curr. Protein Pept. Sci.* **2008,** 9, 507-540.
84. McNaught, K. S. P.; Olanow, C. W., Protein Aggregation in the Pathogenesis of Familial and Sporadic Parkinson's Disease. *Neurobiol. Aging* **2006,** 27, 530-545.
85. Polymeropoulos, M. H.; Lavedan, C.; Leroy, E.; Ide, S. E.; Dehejia, A.; Dutra, A.; Pike, B.; Root, H.; Rubenstein, J.; Boyer, R.; Stenroos, E. S.; Chandrasekharappa, S.; Athanassiadou, A.; Papapetropoulos, T.; Johnson, W. G.; Lazzarini, A. M.; Duvoisin, R. C.; Di Iorio, G.; Golbe, L. I.; Nussbaum, R. L., Mutation in the α-Synuclein Gene Identified in Families with Parkinson's Disease. *Science* **1997,** 276, 2045-2047.
86. Maries, E.; Dass, B.; Collier, T. J.; Kordower, J. H.; Steece-Collier, K., The Role of α-Synuclein in Parkinson's Disease: Insights from Animal Models. *Nat. Rev. Neurosci.* **2003,** 4, 727-738.
87. Drescher, M.; Huber, M.; Subramaniam, V., Hunting the Chameleon: Structural Conformations of the Intrinsically Disordered Protein Alpha-Synuclein. *ChemBioChem* **2012,** 13, 761-768.
88. Mandal, P.; Pettegrew, J.; Masliah, E.; Hamilton, R.; Mandal, R., Interaction between Aβ Peptide and α-Synuclein: Molecular Mechanisms in Overlapping Pathology of Alzheimer's and Parkinson's in Dementia with Lewy Body Disease. *Neurochem. Res.* **2006,** 31, 1153-1162.
89. Iwai, A.; Masliah, E.; Yoshimoto, M.; Ge, N.; Flanagan, L.; Rohan de Silva, H. A.; Kittel, A.; Saitoh, T., The Precursor Protein of Non-Aβ Component of Alzheimer's Disease Amyloid is a Presynaptic Protein of the Central Nervous System. *Neuron* **1995,** 14, 467-475.

90. Davidson, W. S.; Jonas, A.; Clayton, D. F.; George, J. M., Stabilization of α-Synuclein Secondary Structure upon Binding to Synthetic Membranes. *J. Biol. Chem.* **1998,** 273, 9443-9449.
91. Jo, E.; McLaurin, J.; Yip, C. M.; St. George-Hyslop, P.; Fraser, P. E., α-Synuclein Membrane Interactions and Lipid Specificity. *J. Biol. Chem.* **2000,** 275, 34328-34334.
92. Hashimoto, M.; Hsu, L. J.; Xia, Y.; Takeda, A.; Sisk, A.; Sundsmo, M.; Masliah, E., Oxidative Stress Induces Amyloid-Like Aggregate Formation of NACP/α-Synuclein in vitro. *NeuroReport* **1999,** 10, 717-721.
93. Games, D.; Seubert, P.; Rockenstein, E.; Patrick, C.; Trejo, M.; Ubhi, K.; Ettle, B.; Ghassemiam, M.; Barbour, R.; Schenk, D.; Nuber, S.; Masliah, E., Axonopathy in an α-Synuclein Transgenic Model of Lewy Body Disease Is Associated with Extensive Accumulation of C-Terminal-Truncated α-Synuclein. *Am. J. Pathol.* **2013,** 182, 940-953.
94. Kanda, S.; Bishop, J. F.; Eglitis, M. A.; Yang, Y.; Mouradian, M. M., Enhanced Vulnerability to Oxidative Stress by α-Synuclein Mutations and C-Terminal Truncation. *Neurosci.* **2000,** 97, 279-284.
95. Li, W.; West, N.; Colla, E.; Pletnikova, O.; Troncoso, J. C.; Marsh, L.; Dawson, T. M.; Jäkälä, P.; Hartmann, T.; Price, D. L.; Lee, M. K., Aggregation Promoting C-Terminal Truncation of α-Synuclein is a Normal Cellular Process and is Enhanced by the Familial Parkinson's Disease-Linked Mutations. *Proc. Natl. Acad. Sci. U.S.A.* **2005,** 102, 2162-2167.
96. Winner, B.; Jappelli, R.; Maji, S. K.; Desplats, P. A.; Boyer, L.; Aigner, S.; Hetzer, C.; Loher, T.; Vilar, M. a.; Campioni, S.; Tzitzilonis, C.; Soragni, A.; Jessberger, S.; Mira, H.; Consiglio, A.; Pham, E.; Masliah, E.; Gage, F. H.; Riek, R., In Vivo Demonstration that α-Synuclein Oligomers are Toxic. *Proc. Natl. Acad. Sci. U.S.A.* **2011,** 108, 4194-4199.
97. Jellinger, K. A.; Attems, J., Neuropathological Evaluation of Mixed Dementia. *J. Neurol. Sci.* **2007,** 257, 80-87.
98. Mandal, P.; Pettegrew, J.; Masliah, E.; Hamilton, R.; Mandal, R., Interaction between Aβ Peptide and α Synuclein: Molecular Mechanisms in Overlapping Pathology of Alzheimer's and Parkinson's in Dementia with Lewy Body Disease. *Neurochem. Res.* **2006,** 31, 1153-1162.

99. Tsigelny, I. F.; Crews, L.; Desplats, P.; Shaked, G. M.; Sharikov, Y.; Mizuno, H.; Spencer, B.; Rockenstein, E.; Trejo, M.; Platoshyn, O.; Yuan, J. X. J.; Masliah, E., Mechanisms of Hybrid Oligomer Formation in the Pathogenesis of Combined Alzheimer's and Parkinson's Diseases. *PLOS ONE* **2008,** 3, e3135.
100. Irwin, D. J.; Lee, V. M. Y.; Trojanowski, J. Q., Parkinson's Disease Dementia: Convergence of α-Synuclein, Tau and Amyloid-β Pathologies. *Nat. Rev. Neurosci.* **2013,** 14, 626-636.
101. Hamilton, R. L., Lewy Bodies in Alzheimer's Disease: A Neuropathological Review of 145 Cases Using α-Synuclein Immunohistochemistry. *Brain Pathol.* **2000,** 10, 378-384.
102. Mandal, P.; Pettegrew, J.; Masliah, E.; Hamilton, R.; Mandal, R., Interaction between Aβ Peptide and α Synuclein: Molecular Mechanisms in Overlapping Pathology of Alzheimer's and Parkinson's in Dementia with Lewy Body Disease. *Neurochem Res* **2006,** 31, 1153-1162.
103. Tsigelny, I. F.; Crews, L.; Desplats, P.; Shaked, G. M.; Sharikov, Y.; Mizuno, H.; Spencer, B.; Rockenstein, E.; Trejo, M.; Platoshyn, O.; Yuan, J. X. J.; Masliah, E., Mechanisms of Hybrid Oligomer Formation in the Pathogenesis of Combined Alzheimer's and Parkinson's Diseases. *PLOS ONE* **2008,** 3, e3135.
104. Morales, R.; Moreno-Gonzalez, I.; Soto, C., Cross-Seeding of Misfolded Proteins: Implications for Etiology and Pathogenesis of Protein Misfolding Diseases. *PLOS Pathog* **2013,** 9, e1003537.
105. Drenth, J., *Principles of Protein X-ray Crystallography*. Springer: 2007.
106. Duer, M. J., Solid-state NMR spectroscopy: A Tool for Molecular-Level Structure Analysis and Dynamics. *Biomineralization Sourcebook: Characterization of Biominerals and Biomimetic Materials* **2014**, 153.
107. Kessler, H.; Bermel, W.; Muller, A.; Pook, K. H., Modern Nuclear Magnetic Resonance Spectroscopy of Peptides. *Conformation in Biology and Drug Design: The Peptides: Analysis, Synthesis, Biology* **2014**, 437.
108. Burger, V.; Gurry, T.; Stultz, C., Intrinsically Disordered Proteins: Where Computation Meets Experiment. *Polymers* **2014,** 6, 2684-2719.
109. Jensen, M. R.; Blackledge, M., Testing the Validity of Ensemble Descriptions of Intrinsically Disordered Proteins. *Proc. Natl. Acad. Sci. U.S.A.* **2014,** 111, E1557-E1558.

110. Ball, K. A.; Phillips, A. H.; Nerenberg, P. S.; Fawzi, N. L.; Wemmer, D. E.; Head-Gordon, T., Homogeneous and Heterogeneous Tertiary Structure Ensembles of Amyloid-β Peptides. *Biochemistry* **2011,** 50, 7612-7628.

111. Lee, C.; Ham, S., Characterizing Amyloid-Beta Protein Misfolding from Molecular Dynamics Simulations with Explicit Water. *J. Comput. Chem.* **2010,** 32, 349-355.

112. Zhang, S.; Iwata, K.; Lachenmann, M. J.; Peng, J. W.; Li, S.; Stimson, E. R.; Lu, Y. a.; Felix, A. M.; Maggio, J. E.; Lee, J. P., The Alzheimer's Peptide Aβ Adopts a Collapsed Coil Structure in Water. *J. Struct. Biol.* **2000,** 130, 130-141.

113. Mundra, R. V.; Wu, X.; Sauer, J.; Dordick, J. S.; Kane, R. S., Nanotubes in Biological Applications. *Curr. Opin. Biotech.* **2014,** 28, 25-32.

114. Tonga, G. Y.; Moyano, D. F.; Kim, C. S.; Rotello, V. M., Inorganic Nanoparticles for Therapeutic Delivery: Trials, Tribulations and Promise. *Curr. Opin. Colloid Interface Sci.* **2014,** 19, 49-55.

Chapter 2

Methodology

"…everything that is living can be understood

in terms of the jiggling and wiggling of atoms."

-Richard Feynman

2.1 Introduction

As discussed in the first chapter, the major objective of this thesis is to characterise the early structural transitions and interactions of a representative intrinsically disordered protein Aβ. Molecular level understanding of structural and functional details in physiological conditions is the pre-requisite to control pathological conformational transformations of various IDPs. Recent studies have established direct correlation between conformational flexibility and amyloidogenic propensity of various IDPs[1]. Hence, protein dynamics is considered as a possible predictor of pathogenicity of many diseases associated with IDPs[1]. Biological molecules are characterised by motions at various timescales; bond vibrations are the fastest with time period of the order of femtoseconds[2]. It has been observed that the dynamics of surrounding water molecules is coupled with the dynamics of proteins in general[3-5]. Therefore, to understand the dynamics of biomolecules as well as the surrounding solvents we have to capture the structural evolution of the system at femtosecond timescales. Such sophisticated dynamic propagation pathways of solvated IDPs can be captured using complementary computational and experimental methods. Atomistic MD simulations with current generation empirical force fields are a well accepted method for probing the structural, dynamical and interfacial characteristics of biomolecules. This chapter includes overview of computational methods with an emphasis on MD method and the associated statistical analyses used in this work. Further, we briefly describe experimental techniques that are complementary to the MD methods.

2. 2 An Overview of Different Computational Methods

To study the dynamics of different systems, various computational tools are available based on quantum or classical mechanics[2]. According to the size of the system we can choose appropriate technique and each of these techniques provide details of dynamics at various time scales as described in Figure 2.1. Unlike classical mechanics, quantum mechanical (QM) model explicitly include electrons in the calculations[2]. Hence, various quantum mechanical models are generally used to study the 'bond breaking and making' process of chemical reactions[2]. Because of the explicit consideration of the electrons, the calculations become extremely time consuming for larger system. Therefore, these techniques can be adopted only for systems with limited number of atoms.

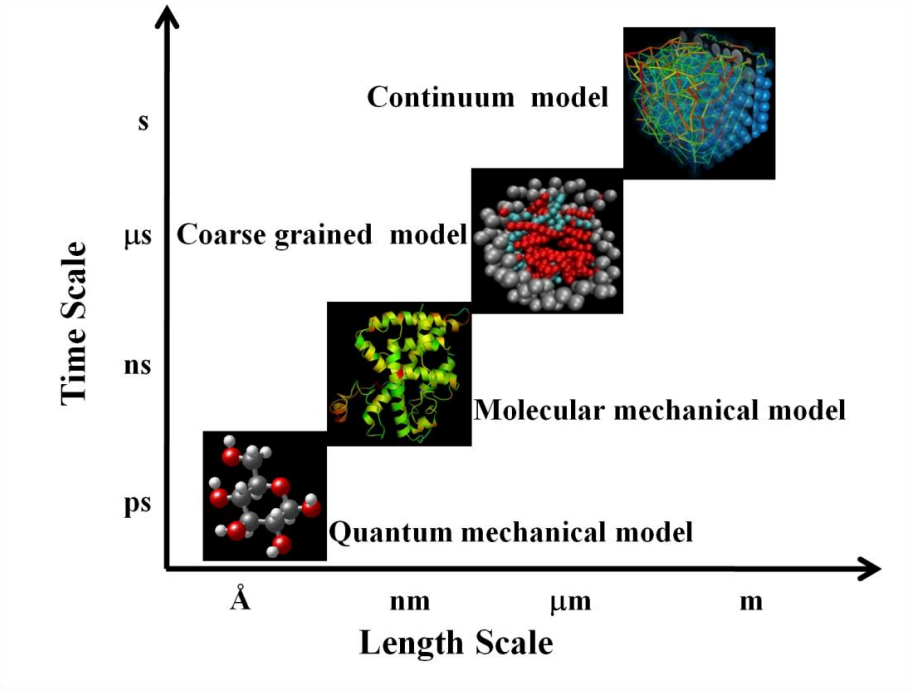

Figure 2.1: Various computational models for different time and length scale.

Molecular mechanical models ignore the electrons of individual atoms and consider only the nuclear motions to calculate the properties of the system[2, 6]. Because of this approximation, systems with significant number of atoms, especially biological molecules can be studied using these techniques. Molecular Dynamics (MD) Simulation is one of the most important methods based on molecular mechanics (MM)[2, 6]. Large number of studies on protein folding, misfolding, aggregation and other biological processes which involve structural alterations have been done by several groups using MD simulations.

Eventhough, MD simulation is considered as the most appropriate computational method to study the dynamics of proteins, it is insufficient for probing the reactive centres of a molecule. The development of QM/MM method enabled the efficient modelling of reactive biomolecular systems[7]. The chemically active center of interest in a biomolecule is treated with QM and the rest of the system treated with MM in this method[7]. Reasonable computational cost along with appreciable accuracy is achieved in this method by incorporating the advantages of QM and MM methods[7].

The all atomistic studies are again difficult for even larger systems because of the requirement of huge computational resources. Instead of considering explicit atoms,

group of atoms are approximated as a single unit in coarse grained model[8, 9]. In biological research, this approach is generally used to get an overall mechanistic understanding about the interactions and dynamics of very large molecules[9]. The detailed and accurate secondary structural information and the dynamics of proteins are unable to probe with this method. In continuum model, matter in the body is considered as a continuum without any free space[10]. This method, because of the large scale approximations can provide only certain properties of the systems which are independent of the structure of the system.

As the aim of this thesis is to understand atomistic details of the early dynamics and interactions of an IDP, we have opted MD simulation technique for this study. The detailed theoretical description of this method is provided in the next section.

2.3 Molecular Dynamics Simulation Method

MD simulation is a deterministic method, which follows laws of classical mechanics to describe the time evolution of molecules constituted by a set of interacting atoms[2]. By integrating Newton's equations of motion, this method generate set of coordinates and velocities at consecutive time intervals[2]. For a simple atomic system with mass *m* and positional coordinate *r*, Newton's second law can be written as

$$F = m\frac{d^2r}{dt^2} \tag{2.1}$$

By knowing the positions and velocities at time *t* one can calculate the positions and velocities of the system after a small time interval δt as follows,

$$r(t+\delta t) = r(t) + v(t)\delta t + \frac{F(t)}{2}\delta t^2 \tag{2.2}$$

$$v(t+\delta t) = v(t) + \frac{F(t+\delta t)+F(t)}{2\mathrm{m}}\delta t \tag{2.3}$$

But, to solve these equations we have to calculate the force acting on each atom, for that we can use the equation

$$F = -\nabla V \tag{2.4}$$

Where, *V* is the potential energy of the system which is a function of nuclear coordinates of atoms. To calculate the potential energy surface of a system, empirical force fields are generally used[2, 6]. A set of successive positions and velocities or the 'trajectory' of the system can be calculated by continuing the above equations.

2.4 Force Field

The potential energy functions for calculating the intra- and inter- molecular interactions of a biological system constructed by various bonded and non-bonded interaction terms[2]. One of the functional forms of this energy function for an N atom system is given below,

$$V(r^N) = \sum_{bonds} k_b (b - b_0)^2 + \sum_{angles} k_\theta (\theta - \theta_0)^2 + \sum_{dihedrals} \sum_{n=1}^{N} k_\varphi^{(n)} [1 + \cos((n\varphi - \delta)] + \sum_{impropers} k_\omega (\omega - \omega_0)^2 + \sum_{i=1}^{N} \sum_{j=i+1}^{N} \left(4\varepsilon_{ij} \left[\left(\frac{\sigma_{ij}}{r_{ij}} \right)^{12} - \left(\frac{\sigma_{ij}}{r_{ij}} \right)^{6} \right] + \frac{q_i q_j}{4\pi\varepsilon_0 r_{ij}} \right) \quad (2.5)$$

The first four terms in eqn. 2.5 are for bonded interactions and the last two terms calculate the non-bonded interactions. The total potential $V(r^N)$ is a function of positional coordinates (r) of N atomic nucleus[2]. The first term describes the energy deviation during bond stretching and which is modelled using harmonic potential; b is the bond length, b_0 is the equilibrium bond length and k_b is the force constant. The second term is also modelled using harmonic potential and this term gives the total energy change during the angle bending motions in a molecule; k_θ is the force constant; θ and θ_0 are the angle between three consecutive atoms and its equilibrium value, respectively. The third term gives the torsional potential (dihedral term) arises due to the rotational motion of the bonds. Every four consecutive atoms in a molecule are associated with a dihedral. The cosine function represents the periodicity of this function. In this term φ is the torsion angle; k_φ is the height of rotational energy barrier; n is the multiplicity which represents the number of minimum points in the function during a 360^0 rotation of a bond; the phase factor δ determines where the torsion angle passes through the minimum values. The last term in the bonded interaction part of eqn. 2.5 describes improper torsional potential using improper torsion angle ω and the parameters ω_0 and k_ω.

The bonded interaction terms concern only about the intra-molecular interactions of the molecule but, the non-bonded potential is calculated between all pairs of atoms

except those pairs included in the calculation of bonded interaction potential[2]. The non-bonded terms in a force field contains van der Waal's and electrostatic interactions and these terms modelled generally as Lenard-Jones and coulomb potentials, respectively.

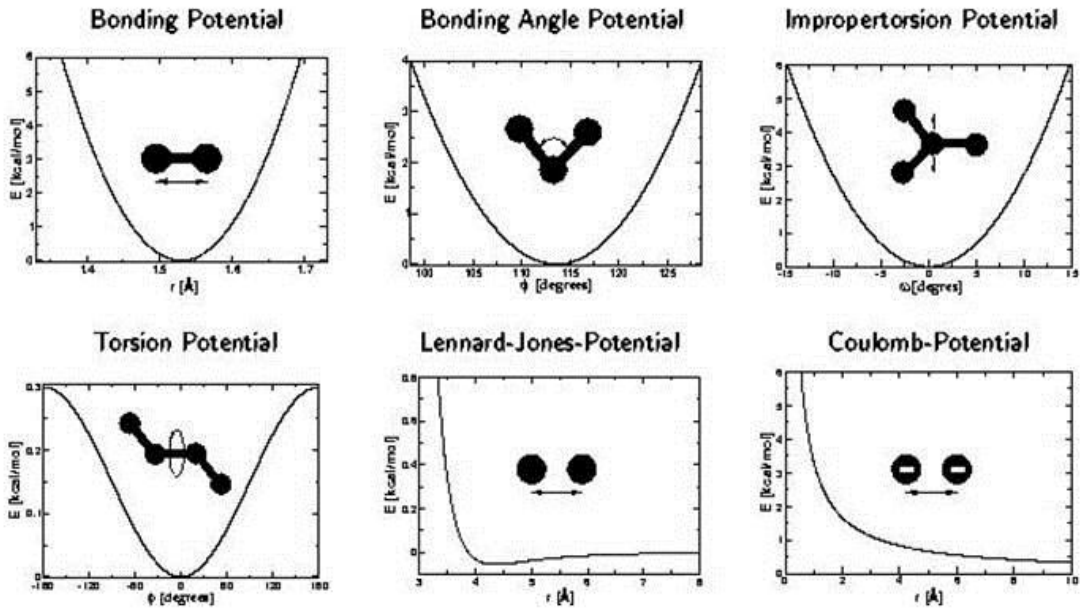

Figure 2.2: Schematic representation of different contributing potential functions to the force field.

The first term in the non-bonded interaction terms in eqn. 2.5 represents van der Waals interaction potential between two atoms *i* and *j* with inter atomic distance r_{ij}. As two atoms are brought together from infinite separation, the negative term ($1/r^6$) in the square bracket dominates hence, energy becomes more negative. Atoms experience increase in attraction with decrease in distance and attain an energy minimum at a closer distance. At distances closer than the energy minimum the positive term ($1/r^{12}$) starts to dominate and energy becomes positive rapidly. The parameter ε_{ij} represents the depth of the potential energy well and σ_{ij} represents the collision diameter or the distance at which the energy is zero. These two parameters depend up on the nature of the interacting atoms. The second non-bonded interaction term describe the electrostatic interaction between pairs of atoms *i* and *j* with partial charges q_i and q_j, respectively, separated by a distance r_{ij} using Coulomb's law.

A functional form and all the parameters associated with it collectively known as a force field[2]. Figure 2.2 depicts different contributing factors of a force field with functional form as given in eqn. 2.5. The parameters of a force field are mainly obtained from experimental or quantum mechanical studies of small molecules or fragments and

these parameters can be used to study much large molecules[2]. Transferability of parameters is a significant aspect of force field[2]. Many empirical force fields are available for different biological molecules. For conducting MD simulations for this thesis work we have adopted all atomistic CHARMM 22 force field for the protein molecules and water[11-13].

2.5 Solvent Models

Characteristic functional properties and dynamics of biomolecules are highly depending on its interaction with the surrounding water environment in the cell. Hence, incorporation of solvent is essential in computational dynamic studies of biomolecules. Several implicit and explicit water models are available for conducting such studies.

2.5.1 Implicit Solvent Model

Implicit model consider the solvent as a dielectric continuum. Among different implicit solvent models we have chosen Generalised Born model[14] for our studies. This model assumes the solute as a set of charged spheres with internal dielectric constant lower than the external solvent[14]. This model has functional form as shown below;

$$G_s = \frac{1}{8\pi}\left(\frac{1}{\varepsilon_0} - \frac{1}{\varepsilon}\right)\sum_{i,j}^{N} \frac{q_i q_j}{\sqrt{r_{ij}^2 + a_{ij}^2\, e^{-D}}} \qquad (2.6)$$

Where, $D = \left(\frac{r_{ij}}{2a_{ij}}\right)^2$; $a_{ij} = \sqrt{a_i a_j}$; ε_0 is the permittivity of the free space; ε is the dielectric constant of the solvent being modelled; q_i and q_j are the electrostatic charges on particle i and j, respectively; r_{ij} is the distance between the atoms i and j; a_i and a_j are the Born radius of atom i and j, respectively. The Born radius of an atom is inversely related to its screening effect. The implicit solvent model reduces the computational cost of simulations but, explicit consideration of solvent is necessary to monitor specific characteristic dynamics of different biological systems.

2.5.2 Explicit Water Models

A wide range of water models are available for studies which require explicit consideration of solvent molecules. Simple water models like TIP3P, SPC, SPC/E, TIP4P, TIP5P maintained a rigid geometry and the interaction between molecules is described by pair wise Coulombic and Lennard-Jones potential[2, 6]. The parameterisation of these models usually carries out by calculating and comparing different thermodynamic and structural properties using MD or MC (Monte Carlo) simulations[2]. At ambient temperatures most of these models yield satisfactory agreement with bulk water[15]. The empirical force fields for biomolecules are generally developed in

combination with a specific water model. Hence, it is very important to consider the compatibility of the water model with the selected force field. The all atom CHARMM 22 force field developed in conjunction with TIP3P water model[11-13]. It is a model with rigid geometry and three electrostatic interaction sites. The van der Waals interaction between two water molecules ignores hydrogen atoms and it is modelled using LJ function with single interaction site located at the oxygen atom.

2.6 Practical Aspects of MD Simulations

The basic requirements to start an MD simulation are the selection of an initial configuration of the system and the option of an appropriate energy model to describe the internal interactions of the system. For protein simulations, the initial coordinates can be obtained from X-ray crystallography, NMR or by theoretical modelling[6]. It can be also modelled by combining these experimental and theoretical methods. Initial velocities of each atom in the system can be estimated by utilising the *Maxwell-Boltzmann equation*[2] (eqn. 2.7), which gives the probability, $p(v_{ix})$ of an atom i of mass m_i to have velocity v_{ix} at a particular temperature T in x direction.

$$p(v_{ix}) = \left(\frac{m_i}{2\pi k_B T}\right)^{1/2} \exp\left[-\frac{1}{2}\frac{m_i v_{ix}^2}{k_B T}\right] \qquad (2.7)$$

A central molecule with its various influencing factors like solvents, ions, model surfaces, other molecules etc. can be modelled together while setting up a simulation box. To make these simulations more realistic to obtain various macroscopic properties of the system, suitable boundary conditions need to be adopted[2]. It is possible to make a system infinite in special extent with minimum number of atoms by duplicating the central simulation box periodically in all directions[2].

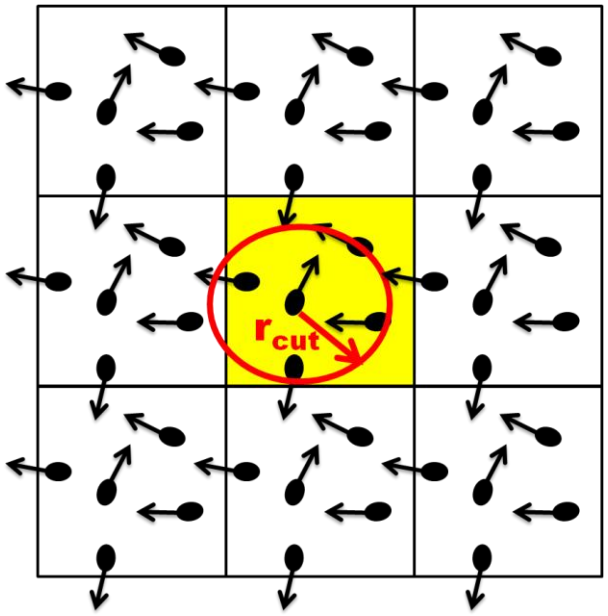

Figure 2.3: Pictorial representation of periodic boundary conditions in two dimensions; r_{cut} represents cutoff distance.

All atoms outside the central box are considered as the image of the atoms in the simulation box and the distance of such an image from the original atom can be calculated by adding or subtracting the integral multiples of the box sides[2]. Thus, the number of particles in the central box remains same. Duplication of interactions between atom pairs is avoided by the implementation of '*minimum image convention*'[2]. By applying such '*periodic boundary conditions*' each atom in the simulation box experience bulk like environment and if a particle leave the central box during the simulation its image enters through the opposite side as shown in Figure2.3[2]. According to this convention each atoms sees just one and only one image of every other atom in the infinitely replicated system[2]. So, an atom or its image whichever is in the minimum distance from its pair will be taken care while doing interaction energy calculation[2].

To reduce the computational cost of pair wise non-bonded interactions, a cutoff is employed to the distance between the atom pairs[2, 6]. The non-bonded interactions beyond the cutoff distance are assumed to be zero[2, 6]. To avoid the interaction of an atom with its own image and with multiple periodic images of the same atom cutoff distance generally set less than half of the shortest side of the simulation box[2, 6]. Smoothening functions are often applied in simulations so that sharp energetic discontinuity at the cutoff distance can be avoided[2, 6]. By implementing a non-bonded neighbour list the computational cost for the energy calculation can be further reduced because the atoms within the cutoff won't

change during a significant number of simulation steps[2, 6]. This list keeps the record of neighbours for each atom within a distance slightly greater than the cutoff[2, 6]. This avoids the calculation of distance in each step[2, 6]. In certain systems, long range electrostatic interactions extend beyond the cutoff distance. The most efficient way to calculate such long range interactions is the *Particle Mesh Ewald summation* method[16]. The summation over point charges in the generic interaction potential is replaced in this method with two summations; one in real space for the short-ranged interactions and the other in Fourier space for long range interactions[16].

There are several algorithms include the verlet algorotm[17], the Beeman's algorithm[18], the leap frog algorithm[19] and the velocity Verlet algorithm[20] for integrating the equations of motion. These strategies are based on finite difference method to generate MD trajectories and using Taylor series expansion[2]. It is very important to choose an appropriate time step for the simulation. For a flexible molecule the time step should be about one-tenth of the time required for its fastest motion[2]. It was estimated that the stretching motion of the bonds with H atoms are the fastest and the time period is approximately 10 fs[2]. Hence a time step of 1 fs will be typical for an unrestrained system[2]. In case of conformationally flexible molecules like proteins it is a common practice to restrain the bond vibrations of less importance to reduce the computational cost of the simulations[2, 6]. In such restrained simulations, time step of 2 fs is reported as reasonable[2, 6]. *SHAKE algorithm* is one of the most commonly using method for applying various constrains on fastest vibrations of the molecule[21].

An MD simulation can be performed under various thermodynamic ensembles- NVE, NVT or NPT. To maintain constant temperature and pressure various methods are implemented with different simulation packages[2]. Before generating the trajectory of a system for the analysis, energy minimisation and equilibration of the initial system needs to be performed[2]. Energy minimization relieve unfavourable interactions in the system and generate configuration corresponds to its most stable state[2]. There are several algorithms like steepest descents method, conjugate gradients method, Newton-Raphson method etc[2, 6]. When the system becomes well equilibrated various parameters achieve stable values. The production run for the desired time period can be started after the equilibration and the resultant trajectory can be used for the direct visualisation and for various analyses.

2.7 Enhanced Simulation Techniques

The potential energy surface of biomolecules consists of large no of local energy minima and the structure gets trapped in such minima during conventional MD conformational sampling[6]. The structural and functional evolution of many proteins takes long time duration and many such transitions are not accessible with normal MD simulations[6]. These are the most challenging issues with the conventional MD simulation. There are different enhanced simulation techniques those ensure improved conformational space sampling. Accelerated MD (AMD) and Replica Exchange MD (REMD) are the two enhanced techniques used for the work reported in this thesis.

2.7.1 Accelerated Molecular Dynamics Simulation

AMD ensures enhanced sampling within shorter durations by modifying the potentialenergy surface ($V(\vec{r})$) with a bias potential $\Delta V(\vec{r})$ [22, 23].

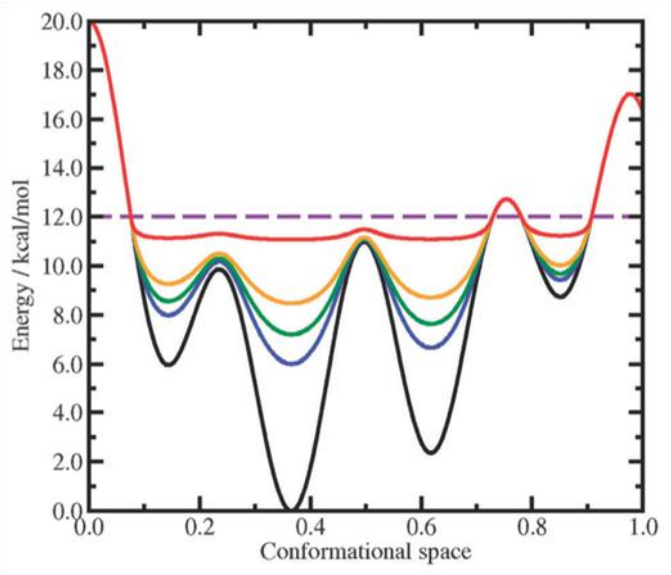

Figure 2.4. Modified potential energy surface with different bias potential. Reprodced from Ref. 23 with the permission from AIP Publishing LLC.

The magnitude of the bias potential $\Delta V(\vec{r})$ is determined by two parameters, boost energy (E_b) and acceleration parameter (α)[22, 23]. The addition of this potential reduces the barrier height of the original potential thereby accelerates the exchange between different low energy conformational states[22, 23]. Figure 2.4 depicts the modified potential energy surface in comparison with the original potential. The extent of acceleration enhances and reduces by increasing values of E_b and α, respectively[22, 23].

The modified potential $V^*(\vec{r})$ is given as[22, 23],

$$V^*(\vec{r}) = V(\vec{r}), \qquad V(\vec{r}) \geq E_b \tag{2.8}$$

$$V^*(\vec{r}) = V(\vec{r}) + \Delta V(\vec{r}), \qquad V(\vec{r}) < E_b \tag{2.9}$$

Here, the bias potential $\Delta V(\mathbf{r})$ is obtained as,

$$\Delta V(\vec{r}) = \frac{\left(E_b - V(\vec{r})\right)^2}{E_b - V(\vec{r}) + \alpha} \tag{2.10}$$

In accordance with the optimized AMD methods preliminary, short unbiased simulations were performed to obtain the mean dihedral energies (V_{dih}), and E_b was set such that their difference was 4 kcal mol^{-1} times the number of residues in the protein[22, 23].

2.7.2 Replica Exchange Molecular Dynamics Simulation

To overcome the protein folding problem with multiple minima, Y. Sugita and Y. Okamoto developed a new simulation technique called REMD. Instead of simulating a single system at a particular temperature, REMD technique allows series of simultaneous simulations of non-interacting systems known as replicas at a range of temperatures[24]. At particular intervals the temperatures of each simulation get swapped by reassigning the velocities and this process is known as replica exchange[24]. Conventional simulations at room temperature or physiological temperature tend to get trapped at local free energy minima of the system, whereas by selecting range of temperature from low to high values it is possible to overcome this limitation in REMD[24]. An optimal temperature distribution is an essential requirement for a successful REMD simulation[24]. The higher temperature replicas cross the high energy barriers easily and the low temperature ones explore the energy minima just like the conventional MD[24]. It has been evidenced that REMD ensures efficient conformational space sampling from different studies on protein folding.

2.8 Analysis of MD Trajectories

To obtain structural, dynamic, energetic and functional insights about the system, one should suitably process and analyse MD simulation trajectories using appropriate techniques. Visualisation of significant events during the propagation of the trajectory is possible by saving the atomic positions and velocities of the system at reasonable time intervals., It is also possible to extract information regarding secondary structure, interaction energies, inter/intra molecular distances, H-bond formation, salt-bridge

formation etc. from the trajectory of the simulated system. Some of the conventional analytical methods are briefly described below.

Root Mean Square Deviation (RMSD) is one of the conventional analytical tools to understand the conformational changes of a protein with respect to a reference structure along the simulation time. It measures the average distance between atoms of superimposed conformations and it can be mathematically represented as

$$RMSD = \sqrt{\frac{\sum_{i=1}^{N} d_i^2}{N}} \tag{2.11}$$

where d_i is the distance between N equivalent atom pairs.

Root Mean Squared Fluctuation (RMSF) measures the average deviation in position of a particle i with respect to its position in a reference structure. In case of protein trajectory analysis, RMSF is a useful tool to understand the residue wise deviation of the system during the simulation with respect to the initial structure. The mathematical representation of RMSF is as follows

$$RMSF = \sqrt{\frac{\sum_{t_j=1}^{T} (x_i(t_j) - x_i(r))^2}{T}} \tag{2.12}$$

Where T is the total time of simulation, x_i is the position of particle i at time t_j and $x_i(r)$ is the reference position of particle i.

Radius of Gyration (R_g) is an effective analytical method to describe the degree of compactness of a protein due to secondary structural change and/or local movements of different segments. Lower the value of R_g, compactness will be high. Mathematically R_g can be calculated as the root mean square distance between the object's different parts from its center of mass or an axis passing through its center of mass.

Ramachandran Diagram depicts the distribution of dihedral angles φ versus ψ of amino acid residues in a protein and it is first introduced by G. N. Ramachandran in 1963[25, 26]. It is a method to predict the secondary structural preferences of different residues of the protein from the simulated trajectory. The distribution of dihedral angles for all the amino-acids except Gly and Pro falls in the allowed conformational regions in the diagram as shown in Figure 2.5. In the diagram the white region corresponds to sterically disallowed region; regions with no steric hindrance is represented in red colour and these regions corresponds to α-helix and β-sheet conformations; if slightly shorter van der Waals radii are used for the calculations, the dihedral angle distribution will be fall in the yellow regions which corresponds to left handed α-helix conformation. The

sidechain of Gly contains only Hydrogen hence, its backbone is more flexible and the allowed area for dihedral angles is larger in the distribution plot. On the contrary in case of cyclic amino acid Pro, only limited combinations are allowed for φ and ψ angles because of its sterically hindered backbone movement.

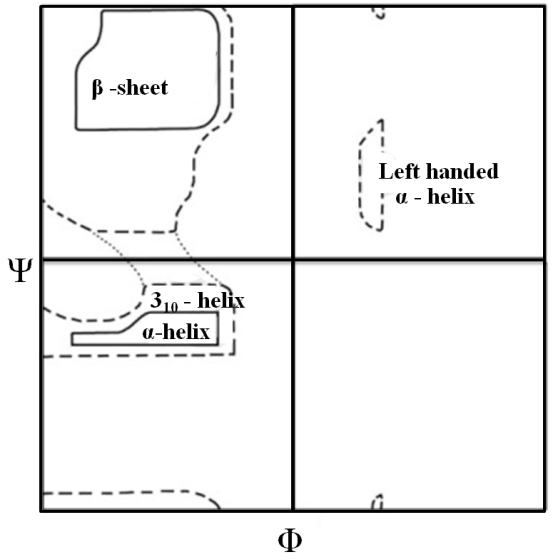

Figure 2.5 Ramachandran diagram. Sterically allowed regions are depicted in the figure.

Correlation Functions statistically describe spatial or temporal correlation between different random variables from a simulated trajectory. The strength of correlation can be quantified using correlation coefficients of that particular correlation function. If we consider the correlation between two variables representing two different quantities measured at two different points then the correlation function is referred as cross correlation function and if the variables represent same quantity then it is known as autocorrelation function. One of the major advantages of MD simulation is the temporal evolution of different configurations of the protein and hence, *time correlation function* can be used to find the correlation of variables at different instance of the simulation trajectory. It is an efficient method to study the time dependent dynamic properties of protein-water systems. Mathematical form of a normalised autocorrelation function of the variable x_i at time $t = 0$ and $t = t$ for N values is given below.

$$C_{xx}(t) = \frac{1}{N}\sum_{1}^{N}\frac{\langle x_i(t).x_i(0)\rangle}{\langle x_i(0).x_i(0)\rangle} \qquad 2.13$$

To simplify the analysis, there are various clustering techniques which can categorise the representative sets of structures from the large number of conformations generated using MD trajectories.

Principal Component Analysis (PCA) is a trajectory processing method that uses orthogonal linear transformation to convert a set of data to a new coordinate system of linearly uncorrelated variables known as principal components (PCs). The highest principal component has the highest variance and each PCs is orthogonal to all the other PCs because these PCs are the eigen vectors of the covariance matrix. There may exist as many PCs as the dimensionality of the data set but in most of the cases only first few PCs are only necessary to explain the significant variations in the data. It is conventional to plot the first and second PCs to monitor the clustering of different conformations and this will help to extract the representative conformations of different clusters from the biological molecular simulation data.

Various software packages such as Visual Molecular Dynamics (VMD)[27], Pymol[28], Carma[29] etc. are available for visualisation and analyses of MD trajectories. However, it is customary to develop inhouse scripts and analysis codes in order to extract statistically relevant quantities from the phase space information contained in the trajectories.

2.9 Experimental Techniques Complementary with MD Simulations for IDP Studies

Conformational fluctuation plays an essential role in determining the function of IDPs and because of the frequent fluctuation in its secondary structure, conventional experimental or computational methods are independently insufficient to probe the unique structure and dynamics of this class of peptides and proteins. Eventhough MD simulations can be effectively used for the characterisation of dynamics and interactions of IDPs in different environments, various experimental techniques are required to validate the structural properties. Here, we have briefly describe some of the most important experimental techniques which are complementary with computational methods to study IDPs.

Nuclear Magnetic Resonance (NMR) spectroscopy and *X-ray crystallography* are widely used for finding the ensemble averaged structure for globular proteins, while these methods provide possible boundaries of the conformational ensemble sampled by IDPs[30]. *NMR spectroscopy* can provide local information about secondary structure propensities

using chemical shift measurements. Secondary chemical shift quantify the deviation between measured chemical shift for each residue and the same for a random coil structure[30-32]. The local structure information obtained using chemical shift comparison will be ensemble average information because the time scale of the structural fluctuation of IDP is relatively faster than the experimental time scale. The long-range residual interactions of IDPs are inherently transient and difficult to detect, Paramagnetic Relaxation Enhancement (PRE) measures long range contacts up to ~ 25 Å by tagging a specific amino acid with a paramagnetic probe[30-32]. Another NMR measurement, Nuclear Overhauser Effect (NOE) can provide details of short-range interactions of residues within ~ 8Å distance. The observed intensities of PRE and NOE exponentially depends on distance hence, the conformational information evolved from these measurements will provide internal contacts within a certain distance limit. Frequent fluctuations also reduce the NOE intensities[31, 32]. Residual Dipolar Coupling (RDC) is established as a reliable measurement to provide information about relative orientation of covalently bonded pair of nuclei[31, 32]. Different local secondary structure can be distinguished by analysing the amplitude and sign of RDCs. A major limitation of solution state NMR is the requirement of non-physiological solvent and experimental conditions because of the rapid aggregation of IDPs in water.

Small Angle X-ray Scattering (SAXS) experiments together with advanced analytical techniques are developed to study the overall shape and size of proteins including IDPs[31-34]. Effect of environmental perturbations on the structural responses of IDPs can effectively monitor using SAXS[31-34]. Several studies reported such structural alterations of different IDPs with changes in temperature, PH, presence of crowding agents, specific ions etc[35, 36]. Structural changes exerted by point mutations have also been studied using this technique[33]. Eventhough it is often used as a complementary method with NMR, Fluorescence spectroscopic techniques and other x-ray crystallographic techniques for IDP characterisation, this method also limited to give ensemble average information about the disordered proteins[33, 34]. *X-ray crystallography* is generally helpful for identifying the disordered regions of large proteins but the lack of crystal structure of disordered protein and peptides is a challenging factor for this method.

Visualisation of the topography of an entire protein with minimal perturbation to the molecule in near physiological condition is possible by using *High Speed Atomic Force Microscopy (HS-AFM)*[37, 38]. By taking the images in an approximate rate of ten

images per second, the global changes in the proteins can be visualised without staining or labelling the protein[37, 38]. But this technique is presently insufficient to capture the local and fast dynamics of the proteins[38].

Recent development in different fluorescence based techniques is enabled single molecular level conformational and dynamics studies of IDPs[39, 40]. These techniques replace the ensemble averaging of IDPs with single molecule level information[39, 40]. The combination of different such single molecule methods generate complementary information. *Single molecule Förster Resonance Energy Transfer (smFRET)* popularly used to study the conformational state, co-existence of different conformational states and the transition between them[39-41]. *Fluorescence correlation spectroscopy (FCS)* in combination with FRET can give insights about the rapid conformational dynamics of proteins[39, 40]. Different aggregation states and the aggregation kinetics of different proteins can be studied using *Fluorescence coincidence analysis*[39, 40]. Development of *Fluorescence microscopy* is promising for IDP studies and the Nobel Prize (2014) in Chemistry was awarded for the development of super resolved Fluorescence microscope. Imaging of amyloidogenic peptides and proteins in a living cell is possible by incorporating FRET imaging techniques with Fluorescence microscopy[42].

Apart all these methods circular dichroism, IR spectroscopy, etc are conventionally used as complementary to other experimental techniques for the identification and characterisation of IDPs and IDRs. Combination of appropriate experimental techniques and different analytical processing of experimental data are helpful to extract information about the structure and dynamics of the protein. Different observations from experimental techniques are always required to be validated using theoretical and computational techniques[43]. Hence, we can say the computational and experimental techniques are complementary to each other in IDP studies.

2.10 References

1. Das, J. K.; Mall, S. S.; Bej, A.; Mukherjee, S., Conformational Flexibility Tunes the Propensity of Transthyretin to form Fibrils through Non-Native Intermediate States. *Angew. Chem.* **2014,** 126, 12995-12998.
2. Andrew, R. L., *Molecular Modelling Principles and Applications.* Pearson Education Ltd., 2nd edition, 2001

3. Bagchi, B., Water Dynamics in the Hydration Layer around Proteins and Micelles. *Chem. Rev.* **2005,** 105, 3197-3219.
4. Bizzarri, A. R.; Cannistraro, S., Molecular Dynamics of Water at the Protein-Solvent Interface. *J. Phys. Chem. B* **2002,** 106, 6617-6633.
5. Li, T.; Hassanali, A. A.; Kao, Y.-T.; Zhong, D.; Singer, S. J., Hydration Dynamics and Time Scales of Coupled Water-Protein Fluctuations. *J. Am. Chem. Soc.* **2007,** 129, 3376-3382.
6. Adcock, S. A.; McCammon, J. A., Molecular Dynamics: Survey of Methods for Simulating the Activity of Proteins. *Chem. Rev.* **2006,** 106, 1589-1615.
7. Warshel, A.; Levitt, M., Theoretical Studies of Enzymic Reactions: Dielectric, Electrostatic and Steric Stabilization of the Carbonium Ion in the Reaction of Lysozyme. *J. Mol. Biol.* **1976,** 103, 227-249.
8. Voegler Smith, A.; Hall, C. K., α-Helix Formation: Discontinuous Molecular Dynamics on an Intermediate-Resolution Protein Model. *Proteins: Struct., Funct., Bioinf.* **2001,** 44, 344-360.
9. Tozzini, V., Coarse-Grained Models for Proteins. *Curr. Opin. Struct. Biol.* **2005,** 15, 144-150.
10. Roberts, A. J., *A One-Dimensional Introduction to Continuum Mechanics*. World Scientific: 1994.
11. Mackerell, A. D., Empirical Force Fields for Biological Macromolecules: Overview and Issues. *J. Comp. Chem.* **2004,** 25, 1584-1604.
12. MacKerell, A. D.; Bashford, D.; Bellott; Dunbrack, R. L.; Evanseck, J. D.; Field, M. J.; Fischer, S.; Gao, J.; Guo, H.; Ha, S.; Joseph-McCarthy, D.; Kuchnir, L.; Kuczera, K.; Lau, F. T. K.; Mattos, C.; Michnick, S.; Ngo, T.; Nguyen, D. T.; Prodhom, B.; Reiher, W. E.; Roux, B.; Schlenkrich, M.; Smith, J. C.; Stote, R.; Straub, J.; Watanabe, M.; Wiórkiewicz-Kuczera, J.; Yin, D.; Karplus, M., All-Atom Empirical Potential for Molecular Modeling and Dynamics Studies of Proteins. *J. Phys. Chem. B* **1998,** 102, 3586-3616.
13. Mackerell, A. D.; Feig, M.; Brooks, C. L., Extending the Treatment of Backbone Energetics in Protein Force Fields: Limitations of Gas-phase Quantum Mechanics in Reproducing Protein Conformational Distributions in Molecular Dynamics Simulations. *J. Comp. Chem.* **2004,** 25, 1400-1415.
14. Koehl, P., Electrostatics Calculations: Latest Methodological Advances. *Curr. Opin. Struct. Biol.* **2006,** 16, 142-151.

15. Mark, P.; Nilsson, L., Structure and Dynamics of the TIP3P, SPC, and SPC/E Water Models at 298 K. *J. Phys. Chem. A* **2001,** 105, 9954-9960.
16. Essmann, U.; Perera, L.; Berkowitz, M. L.; Darden, T.; Lee, H.; Pedersen, L. G., A Smooth Particle Mesh Ewald Method. *J. Chem. Phys.* **1995,** 103, 8577-8593.
17. Verlet, L., Computer "Experiments" on Classical Fluids. I. Thermodynamical Properties of Lennard-Jones Molecules. *Phys. Rev.* **1967,** 159, 98-103.
18. Beeman, D., Some Multistep Methods for Use in Molecular Dynamics Calculations. *J. Comput. Phys.* **1976,** 20, 130-139.
19. Hockney, R. W. *Potential Calculation and Some Application*, Langley Research Center, Hampton, Va.: 1970.
20. Swope, W. C.; Andersen, H. C.; Berens, P. H.; Wilson, K. R., A Computer Simulation Method for the Calculation of Equilibrium Constants for the Formation of Physical Clusters of Molecules: Application to Small Water Clusters. *J. Chem. Phys.* **1982,** 76, 637-649.
21. Ryckaert, J.-P.; Ciccotti, G.; Berendsen, H. J. C., Numerical Integration of the Cartesian Equations of Motion of a System with Constraints: Molecular Dynamics of n-Alkanes. *J. Comput. Phys.* **1977,** 23, 327-341.
22. Hamelberg, D.; de Oliveira, C. A. F.; McCammon, J. A., Sampling of Slow Diffusive Conformational Transitions with Accelerated Molecular Dynamics. *J. Chem. Phys.* **2007,** 127, 155102-155109.
23. Hamelberg, D.; Mongan, J.; McCammon, J. A., Accelerated Molecular Dynamics: A Promising and Efficient Simulation Method for Biomolecules. *J. Chem. Phys.* **2004,** 120, 11919-11929.
24. Sugita, Y.; Okamoto, Y., Replica-exchange Molecular Dynamics Method for Protein Folding. *Chem. Phys. Lett.* **1999,** 314, 141-151.
25. Ramachandran, G. N.; Ramakrishnan, C.; Sasisekharan, V., Stereochemistry of Polypeptide Chain Configurations. *J. Mol. Biol.* **1963,** 7, 95-99.
26. Ramachandran, G. N.; Sasisekharan, V.; C.B. Anfinsen, M. L. A. J. T. E.; Frederic, M. R., Conformation of Polypeptides and Proteins In *Advances in Protein Chemistry*, Academic Press: 1968; Vol. Volume 23, pp 283-437.
27. Humphrey, W.; Dalke, A.; Schulten, K., VMD: Visual Molecular Dynamics. *J. Mol. Graph.* **1996,** 14, 33-38.
28. WL, D., PyMOL: an Open-source Molecular Graphics Tool. *CCP4 Newslett. Protein Crystallogr.* **2002,** 40.

29. Glykos, N. M., Software News and Updates Carma: A molecular dynamics Analysis Program. *J. Comp. Chem.* **2006,** 27, 1765-1768.
30. Eliezer, D., Biophysical Characterization of Intrinsically Disordered Proteins. *Curr. Opin. Struct. Biol.* **2009,** 19, 23-30.
31. Jensen, M. R.; Blackledge, M., Testing the Validity of Ensemble Descriptions of Intrinsically Disordered Proteins. *Proc. Natl. Acad. Sci. U.S.A.* **2014,** 111, E1557-E1558.
32. Jensen, M. R. b.; Salmon, L. c.; Nodet, G.; Blackledge, M., Defining Conformational Ensembles of Intrinsically Disordered and Partially Folded Proteins Directly from Chemical Shifts. *J. Am. Chem. Soc.* **2010,** 132, 1270-1272.
33. Bernado, P.; Svergun, D. I., Structural Analysis of Intrinsically Disordered Proteins by Small-angle X-ray Scattering. *Mol. Biosyst.* **2012,** 8, 151-167.
34. Uversky, V. N.; Dunker, A. K.; Bernadó, P.; Svergun, D., Analysis of Intrinsically Disordered Proteins by Small-Angle X-ray Scattering. In *Intrinsically Disordered Protein Analysis*, Springer New York: 2012; Vol. 896, pp 107-122.
35. Uversky, V. N.; Dunker, A. K.; Smith, M.; Jelokhani-Niaraki, M., pH-Induced Changes in Intrinsically Disordered Proteins. *In Intrinsically Disordered Protein Analysis*, Springer New York: 2012; Vol. 896, pp 223-231.
36. Shkumatov, A. V.; Chinnathambi, S.; Mandelkow, E.; Svergun, D. I., Structural Memory of Natively Unfolded Tau Protein Detected by Small-Angle X-ray Scattering. *Proteins: Struct., Funct., Bioinf.* **2011,** 79, 2122-2131.
37. Milhiet, P.-E.; Yamamoto, D.; Berthoumieu, O.; Dosset, P.; Le Grimellec, C.; Verdier, J.-M.; Marchal, S.; Ando, T., Deciphering the Structure, Growth and Assembly of Amyloid-like Fibrils Using High-speed Atomic Force Microscopy. *PLOS One* **2010,** 5, e13240.
38. Ando, T.; Uchihashi, T.; Kodera, N., High-Speed AFM and Applications to Biomolecular Systems. *Annu. Rev. Biophys.* **2013,** 42, 393-414.
39. Brucale, M.; Schuler, B.; Samorì, B., Single-Molecule Studies of Intrinsically Disordered Proteins. *Chem. Rev.* **2014,** 114, 3281-3317.
40. Banerjee, P. R.; Deniz, A. A., Shedding Light on Protein Folding Landscapes by Single-Molecule Fluorescence. *Chem. Soc. Rev.* **2014,** 43, 1172-1188.
41. Ziv, G.; Haran, G., Protein Folding, Protein Collapse, and Tanford's Transfer Model: Lessons from Single-Molecule FRET. *J. Am. Chem. Soc.* **2009,** 131, 2942-2947.

42. Theillet, F.-X.; Binolfi, A.; Frembgen-Kesner, T.; Hingorani, K.; Sarkar, M.; Kyne, C.; Li, C.; Crowley, P. B.; Gierasch, L.; Pielak, G. J.; Elcock, A. H.; Gershenson, A.; Selenko, P., Physicochemical Properties of Cells and Their Effects on Intrinsically Disordered Proteins (IDPs). *Chem. Rev.* **2014,** 114, 6661-6714.
43. Burger, V.; Gurry, T.; Stultz, C., Intrinsically Disordered Proteins: Where Computation Meets Experiment. *Polymers* **2014,** 6, 2684-2719.

CHAPTER 3

Early Conformational Dynamics of Aβ_{42} Peptide Monomer in Biologically Relevant Environments

"Nothing in life is to be feared, it is only to be understood.

Now is the time to understand more, so that we may fear less."

-Marie Curie

Abstract

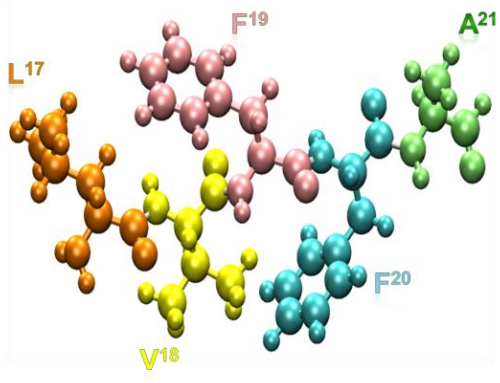

The studies on the early conformational dynamics of monomeric A$\beta_{1\text{-}42}$ in two biologically relevant environments are included in this chapter. The first part of this chapter describes the early dynamics of the peptide in aqueous environment. This study revealed the extent of hydrophobicity of the Central Hydrophobic Core (CHC) of Aβ, $L_{17}VFFA_{21}$, in the early observed structural collapse of the monomeric peptide by mutating the central residue of the CHC i.e., F_{19} with Tyrosine and Isoleucine. Results showed that the change in hydrophobicity of the residue causes significant alteration in the early observed structural collapse of the peptide. The second part of this chapter depicts the effect of a model hydrophilic nano surface on the early conformational dynamics of Aβ_{42} using hydrophilic TiO_2 (rutile) surface and found a distance dependent change in the intrinsic behavior of the peptide. The early characteristic structural collapse of the peptide is disrupted, while the β-sheet propensity is sharply enhanced with increased proximity to the surface. These results may have implications in Aβ self-assembly and fibrillogenesis on hydrophilic surfaces, and should be taken into consideration in the design of novel nanomaterials for perturbing amyloidogenic behavior.

3.1. Role of Hydrophobicity of Central Hydrophobic Core in the Early Dynamics of A$\beta_{1\text{-}42}$ in Water

3.1.1 Introduction

Aβ, being an IDP, exists in different conformational states[1-7]. The peptide has conformational preferences in different environmental conditions. It has been reported in literature that Aβ_{42} is predominantly in α-helical conformation in lipid mimicking environment[8, 9], however in water it adopts collapsed coil structure[6, 7]while the peptide monomer is found to be in β-sheet conformation in the amyloid plaque[10, 11]. Various studies reported the most populated conformations of Aβ by integrating different experimental and simulation techniques[1, 5, 12, 13]. The broadness of the conformational ensemble of Aβ monomer makes the characterization of the aggregation process difficult from the very early stage itself. However, it is significant to understand the early dynamics of Aβ at the monomeric level to prevent its conformational transformations to the aggregation prone structure and further formation of toxic oligomers and fibrils.

As discussed in the introduction, Aβ is derived from APP which is an integral membrane protein with large helical content[14, 15]. It has been reported that the activity of one of the enzymes involved in the cleavage of this peptide from its precursor, γ-secretase, can be inhibited by a specific helical species, suggesting that the proteolytic enzyme interacts with helical part of APP[16]. NMR studies demonstrated that the peptide exhibits increased helicity in a lipid like environment[8, 9]. Partially folded helix conformation is reported as an early intermediate stage in the fibril assembly[17] and several studies reported the significance of Aβ in the helical conformation[18, 19]. Because of all these it has been widely hypothesized that Aβ monomer just after its cleavage from the APP presumably contains significant helical content. It is also presumed that, after cleavage from APP, the Aβ peptide monomer in helical conformation goes into water rich extracellular space leading to conformational changes and thereafter self assembles into soluble oligomers and insoluble fibrils[4, 19-21]. So during the aggregation process a freshly cleaved Aβ should eventually undergo a conformational transition possibly from α-helix to β-sheet and the important dynamics involved in this pathway is still unclear. Hence, a model structure of the peptide which is in helical conformation has been taken for this study.

The intrinsic properties and characteristic structural dynamics of amyloid peptides are highly depending on its primary structure. Eventhough Aβ is an amphiphilic peptide, it is predominantly hydrophobic in nature and contains continuous hydrophobic patches;

the N-terminal region is mainly composed of hydrophilic residues. Several studies have focused on the role of different hydrophobic segments like L_{17}-A_{21}, A_{30}-M_{35} and A_{36}-A_{42} in the amyloid toxicity and the results showed that these regions promote aggregation hence, these regions are responsible for neurotoxicity[4, 22-26]. Previous studies showed that the early dynamics of the monomeric peptide in aqueous media is characterized by a structural collapse initiated by nonlocal interactions between the central hydrophobic core (CHC) of the peptide $L_{17}VFFA_{21}$ with the C-terminal hydrophobic region[4, 24, 27].

From different experimental and computational studies it has been hypothesized that the intrinsic structural collapse of Aβ peptide monomer is as an essential mechanistic event in the early aggregation pathway in water[4, 7, 25]. Hence, CHC is a key region of focus in the drug development strategies [26, 28-30]. The stabilization of the central helix of the monomeric peptide is considered as a plausible method to prevent aggregation[26]. Several studies focused on the properties of CHC and studied the interaction of many drug molecules with the same region[26, 31, 32]. Study of Aβ_{42} on single walled carbon nanotube (SWCN) surface has shown that the adsorption of the N-terminal CHC region on the nano tube prevents the intrinsic hydrophobic collapse of the monomeric peptide unit[24]. Hence, it requires further studies to understand the mechanism of the observed hydrophobic collapse and the role of CHC in this phenomenon for designing biocompatible drug molecules. This study showed that the perturbation of hydrophobicity of the CHC will alter the structural and dynamical path way of the peptide significantly. The results from this study provide more insights into the mechanism of the structural collapse and the specialities of the CHC.

3.1.2 Methods

A helical conformation of Aβ peptide was reported by Tomacelli et al. in 70:30 H_2O/HFIP mixture - a lipid mimicking environment[9]. It has been experimentally observed that the Aβ peptide undergo alpha helix to beta sheet transition by gradually increasing the polarity of the medium[8, 9]. Hence, this helical structure was taken and explicitly solvated in water TIP3P to monitor the conformational transition pathway of the helical peptide. The initial structure contains two helical regions, a well ordered N-terminal helix H1 (TYR10 to ASP23) and a comparatively disordered C-terminal helix H2 (LYS28 to GLY38)[9]. The NH_3^+ and the COO^- groups were added to the N- and the C-termini, respectively of the peptide, which was solvated in a rectangular box of water with the TIP3P water model[33], the box initially measured, approximately, 95Å x 62Å x 50Å. The

system was neutralized with the addition of three Na^+ counter ions. The CHARMM22 force field with cmap correction[34, 35] was used for the peptide and the NAMD2.7 package[36] was used for all the simulations. Energy minimization, using the conjugate gradient technique, was performed on the solvated peptide for 20000 steps. All simulations were carried out in the NPT ensemble, with the Nosé-Hoover Langevin piston algorithm[37, 38] used for maintaining a 1 atm pressure. The temperature was held constant at 300 K using Langevin dynamics, with a collision frequency of 1 ps^{-1}. Bond lengths with hydrogen atoms were held constant using the SHAKE algorithm.[39] The simulation timestep used was 2.0 femto seconds (fs), and coordinates were saved every ps. Three-dimensional orthorhombic periodic boundary conditions were employed. Electrostatic interactions were calculated with the particle mesh Ewald (PME) method.[40] The cutoff distance for non-bonded interactions was set to 12 Å, with a smoothing function employed from 10.5 Å. Five trajectories of 80 ns length produced for both the systems with slightly different initial velocities. The initial structure was subsequently mutated with isolusine and tyrosine at 19^{th} residue. Three trajectories of 80 ns were generated at physiological conditions using the same methodological procedures.

3.1.3 Results

3.1.3.1 Characteristics of Structural Collapse

We have observed a drastic decrease in the radius of gyration of the peptide during the simulation in each of the trajectories as shown in Figure 3.1.1(a). The average decrease in R_g was found to be ~ 3.0 Å. The decrease in R_g generally results because of the compactness of the system, which can be attributed to the secondary structural change or internal structural collapse occurring in the system. Earlier reports showed that Aβ prefer to be in collapsed state in aqueous environment[4, 7, 11, 24, 25], we defined a parameter $d_{collapse}$ which is the inter-strand distance between segments $L_{17}VFFAEDVGS_{26}$ and $K_{28}GAIIGLMVGGVVIA_{42}$. Figure 3.1.1(b) depicts the evolution of $d_{collapse}$ for the five individual trajectories and the average over five trajectories. The inter-strand distance is found to be reduced from its initial value, 16.6 Å to a final value 8.75 Å on the average. Thus, the selected peptide conformation undergoes structural collapse in the very early stage of its transformation. Similarity in the temporal pattern of R_g and $d_{collapse}$ indicate that these two parameters are directly correlated.

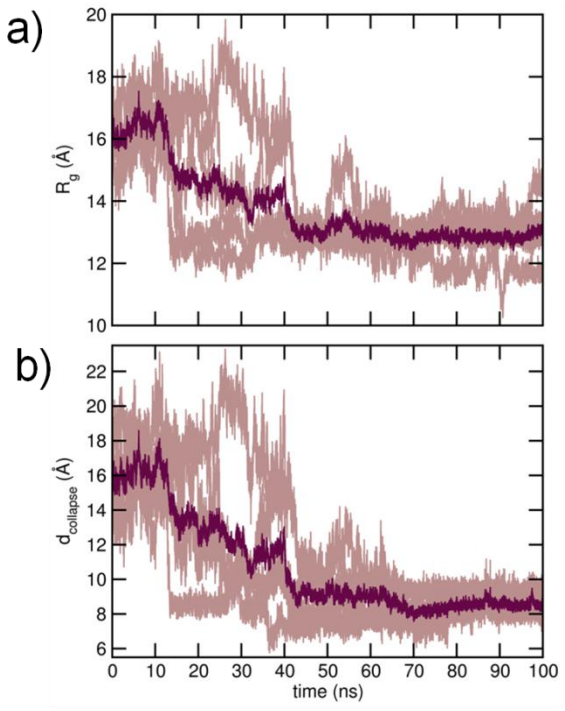

Figure 3.1.1. (a) Evolution of radius of gyration (b) Evolution of $d_{collapse}$. The values for the individual trajectories are represented in *Brown* and the average values over all trajectories are represented in *Maroon*.

It was evidenced from the above calculations, the peptide attain a metastable equilibrium state after the collapse. Hence, it seems that the collapsed state is a stable conformational state. The driving interaction for such a structural collapse has been analyzed and it was noticed that the non-bonded interaction between CHC and hydrophobic segments, and $V_{36}GGVVIA_{42}$, on the C- terminal region of the peptide is significantly correlated with the collapse of the peptide. Figure 3.1.2 (a and b) shows the evolution of interaction strength of CHC with both of the C-terminal hydrophobic segments separately for each of the trajectories and their average.

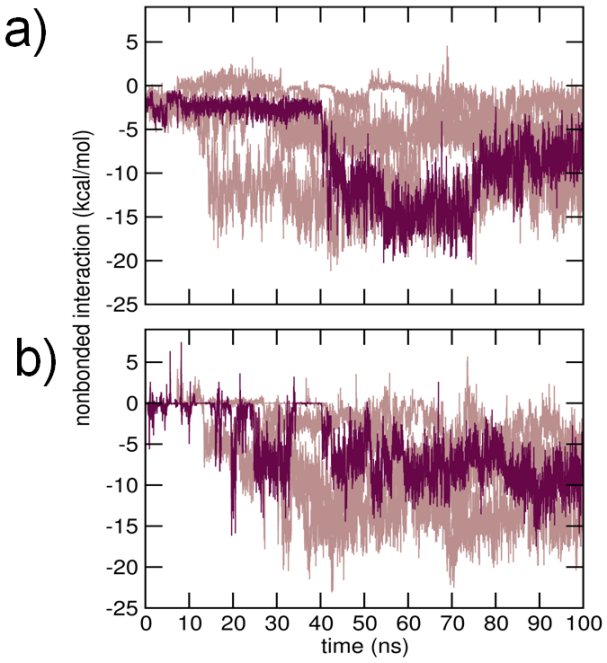

Figure 3.1.2. Evolution of interaction energy between the central hydrophobic core (CHC) and the C-terminal hydrophobic segments (a) A_{30}IIGLM_{35} (b) V_{36}GGVVIA_{42}. The values for the individual trajectories are represented in *Brown* and the average values over all trajectories are represented in *Maroon*.

3.1.3.2 Extend of hydrophobicity of CHC in the Structural Collapse

As we have observed CHC has crucial role in the structural collapse of the peptide, to understand the extent of hydrophobicity on this early conformational transition, the hydrophobicity of this segment was perturbed using mutations. Here the central residue of CHC i.e. the Phe (F_{19}) is mutated with Tyr (Y) and Ile (I) consecutively and these mutated systems are designated as F19Y and F19I, respectively. The wild type is denoted as F19.

Phe is a hydrophobic and aromatic residue and has significant role in the collapse of the peptide, as observed through adsorption studies of the peptide with single walled carbon nanotube. Hence, this central residue has been mutated with Ile and Tyr. According to Fauchere–Pliska scale the hydrophobicity indices of Phe, Ile and Tyr are 1.79,1.80 and 0.96, respectively[41]. Here, Ile is equally hydrophobic to Phe but having aliphatic sidechain and Tyr is aromatic but less hydrophobic than Phe (Figure 3.1.3). In F19I, the mutation causes alteration in the aromatic character but not shifting the

hydrophobicity significantly. While, in F19Y the hydrophobicity of the residue is perturbed but maintained the aromatic character.

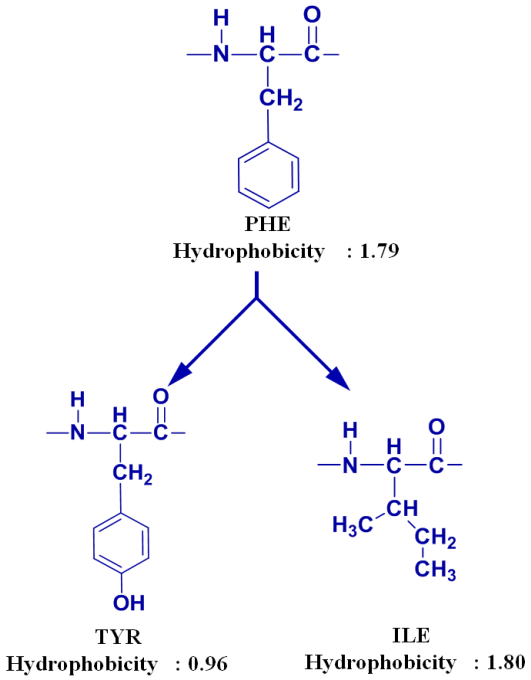

Figure 3.1.3. The chemical structure of Phenylalanine (PHE), Tyrosine (TYR) and Isoleusine (ILE). The corresponding hydrophobicity according to Fauchere–Pliska scale is given with the structure.

The dynamics, especially the early observed CHC driven compactness of the monomer peptide and the structural variations of the peptide in F19I and F19Y were analyzed in comparison with F19. Figure 3.1.4, represents the distribution of $d_{collapse}$ in the three systems for last 10 ns of each trajectories. The initial value of this parameter is 16.7 Å in the F19 structure. It was observed that the collapse propensity of F19Y significantly reduced compared to the F19I, in which the maximum population was found to lie near to that of the wild type but with reduced compactness.

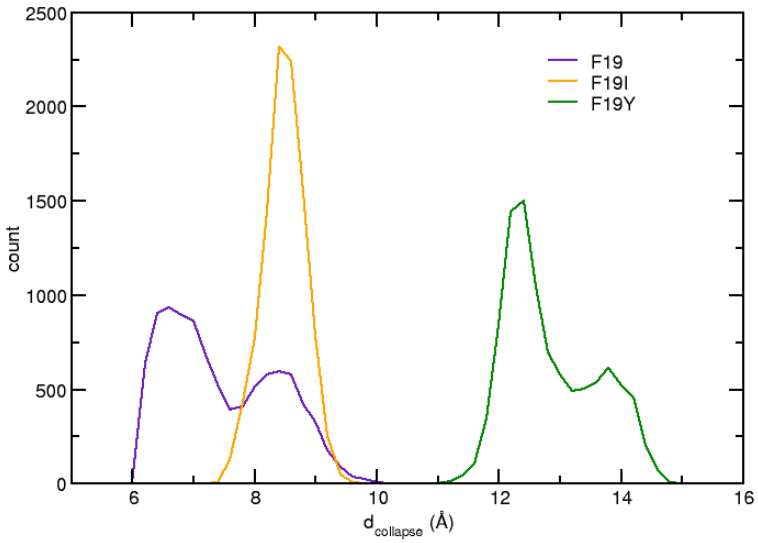

Figure 3.1.4. Population distributions of the peptide's $d_{collapse}$ (in Å), over the last 10 ns of the simulations.

System	**<$d_{collapse}$>**	**<Interaction Energy> (kcal mol^{-1})**	
	(Å)	**CHC- A_{30}IIGLM$_{35}$**	**CHC- V_{36}GGVVIA$_{42}$**
F19	8.3 (0.9)	-10.1 (2.8)	-4.86 (2.6)
F19I	8.38 (0.9)	-6.83 (3.6)	-5.44 (2.5)
F19Y	12.77 (5.6)	-4.10 (3.5)	-3.68 (3.0)

Table 3.1.1. The mean values of $d_{collapse}$ and interaction energies between CHC with A-$_{30}$IIGLM$_{35}$ and V$_{36}$GGVVIA$_{42}$ averaged over the last 10 ns of the simulations; the standard deviations are given in the bracket.

The nonbonded interaction energy between the CHC region and the C-terminal hydrophobic patches were calculated for comparison and the average over last 10 ns of trajectories for all the three systems are listed in the Table 3.1. The interaction strengths were found to be significantly weaker in case of F19Y compared to F19 system, but in case of F19I system the interaction strengths were not drastically different but slightly weaker that the F19 system. The variation in the interaction strength is in correlation with the variation in $d_{collapse}$ value of the three systems. These results give evidence for the

significance of the hydrophobicity of the F19 and hence the CHC in the early observed intrinsic dynamics of the peptide.

3.1.4 Discussions and Conclusions

We have investigated the early observed dynamics of Aβ_{42} and found that the early dynamics is characterized by structural collapse. This structural collapse found to be driven by the nonbonded interactions of CHC with C-terminal hydrophobic domain. Structural compactness is considered widely as an essential requirement for the aggregation of the peptide[4, 7, 25]. Earlier studies reported possible mechanism of the aggregation through the collapsed intermediate stages[4]. Not only in the helical conformation but in the random coil state of the peptide also the structural collapse is reported as a spontaneous conformational transition[7]. Most importantly, the peptide ultimately attains collapsed beta sheet conformation in its fibrilar state[10]. The dynamics and interactions involved in the structural collapse have implications in the aggregation pathway of the peptide. Here it is very important to mention that the helical conformation has collapsed spontaneously hence the collapse is possibly one of the early events in the conformational transition of the monomeric peptide. An earlier study with different force field also reported the propensity of the peptide to collapse[4] and in our study the collapsed state found to be a metastable state.

It was found from this study that the perturbation of hydrophobicity in the central position of the CHC significantly alter the characteristic dynamics of Aβ. Hence, it can assume that F19 as a key residue in the CHC and also in the peptide. A separate study has shown that the presence of a hydrophobic surface (SWCN) can prevent the collapse of the peptide because of the spontaneous adsorption of the peptide on the surface[24]. Here also the alteration of hydrophobicity of the CHC by mutating F_{19} with Tyr causes significant decrease in the adsorption of the peptide on the surface[24]. The hydrophobic and aromatic properties of F_{19} make it a key target in the drug development strategic studies[24].

The results reiterate the importance of CHC as well as the C-terminal hydrophobic segments in the intrinsic dynamics of the full length Aβ_{42} peptide in aqueous environment. These results are anticipated to help in designing suitable drug molecules to prevent early pathogenic dynamics of the peptide and encourage extending the study to other residues of the CHC. This study limited by the sampling; enhanced sampling and further studies are required to understand the role of water in the structural collapse, role of collapse in the dimerisation and subsequent aggregation process.

3.2. Structural Response of an Isolated Aβ_{1-42} Monomer Localized in the Vicinity of the Hydrophilic TiO_2 Surface

3.2.1 Introduction

Protein surface interaction studies have been capturing the attention of multiple areas of research during the last decade. The adsorption of biomolecules on specific surfaces, such as those made available on nanomaterials such as graphene and carbon nanotubes[24, 28, 42]; self-assembled systems such as monolayers, bilayers, micelles, and lipid membranes[24, 28, 42-47]; polymers such as polyethylene glycol and teflon[19, 44]; and silicates and metal oxides[19, 42, 48], may lead to altered activity, selectivity and structural stability. The effects arise from a complex interplay between the physico-chemical nature of the surface[28, 45, 47, 49-52]and the nature and strength of its interaction with biomolecules[28, 44, 45]. Further, at higher concentrations, surfaces can affect these phenomena as well as the kinetics of biomacromolecular self-assembly by facilitating macromolecular crowding by reducing the available spatial dimensions from three to two[53-55].

Harnessing the influence of nanomaterials on the behavior of peptides and proteins is increasingly being considered in the development of novel therapeutic strategies[56-59], if issues pertaining to their solubility and toxicity can be successfully addressed[58, 59]. Particularly, a number of recent studies have attempted to directly understand how the interactions arising from the nanomaterials themselves affect the self-assembly pathways of the Aβ monomer or the stability of its fibrillar aggregates [23, 24, 28]. A variety of experiments and simulations demonstrate the differential role played by the surface properties on the observed effects. For example, while fibrillation is noted to occur with ease on the planar, hydrophobic surface of a graphene layer, the hydrophilic mica surface induces the formation of pseudomicellar globular aggregates [42]. We have recently reported that the peptide adsorbs spontaneously on the hydrophobic surface of single-walled carbon nanotube [24], and other studies have shown that the curved nanotube surface can destabilize fibrils and induce β-barrel formation by Aβ segments [28, 60]. Fibrillogenesis of Aβ and the islet amyloid peptide are enhanced at the air-water interface[41]. It has been demonstrated experimentally that hydrophillic TiO_2 nanoparticles are capable of promoting Aβ fibrillar aggregation [61]. Aβ fibrillization rates on self-assembled monolayers depend on the monolayer composition and the oligomer size [6]. Importantly, surface induced macromolecular crowding effects play key roles in the aggregation of Aβ[19, 43], with physical aspects, such as the surface area and curvature

having a significant bearing[61-64]. Further, experimental studies comparing the effects of hydrophobic and hydrophilic surfaces show that while the former induces α-helicity and the latter is responsible for enhancing β-sheet content, both enhance lateral association of the peptide[19].

Hydrophilic nanoparticles, being water soluble, may additionally be used as effective drug carriers. However, this necessitates that their intrinsic effects on the targeted biomolecule should be clearly understood. Although a number of studies have focused on the aggregation and polymorphism of Aβ_{42} on different hydrophilic nano surfaces[19, 42, 61, 65], there remains a relative lack of understanding of the intrinsic behavior of Aβ_{42} in its monomeric state in the vicinity of nanomaterials such as silicates and metal oxides. In this work, we have used atomistic molecular dynamics (MD) simulations to study, at the 'single-molecular' level, the effect of the model hydrophilic surface, rutile TiO_2 (001), on the structural propensities of isolated, monomeric Aβ. We have considered the structure of the full-length peptide obtained in a lipid-mimicking environment, considered to have some similarities with the peptide freshly cleaved from APP [9], as the starting Aβ conformation. The hydrophobic peptide, on being restrained in the vicinity of the rutile surface, loses its helical character; a proportionate increase in β-sheet character is observed. These effects are more pronounced with increasing proximity, and at about 16 Å from the surface, the peptide's conformational behavior is similar to that of the free peptide. We discuss implications of the observed structural responses in the design of novel nanoparticles targeted for the self-assembly or amyloidogenesis of Aβ.

3.2.2 Computational Methods

MD Simulations

We have carried out atomistic Molecular Dynamics simulations of A$\beta_{1\text{-}42}$ in implicit solvent on TiO_2 (001) monolayer using NAMD2.8 package [36]. The initial coordinates of the peptide have been taken from PDB database, which is a solution state NMR structure in 70:30 H_2O: HFIP mixture (PDB ID: 1Z0Q) with high helical content and is comparable to an early conformation of the Aβ peptide in the pathogenic aggregation pathway [9] NH_3^+ and COO^- groups were added to the N- and C- termini of the peptide respectively. TiO_2 (001) monolayer surface of the dimension 90 Å × 90 Å with lattice parameters a = 4.597 Å and b = 2.9587 Å was constructed using the software Material Studio5.5. We have used the all atom CHARMM22 force field with CMAP correction [66] for protein. The parameters for TiO_2 have been taken from Borodin *et al* [46], with partial charges of -1.098

e and +2.196 *e* for oxygen and titanium, respectively. These parameters have been successfully applied earlier to study protein adsorption on TiO_2 [48]. We modeled three systems, A, B and C, in which the TiO_2 sheet was fixed parallel to XY plane and all internal degrees of freedom of the sheet were frozen. The center of mass of the peptide is restrained at 8, 10 and 16 Å away from the TiO_2 surface for systems A, B and C, respectively, with a harmonic force of force constant 4.0 kcal mol^{-1} $Å^{-2}$. All the three systems on surface were solvated using Generalised Born Implicit Solvent (GBIS) model [67, 68] with a dielectric constant of 78.5 and ionic concentration of 0.2. Energy minimization of 20,000 steps was carried out with the conjugate gradient technique. A free peptide system, 'F', was also simulated in implicit solvent, for comparison. All our simulations were done at 310K, with simulation time step of 2 fs. The coordinates were saved at each picosecond, and each system was simulated for 100 ns.

Structural Persistence Parameter

We have earlier defined the structural persistence parameter, *P* that yields the 'global' extent of structural evolution over a reference structure [24] . To summarize briefly,

$$P = \frac{1}{N_{res}} \sum_{j=1}^{N_{res}} e^{-(\Delta\phi_j / \Delta\phi_{\max})} . e^{-(\Delta\psi_j / \Delta\psi_{\max})} \qquad (3.1)$$

$\Delta\varphi_j$ and $\Delta\psi_j$ are the changes in the φ and ψ torsional angles of residue *j* over the reference at a given point in time, and $\Delta\varphi_{max}$ and $\Delta\psi_{max}$ represent the maximal changes that can occur in the torsional angles. N_{res} represents the total number of amino acid residues in the protein. For a structure that is exactly identical to the reference, *P* attains a value of 1, and for a structure where every residue attains the maximum possible change, *P* is $\sim e^{-2}$. The (φ, ψ) angles were directly estimated using the VMD program [69]. VMD was also used for visualization purposes.

3.2.3 Results

In Figure 3.2.1, the peptide structures at the end of the A, B, C and F simulations are represented. Structurally, the free peptide appears to most closely resemble the peptide at the end of the simulated trajectory C. The root mean squared deviations (RMSD) of the peptide backbone relative to the initial starting structure, as well as the value of the persistence *P*, over the simulated trajectories are depicted in Figure 3.2.2. The RMSD of the free peptide is distinctly lower than that of systems A and B, especially in the latter

parts of the trajectory. However, the RMSD of the peptide held at 16 Å from the surface (system C) is comparable to that of the free peptide.

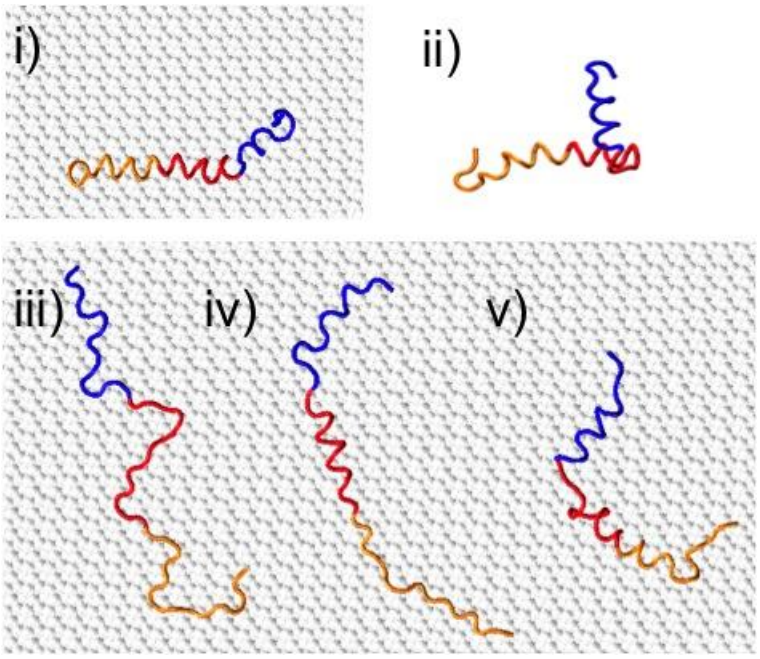

Figure 3.2.1.. *i)* Top view of the initial setup of A$\beta_{1\text{-}42}$ on TiO_2 surface, *ii)* final peptide structure in system F, *iii)* top view of final peptide structure in system A, *iv)* top view of final peptide structure in system B, *v)* top view of final peptide structure in system C. The N-terminal segment (residues 1 to 15), middle segment (residues 16 to 28), and the C-terminal segment (residues 29 to 42) are shown in orange, red and blue, respectively.

As described earlier, the structural persistence, *P* is a useful measure for estimating the global level of structural evolution over time [24]. The evolution of *P* relative to the original conformation shows that a significantly large degree of the secondary structure is retained over timescales of a few hundred nanoseconds. We point out here that the CHARMM force field has been noted to have an α-helical bias[70, 71]. The value of *P* is distinctly lower for the peptide held in the vicinity of the rutile surface. Its increasing value from system A to system C indicates that the rutile surface has a strong, distance-dependent propensity to disrupt the original structure, despite the inherent helical bias of the force field.

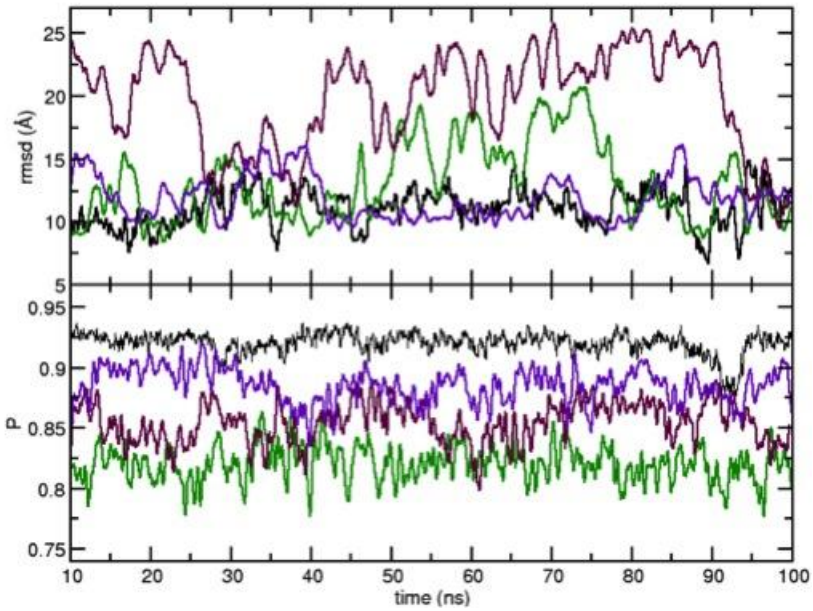

Figure 3.2.2. *i)* Evolution of the peptide's backbone root mean squared deviation (rmsd, in Å), and *ii)* evolution of structural persistence *P*, relative to the starting structure. Data for system A is in green; for system B in maroon; for system C in indigo; and for system F in black.

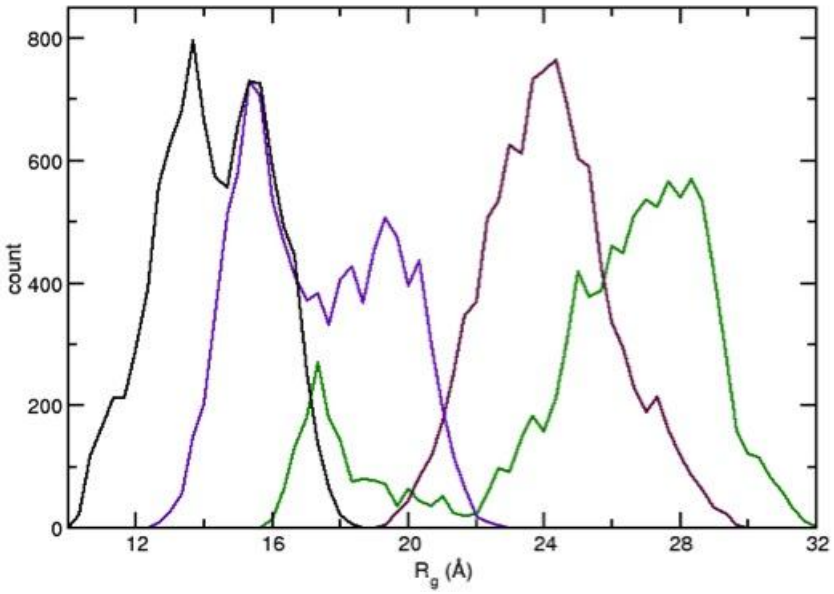

Figure 3.2.3. Population distribution of the peptide's radius of gyration (in Å) over the last 10 ns of the simulations. Data for system A, B, C and F are depicted in green, maroon, indigo and black, respectively.

The propensity of the free Aβ monomer to collapse spontaneously has been pointed out by previous studies[4, 24, 25]. In our simulations of the free peptide in explicit

water, the peptide's radius of gyration (R_g) decreased by ~23%, from the original value of 16.5 Å to the final value of 12.7 Å [24]. In Figure 3.2.3, we have compared distributions of the peptide's R_g values over the last 10 ns of the A, B, C and F simulations; the mean R_g value in these systems are 25.4 (±3.7), 24.0 (±1.8), 17.1 (±2.1) and 14.2 (±1.6) Å, respectively. Thus, while the intrinsic collapse propensity of the free peptide remains largely unaffected in implicit aqueous environment, it is significantly compromised with proximity to the rutile surface.

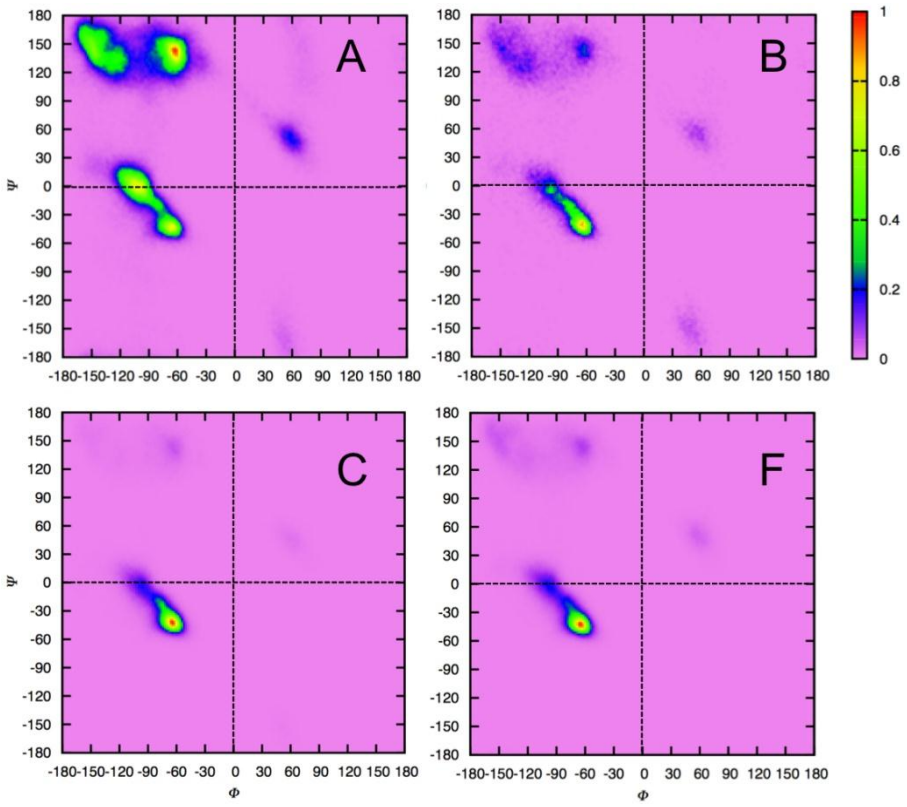

Figure 3.2.4. Distribution of the (φ, ψ) torsional angles (in degrees), for the peptides residues in the systems A, B, C and F, over the last 10 ns of the simulated trajectories. The terminal residues and the glycines have not been considered.

As discussed previously, the Aβ peptide's aggregation is marked by the formation of fibrillar structures with high cross β-sheet content. It still remains to be completely understood if fibril formation is preceded by initial nucleation involving sequential assembly of misfolded monomeric units, and whether the high β-sheet content of stable fibrils results from co-operative structural realignment [10, 72]. In any case, sharp changes in structural content may be important vis-à-vis unraveling mechanisms of the peptide's self-assembly, fibrillogenesis and neurotoxicity, and for providing a basis in the design of

novel therapeutic materials to target AD. Our analyses described so far show that the rutile surface perturbs intrinsic propensities of the free Aβ monomer in a distance-dependent manner. Particularly, the sharp drop in *P* for the systems where the peptide is close to the surface indicate that the secondary structural propensities are drastically altered as compared to the free peptide. For a direct estimate of the secondary structural propensities, in Figure 3.2.4, we have plotted the (φ, ψ) torsional angles, or the Ramachandran diagrams, for the peptide in the A, B, C and F systems, with data taken from the last 10 ns of their simulation trajectories. All residues, except the terminal residues Asp1 and Ala42, and the Glycines (at positions 9, 25, 29, 33, 37 and 38), have been considered in the plots. For ease of comparison, the scales have been normalized such that the maximum intensity is 1. The Ramachandran diagram for the free peptide has the maximum peak intensity near (-60°, -45°). In system A, the maximum peak intensity shifts significantly, to near (-60°, +145°) in the upper left quadrant. A diffuse peak, of about 40% the intensity of the maximum, is found in the vicinity of (-150°, +145°). Compared to the free peptide, the helical peak is significantly weakened, and connected to another peak located in the vicinity of (-110°, 0°). In system B, although the dominant peak remains in the vicinity of (-60°, -45°) like the free peptide, there are small but noticeable populations near the regions (-60°, +145°) and (-150°, +145°). Compared to the free peptide, the peak near (-60°, -45°) is significantly weakened and connected to another peak located near (-110°, 0°). The Ramachandran diagram for system C is closest in form to that of the free peptide, with a single, intense peak at (-60°, -45°), and the near absence of populations in the upper left quadrant.

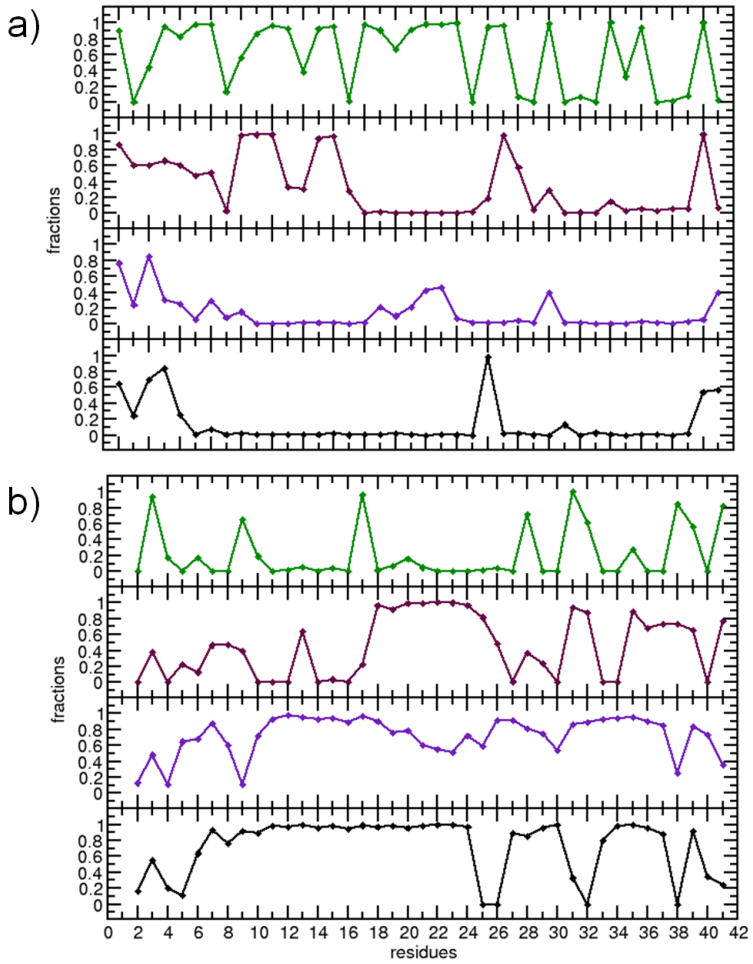

Figure 3.2.5. a) Residue wise *β*-sheet probability, b) residue wise helical probability, over the last 10 ns of simulations. Data for systems A, B, C and F are depicted in green, maroon, indigo and black, respectively.

The data discussed above indicates that close proximity to the rutile surface affects the natural secondary structure propensities of the A*β* peptide, and in fact, induces a significant fraction of *β*-sheet content. In Figure 3.2.5, we have shown the residue wise *β*-sheet (a) and helical propensities (b) over the last 10 ns of the A, B, C and F trajectories. This calculation has been done purely on the basis of the position within the Ramachandran diagram. A right-handed helical conformation corresponds to (φ, ψ) limits within (-170°, -90°) and (-30°, 0°), and a *β*-sheet conformation to limits within (-30°, 15°) and (-180°, 180°). Although the classification does not explicitly take into account the backbone hydrogen-bonding, it is sufficient to mark sharp changes in the secondary structure propensity of individual residues. Away from the termini, the only residue that shows marked *β*-sheet propensity of the free residue is Ser26; it could be due to the

presence of a neighboring Glycine. Significant *β*-sheet propensity emerges in the presence of the rutile surface, and increases from system A to C. The increased *β*-sheet propensity is commensurate with decreased helical propensity, which is most marked in the absence of the surface.

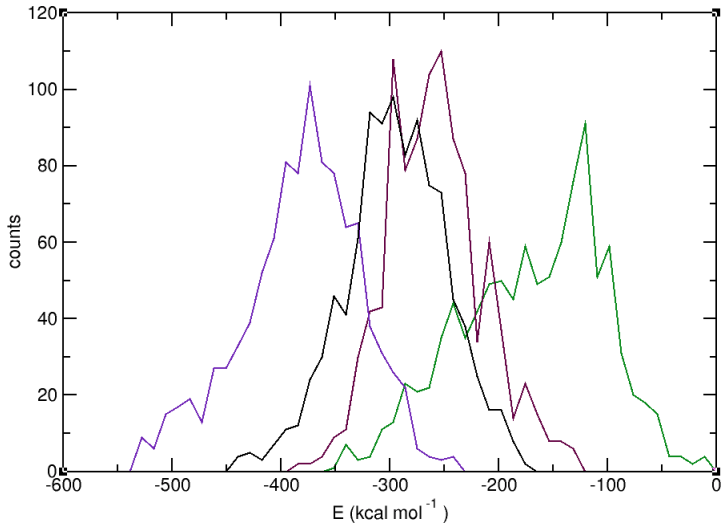

Figure 3.2.6. Population distribution of the peptide's internal non-bonded energy, E, over the last 10 ns of the simulations. Data for systems A, B, C and F are depicted in green, maroon, indigo and black, respectively. The mean values of the energies for systems A, B, C and F are -164.3 kcal mol^{-1}, -253.7 kcal mol^{-1}, -376.3 kcal mol^{-1}, and -289.6 kcal mol^{-1}, respectively.

In Figure 3.2.6, we have shown the histogram of the total electrostatic interaction energy of the peptide with the surface for system A, B and C. Electrostatic interactions of System A and B with the surface are significantly lower than system C, where the interaction energy is observed to be negligible.

3.2.4 Discussion and Conclusions

In this paper, we have examined the structural response of the full-length, monomeric A*β* to increased proximity of the hydrophilic TiO_2 (001) rutile surface. The peptide held in the vicinity of the surface displayed both global and local level structural differences in comparison to the free monomer. Most importantly, *β*-sheet populations are found to markedly increase with increasing proximity to the rutile surface. It would be useful to probe if the enhanced *β*-sheet propensity on the rutile surface is responsible for enhancing the nucleation process, as described experimentally by *in vitro* thioflavin T fluorescence studies performed with TiO_2 nanoparticles [61].

We mention here that recent experiments and computational studies show that hydrophilic surfaces, in general, appear to induce higher β-sheet content in the Aβ_{42} structure[19, 49, 61]. However, its conformational behavior and self-assembly kinetics on phospholipid monolayers and bilayers, and therefore on cellular membranes is determined by the interplay of several factors, and appears to be more complex. For example, hydrophilic interactions (arising due to the lipid head groups) and long-range hydrophobic interactions (arising due to lipid tails within the hydrophobic core)[44, 45, 50] have been noted to play important roles in Aβ adsorption on these surfaces. It has been reported that the dimyristoylphosphatidylcholine (DMPC) monolayer induces chain extension and the formation of structures with high β-sheet content in the Aβ monomer [44]. However, while free energy calculations show thermodynamic favorability of Aβ localization on dipalmitoylphoshatidylcholine (DPPC) and dioleoylphosphatidylserine (DOPS) bilayers [56, 73], these anionic surfaces may not induce a significant random coil to β-sheet structural conversion [56, 73]. Further, it has been demonstrated very recently that the palmitoyloleoylphosphatidylethanolamine (POPE) bilayer is capable of destabilizing pre-formed protofilaments of Aβ, resulting in a small but distinct loss in β-sheet character[45, 50]. Interestingly, in the vicinity of the phospholipid bilayers, the salt bridge between K28 and E22 or D23, understood to be one of the key stabilizing factors for the peptide's strand-turn-strand motif, is not promoted in the peptide monomer [56, 73] and largely disrupted in the protofibril [45, 50]. Our simulations show that the probability of formation of either the (D23, K28), or the (E22, K28) salt bridge is very low, and that their interaction strength with the rutile surface is distinctly weaker in comparison to the interaction strength recently reported with the POPE bilayer (see Figure AI-1 and AI-2 in Appendix I).

We further point out that recent studies have shown that solvent free energy plays a role in the dimerization of the full-length peptide [74]. Thus, any studies of peptide oligomerization on the rutile surface will have to be performed in explicit solvent environment. We mention here, however, that our preliminary simulations of the peptide-rutile complexes in explicit TIP3P water indicate qualitative agreement with the overall structural response presented in this study. Detailed investigation in explicit solvent environment is essential to decouple the effect of interaction of the peptide with the hydrophilic surface and with the water molecules confined around the peptide on the surface. We do not find a clear correlation between the proximity to the rutile surface and

the peptide's internal energy. While the peptide's internal non-bonded energy decreases sharply in system A compared to the free peptide, it appears to be closer to that of the free peptide in system B than in system C. We further note that the change in the *β*-sheet propensity from system A to C in non-uniform, *ie*., the domains that display high *β*-sheet propensity in A do not display progressively diminishing propensity from B to C (see $L_{17}VFFA_{21}$ in Figure 3.2.5 (a), for example). Enhanced sampling, coupled with residue-wise studies of conformational propensities, will help unravel definitive connections between the distance from the surface and overall structural response. Further studies will also be required to determine whether the enhanced *β*-sheet propensity is a representation of the peptide's response to all hydrophilic surfaces, or specifically to the rutile surface considered here.

The results presented here may have implications in the design of novel, hybrid nanoparticles targeted for disrupting the self-assembly of A*β*. Hydrophobic nanoparticles, while displaying significant abilities to disrupt the natural characteristics of monomeric and fibrillized A*β* [23, 24, 28, 75], have inherently low solubility, which poses a challenge in delivering them through aqueous media. While a variety of non-covalent functionalization techniques are being investigated for the dispersion of such nanoparticles in water [26, 76], this may also plausibly be achieved via hybridization with hydrophilic nanomaterials such as TiO_2 [77]. Our results indicate that the design of such composites should carefully take into consideration the structural responses of the targeted peptide to the individual constituents, as well as to the hybrid nanomaterial.

3.3 References

1. Bandura, A. V.; Sykes, D. G.; Shapovalov, V.; Troung, T. N.; Kubicki, J. D.; Evarestov, R. A., Adsorption of Water on the TiO2 (Rutile) (110) Surface: A Comparison of Periodic and Embedded Cluster Calculations. *J. Phys. Chem. B* **2004,** 108, 7844-7853.
2. Chong, S.-H.; Yim, J.; Ham, S., Structural Heterogeneity in Familial Alzheimer's Disease Mutants of Amyloid-Beta Peptides. *Mol. Biosyst.* **2013,** 9, 997-1003.
3. Fisher, C.; Ullman, O.; Stultz, C., Comparative Studies of Disordered Proteins with Similar Sequences: Application to Aβ40 and Aβ42. *Biophys. J.* **2013,** 104, 1546-1555.
4. Lee, C.; Ham, S., Characterizing Amyloid-beta Protein Misfolding from Molecular Dynamics Simulations with Explicit Water. *J. Comput. Chem.* **2010,** 32, 349-355.

5. Rosenman, D. J.; Connors, C. R.; Chen, W.; Wang, C.; García, A. E., Aβ Monomers Transiently Sample Oligomer and Fibril-like Configurations: Ensemble Characterization Using a Combined MD/NMR Approach. *J. Mol. Biol.* **2013,** 425, 3338-3359.
6. Sgourakis, N. G.; Merced-Serrano, M.; Boutsidis, C.; Drineas, P.; Du, Z.; Wang, C.; Garcia, A. E., Atomic-level Characterization of the Ensemble of the Aβ (1-42) Monomer in Water Using Unbiased Molecular Dynamics Simulations and Spectral algorithms. *J. Mol. Biol.* **2011,** 405, 570-583.
7. Zhang, S.; Iwata, K.; Lachenmann, M. J.; Peng, J. W.; Li, S.; Stimson, E. R.; Lu, Y. a.; Felix, A. M.; Maggio, J. E.; Lee, J. P., The Alzheimer's Peptide Aβ Adopts a Collapsed Coil Structure in Water. *J. Struct. Biol.* **2000,** 130, 130-141.
8. Crescenzi, O.; Tomaselli, S.; Guerrini, R.; Salvadori, S.; D'Ursi, A. M.; Temussi, P. A.; Picone, D., Solution Structure of the Alzheimer Amyloid β-Peptide (1–42) in an Apolar Microenvironment. *Eur. J. Biochem.* **2002,** 269, 5642-5648.
9. Tomaselli, S.; Esposito, V.; Vangone, P.; van Nuland, N. A.; Bonvin, A. M.; Guerrini, R.; Tancredi, T.; Temussi, P. A.; Picone, D., The alpha-to-beta Conformational Transition of Alzheimer's Abeta-(1-42) Peptide in Aqueous Media is Reversible: A Step by Step Conformational Analysis Suggests the Location of beta Conformation Seeding. *ChemBioChem* **2006,** 7 , 257-267.
10. Hall, C. K., Thermodynamic and Kinetic Origins of Alzheimer's and Related Diseases: A Chemical Engineer's Perspective. *AIChE J.* **2008,** 54, 1956-1962.
11. Petkova, A. T.; Ishii, Y.; Balbach, J. J.; Antzutkin, O. N.; Leapman, R. D.; Delaglio, F.; Tycko, R., A Structural Model for Alzheimer's β-Amyloid Fibrils Based on Experimental Constraints from Solid State NMR. *Proc. Natl. Acad. Sci. U.S.A.* **2002,** 99, 16742-16747.
12. Ball, K. A.; Phillips, A. H.; Nerenberg, P. S.; Fawzi, N. L.; Wemmer, D. E.; Head-Gordon, T., Homogeneous and Heterogeneous Tertiary Structure Ensembles of Amyloid-β Peptides. *Biochemistry* **2011,** 50, 7612-7628.
13. Luhrs, T.; Ritter, C.; Adrian, M.; Riek-Loher, D.; Bohrmann, B.; Dobeli, H.; Schubert, D.; Riek, R., 3D Structure of Alzheimer's Amyloid-β(1-42) Fibrils. *Proc. Natl. Acad. Sci. U.S.A.* **2005,** 102, 17342-17347.
14. Gralle, M.; Ferreira, S. T., Structure and Functions of the Human Amyloid Precursor Protein: The Whole is More than the Sum of its Parts. *Prog. Neurobiol.* **2007,** 82, 11-32.

15. Kang, J.; Lemaire, H.-G.; Unterbeck, A.; Salbaum, J. M.; Masters, C. L.; Grzeschik, K.-H.; Multhaup, G.; Beyreuther, K.; Muller-Hill, B., The Precursor of Alzheimer's Disease Amyloid A4 Protein Resembles a Cell-Surface Receptor. *Nature* **1987,** 325, 733-736.

16. Imamura, Y.; Watanabe, N.; Umezawa, N.; Iwatsubo, T.; Kato, N.; Tomita, T.; Higuchi, T., Inhibition of γ-Secretase Activity by Helical β-Peptide Foldamers. *J. Am. Chem. Soc.* **2009,** 131, 7353-7359.

17. Abedini, A.; Raleigh, D. P., A Critical Assessment of the Role of Helical Intermediates in Amyloid Formation by Natively Unfolded Proteins and Polypeptides. *Protein Eng. Des. Sel.* **2009,** 22, 453-459.

18. Fezoui, Y.; Teplow, D. B., Kinetic Studies of Amyloid β-Protein Fibril Assembly. *J. Biol. Chem.* **2002,** 277, 36948-36954.

19. Giacomelli, C. E.; Norde, W., Conformational Changes of the Amyloid β-Peptide (1–40) Adsorbed on Solid Surfaces. *Macromol. Biosci.* **2005,** 5, 401-407.

20. Yang, C.; Li, J.; Li, Y.; Zhu, X., The Effect of Solvents on the Conformations of Amyloid β-Peptide (1-42) Studied by Molecular Dynamics Simulation. *Comp. Theor. Chem.* **2009,** 895, 1-8.

21. Yang, C.; Zhu, X.; Li, J.; Chen, K., Molecular Dynamics Simulation Study on Conformational Behavior of Aβ (1-40) and Aβ (1-42) in Water and Methanol. *Comp. Theor. Chem.* **2009,** 907, 51-56.

22. Baumketner, A.; Shea, J.-E., The Structure of the Alzheimer Amyloid β 10-35 Peptide Probed through Replica-Exchange Molecular Dynamics Simulations in Explicit Solvent. *J. Mol. Biol.* **2007,** 366, 275-285.

23. Smoak, E. M.; Dabakis, M. P.; Henricus, M. M.; Tamayev, R.; Banerjee, I. A., Interactions of Amyloid Aβ(1–42) Peptide with Self-Assembled Peptide Nanospheres. *J. Pept. Sci.* **2011,** 17, 14-23.

24. Chatterjee, P.; Sengupta, N., Effect of the A30P Mutation on the Structural Dynamics of Micelle-Bound αSynuclein Released in Water: A Molecular Dynamics Study. *Eur. Biophys. J.* **2012,** 41, 483-489.

25. Bernstein, S. L.; Wyttenbach, T.; Baumketner, A.; Shea, J.-E.; Bitan, G.; Teplow, D. B.; Bowers, M. T., Amyloid β-Protein: Monomer Structure and Early Aggregation States of Aβ 42 and Its Pro19 Alloform. *J. Am. Chem. Soc.* **2005,** 127, 2075-2084.

26. Li, J.; Liu, R.; Lam, K. S.; Jin, L.-W.; Duan, Y., Alzheimer's Disease Drug Candidates Stabilize Aβ Protein Native Structure by Interacting with the Hydrophobic Core. *Biophys. J.* **2011,** 100, 1076-1082.

27. Sgourakis, N. G.; Yan, Y.; McCallum, S. A.; Wang, C.; Garcia, A. E., The Alzheimer's Peptides Aβ40 and 42 Adopt Distinct Conformations in Water: A Combined MD / NMR Study. *J. Mol. Biol.* **2007,** 368, 1448-1457.

28. Arce, F. T.; Jang, H.; Ramachandran, S.; Landon, P. B.; Nussinov, R.; Lal, R., Polymorphism of Amyloid β Peptide in Different Environments: Implications for Membrane Insertion and Pore Formation. *Soft Matter* **2011,** 7, 5267-5273.

29. Lockhart, C.; Kim, S.; Klimov, D. K., Explicit Solvent Molecular Dynamics Simulations of Aβ Peptide Interacting with Ibuprofen Ligands. *J. Phys. Chem. B* **2012,** 116, 12922-12932.

30. Viet, M. H.; Ngo, S. T.; Lam, N. S.; Li, M. S., Inhibition of Aggregation of Amyloid Peptides by Beta-Sheet Breaker Peptides and their Binding Affinity. *J. Phys. Chem. B* **2011,** 115, 7433-7446.

31. Ito, M.; Johansson, J.; Stromberg, R.; Nilsson, L., Unfolding of the Amyloid β-Peptide Central Helix: Mechanistic Insights from Molecular Dynamics Simulations. *PLOS ONE* **2011,** 6, e17587.

32. Lemkul, J. A.; Bevan, D. R., The Role of Molecular Simulations in the Development of Inhibitors of Amyloid β-Peptide Aggregation for the Treatment of Alzheimer's Disease. *ACS Chem. Neurosci.* **2012,** 3, 845-56.

33. Jorgensen, W. L.; Chandrasekhar, J.; Madura, J. D.; Impey, R. W.; Klein, M. L., Comparison of Simple Potential Functions for Simulating Liquid Water. *J. Chem. Phys.* **1983,** 79, 926-935.

34. Mackerell, A. D., Empirical Force Fields for Biological Macromolecules: Overview and Issues. *J. Comput. Chem.* **2004,** 25, 1584-1604.

35. MacKerell, A. D.; Bashford, D.; Bellott; Dunbrack, R. L.; Evanseck, J. D.; Field, M. J.; Fischer, S.; Gao, J.; Guo, H.; Ha, S.; Joseph-McCarthy, D.; Kuchnir, L.; Kuczera, K.; Lau, F. T. K.; Mattos, C.; Michnick, S.; Ngo, T.; Nguyen, D. T.; Prodhom, B.; Reiher, W. E.; Roux, B.; Schlenkrich, M.; Smith, J. C.; Stote, R.; Straub, J.; Watanabe, M.; Wiorkiewicz-Kuczera, J.; Yin, D.; Karplus, M., All-Atom Empirical Potential for Molecular Modeling and Dynamics Studies of Proteins. *J. Phys. Chem. B* **1998,** 102, 3586-3616.

36. Kalé, L.; Skeel, R.; Bhandarkar, M.; Brunner, R.; Gursoy, A.; Krawetz, N.; Phillips, J.; Shinozaki, A.; Varadarajan, K.; Schulten, K., NAMD2: Greater Scalability for Parallel Molecular Dynamics. *J. Comput. Phys.* **1999,** 151, 283-312.

37. Martyna, G. J.; Tobias, D. J.; Klein, M. L., Constant Pressure Molecular Dynamics Algorithms. *J. Chem. Phys.* **1994,** 101, 4177-4189.

38. Feller, S. E.; Zhang, Y.; Pastor, R. W.; Brooks, B. R., Constant Pressure Molecular Dynamics Simulation: The Langevin Piston Method. *J. Chem. Phys.* **1995,** 103, 4613-4621.

39. Ryckaert, J.-P.; Ciccotti, G.; Berendsen, H. J. C., Numerical Integration of the Cartesian Equations of Motion of a System with Constraints: Molecular Dynamics of n-Alkanes. *J. Comp. Phys.* **1977,** 23, 327-341.

40. Essmann, U.; Perera, L.; Berkowitz, M.; Darden, T.; Lee, H.; Pedersen, L., A Smooth Particle Mesh Ewald Method. *J. Chem. Phys.* **1995,** 103, 8577-8593.

41. Fauchere, J. L.; Pliska, V., Hydrophobic Parameters π. of Amino Acid Side Chains from the Partitioning of N-Acetyl-Amino Acid Amides. *Eur. J. Med. Chem.* **1983,** 18, 379-375.

42. Kowalewski, T.; Holtzman, D. M., In Situ Atomic Force Microscopy Study of Alzheimer's β-Amyloid Peptide on Different Substrates: New Insights into Mechanism of β-Sheet Formation. *Proc. Natl. Acad. Sci. U.S.A.* **1999,** 96, 3688-3693.

43. Bokvist, M.; Gröbner, G., Misfolding of Amyloidogenic Proteins at Membrane Surfaces: The Impact of Macromolecular Crowding. *J. Am. Chem. Soc.* **2007,** 129, 14848-14849.

44. Brambilla, D.; Verpillot, R.; Le Droumaguet, B.; Nicolas, J.; Taverna, M.; Kóňa, J.; Lettiero, B.; Hashemi, S. H.; De Kimpe, L.; Canovi, M.; Gobbi, M.; Nicolas, V.; Scheper, W.; Moghimi, S. M.; Tvaroška, I.; Couvreur, P.; Andrieux, K., PEGylated Nanoparticles Bind to and Alter Amyloid-Beta Peptide Conformation: Toward Engineering of Functional Nanomedicines for Alzheimer's Disease. *ACS Nano* **2012,** 6, 5897-5908.

45. Tofoleanu, F.; Buchete, N.-V., Alzheimer Aβ Peptide Interactions with Lipid Membranes: Fibrils, Oligomers and Polymorphic Amyloid Channels. *Prion* **2012,** 6, 339-345.

46. Borodin, O.; Smith, G. D.; Bandyopadhyaya, R.; Byutner, O., Molecular Dynamics Study of the Influence of Solid Interfaces on Poly (Ethylene Oxide) Structure and Dynamics. *Macromolecules* **2003,** 36, 7873-7883.

47. Zhao, J.; Wang, Q.; Liang, G.; Zheng, J., Molecular Dynamics Simulations of Low-Ordered Alzheimer β-Amyloid Oligomers from Dimer to Hexamer on Self-Assembled Monolayers. *Langmuir* **2011,** 27, 14876-14887.

48. Utesch, T.; Daminelli, G.; Mroginski, M. A., Molecular Dynamics Simulations of the Adsorption of Bone Morphogenetic Protein-2 on Surfaces with Medical Relevance. *Langmuir* **2011,** 27, 13144-13153.

49. Kim, S.; Klimov, D., Binding to the Lipid Monolayer Induces Conformational Transition in Aβ Monomer. *J. Mol. Model.* **2012,** 19, 737-750.

50. Tofoleanu, F.; Buchete, N.-V., Molecular Interaction of Alzheimer's Aβ protofilaments with Lipid Membranes. *J. Mol. Biol.* **2012,** 421, 572-586.

51. Wang, Q.; Zhao, J.; Yu, X.; Zhao, C.; Li, L.; Zheng, J., Alzheimer Aβ1-42 Monomer Adsorbed on the Self-Assembled Monolayers. *Langmuir* **2012,** 26, 12722-12732.

52. Yu, X.; Wang, Q.; Lin, Y.; Zhao, J.; Zhao, C.; Zheng, J., Structure, Orientation, and Surface Interaction of Alzheimer Amyloid-β Peptides on the Graphite. *Langmuir* **2012,** 28, 6595-6605.

53. Chatelier, R. C.; Minton, A. P., Adsorption of Globular Proteins on Locally Planar Surfaces: Models for the Effect of Excluded Surface Area and Aggregation of Adsorbed Protein on Adsorption Equilibria. *Biophys. J.* **1996,** 71, 2367-2374.

54. Minton, A. P., Adsorption of Globular Proteins on Locally Planar Surfaces. II. Models for the Effect of Multiple Adsorbate Conformations on Adsorption Equilibria and Kinetics. *Biophys. J.* **1999,** 76, 176-187.

55. Minton, A. P., The Influence of Macromolecular Crowding and Macromolecular Confinement on Biochemical Reactions in Physiological Media. *J. Biol. Chem.* **2001,** 276, 10577-10580.

56. Davis, C. H.; Berkowitz, M. L., Interaction Between Amyloid-β (1-42) Peptide and Phospholipid Bilayers: A Molecular Dynamics Study. *Biophys. J.* **2009,** 96, 785-797.

57. Chen, P. C.; Mwakwari, S. C.; Oyelere, A. K., Gold Nanoparticles: From Nanomedicine to Nanosensing. *Nanotechnol. Sci. Appl.* **2008,** 2008, 45 - 66.

58. Yang, W.; Thordarson, P.; Gooding, J. J.; Ringer, S. P.; Braet, F., Carbon Nanotubes for Biological and Biomedical Applications. *Nanotechnology* **2007,** 18, 412001.

59. Kostarelos, K.; Lacerda, L.; Pastorin, G.; Wu, W.; WieckowskiSebastien; Luangsivilay, J.; Godefroy, S.; Pantarotto, D.; Briand, J.-P.; Muller, S.; Prato, M.; Bianco, A., Cellular Uptake of Functionalized Carbon Nanotubes is Independent of Functional Group and Cell Type. *Nat. Nano* **2007,** 2, 108-113.

60. Chebaro, Y.; Jiang, P.; Zang, T.; Mu, Y.; Nguyen, P. H.; Mousseau, N.; Derreumaux, P., Structures of Aβ 17-42 Trimers in Isolation and with Five Small-Molecule Drugs Using a Hierarchical Computational Procedure. *J. Phys. Chem. B* **2012,** 116, 8412-8422.

61. Wu, W.-h.; Sun, X.; Yu, Y.-p.; Hu, J.; Zhao, L.; Liu, Q.; Zhao, Y.-f.; Li, Y.-m., TiO2 Nanoparticles Promote β-Amyloid Fibrillation In Vitro. *Biochem. Biophys. Res. Commun.* **2008,** 373, 315-318.

62. Colvin, V. L.; Kulinowski, K. M., Nanoparticles as Catalysts for Protein Fibrillation. *Proc. Natl. Acad. Sci. U.S.A.* **2007,** 104, 8679-8680.

63. Kurylowicz, M.; Giuliani, M.; Dutcher, J. R., Using Nanoscale Substrate Curvature to Control the Dimerization of a Surface-Bound Protein. *ACS Nano* **2012,** 6, 10571-10580.

64. Linse, S.; Cabaleiro-Lago, C.; Xue, W.-F.; Lynch, I.; Lindman, S.; Thulin, E.; Radford, S. E.; Dawson, K. A., Nucleation of Protein Fibrillation by Nanoparticles. *Proc. Natl. Acad. Sci. U.S.A.* **2007,** 104, 8691-8696.

65. Miller, Y.; Ma, B.; Nussinov, R., Zinc Ions Promote Alzheimer Aβ Aggregation via Population Shift of Polymorphic States. *Proc. Natl. Acad. Sci. U.S.A.* **2010,** 107, 9490-9495.

66. Brooks, B. R.; Bruccoleri, R. E.; Olafson, B. D.; States, D. J.; Swaminathan, S.; Karplus, M., CHARMM: A Program for Macromolecular Energy, Minimization, and Dynamics Calculations. *J. Comput. Chem.* **1983,** 4, 187-217.

67. Onufriev, A.; Bashford, D.; Case, D. A., Exploring Protein Native States and Large-Scale Conformational Changes with a Modified Generalized Born Model. *Proteins: Struct., Funct., Bioinf.* **2004,** 55, 383-394.

68. Onufriev, A.; Bashford, D.; Case, D. A., Modification of the Generalized Born Model Suitable for Macromolecules. *J. Phys. Chem. B* **2000,** 104, 3712-3720.

69. Humphrey, W.; Dalke, A.; Schulten, K., VMD: Visual Molecular Dynamics. *J. Mol. Graph.* **1996,** 14, 33-38.

70. Best, R. B.; Buchete, N.-V.; Hummer, G., Are Current Molecular Dynamics Force Fields too Helical? *Biophys. J.* **2008,** 95, L07-L09.

71. Tulip, P. R.; Gregor, C. R.; Troitzsch, R. Z.; Martyna, G. J.; Cerasoli, E.; Tranter, G.; Crain, J., Conformational Plasticity in an HIV-1 Antibody Epitope. *J. Phys. Chem. B* **2012,** 114, 7942-7950.

72. Miller, Y.; Ma, B.; Nussinov, R., Polymorphism in Alzheimer Aβ Amyloid Organization Reflects Conformational Selection in a Rugged Energy Landscape. *Chem. Rev.* **2010,** 110, 4820-4838.

73. Davis, C. H.; Berkowitz, M. L., Structure of the Amyloid-β (1-42) Monomer Absorbed to Model Phospholipid Bilayers: A Molecular Dynamics Study. *J. Phys. Chem. B* **2009,** 113, 14480-14486.

74. Chong, S.-H.; Ham, S., Impact of Chemical Heterogeneity on Protein Self-Assembly in Water. *Proc. Natl. Acad. Sci. U.S.A.* **2012,** 109, 7636-7641.

75. Andujar, S. A.; Lugli, F.; Hofinger, S.; Enriz, R. D.; Zerbetto, F., Amyloid-β Fibril Disruption by C60-Molecular Guidance for Rational Drug Design. *Phys. Chem. Chem. Phys.* **2012,** 14, 8599-8607.

76. Vaisman, L.; Wagner, H. D.; Marom, G., The Role of Surfactants in Dispersion of Carbon Nanotubes. *Adv. Colloid Interface Sci.* **2006,** 128, 37-46.

77. Haass, C.; Selkoe, D. J., Soluble Protein Oligomers in Neurodegeneration: Lessons from the Alzheimer's Amyloid β-Peptide. *Nat. Rev. Mol. Cell Biol.* **2007,** 8, 101-112.

Chapter 4

Microscopic Hydration Properties of the A$\beta_{1\text{-}42}$ Peptide Monomer and the Globular Protein Ubiquitin: A Comparative Molecular Dynamics Study

"Measure what can be measured,

and make measurable what cannot be measured."

-Galileo Galilei

Abstract

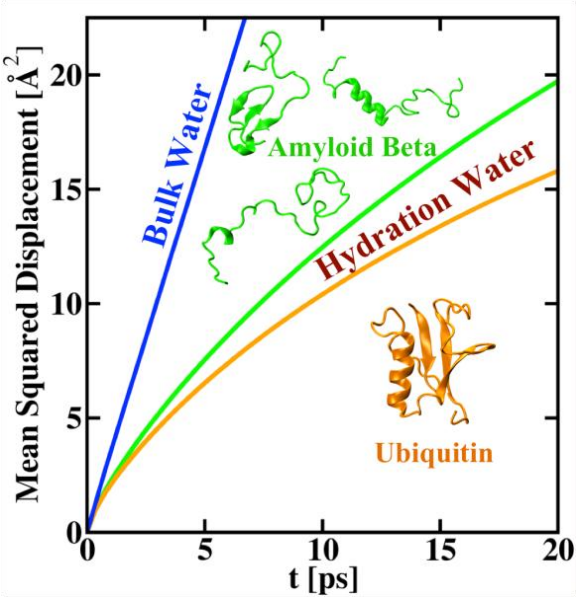

In this chapter, a comparative study of the microscopic properties of water molecules present in the hydration layer of eight selected conformations of amyloid beta (1-42) which is an IDP, and a globular protein, ubiquitin (UBQ) is included. It is noticed that irrespective of the conformational heterogeneity among the Aβ monomers, water molecules hydrating their surfaces exhibit relatively faster dynamics as compared to water molecules hydrating UBQ. Importantly, the conformational heterogeneity of the Aβ monomers has been found to affect the translational and rotational motions of hydration water molecules in a non-uniform manner. Detailed investigation of the time scale of hydrogen bond relaxations at the surface and their energetics revealed the possibility of heterogeneous confinement around different Aβ conformations. The distribution of water density fluctuation around Aβ conformations are broader compared to UBQ because of its predominant hydrophobic nature. Significant heterogeneity in the density fluctuation among the Aβ monomers suggests that the structural propensities could affect the peptide's effective surface hydrophobicity.

4.1 Introduction

As discussed in the introduction Intrinsically disordered proteins (IDPs) belong to a class of protein sequences that do not possess uniquely folded native structures at physiological conditions.[1] The ability of IDPs to play important biological roles despite the absence of well-defined structure has defied the classic protein structure-function paradigm, and triggered vast research on this protein sub-family.[2] The 4 kDa Amyloid beta (Aβ) peptide has been considered a representative IDP system in recent studies.[3-5] While the 'Amyloid hypothesis' implicates the peptide's fibrillar aggregates (known an 'amyloids') in AD onset, emerging research indicates higher neurotoxicity of its soluble forms.[6] The full length Aβ peptide monomer adopts helical motifs in solvents with low polarity,[7,8] but inhabits a wide conformational ensemble in aqueous environment.[4,9,10] Aβ is thought to follow a nucleated polymerization mechanism, wherein a disordered, activated nucleus triggers the self-assembly pathway that eventually results in the formation of polymorphic protofibrillar and fibrillar aggregates.[11-13] Aβ is considered a paradigm for describing the conformational behavior for amyloidogenic proteins.[14]

Recent advances have significantly unraveled the physical origins of IDP behavior.[2] Amongst various key factors, the solvent environment has been found to have profound influence over the self-assembly behavior of proteins such as Aβ.[15] Alterations to the solvent environment can influence conformational flexibilities, structural ordering and self-assembly kinetics of such disordered proteins.[8,16-18] In Aβ, interior hydration plays crucial roles in the stability of protofibrillar assemblies.[15,19,20] Further, the solvation free energy has been shown as an important component in the total free energy of dimerization of full length Aβ.[21]

Despite emerging knowledge on the role of solvent in the conformational and protein self-assembly behavior, little is known about the dynamical coupling of solvent molecules with the protein surface of disordered, assembly-prone proteins such as Aβ. In contrast, hydration dynamics of natively folded proteins have been studied in great detail via advanced spectroscopic techniques and computer simulations.[22-28] In these systems, coupling with the protein surface causes marked deviations from bulk behavior in water molecules hydrating the surface. Their dynamical slowdown is reflected in their distinctly sub-linear diffusion, longer tumbling times and longer mean residence times in the hydration layer.[22-28] The water molecules hydrating the surface of a protein are often

termed as 'biological water',[29] due to their indispensable role in guiding the structure, dynamics, and hence the function of the protein.[30] Importantly, it is shown that protein dynamical transitions and folding are 'slaved' to solvent dynamics.[31,32] The anharmonic motions of the protein atoms have been found to be coupled to the hydrogen bond dynamics at the interface.[33] Recent work from our group showed that the conformational flexibility of key secondary structural elements of folded proteins affects the local heterogeneity in hydration water dynamics.[34,35]

As in the case of natively structured proteins, important signatures of solvent influences on an assembly prone protein can be obtained by exploring the extent of its dynamical coupling with the surrounding solvent layer. However, due to inherent complex nature of the problem and lack of thermodynamically stable structures, no significant attempt has been made so far to explore the dynamical features of water molecules hydrating the surfaces of such proteins. To the best of our knowledge, the present study reports for the first time an in-depth analysis of the correlated dynamical behavior of water molecules hydrating an important protein in this class, namely, the Aβ peptide. We emphasize at this point that as the conformational ensembles of disordered proteins such as Aβ are widely distributed, it is essential to monitor the protein-water dynamical coupling of these systems by averaging of key properties over multiple representative conformations. Interestingly, in the case of globular proteins, it has been demonstrated recently that the distribution of reorientation dynamics of individual water molecules within the hydration shell and therefore the overall hydration shell dynamics are independent of the size and the secondary structural contents of the proteins.[36] In this study, we have used atomistic molecular dynamics simulations to study key dynamical and energetic aspects of water molecules hydrating a variety of monomeric A$\beta_{1\text{-}42}$ conformations. For comparison, we have performed equivalent analyses of solvent behavior on the surface of a folded globular protein, namely, ubiquitin (UBQ). Preliminary analysis with van Hove autocorrelation function suggests faster movement of surface water molecules in the Aβ ensemble over UBQ. Detailed analysis revealed a small but distinct shift towards bulk-like character of the hydration water molecules of Aβ over those of UBQ. However, the diffusion remained sub-linear, while the rotational relaxation and the hydrogen bond dynamics were found to be significantly slower than that of bulk water, indicating strong protein-water dynamical coupling even in the structurally disordered Aβ. Overall, such differences in hydration layer behavior with

UBQ appeared to be independent of the conformational characteristics of Aβ. Interestingly, however, the solvent on the Aβ surface displayed degrees of heterogeneity not associated with natively folded proteins.

4.2 Methods

4.2.1 System Setup and Simulation Protocols

Molecular Dynamics Simulations

Molecular dynamics (MD) simulations for eight different conformations of full length A$\beta_{1\text{-}42}$ (AB1 to AB8) and ubiquitin (UBQ) were performed using NAMD2.8 package.[37] The methods used to generate the peptide conformations are described below. The CHARMM all atom force field with the CMAP correction was used.[38-40] The NH_3^+ and COO^- groups were added to the N- and C-terminii of all the peptide and protein conformations. All the initial structures were solvated with TIP3P water molecules[41] followed by addition of counter ions in order to afford charge neutral systems. The minimum distance from a protein atom to the edge of the simulation box was at least 14 Å. After 10,000 steps of conjugate gradient energy minimization, 6 ns of simulations were carried out in the isothermal-isobaric (NPT) ensemble with orthorhombic periodic boundary conditions for equilibration of the systems. Constant temperature of 310 K was maintained with Langevin dynamics (collision frequency of 1 ps^{-1}) and the Langevin piston Nosé-Hoover method[42] maintained the constant pressure of 1 atm. The cutoff radius for the Lennard- Jones interactions was set to 12 Å. The SHAKE algorithm[43] was used for constraining bonds involving hydrogens. Electrostatic interactions were calculated with particle-mesh Ewald,[44] and a simulation timestep of 1 fs was used. The equilibration was followed by 2 ns of simulations in the canonical (NVT) ensemble, with snapshots saved every 8 fs. These snapshots were used for all analyses presented in the study.

4.2.2 Generation of Initial Monomer Conformations

Ubiquitin

The initial structure of the 76 residue, natively folded protein Ubiquitin was taken from Protein Data Bank (PDB: 1UBQ).[45]

Aβ Conformations

Recent reports indicate that the Aβ monomeric ensemble is characterized by significant conformational heterogeneity.[4,9,46-50] Here, we point out that a recent study has shown that despite subtle differences in the isoforms, varying force fields largely converge in the important structural characteristics of the Aβ ensembles generated.[50] We generated a variety of full-length Aβ monomeric conformations with multiple methods that have been used widely for rapid sampling of protein conformational space, such as 'Replica Exchange Molecular Dynamics' (REMD) and 'Accelerated Molecular dynamics' (AMD).[48,50,51] The structure generation protocols are discussed in brief below. Keeping in mind the structural heterogeneity of the ensemble, eight individual Aβ conformations with varying secondary structural content were selected for our study. The structural basis of these selections, based on previous reports, is discussed in the next section.

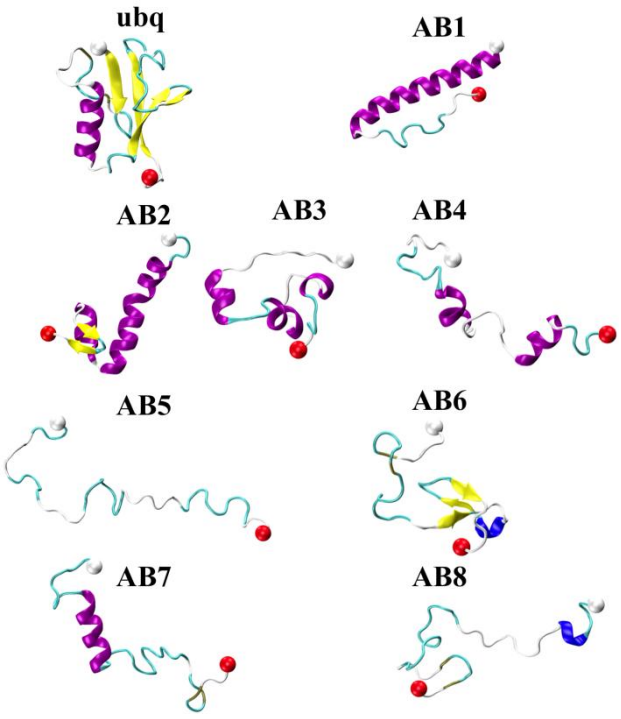

Figure4.1. Representative snap shots of A$\beta_{1\text{-}42}$ and UBQ from the simulated trajectories.

The solution state NMR structure of A$\beta_{1\text{-}42}$ peptide in a 70:30 mixture of water and hexafluoro-2-propanol has been reported in Protein Data Bank (PDB: 1Z0Q)[8]. This structure is predominantly helical, and has been used in several recent simulation

studies.[52,53] This structure was simulated in the NPT ensemble for 150 ns, and the end point conformation was designated as 'AB1'.

REMD[54] simulation method was carried out for the 1Z0Q structure, with 64 replicas spanning the temperature range from 330 K to 600 K. Exchange time among the replicas was set to 0.25 ps and the acceptance ratio was found to be greater than 10%. Each replica was simulated for 10 ns and hence the total simulation time was 640 ns. The Aβ conformations AB2, AB3 and AB4 were taken at the end point of the trajectories at 530K, 600K and 594K, respectively.

The 1Z0Q structure was simulated in the gas phase at a temperature of 373 K for 5 ns, generating several random coil conformations. A few snapshots were simulated in explicit water for up to 100 ns following the protocol described, and some were found to develop C-terminal beta sheet character. Representative snapshots of a random coil conformation and one with C-terminal beta sheet were designated AB5 and AB6, respectively.

AMD is a technique that ensures enhanced sampling of an ensemble in a short time by reducing the energy barrier between different states of the system. Details of the AMD technique are provided in Chapter 2 (section 2.7.1). AMD was performed on the 1Z0Q structure. The value of the dihedral boost, E_b, was fixed such that its difference with the mean dihedral energy in unbiased simulations was 4 kcal mol^{-1} times the number of residues in the peptide in accordance with recently optimized protocols.[57] The structure thus obtained was designated AB7.

A monomeric unit of a parallel beta sheet structure was taken from the pentameric Aβ_{17-42} (PDB ID: 2BEG)[58], and the N-terminal sequence D_1AEFRHDSGYEVHHQK$_{16}$ generated with the VMD tool[59] in an extended orientation (dihedral angles, $\psi = 180^0$ and $\varphi = 180^0$), was attached to get the full length Aβ_{1-42}. This conformation was simulated in the NPT ensemble for 5 ns, and the end point designated as AB8.

4.3 Results and Discussions

4.3.1 Characteristics of the Aβ Conformations

Aβ, unlike natively folded globular proteins, is characterized by large conformational fluctuations. Therefore, to probe the influence of the conformational heterogeneity of Aβ on its hydration layer, we have selected multiple monomeric conformations that describe

the differential aspects of the Aβ conformational ensemble. We first note that helicity of the amyloid precursor protein (APP) is essential for its efficient enzymatic cleavage[60], and thus nascent Aβ has been hypothesized to be in a helical conformation just after release into the aqueous cytoplasm.[8,47] The helical structure is also evident when solvents of lower polarity are added.[7,8] However, in pure aqueous solution, the ensemble is characterized by collapsed coil structure,[9,46] Extensive computer simulations indicate an enhanced probability for helicity at N-terminal region[4] and a preferential anti-parallel beta sheet motif in the C-terminal region.[3,4,50] In Figure 4.1, we present representative snapshots of the Aβ conformations used in this study, along with a representative snapshot of UBQ conformation. The conformer AB1 is characterized by the highest degree of helicity in the N-terminal and turn regions, and by the absence of any beta-sheet structure. In comparison to AB1, the conformations AB2, AB3 and AB4 have reduced helicities in the N-terminal and turn regions, but a small extent of C-terminal helicity as reported earlier.[61] Among these three structures, AB2 is also characterized by the presence of an anti-parallel beta sheet in the C-terminal region. The conformation AB5 is predominantly characterized by the presence of turns and coils, and has negligible helicity in the N-terminal region. While the helical conformations are completely absent in the AB6 conformation, there is a small extent of 3_{10}- helicity in the N-terminal and turn regions. However, this conformation is characterized by the distinct presence of beta-sheet conformations in the central hydrophobic core ($F_{19}FA_{21}$) and in the C-terminal domain $K_{28}GAI_{31}$ and $M_{35}VGG_{38}$. We point out that the AB6 structure is comparable to the highly populated conformation reported in recent studies that plays significant roles in pathological aggregation of Aβ.[62,63] AB7 is also characterized by the presence of C-terminal beta-sheet and isolated bridge propensities, in addition to a reduced extent of N-terminal helicity in comparison to AB2. The AB8 conformation has marginal 3_{10} helicity in the N-terminal and turn regions, but has distinct anti-parallel beta-strands in the C-terminal region. In Table 4.1, we have presented the mean secondary structure percentages of the N-terminal, turn, and C-terminal domains and in Figure 4.2, we have shown the residue-wise secondary structural content over the 2 ns analysis runs for the eight Aβ conformations.Eventhough, the conformations are highly flexible, the calculations of root mean squared fluctuations (RMSF) of the non-hydrogen atoms (provided in Appendix-II, Figure AII-1), and the structural persistence, Q[64,65](mean

values of Q are listed in Appendix-II, Table AII-1) showed that the structural characteristics are conserved to a large extent during the analysis periods.

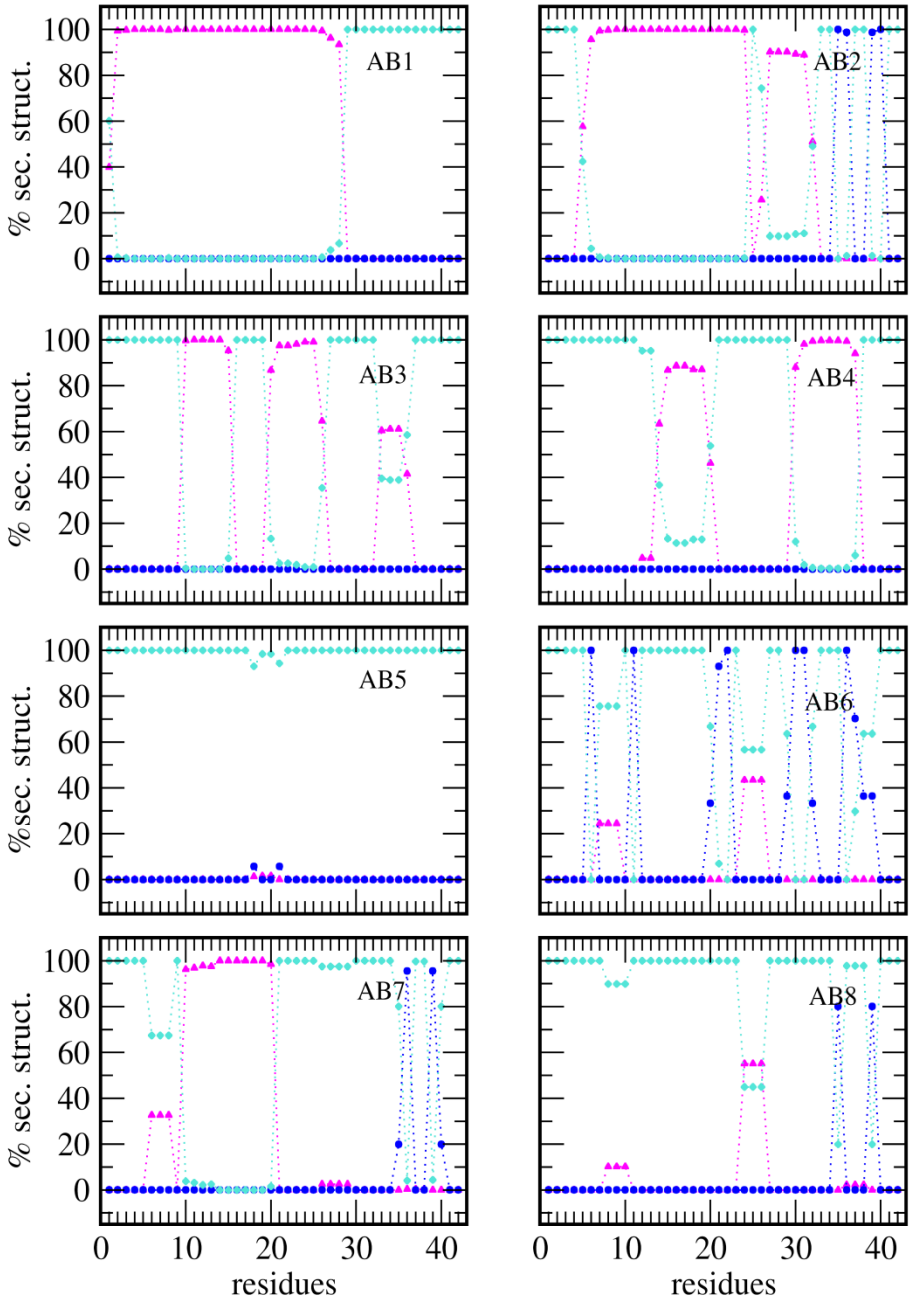

Figure 4.2. Residue-wise secondary structural content averaged over the 2 ns analysis run for the eight Aβ conformations. Total percentage of helix is represented using magenta; percentage of β-sheet is in blue and total percentage of turn and coil is in cyan.

secondary structure		Aβ conformations							
		AB1	AB2	AB3	AB4	AB5	AB6	AB7	AB8
N- terminus (res 1-21)	α-helix	97.02	78.62	37.05	24.74	0.0	0.0	51.46	0.0
	3_{10}-helix	0.0	0.02	0.03	0.80	0.21	3.14	5.07	1.43
	π-helix	0.0	0.0	0.0	1.10	0.0	0.0	0.0	0.0
	β-sheet	0.0	0.0	0.0	0.0	0.0	5.93	0.0	0.0
	isolated bridge	0.0	0.0	0.0	0.0	0.56	9.52	0.0	0.0
	turn & coil	2.98	21.36	62.92	73.36	99.22	81.41	43.47	98.57
turn (res 22-29)	α-helix	86.43	73.33	56.87	0.0	0.0	0.0	1.19	0.0
	3_{10}-helix	0.0	1.35	0.72	0.0	0.0	16.0	0.06	20.36
	π-helix	0.0	0.0	0.0	0.0	0.0	0.0	0.0	0.0
	β-sheet	0.0	0.0	0.0	0.0	0.0	16.34	0.0	0.0
	isolated bridge	0.0	0.0	0.0	0.0	0.0	0.78	0.0	0.0
	turn & coil	13.53	25.32	42.42	100.0	100.0	66.87	98.75	79.64
C-terminus (res 30-42)	α-helix	0.0	17.09	12.35	59.58	0.0	0.0	0.0	0.0
	3_{10}-helix	0.0	0.33	4.73	0.20	0.0	0.0	0.04	0.44
	π-helix	0.0	0.0	0.0	0.0	0.0	0.0	0.0	0.0
	β-sheet	0.0	30.52	0.0	0.0	0.0	34.09	6.42	0.0
	isolated bridge	0.0	0.12	0.0	0.0	0.0	2.47	11.54	12.25
	turn & coil	100.0	51.93	82.93	40.22	100.0	63.44	82.01	87.31

Table 4.1. Secondary structure details of Aβ conformations; Average secondary structural content (in percentage) of the N- and C-termini, and turn regions.

We further point out that conformational collapse of the Aβ monomer is considered a key early event in the peptide's self-assembly pathway.[46,47,66,67] Such compaction is attributed mainly to the interactions between key regions in the N- and C-terminal domains. In the previous chapter, we have characterized the extent of Aβ compactness with the parameter '$d_{collapse}$', defined as the center of mass distance between the domains L_{17}VFFAEDVGS$_{26}$ and K_{28}GAIIGLMVGGVVIA$_{42}$.[65-67]

conf.	<$d_{collapse}$>	<R_g>	<SASA>	< E_{tot-PW} >
AB1	9.05	12.68	89.77	-4.49
AB2	10.38	12.12	90.12	-4.14
AB3	7.57	11.17	99.42	-4.04
AB4	23.60	18.58	114.26	-3.81
AB5	24.58	19.26	125.22	-3.64
AB6	5.94	11.70	93.41	-4.16
AB7	16.50	15.44	106.67	-3.78
AB8	10.90	14.82	109.73	-4.07
AB-avg	13.57	14.47	103.58	-4.02
UBQ	-	12.40	73.36	-5.42

Table 4.2. Degree of compactness and interaction strength with hydration water. Average values of $d_{collapse}$ (in Å), R_g (in Å), SASA (in Å^2), and E_{tot-PW} (in kcal mol^{-1}) for the Aβ conformations and UBQ. Data averaged over the eight Aβ conformations are specified as AB-avg.

In Table 4.2, we have listed the mean $d_{collapse}$ values over the trajectories of the eight Aβ conformations, along with the mean values of their radius of gyration (R_g) and the solvent accessible surface area (SASA) per residue calculated with the VMD software.[59] The SASA was obtained by calculating the total area covered by running a spherical probe of 1.8Å radius over the peptide surface. R_g and SASA are found to correlate reasonably well

with the $d_{collapse}$ values (see FigureAII-2 in Appendix II). Despite their conformational differences, we find that the level of compactness of AB1, AB2, and AB6 are comparable. Interestingly, UBQ conformation has the lowest SASA and relatively low R_g values despite its longer sequence compared to Aβ, reflecting its high degree of compactness.

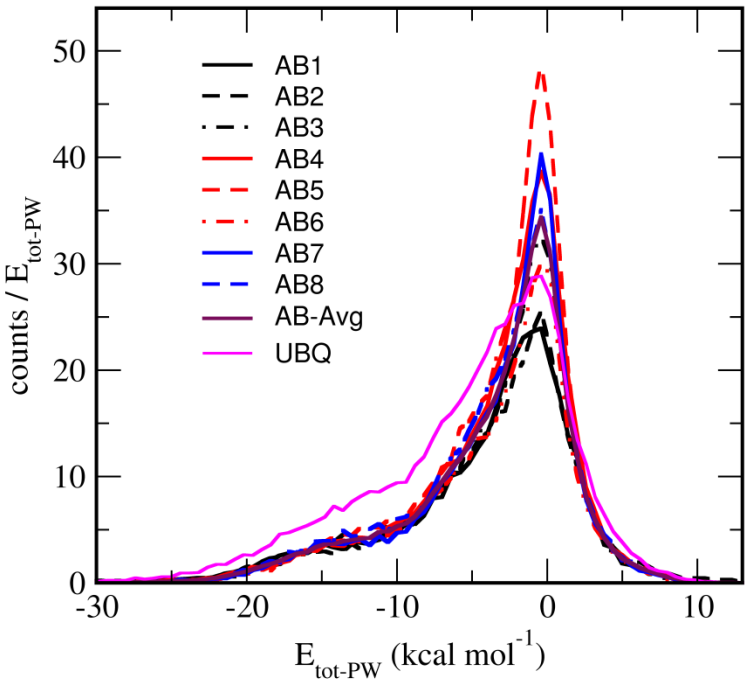

Figure 4.3. Distributions of the interaction energy ($E_{tot\text{-}PW}$) of the first hydration layer water molecules with the protein for different Aβ peptide conformations and UBQ. The corresponding distribution averaged over the Aβ monomers are also shown for comparison.

For a preliminary comparison and insights into the association of the hydration water molecules at the protein surface in the Aβ conformations and in UBQ, we have evaluated the total (i.e., electrostatic and van der Waals) interaction strengths, $E_{tot\text{-}PW}$, of individual water molecules residing in the hydration layer with the entire protein molecule. It may be noted here that all the calculations presented in the remaining manuscript are carried out by considering those water molecules that reside within a distance of 5 Å from the protein. This is consistent with earlier reports[68] where it was shown that the effects of a protein on water properties are primarily restricted to the first hydration layer (within ~5 Å). In Figure 4.3 we have presented the distributions of $E_{tot\text{-}PW}$, averaged over equi-spaced snapshots as obtained from the simulated trajectories and

normalized such that the integrals of the distributions correspond to the total number of hydration water molecules.[28] As evident from the figure, the protein-water (PW) interactions are heterogeneous in nature, which agrees well with earlier reports.[28] However, the spread in $E_{tot\text{-}PW}$ in the Aβ conformations is found to be less compared to the corresponding distribution for UBQ. The mean values of the interaction strengths ($<E_{tot\text{-}PW}>$) are included in Table 4.2. We find that the PW interaction strengths on average are reduced by about 1.4 kcal mol^{-1} for the Aβ conformations as compared to UBQ. It may be noted here that compared to the Aβ monomers, more negative $<E_{tot\text{-}PW}>$ value or higher PW interaction strength for a tagged water present in the vicinity of UBQ is likely to arise due to its larger number of residues and more compact structure. However, we did not find any correlation between the mean total PW interaction strength with the overall secondary structure content and the degree of compactness of the Aβ conformations.

4.3.2 Dynamics of Hydration Water

4.3.2.1 Translational Dynamics

In this section, we explore and compare the microscopic dynamics of water molecules hydrating the Aβ monomers. The influence of heterogeneous conformations of the monomers and their flexibilities on the mobility of the nearby water molecules has been studied in detail. To assess and compare water translational dynamics, we first calculate the evolutions of the van Hove autocorrelation function $G_s(r, t)$ for those water molecules that were present initially ($t = 0$) in the first hydration layers of the protein conformations. $G_s(r, t)$ is a space-time autocorrelation function which gives the probability density of finding a particle i at time t, if the particle was at the origin at $t = 0$. The function is defined for an N particle system as[69]

$$G_s(r,t) = \frac{1}{N}\sum_{i=1}^{N}\left\langle \delta[r + r_i(0) - r_i(t)]\right\rangle \qquad (4.1)$$

where $r_i(t)$ denotes the position of the i^{th} particle at time t. For purely homogeneous diffusion, $G_s(r, t)$ is a Gaussian function of the position r at all times t. In Figure 4.4 (upper panel), we present $4\pi r^2 G_s(r, t)$, or $P(r; t)$, the probability of a water molecule residing in the hydration layer at time $t = 0$, to have moved a distance r in time t at 5, 20, 50 and 100 ps, respectively.

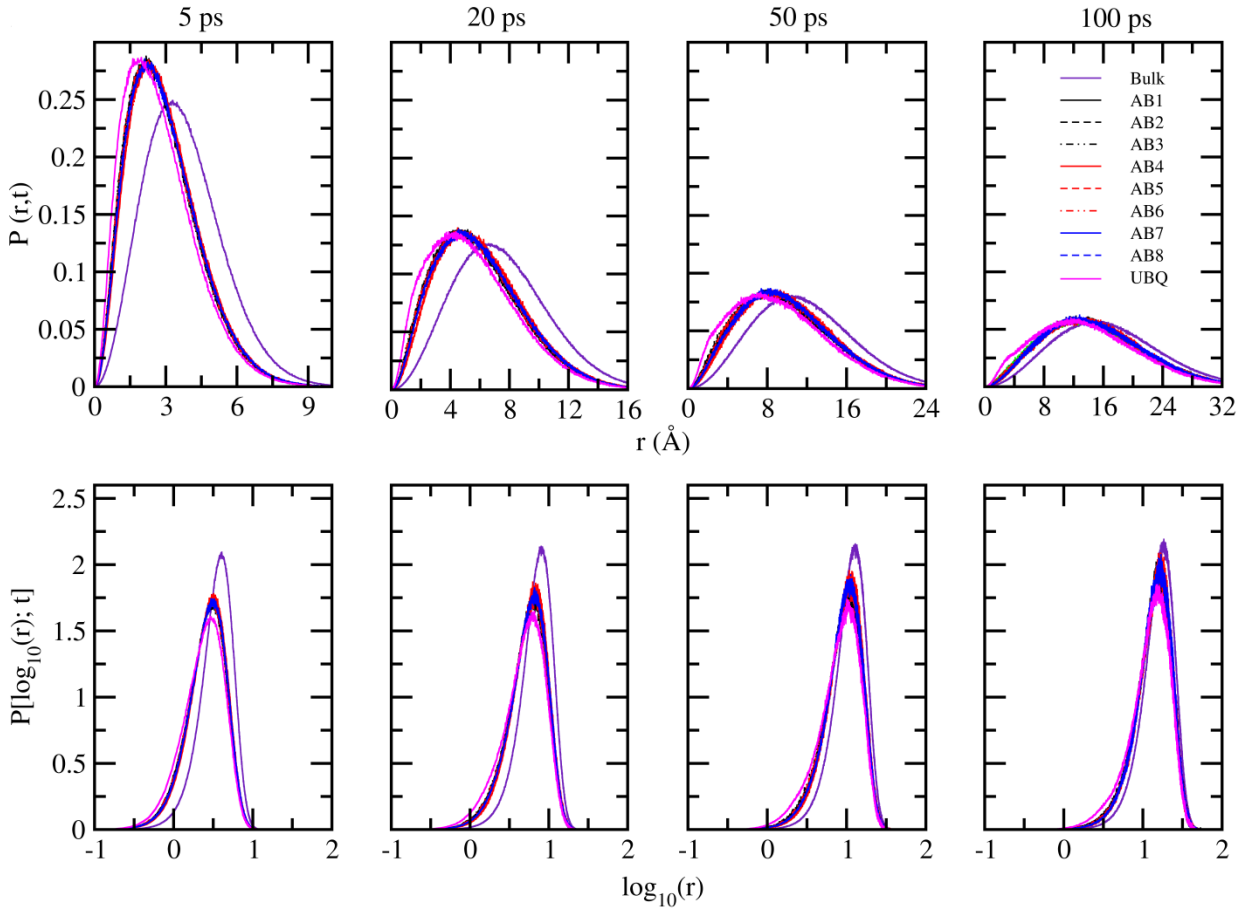

Figure 4.4. $P(r; t)$ as a function of r (top panel) and $P(\log_{10}(r); t)$ as a function of $\log_{10}(r)$ (bottom panel) for the first hydration layer water molecules around different Aβ peptide conformations and UBQ. As a reference, the corresponding functions for pure bulk water are included.

The calculations are carried out for water molecules around all the Aβ monomers and UBQ. As a reference, the corresponding data for pure bulk water as obtained from a separate MD simulation of TIP3P water under identical conditions is also included in the figure. Compared to water in pure bulk phase, slower diffusion of protein surface water at short times is evident from the figure. The results indicate near-identical mobility of water molecules around the Aβ monomers. However, compared to UBQ, small but noticeably higher mobility of water molecules hydrating the flexible Aβ molecules can be seen. It is known that for homogeneous diffusion, peak heights of the logarithm of the single particle displacement, $P(\log_{10}(r); t)$, calculated as $ln(10)[4\pi r^3 G_s(r, t)]$, remains constant (~2.13) with time.[70,71] We have plotted $P(\log_{10}(r); t)$ *vs.* $\log_{10}(r)$ for the hydration layer water molecules around all the protein systems, as shown in the lower panel of Figure 4.4. While the peak heights for bulk water remain nearly constant with time, they are

distinctly lower for the protein hydration water, particularly at short times. It is evident that at shorter time scale (within a few tens of picoseconds), the water molecules exhibit constrained motions near the protein surface. In other words, a protein extends its influence on nearby water molecules for a duration up to a few tens of picoseconds. A closer examination of the data further reveals that while the peak heights for AB1 to AB8 are nearly the same, they are marginally higher compared to that observed for UBQ. This is an important finding that signifies that the water molecules around the flexible Aβ monomers tend to leave the first hydration layers relatively faster than those around the more compact globular UBQ. The peak positions in $P(r; t)$, and the peak heights in $P(\log_{10}(r); t)$ are provided in the Table 4.3.

conf.	peak position of P(r, t)				peak height of $P(\log_{10}(r); t)$			
	5 ps	20 ps	50 ps	100 ps	5 ps	20 ps	50 ps	100 ps
AB1	2.2	4.5	7.8	11.8	1.7	1.8	1.9	2.0
AB2	2.2	4.5	7.8	12.3	1.7	1.8	1.9	2.1
AB3	2.3	4.2	8.1	11.9	1.7	1.8	1.8	2.0
AB4	2.3	5.3	8.2	11.9	1.8	1.9	2.0	2.1
AB5	2.2	5.4	8.4	12.0	1.8	1.8	2.0	2.1
AB6	2.3	4.5	7.3	12.5	1.7	1.8	1.9	2.0
AB7	2.1	4.6	8.3	12.8	1.7	1.8	1.9	2.1
AB8	2.2	4.5	7.4	11.3	1.7	1.8	1.9	2.1
UBQ	2.0	4.4	7.3	11.6	1.6	1.7	1.7	1.9
bulk water	3.3	6.6	10.5	14.9	2.1	2.1	2.2	2.2

Table 4.3. Peak positions of P((r);t) and peak heights of $P(\log_{10}(r); t)$ (in Å) for the first hydration layer water molecules around different Aβ peptide conformations and UBQ. As a reference, the corresponding data for pure bulk water are also listed.

It is evident from the above discussion that the water molecules hydrating the flexible Aβ monomers exhibit relatively faster mobility as compared to those around the globular protein UBQ. To obtain a more quantitative understanding of the effects of conformational heterogeneities of the Aβ conformers on the diffusive behavior of the hydration water molecules, we have directly probed water translational motions by

calculating their mean square displacements (MSD), as a function of time. MSD is defined as,

$$\left\langle \Delta r^2 \right\rangle = \left\langle \left| r_i(t) - r_i(0) \right|^2 \right\rangle \tag{4.2}$$

where r_i(t) and r_i(0) are the position vectors of the oxygen atom of the *i*-th water molecule present in the first hydration layer at time *t* and at *t* = 0, respectively. The angular brackets denote that the averaging is carried out over different time origins and over the tagged water molecules. The calculations are carried out for water molecules around different Aβ monomers and UBQ, and the results are shown in Figure 4.5. The corresponding result for pure bulk water is included in the figure for comparison.

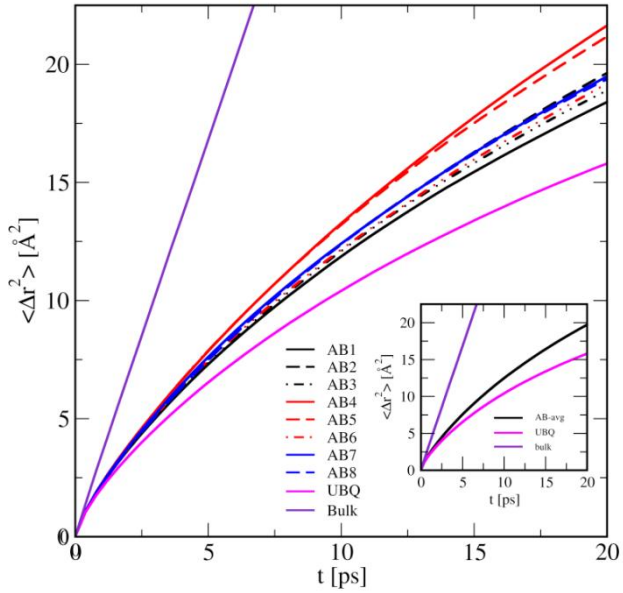

Figure 4.5. Mean square displacement (MSD) of water molecules present in the first hydration layers of different Aβ peptide conformations and UBQ. The MSD of water in pure bulk state is shown for comparison. The results for UBQ, pure bulk water, and that averaged over the Aβ monomers are also included in the inset.

We have also calculated water MSD averaged over all the Aβ monomers, as shown in the inset of the figure. It can be seen that compared to water in pure bulk phase, translational motions of water molecules present in the hydration layers of conformationally disordered Aβ monomers and the globular UBQ are significantly restricted. Such restricted water motions at biomolecular interfaces are well known.[35,69,72-74] Importantly, we notice that though water motions around the Aβ monomers are distinctly faster than that around UBQ, heterogeneity in solvent dynamical environment exists around the Aβ

conformations. The calculations reveal that although the differences are small, but among the 8 Aβ conformations studied, water molecules around AB1 exhibit the slowest and those around AB4 exhibit the fastest motions. It may be noted that unlike a globular protein, such as UBQ, Aβ being an IDP does not have a unique three-dimensional structure, and exhibits fluctuations among different conformations separated by low energy barriers under physiological conditions.[2,75] The present results along with the distributions of van Hove function as discussed earlier (Figure 4.4) show that the intrinsic flexibility of Aβ and its frequent oscillations among different conformational states lead to relatively more dynamic hydration layer around it as compared to that around UBQ. The results further suggest that the flexibility of Aβ leads to nonuniform degree of confinement around its different conformations, thereby affecting the hydration water motions heterogeneously. We believe that the relatively more dynamic nature of the hydration layers around Aβ monomers is an important observation, as the water molecules in the vicinity of the monomers can then be easily displaced during the dewetting transition associated with the fibrillation process in amyloid pathology.[19]

We have calculated the diffusion coefficients (D_E) of water molecules hydrating the Aβ monomers and UBQ from the slopes of the corresponding MSD curves using the Einstein's formulation,[76]

$$D_E = \lim_{\Delta t \to \infty} \frac{\left\langle \Delta r^2 \right\rangle}{2d\Delta t} \tag{4.3}$$

where d is the dimensionality of the system. The D_E values obtained along with that averaged over the Aβ monomers and for pure bulk water are listed in Table 4.4. It is apparent from the data that with respect to bulk water the translational mobility of hydration water around UBQ is about 7 times slower, while the extent of retardation around the Aβ monomers is 4 to 5.5 times (average D_E value being 4.9 times lower). Besides, the water molecules around the Aβ monomers are found to diffuse on a time scale 23-60 % faster than those around UBQ. Heterogeneous translational motions among the Aβ hydration water molecules are also evident from the data. We find that the water molecules around the AB4 monomer exhibit 30 % faster translational mobility as compared to the slowest moving water around AB1. It may be noted that the diffusion of water in the vicinity of a large macromolecule is in general sublinear in nature.[69] Therefore, relative comparisons between the D_E values as discussed above are more meaningful than their absolute values.

conf.	D_E (10^{-5} cm^2s^{-1})	$<\tau_\mu>$ (ps)
AB1	1.01	11.03
AB2	1.12	9.30
AB3	1.05	10.82
AB4	1.31	8.09
AB5	1.24	9.08
AB6	1.10	9.55
AB7	1.10	8.65
AB8	1.07	10.58
AB-avg	1.13 (0.05)	9.64 (0.46)
UBQ	0.82	13.50
bulk water	5.52	1.92

Table 4.4. The translational diffusion coefficients (D_E) and average reorientational time constants ($<\tau_\mu>$) of the first hydration layer water molecules around different Aβ peptide conformations and UBQ. The corresponding data averaged over the Aβ monomers (AB-avg) and that for pure bulk water are listed for comparison.

4.3.2.2 Rotational Dynamics

We now investigate the influence of heterogeneous conformational fluctuations of the Aβ peptide conformers on the rotational motions of water molecules hydrating their surfaces. Once again, the results are compared with that observed for the UBQ system. The calculations are carried out by measuring the time scale of reorientations of water dipoles, $\hat{\mu}$, defined as the unit vector connecting the oxygen atom of a water molecule to the center of the line joining the two hydrogen atoms. Time evolution of $\hat{\mu}$ has been studied by measuring the dipole-dipole time correlation function (TCF), $C_\mu(t)$, defined as

$$C_\mu(t) = \frac{\langle \hat{\mu}_i(0).\hat{\mu}_i(t) \rangle}{\langle \hat{\mu}_i(0).\hat{\mu}_i(0) \rangle} \tag{4.5}$$

Here, $\hat{\mu}_i(t)$ is the unit dipole moment vector of the i^{th} water molecule at time t. Again, the calculations are carried out by averaging over the water molecules selected at different reference initial times. The results obtained for the water molecules hydrating the Aβ monomers and UBQ are displayed in Figure 4.6. For comparison, the result for pure bulk

water is also included in the figure. $C_\mu(t)$ averaged over all the Aβ conformations are shown in the inset of the figure.

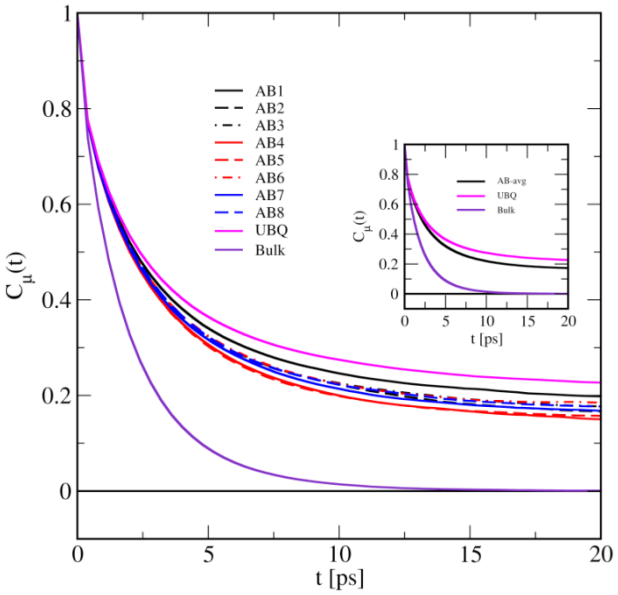

Figure 4.6. Reorientational time correlation function, $C_\mu(t)$, of water molecules present in the first hydration layers of different Aβ peptide conformations and UBQ. The corresponding function for water in pure bulk state is shown for comparison. The results for UBQ, pure bulk water, and that averaged over the Aβ monomers are also included in the inset.

First, it can be seen that the rotational motions of water molecules present in the first hydration layers around the Aβ monomers and the UBQ are significantly restricted. Consistent with the translational diffusion, the rotational motions of water molecules hydrating UBQ are also affected to a greater extent. Importantly, comparison of the results with that shown in Figure 4.6 reveals that the relative degree of heterogeneity in water rotational motions around different conformations of the Aβ peptide is similar to that noticed for their translational motions. Therefore, the conformational flexibility of the Aβ peptide affects both translational and rotational motions of hydration layer water molecules in a similar fashion.

The slow long-time decay of the $C_\mu(t)$ curves as evident from Figure 4.6 can be described by a multi-exponential law. We have fitted each of the decay curves with triexponentials of the form,

$$C_\mu(t) = \sum_{i=1}^{3} A_i e^{-t/\tau_i} \qquad (4.6)$$

where τ_i and A_i are the corresponding time constants and amplitudes, respectively. The amplitude-weighted average water reorientational times ($<\tau_\mu>$) as obtained from such fits for different Aβ monomers and UBQ are listed in Table 4.4. For comparison, the data for pure bulk water and that averaged over all the Aβ conformations are also listed in the table. Compared to water in pure bulk state, significant longer duration taken by hydration water molecules to reorient themselves is clearly evident from the data. With respect to bulk water, we find that water molecules around UBQ take about 7 times longer to reorient, while those around the Aβ monomers take 4-6 times longer durations. However, the water molecules hydrating the flexible Aβ monomers reorient on a time scale 18-40 % faster than that for UBQ. Once again, among the Aβ monomers, fastest and slowest water reorientations have been noticed around AB4 and AB1, respectively. A comparison between the D_E and the $<\tau_\mu>$ values provide evidence for near-identical relative influence of the Aβ monomers and UBQ on translational and rotational motions of hydration layer water molecules.

4.3.2.3 Role of Conformational Flexibility

One important issue in understanding the hydration behavior of a structurally disordered protein, such as Aβ is the role played by its conformational flexibility on the microscopic properties of the surrounding water layer. We herein attempt to understand such role in the observed heterogeneity in the hydration layer behavior around different Aβ monomer conformations. For that, we have performed two additional simulations with the Aβ conformations whose hydration waters exhibit the fastest (AB4) and the slowest (AB1) translational motions (see Figure 4.5), by restricting the peptide conformational flexibility with the application of harmonic restraints (2 kcal mol^{-1} $Å^{-2}$) to their non-hydrogen atoms. These simulations were carried out in the NVT ensemble for 2 ns each following the same protocols as described earlier. In a recent study[74], it is shown that even for a folded globular protein, loss of conformational flexibility leads to an increasingly restricted hydration water motions. In light of this, the UBQ conformation was also similarly restrained and simulated. In Figure 4.7 we compare (a) the distributions of the total PW interaction strength, $E_{tot\text{-}PW}$, and (b) the MSD, $<\Delta r^2>$, for the hydration layer water molecules, between the restrained and the unrestrained systems. As a reference, the data for pure bulk water are included in Figure 4.7b. It can be seen from the results (Figure 4.7a) that the loss in conformational flexibility has a relatively small effect on the net PW interaction strengths. This is evident from the calculated average interaction energies ($<E_{tot\text{-}PW}>$) as listed in Table 4.5.

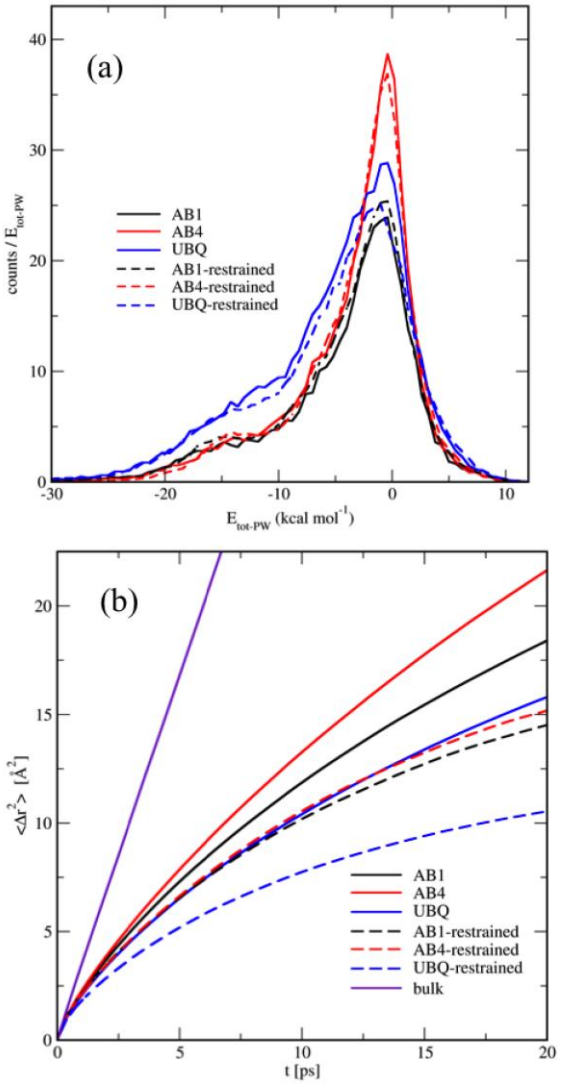

Figure 4.7. Comparison of (a) distributions of the total protein-water interaction strength, $E_{tot\text{-}PW}$, and (b) the mean square displacement (MSD) of the hydration layer water molecules, between the restrained and the flexible Aβ conformations AB1 and AB4, and those of UBQ. The MSD of water in pure bulk state is shown for comparison.

However, we notice that the absence of protein flexibility has a pronounced influence on the degree of restriction of the translational motions of water molecules hydrating the Aβ conformations as well as UBQ. In consistent with our earlier work,[74] the results show that irrespective of whether it is a globular protein or a disordered one, enhanced confinement at the surface on restraining the protein's flexibility results in increasingly restricted hydration water motions.

Type	conf	$< E_{tot\text{-}PW} >$ (kcal mol^{-1})	D_E (10^{-5} cm^2s^{-1})
restrained	AB1	-4.48	0.72
	AB4	-3.60	0.76
	UBQ	-5.46	0.46
flexible	AB1	-4.49	1.01
	AB4	-3.81	1.31
	UBQ	-5.42	0.82

Table 4.5. The average protein-water interaction strength ($<E_{tot\text{-}PW}>$), translational diffusion coefficients (D_E) for the first hydration layer water molecules around the Aβ conformations AB1 and AB4, and UBQ in restrained and flexible systems.

Interestingly, it is found that though the hydration water molecules around restrained AB1 and AB4 exhibit increasingly retarded mobility, but the relative differences between those decrease significantly as compared to the corresponding flexible or unrestrained forms. It is clear that in absence of conformational flexibility, the hydration environment around the Aβ monomers becomes nearly homogeneous. We have calculated the hydration water diffusion coefficients (D_E) following eq. 6 for the restrained systems, which are listed in Table 4.5 along with the corresponding data for the flexible systems. Note that in absence of conformational flexibility, water diffusivity close to the protein surface decreases by 30-45 %. Further, near- identical dynamic environment in the hydration layers of AB1 and AB4 in their restrained forms is clearly evident from the data. Our analysis clearly suggests that the relatively faster heterogeneous water motions around the Aβ monomers as compared to that around UBQ can largely be attributed to higher flexibility of the disordered Aβ conformers, rather than their relatively weaker interactions with surrounding solvent.

4.3.3. Hydrogen Bond Dynamics

It is clear from our discussion so far that the conformational disorders of the Aβ monomers affect the mobility of hydration water molecules in a heterogeneous manner. Such heterogeneous influence of Aβ and UBQ on the dynamics of surrounding water molecules is expected to be coupled with the time scale associated with the formation and breaking of hydrogen bonds at the interface. We examine such influence in this section.

It is known that the presence of a macromolecule like a protein modifies the regular water-water (WW) hydrogen bond network in aqueous solution with the formation of protein-water (PW) hydrogen bonds.[35,69,74] Microscopic information on the dynamics of hydrogen bonds can be obtained from MD simulations through the calculation of different time correlation functions.[77-82] In this section, we investigate the hydrogen bond dynamics around different configurations of Aβ, and compare the results with that observed for UBQ. To study hydrogen bonds, it is necessary to define them first. Either a geometry-based[79,82-85] or an energy-based criterion[41,81,86,87] is commonly used to define a hydrogen bond. In our calculations, we have used appropriate geometric criteria to define PW and WW hydrogen bonds. In this approach, the first condition to form a PW hydrogen bond is that the distance between the participating protein atom (donor or acceptor) and the oxygen atom of the tagged water be within 3.3 Å. The second condition for a protein acceptor atom (X) to form a PW hydrogen bond is that the angle between one of the O–H bond vectors of the water and the vector connecting the water oxygen and X be within 35°. Similarly, for a protein donor atom (Y) to form such hydrogen bond, the angle between Y–H bond vector and the vector connecting Y and the water oxygen should be within 35°. Besides, two water molecules are considered to be hydrogen bonded if their inter-oxygen and nonbonded oxygen-hydrogen distances are within 3.5 Å and 2.45 Å, respectively, and the oxygen–oxygen–hydrogen angle is less than 30°.[79,82,85]

We have investigated the dynamics of hydrogen bonds by calculating two time correlation functions (TCF), namely, the intermittent hydrogen bond TCF ($C(t)$), and the continuous hydrogen bond TCF ($S(t)$). The two functions are defined as[77,78,87]

$$C(t) = \frac{\langle h(0)h(t)\rangle}{\langle h(0)h(0)\rangle} \tag{4.7}$$

and

$$S(t) = \frac{\langle h(0)H(t)\rangle}{\langle h(0)h(0)\rangle} \tag{4.8}$$

The definitions are based on two population variables $h(t)$ and $H(t)$. The variable $h(t)$ is considered to be unity if a particular pair of sites (PW or WW) are hydrogen bonded at time t, and zero, otherwise. On the other hand, $H(t)$ is defined as unity when a particular pair of sites remain continuously hydrogen bonded from time $t = 0$ to a later time t, and zero, otherwise. The angular brackets indicate that the averaging is carried out over all the

hydrogen bonds of a particular type (PW or WW) at different time origins. According to the definitions, $C(t)$ corresponds to the probability that a particular hydrogen bond formed at time $t = 0$ will be found intact at a later time t. It is therefore independent of the history of breaking and reformation of hydrogen bonds at intermediate times. Thus, recrossing of the barrier between the bonded and the nonbonded states and the long-time diffusive behavior are included in $C(t)$. Therefore, $C(t)$ can provide information on the time scale of overall hydrogen bond structural reorganization at the interface. The function $S(t)$, on the other hand, describes the probability that a particular hydrogen bond formed at $t = 0$ remains continuously intact at all times up to t. Hence, $S(t)$ provides a true estimate of the lifetime or the survival time of a hydrogen bond.

We first calculate the intermittent hydrogen bond TCF ($C_{PW}(t)$) for the PW hydrogen bonds formed by the residues of the Aβ monomers and UBQ with water molecules at their surfaces, as shown in Figure 4.8a. In Figure 4.8b we show the relaxation patterns of $C_{WW}(t)$ corresponding to the WW hydrogen bonds formed by the first hydration layer water molecules around the proteins. In the insets, we compare the relaxations of $C_{PW}(t)$ and $C_{WW}(t)$ averaged over all the Aβ conformations with that obtained for UBQ. As a reference, the decay of $C_{WW}(t)$ for WW hydrogen bonds in pure bulk water is included in both the figures.

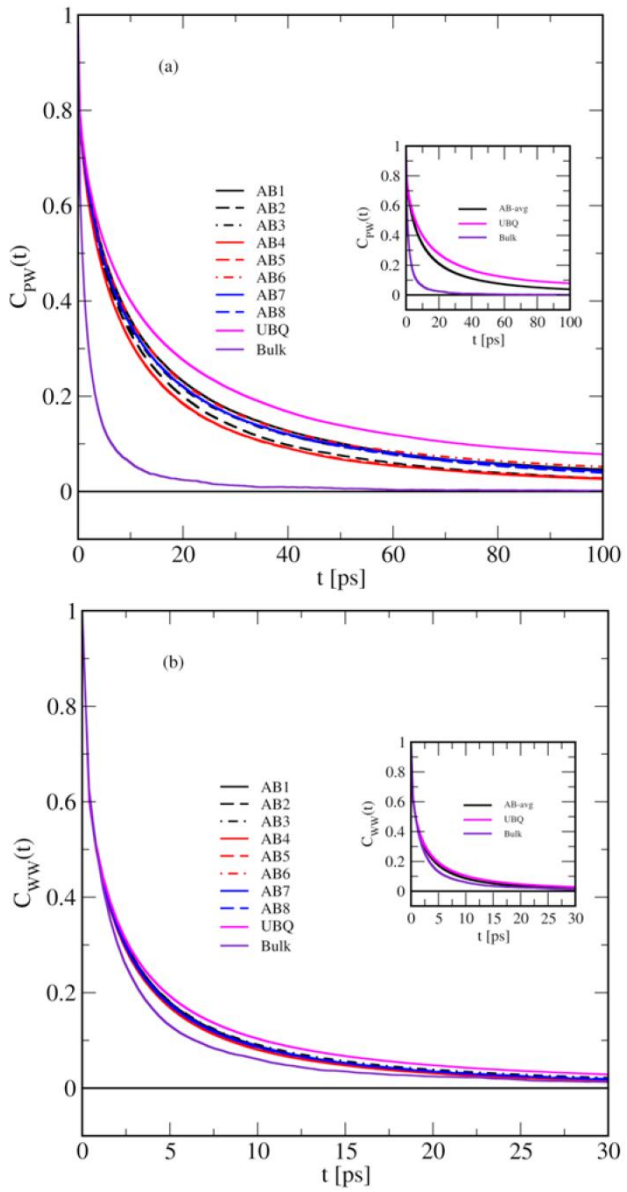

Figure 4.8.(a) Intermittent time correlation function, $C_{PW}(t)$, for the PW hydrogen bonds formed between water molecules and the residues of different Aβ peptide conformations and UBQ. (b) The corresponding function, $C_{WW}(t)$, for the WW hydrogen bonds formed by the first hydration layer water molecules around different Aβ peptide conformations and UBQ. The function $C_{WW}(t)$ for water in pure bulk state is shown for comparison. The results for UBQ, pure bulk water, and that averaged over the Aβ monomers are also included in the insets.

It is evident from the results that regardless of whether the hydration water molecules are involved in PW or WW hydrogen bonds, the relaxations of $C(t)$ are always slower with longer relaxation times than that of bulk water, the effect being more prominent for the PW hydrogen bonds. Such slower relaxations of hydrogen bonds involving the first

hydration layer water molecules correlate well with their restricted translational and rotational motions, as discussed earlier (see Figures 4.5 and 4.6). Importantly, the relaxation of PW hydrogen bonds formed by the UBQ residues is noticeably slower than that corresponding to the Aβ monomers (Figure 4.8a). Besides, a heterogeneous time scale of PW hydrogen bond relaxation among different Aβ monomers is evident from the data. Interestingly, the WW hydrogen bonds formed by the first hydration layer water molecules around the Aβ monomers exhibit near-homogeneous dynamics that is marginally faster than that around UBQ, as observed in Figure 4.8b. This is an important finding, which shows that the heterogeneous motions of water molecules present in the first hydration layers of the Aβ monomers as discussed earlier correlate well with slow non-uniform relaxations of PW hydrogen bonds formed at the protein surfaces. Note that, such non-uniform relaxations of PW hydrogen bonds among the Aβ monomers once again confirm heterogeneous degree of confinement around their fluctuating configurations. To obtain estimates of the PW and WW hydrogen bond relaxation times, we have once again fitted each of the decay curves in Figure 4.8 with triexponentials (eq. 8). The amplitude-weighted average relaxation times ($<\tau_c^{PW}>$ and $<\tau_c^{WW}>$) as obtained from such fits are listed in Table 4.6. For comparison, the corresponding value for pure bulk water and that obtained by averaging over all the Aβ monomers are also listed in the table. It is clear from the data that compared to bulk water, the PW hydrogen bonds take longer durations to relax. In particular, the average relaxation time of PW hydrogen bonds formed by UBQ is 8.5 times more than bulk water, whereas the corresponding hydrogen bonds formed by the Aβ monomers take 4.5-6.5 times longer to relax. Significant heterogeneity in PW hydrogen bond environment around the flexible Aβ monomers is also evident from the corresponding $<\tau_c^{PW}>$ values. Note that compared to the PW hydrogen bonds, the WW hydrogen bonds formed by the first hydration layer water molecules take only marginally longer times (~30 % longer for UBQ and 5-17 % for Aβ monomers) to relax than that for water in pure bulk state. In Figure 4.9 we show the relaxations of continuous hydrogen bond TCFs ($S_{PW}(t)$ and $S_{WW}(t)$) corresponding to the PW and WW hydrogen bonds around the Aβ monomers and UBQ. The data averaged over all the Aβ conformations have also been calculated as shown in the insets. The result for pure bulk water is once again included in the figure as a reference. It can be seen from Figure 4.9a that for each system the function $S_{PW}(t)$ relaxes slowly as compared to bulk water, thereby indicating longer lifetimes of PW hydrogen bonds. Interestingly, unlike

$C_{PW}(t)$, we do not observe any distinct difference in the relaxation patterns of $S_{PW}(t)$ between the Aβ monomers among themselves and that between UBQ and Aβ. The $S_{WW}(t)$ decay curves for the WW hydrogen bonds involving the hydration water molecules show even more interesting behavior.

conf.	$<\tau_c^{PW}>$ (ps)	$(<\tau_c^{WW}>)$ (ps)
AB1	18.06	3.27
AB2	14.58	3.21
AB3	17.02	3.42
AB4	13.63	3.07
AB5	13.49	3.10
AB6	19.03	3.23
AB7	17.72	3.23
AB8	16.95	3.30
AB-avg	16.31 (0.99)	3.23 (0.05)
UBQ	24.86	3.83
bulk water	-	2.93

Table 4.6. Average relaxation times as obtained from the intermittent PW ($<\tau_c^{PW}>$) and WW ($<\tau_c^{WW}>$) hydrogen bond TCFs for the water molecules present in the first hydration layers around different Aβ peptide conformations and UBQ. The corresponding data averaged over the Aβ monomers (AB-avg) and that for pure bulk water are listed for comparison.

It is evident from Figure 4.9b that compared to bulk water the function relaxes noticeably slowly for UBQ. On the other hand, the results for water around the Aβ monomers are found to be almost indistinguishable from that of water in pure bulk state. Again, we have fitted each of the $S_{PW}(t)$ and $S_{WW}(t)$ decay curves with triexponentials (eq. 8) and calculated the amplitude-weighted average lifetimes of the PW and WW hydrogen bonds ($<\tau_s^{PW}>$ and $<\tau_s^{WW}>$), which are listed in Table 4.7. As before, the lifetime of WW hydrogen bonds in pure bulk state and that obtained by averaging over all the Aβ monomers are also listed in the table. It can be seen that compared to bulk water, the PW hydrogen bonds in general exhibit 2-3 times longer lifetimes. On the other hand, though

the WW hydrogen bonds around globular UBQ survive ~40 % longer since their formations, but there is hardly any distinction between the WW hydrogen bond survival times in the hydration layers of the Aβ monomers and that in pure bulk state.

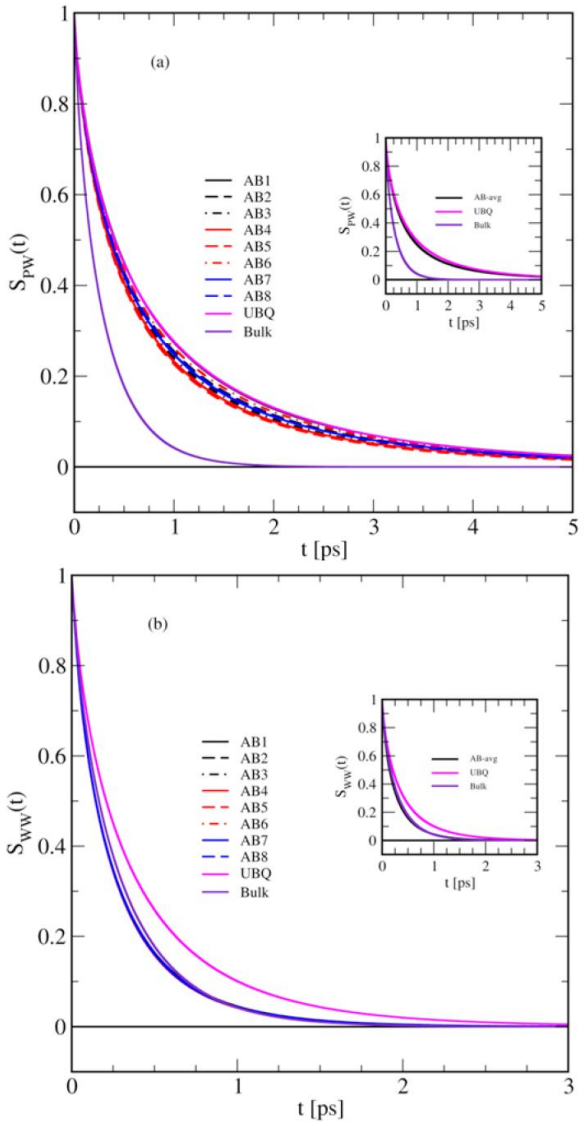

Figure 4.9. (a) Continuous time correlation function, $S_{PW}(t)$, for the PW hydrogen bonds formed between water molecules and the residues of different Aβ peptide conformations and UBQ. (b) The corresponding function, $S_{WW}(t)$, for the WW hydrogen bonds formed by the first hydration layer water molecules around different Aβ peptide conformations and UBQ. The function $S_{WW}(t)$ for water in pure bulk state is shown for comparison. The results for UBQ, pure bulk water, and that averaged over the Aβ monomers are also included in the insets.

Let us attempt to explain the origin of the heterogeneous influence of the proteins on the relaxations of intermittent and continuous hydrogen bond TCFs, as observed above. We already mentioned that the functions $S_{PW}(t)$ and $S_{WW}(t)$ provide absolute estimates of the average durations over which PW and WW hydrogen bonds would survive since their formations, and are independent of water translational and rotational motions. Therefore, the relaxation time scales of these functions should depend on hydrogen bond strengths.

conf.	$<\tau_s^{PW}>$ (ps)	$(<\tau_s^{WW}>)$ (ps)	$(<E_{PW}>)$ (kcal/mol)	$(<E_{WW}>)$ (kcal/mol)
AB1	0.88	0.27	-8.43	-4.08
AB2	0.83	0.27	-8.26	-4.08
AB3	0.75	0.27	-7.52	-4.08
AB4	0.67	0.27	-7.35	-4.08
AB5	0.56	0.27	-7.15	-4.08
AB6	0.85	0.27	-7.54	-4.08
AB7	0.79	0.27	-7.69	-4.08
AB8	0.82	0.27	-7.39	-4.08
AB-avg	0.77 (0.05)	0.27	-7.67 (0.21)	-4.08
UBQ	0.89	0.39	-8.18	-4.06
bulk water	-	0.28		-4.20

Table 4.7. Average relaxation times as obtained from the continuous PW ($<\tau_s^{PW}>$) and WW ($<\tau_s^{WW}>$) hydrogen bond TCFs for the water molecules present in the first hydration layers along with the average interaction energy between a protein residue and a water molecule hydrogen-bonded to It ($<E_{PW}>$) and that between a pair of hydrogen-bonded water molecules ($<E_{WW}>$) around different Aβ peptide conformations and UBQ. The corresponding data averaged over the Aβ monomers (AB-avg) and that for pure bulk water are listed for comparison.

Using the definitions of hydrogen bonds, we have calculated the average interaction energy between a water molecule and the residue of the protein (Aβ or UBQ) (E_{PW}) with which it is hydrogen-bonded. Similarly, the average interaction energy of a pair of

hydrogen-bonded water molecules (E_{WW}) present either in the hydration layer or in the bulk state is also computed. The calculated values are listed in Table 4.7. The energy values averaged over the Aβ monomers are also listed for comparison. It can be seen that on average a PW hydrogen bond is about 2 times stronger than a WW hydrogen bond. Therefore, a PW hydrogen bond once formed at the surface of a protein (Aβ or UBQ) survives longer than a WW hydrogen bond due to its greater strength. Interestingly, we notice that despite identical residue sequence, as observed in case of average total interaction energy between a water molecule in the hydration layer and the protein surface, the PW hydrogen bond strengths among the Aβ monomers are noticeably different (within 10% with respect to the average value). It is known that appropriate geometrical orientation between a residue and a water molecule is necessary to form a PW hydrogen bond. The results indicate that due to heterogeneous conformational features of the Aβ monomers and the degree of confinement around them, the relative orientations of PW hydrogen-bonded pairs are different. As a result the PW hydrogen bond strengths and hence their average lifetimes differ among the Aβ monomers. Note that unlike $<E_{tot\text{-}PW}>$ (see Table 4.2), $<E_{PW}>$ is independent of the size or the number of residues of the protein. However, due to different primary amino acid sequence and their types, $<E_{PW}>$ values between Aβ and UBQ are to a small extent different with PW hydrogen bonds formed by UBQ being marginally stronger than those formed by Aβ. In contrast to the PW hydrogen bonds, we notice identical hydrogen-bonded water pair interaction energy, similar to that for the bulk state, around the Aβ monomers. This is reflected in identical bulk-like WW hydrogen bond lifetimes around them. Surprisingly, despite similar WW hydrogen bond energy near UBQ, these hydrogen bonds survive over relatively longer durations as mentioned before. We believe that such differences in WW hydrogen bond lifetimes around UBQ and Aβ monomers arise due to heterogeneous confinement around them. As already discussed, UBQ with more compact secondary structures can confine hydrogen-bonded water molecules present in its hydration layer more effectively than the disordered Aβ conformations. As a result, hydration layer water molecules around UBQ although form WW hydrogen bonds of similar strength, but they survive over longer periods.

It may be noted that the hydrogen bond properties often depend on their definitions. To verify such dependence on WW hydrogen bond lifetimes, if any, we have recalculated the function $S_{WW}(t)$ for the hydration water molecules around the Aβ monomers and UBQ using an energy-based criterion[87] to define such bonds. According to

this criterion, a WW hydrogen bond is said to have formed if the distance between the oxygen atoms of two water molecules is within 3.5 Å, and the pair energy is less than -2.5 kcal mol^{-1}. Comparison of the results (Figure AII-4, and Table AII-2 in Appendix II) with that discussed above (Figure 4.9b and Table 4.7) clearly shows that the relaxation patterns of $S_{WW}(t)$ and hence the lifetimes of WW hydrogen bonds ($<\tau_s^{WW}>$) around the Aβ monomers are nearly independent of their definition. In contrast, however, we notice that the average WW hydrogen bond lifetime around UBQ depends on the criterion used to define those bonds. In fact, the energy-based criterion leads to relatively shorter $<\tau_s^{WW}>$ in the hydration layer of UBQ, which becomes same as that obtained around the Aβ conformations (Table AII-2). It is clear from the results that the energy-based criterion avoids the influence of nonuniform confinement around the flexible Aβ conformations and compact UBQ as observed in Figure 4.9b. This is an important observation which however, needs to be investigated further.

4.3.4. Water Density Fluctuations

Before concluding, we attempt to obtain preliminary insights into how the observed nonuniform hydration behavior between the Aβ conformers and UBQ are correlated with the nature of the protein surface. Recent research shows a close association of the water density fluctuations in the vicinity of a surface with the physico-chemical nature of the surface.[88-90] It has been shown that water densities within small probe volumes in close vicinity of a surface have Gaussian distributions whose widths increase with increasing surface hydrophobicity. In the case of biomolecules, enhanced water density fluctuation near hydrophobic surfaces can alter interactions and functions.[90] As hydrophobicity plays important roles in the behavior of Aβ,[13,19,66] it may therefore be worthwhile to compare water density fluctuations close to the surface of the Aβ conformers with that around UBQ. From our simulation snapshots, we obtained the water number densities within a probe volume approximated as the product of the SASA and 3 Å. For ease of comparison, we obtained *P(n*),* which is the probability distribution of the water number density divided by the mean density, *n**, normalized by the maximum probability. In Figure 4.10, we have plotted *P(n*)* as a function of *n** fitted to the Gaussian form,

$$P(n^*) = e^{-\frac{(n^*-1)^2}{\alpha}} \qquad (4.9)$$

We have listed the values of α for each of the Aβ conformers and UBQ in Table 4.8.

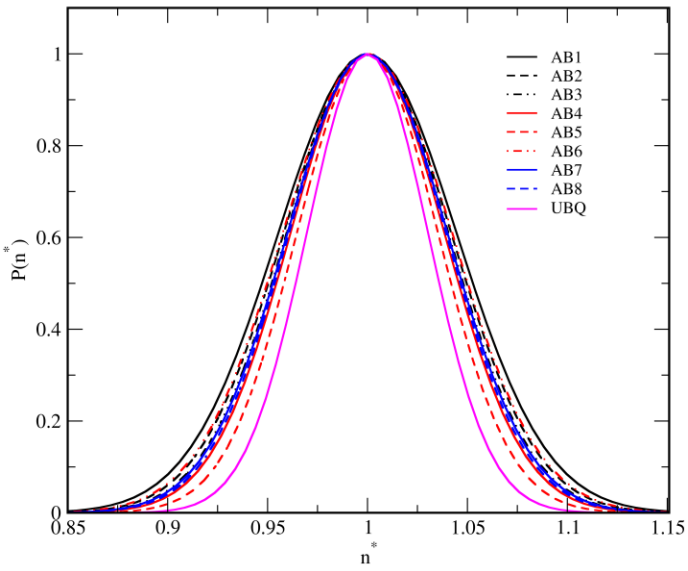

Figure 4.10. Probability distributions of water densities near the surfaces of different Aβ peptide conformations and UBQ fitted to the Gaussian form.

conf.	α (10^{-3})
AB1	4.018
AB2	3.540
AB3	3.316
AB4	2.990
AB5	2.520
AB6	3.638
AB7	3.239
AB8	3.110
UBQ	1.860

Table 4.8. The Values of α Obtained From Fits of the Water Density Distribution $P(n^*)$ to Eq. 11 for the Aβ Peptide Conformations and UBQ.

The distribution corresponding to each Aβ conformer is found to be broader than that obtained for UBQ, demonstrating the overall higher surface hydrophobicity of the Aβ sequence. Interestingly, the water density distributions of the individual Aβ conformations are not identical, with the distributions being marginally narrower for the conformations with lower secondary structural content. This analysis suggests that the

conformational propensities are associated with both surface hydrophobicity as well as the dynamical behavior of the hydration layer. Further investigations that develop and employ more rigorous definitions of the probe volume could help reveal the interplay of conformational fluctuations and surface hydrophobicity and their relationship with the hydration layer behaviors of disordered proteins.

4.4 Conclusions

In this article, we have analyzed the microscopic association of the protein hydration layer with putative Aβ conformations and with the natively folded state of ubiquitin (UBQ), a small globular protein, using atomistic MD simulations. Compared to UBQ, the Aβ monomers demonstrate marginally weaker association with the hydration layer. Detailed analyses of the dynamical behavior of the hydration layers show that the water molecules hydrating the Aβ conformations exhibit faster translational and rotational motions compared to those hydrating UBQ. The heterogeneous motions of the Aβ hydration water molecules are found to be correlated with the relaxation time scales of protein-water (PW) and water-water (WW) hydrogen bonds at the interfaces. It is demonstrated that though the average survival time of a PW hydrogen bond around Aβ and UBQ are nearly the same, the non-uniform influence of the two proteins on water dynamics leads to heterogeneous time scales of overall structural relaxation of PW hydrogen bonds. Further, it is found that the structural variation in Aβ leads to changes in the hydration layer dynamics. Thus, conformational fluctuations and alterations in the degree of surface exposure can affect coupling of the Aβ peptide with the hydration layer and lead to an overall increase in the heterogeneous behavior of the hydration water molecules.

Our results are of biological significance in studies of Aβ self-assembly, where hydration water has been shown to play crucial roles in early oligomeric assembly and in protofibrillar stability.[15,19] The entropic contribution of the hydration waters upon release into the bulk phase is one of the key factors that drive early self-assembly.[21,91,92] Thus, the relative effects of the protein surface on the dynamical behavior of its surrounding water molecules could be an important indicator of its aggregation propensity. However, it remains to be investigated if the observed differences relative to a folded protein are representative of general IDP hydration or is unique to the Aβ peptide. This will require further studies of microscopic hydration properties of multiple IDP sequences of varying surface topology, and detailed investigations of how the key domains associated with

their self-assembly influence local as well as overall hydration dynamics. Some of these aspects are under active investigation in our laboratory.

4.5 References

(1) Dyson, H. J.; Wright, P. E., Intrinsically Unstructured Proteins and Their Functions. *Nat. Rev. Mol. Cell. Biol.* **2005**, *6*, 197-208.

(2) Tompa, P., Intrinsically Disordered Proteins: a 10-Year Recap. *Trends Biochem. Sci.* **2012**, *37*, 509-516.

(3) Ball, K. A.; Phillips, A. H.; Nerenberg, P. S.; Fawzi, N. L.; Wemmer, D. E.; Head-Gordon, T., Homogeneous and Heterogeneous Tertiary Structure Ensembles of Amyloid-β Peptides. *Biochemistry* **2011,** *50*, 7612-7628.

(4) Lin, Y.-S.; Bowman, G. R.; Beauchamp, K. A.; Pande, V. S., Investigating How Peptide Length and a Pathogenic Mutation Modify the Structural Ensemble of Amyloid Beta Monomer. *Biophys. J.* **2012**, *102*, 315-324.

(5) Fisher, C. K.; Ullman, O.; Stultz, C. M., Comparative Studies of Disordered Proteins with Similar Sequences: Application to Aβ40 and Aβ42. *Biophys. J* **2013,** *104* , 1546-1555.

(6) Haass, C.; Selkoe, D. J., Soluble Protein Oligomers in Neurodegeneration: Lessons from the Alzheimer's Amyloid β-Peptide. *Nat. Rev. Mol. Cell. Biol.* **2007**, *8*, 101-112.

(7) Crescenzi, O.; Tomaselli, S.; Guerrini, R.; Salvadori, S.; D'Ursi, A. M.; Temussi, P. A.; Picone, D., Solution structure of the Alzheimer Amyloid B-Peptide (1–42) In An Apolar Microenvironment. *Eur. J. Biochem.* **2002**, *269*, 5642-5648.

(8) Tomaselli, S.; Esposito, V.; Vangone, P.; van Nuland, N. A.; Bonvin, A. M.; Guerrini, R.; Tancredi, T.; Temussi, P. A.; Picone, D., The Alpha-to-Beta Conformational Transition of Alzheimer's Abeta-(1-42) Peptide in Aqueous Media is Reversible: a Step by Step Conformational Analysis Suggests the Location of Beta Conformation Seeding. *ChemBioChem* **2006**, *7*, 257-267.

(9) Sgourakis, N. G.; Yan, Y.; McCallum, S. A.; Wang, C.; García, A. E., The Alzheimer's Peptides Aβ 40 and 42 Adopt Distinct Conformations in Water: a Combined MD / NMR Study. *J. Mol. Biol.* **2007**, *368*, 1448-1457.

(10) Hou, L.; Shao, H.; Zhang, Y.; Li, H.; Menon, N. K.; Neuhaus, E. B.; Brewer, J. M.; Byeon, I.-J. L.; Ray, D. G.; Vitek, M. P.; et al. Solution NMR Studies of the Aβ(1−40) and Aβ(1−42) Peptides Establish that the Met35 Oxidation State Affects the Mechanism of Amyloid Formation. *J. Am. Chem. Soc* **2004**, *126*, 1992-2005.

(11) Massi, F.; Straub, J. E., Energy Landscape Theory for Alzheimer's Amyloid B-Peptide Fibril Elongation. *Proteins: Struct., Funct., Bioinf.* **2001**, *42*, 217-229.

(12) Pellarin, R.; Caflisch, A., Interpreting the Aggregation Kinetics of Amyloid Peptides. *J. Mol. Biol.* **2006**, *360*, 882-892.

(13) Reddy, G.; Straub, J. E.; Thirumalai, D., Dynamics of Locking of Peptides onto Growing Amyloid Fibrils. *Proc. Natl. Acad. Sci. U.S.A.* **2009**, *106*, 11948-11953.

(14) Miller, Y.; Ma, B.; Nussinov, R., Polymorphism in Alzheimer Aβ Amyloid Organization Reflects Conformational Selection in a Rugged Energy Landscape. *Chem. Rev.* **2010**, *110*, 4820-4838.

(15) Thirumalai, D.; Reddy, G.; Straub, J. E., Role of Water in Protein Aggregation and Amyloid Polymorphism. *Acc. Chem. Res.* **2012**, *45*, 83-92.

(16) van der Wel, P. C. A.; Lewandowski, J. z. R.; Griffin, R. G., Solid-State NMR Study of Amyloid Nanocrystals and Fibrils Formed by the Peptide GNNQQNY from Yeast Prion Protein Sup35p. *J. Am. Chem. Soc* **2007**, *129*, 5117-5130.

(17) Shen, C. L.; Murphy, R. M., Solvent Effects on Self-Assembly of Beta-Amyloid Peptide. *Biophys. J.* **1995**, *69*, 640-651.

(18) Tran, H. T.; Mao, A.; Pappu, R. V., Role of Backbone-Solvent Interactions in Determining Conformational Equilibria of Intrinsically Disordered Proteins. *J. Am. Chem. Soc* **2008**, *130*, 7380-7392.

(19) Krone, M. G.; Hua, L.; Soto, P.; Zhou, R.; Berne, B. J.; Shea, J.-E., Role of Water in Mediating the Assembly of Alzheimer Amyloid-Baβ16-22 Protofilaments. *J. Am. Chem. Soc* **2008**, *130*, 11066-11072.

(20) Zheng, J.; Jang, H.; Ma, B.; Tsai, C.-J.; Nussinov, R., Modeling the Alzheimer Aβ17-42 Fibril Architecture: Tight Intermolecular Sheet-Sheet Association and Intramolecular Hydrated Cavities. *Biophys. J.* **2007,** *93*, 3046-3057.

(21) Chong, S.-H.; Ham, S., Impact of Chemical Heterogeneity on Protein Self-Assembly in Water. *Proc. Natl. Acad. Sci. U.S.A.* **2012**, *109*, 7636-7641.

(22) Pal, S. K.; Peon, J.; Bagchi, B.; Zewail, A. H., Biological Water:Femtosecond Dynamics of Macromolecular Hydration. *J. Phys. Chem. B* **2002**, *106*, 12376-12395.

(23) Halle, B., Protein Hydration Dynamics in Solution: a Critical Survey. *Philos. Trans. R. Soc. Lond. B: Biol. Sci.* **2004**, *359*, 1207-1224.

(24) Bandyopadhyay, S.; Chakraborty, S.; Bagchi, B., Exploration of the Secondary Structure Specific Differential Solvation Dynamics Between the Native And Molten Globule States of the Protein HP-36. *J. Phys. Chem. B* **2006**, *110*, 20629-20634.

(25) Ebbinghaus, S.; Kim, S. J.; Heyden, M.; Yu, X.; Heugen, U.; Gruebele, M.; Leitner, D. M.; Havenith, M., An Extended Dynamical Hydration Shell Around Proteins. *Proc. Natl. Acad. Sci. U.S.A.* **2007**, *104*, 20749-20752.

(26) Li, T.; Hassanali, A. A.; Kao, Y.-T.; Zhong, D.; Singer, S. J., Hydration Dynamics and Time Scales of Coupled Water−Protein Fluctuations. *J. Am. Chem. Soc* **2007**, *129*, 3376-3382.

(27) Bhattacharyya, K., Nature of Biological Water: A Femtosecond Study. *Chem. Commun.* **2008**, *25*, 2848-2857.

(28) Sengupta, N.; Jaud, S.; Tobias, D. J., Hydration Dynamics in a Partially Denatured Ensemble of the Globular Protein Human α-Lactalbumin Investigated with Molecular Dynamics Simulations. *Biophys. J.* **2008**, *95*, 5257-5267.

(29) Nandi, N.; Bagchi, B., Dielectric Relaxation of Biological Water. *J. Phys. Chem. B* **1997,** *101*, 10954-10961.

(30) Bagchi, B., Water Dynamics in the Hydration Layer around Proteins and Micelles. *Chem. Rev* **2005,** *105*, 3197-3219.

(31) Fenimore, P. W.; Frauenfelder, H.; McMahon, B. H.; Parak, F. G., Slaving: Solvent Fluctuations Dominate Protein Dynamics and Functions. *Proc. Natl. Acad. Sci. U.S.A.* **2002**, *99*, 16047-16051.

(32) Frauenfelder, H.; Fenimore, P. W.; Chen, G.; McMahon, B. H., Protein Folding is Slaved to Solvent Motions. *Proc. Natl. Acad. Sci. U.S.A.* **2006**, *103*, 15469-15472.

(33) Tarek, M.; Tobias, D. J., Role of Protein-Water Hydrogen Bond Dynamics in the Protein Dynamical Transition. *Phys. Rev. Lett.* **2002**, *88*, 138101.

(34) Sinha, S. K.; Bandyopadhyay, S., Differential Flexibility of the Secondary Structures of Lysozyme and the Structure and Ordering of Surrounding Water Molecules. *J. Chem. Phys.* **2011**, *134*, 115101.

(35) Sinha, S. K.; Bandyopadhyay, S., Local Heterogeneous Dynamics of Water around Lysozyme: a Computer Simulation Study. *Phys. Chem. Chem. Phys.* **2012**, *14*, 899-913.

(36) Fogarty, A. C.; Laage, D., Water Dynamics in Protein Hydration Shells: The Molecular Origins of the Dynamical Perturbation. *J. Phys. Chem. B* **2014**. DOI:10.1021/jp409805p

(37) Kale, L.; Skeel, R.; Bhandarkar, M.; Brunner, R.; Gursoy, A.; Krawetz, N.; Phillips, J.; Shinozaki, A.; Varadarajan, K.; Schulten, K., NAMD2: Greater Scalability for Parallel Molecular Dynamics. *J. Comput. Phys.* **1999**, *151*, 283-312.

(38) Mackerell, A. D., Empirical Force Fields for Biological Macromolecules: Overview and Issues. *J. Comput. Chem.* **2004**, *25*, 1584-1604.

(39) Mackerell, A. D.; Feig, M.; Brooks, C. L., Extending the Treatment of Backbone Energetics in Protein Force Fields: Limitations of Gas-Phase Quantum Mechanics in Reproducing Protein Conformational Distributions in Molecular Dynamics Simulations. *J. Comput. Chem.* **2004**, *25*, 1400-1415.

(40) MacKerell, A. D.; Bashford, D.; Bellott; Dunbrack, R. L.; Evanseck, J. D.; Field, M. J.; Fischer, S.; Gao, J.; Guo, H.; Ha, S.; Joseph-McCarthy, D.; et al. All-Atom Empirical Potential for Molecular Modeling and Dynamics Studies of Proteins. *J. Phys. Chem. B* **1998**, *102*, 3586-3616.

(41) Jorgensen, W. L.; Chandrasekhar, J.; Madura, J. D.; Impey, R. W.; Klein, M. L., Comparison of Simple Potential Functions for Simulating Liquid Water. *J. Chem. Phys.* **1983**, *79*, 926-935.

(42) Feller, S. E.; Zhang, Y.; Pastor, R. W.; Brooks, B. R., Constant Pressure Molecular Dynamics Simulation: the Langevin Piston Method. *J. Chem. Phys.* **1995**, *103*, 4613-4621.

(43) Ryckaert, J.-P.; Ciccotti, G.; Berendsen, H. J. C., Numerical Integration of the Cartesian Equations of Motion of a System with Constraints: Molecular Dynamics of N-Alkanes. *J. Comput. Phys.* **1977**, *23*, 327-341.

(44) Essmann, U.; Perera, L.; Berkowitz, M. L.; Darden, T.; Lee, H.; Pedersen, L. G., A Smooth Particle Mesh Ewald Method. *J. Chem. Phys.* **1995**, *103*, 8577-8593.

45) Vijay-Kumar, S.; Bugg, C. E.; Cook, W. J., Structure of Ubiquitin Refined at 1.8 Å Resolution. *J. Mol. Biol.* **1987**, *194*, 531-544.

(46) Zhang, S.; Iwata, K.; Lachenmann, M. J.; Peng, J. W.; Li, S.; Stimson, E. R.; Lu, Y. a.; Felix, A. M.; Maggio, J. E.; Lee, J. P., The Alzheimer's Peptide Aβ Adopts a Collapsed Coil Structure in Water. *J. Struct. Biol.* **2000**, *130*, 130-141.

(47) Lee, C.; Ham, S., Characterizing Amyloid-Beta Protein Misfolding from Molecular Dynamics Simulations with Explicit Water. *J. Comput. Chem.* **2011**, *32*, 349-355.

(48). Sgourakis, N. G.; Merced-Serrano, M.; Boutsidis, C.; Drineas, P.; Du, Z.; Wang, C.; Garcia, A. E., Atomic-Level Characterization of the Ensemble of the Aβ (1-42) Monomer

in Water Using Unbiased Molecular Dynamics Simulations and Spectral Algorithms. *J. mol. biol.* **2011,** *405*, 570-583.

(49) Chong, S.-H.; Yim, J.; Ham, S., Structural Heterogeneity in Familial Alzheimer's Disease Mutants of Amyloid-beta Peptides. *Mol. BioSyst.* **2013,** *9* , 997-1003.

(50) Rosenman, D. J.; Connors, C. R.; Chen, W.; Wang, C.; García, A. E., Aβ Monomers Transiently Sample Oligomer and Fibril-Like Configurations: Ensemble Characterization Using a Combined MD/NMR Approach. *J. Mol. Biol.* **2013**, *425*, 3338-3359.

(51) Miao, Y.; Nichols, S. E.; McCammon, J. A., Free Energy Landscape of G-Protein Coupled Receptors, Explored by Accelerated Molecular Dynamics. *Phys. Chem. Chem. Phys.* **2014,** *16* , 6398-6406.

(52) Okamoto, A.; Yano, A.; Nomura, K.; Higai, S. i.; Kurita, N., Stable Conformation of Full-Length Amyloid-B (1–42) Monomer in Water: Replica Exchange Molecular Dynamics and Ab Initio Molecular Orbital Simulations. *Chem. Phys. Lett.* **2013**, *577*, 131-137.

(53) Olubiyi, O. O.; Strodel, B., Structures of the Amyloid β-Peptides Aβ1–40 and Aβ1–42 as Influenced by pH and a D-Peptide. *J. Phys. Chem. B* **2012**, *116*, 3280-3291.

(54) Sugita, Y.; Okamoto, Y., Replica-Exchange Molecular Dynamics Method for Protein Folding. *Chem. Phys. Lett.* **1999**, *314*, 141-151.

(55) Hamelberg, D.; de Oliveira, C. A. F.; McCammon, J. A., Sampling of Slow Diffusive Conformational Transitions with Accelerated Molecular Dynamics. *J. Chem. Phys.* **2007**, *127*, 155102-155109.

(56) Hamelberg, D.; Mongan, J.; McCammon, J. A., Accelerated Molecular Dynamics: a Promising and Efficient Simulation Method for Biomolecules. *J. Chem. Phys.* **2004**, *120*, 11919-11929.

(57) Markwick, P. R. L.; McCammon, J. A., Studying Functional Dynamics in Bio-Molecules Using Accelerated Molecular Dynamics. *Phys. Chem. Chem. Phys.* **2011**, *13*, 20053-20065.

(58) Strodel, B.; Lee, J. W. L.; Whittleston, C. S.; Wales, D. J., Transmembrane Structures for Alzheimer's Aβ1–42 Oligomers. *J. Am. Chem. Soc.* **2010,** *132*, 13300-13312.

(59) Humphrey, W.; Dalke, A.; Schulten, K., VMD: Visual Molecular Dynamics. *J. Mol. Graphics* **1996**, *14*, 33-38.

(60) Sisodia, S. S., Beta-Amyloid Precursor Protein Cleavage by a Membrane-Bound Protease. *Proc. Natl. Acad. Sci. U.S.A.* **1992,** *89* , 6075-6079.

(61) Baumketner, A.; Bernstein, S. L.; Wyttenbach, T.; Bitan, G.; Teplow, D. B.; Bowers, M. T.; Shea, J.-E., Amyloid B-Protein Monomer Structure: a Computational and Experimental Study. *Protein Sci.* 2006, *15*, 420-428.

(62) Luhrs, T.; Ritter, C.; Adrian, M.; Riek-Loher, D.; Bohrmann, B.; Dobeli, H.; Schubert, D.; Riek, R., 3D Structure of Alzheimer's Amyloid-β (1-42) Fibrils. *Proc. Natl. Acad. Sci. U.S.A.* **2005**, *102*, 17342-17347.

(63) Khandogin, J.; Brooks, C. L., Linking Folding with Aggregation in Alzheimer's β-amyloid Peptides. *Proc. Natl. Acad. Sci. U.S.A.* **2007,** *104*, 16880-16885.

(64) Chatterjee, P.; Sengupta, N., Effect of the A30P Mutation on the Structural Dynamics of Micelle-Bound αSynuclein Released in Water: a Molecular Dynamics Study. *Eur. Biophys. J.***2012,** *41*, 483-489.

(65) Jose, J. C; Sengupta, N., Molecular Dynamics Simulation Studies of the Structural Response of an Isolated Aβ1-42 Monomer Localized in the Vicinity of the Hydrophilic TiO_2 Surface. *Eur. Biophys. J.* **2013**, *42,* 487-494.

(66) Jana, A. K.; Jose, J. C.; Sengupta, N., Critical Roles of Key Domains in Complete Adsorption of Aβ Peptide on Single-Walled Carbon Nanotubes: Insights with Point Mutations and MD Simulations. *Phys. Chem. Chem. Phys.* **2013,** *15*, 837-844.

(67) Jana, A. K.; Sengupta, N., Adsorption Mechanism and Collapse Propensities of the Full-Length, Monomeric Aβ1-42 on the Surface of a Single-Walled Carbon Nanotube: A Molecular Dynamics Simulation Study. *Biophys. J.* **2012**, *102,* 1889-1896.

(68) Sinha, S. K.; Chakraborty, S.; Bandyopadhyay, S., Thickness of the Hydration Layer of a Protein from Molecular Dynamics Simulation. *J. Phys. Chem. B* **2008**, *112*, 8203-8209.

(69) Bizzarri, A. R.; Cannistraro, S., Molecular Dynamics of Water at the Protein-Solvent Interface. *J. Phys. Chem. B* **2002**, *106,* 6617-6633.

(70) Chong, S.-H., Connections of Activated Hopping Processes with the Breakdown of the Stokes-Einstein Relation and with Aspects of Dynamical Heterogeneities. *Phys. Rev. E* **2008**, *78*, 041501.

(71) Flenner, E.; Szamel, G., Relaxation In a Glassy Binary Mixture: Mode-Coupling-Like Power Laws, Dynamic Heterogeneity, and a New Non-Gaussian Parameter. *Phys. Rev. E* **2005**, *72*, 011205.

(72) Rocchi, C.; Bizzarri, A. R.; Cannistraro, S., Water Dynamical Anomalies Evidenced by Molecular-Dynamics Simulations at the Solvent-Protein Interface. *Phys. Rev. E* **1998**, *57*, 3315-3325.

(73) Pizzitutti, F.; Marchi, M.; Sterpone, F.; Rossky, P. J., How Protein Surfaces Induce Anomalous Dynamics of Hydration Water. *J. Phys. Chem. B* **2007**, *111*, 7584-7590.

(74) Pal, S.; Bandyopadhyay, S., Importance of Protein Conformational Motions and Electrostatic Anchoring Sites on the Dynamics and Hydrogen Bond Properties of Hydration Water. *Langmuir* **2013**, *29*, 1162-1173.

(75) Uversky, V. N.; Dunker, A. K., Understanding Protein Non-Folding. *Biochim. Biophys. Acta.* **2010**, *1804*, 1231-1264.

(76) Allen, M. P.; Tidlesley, D. J., Computer Simulation of Liquids; Clarendon : Oxford. **1987**.

(77) Stillinger, F. H., Theory and Molecular Models for Water. *Adv. Chem. Phys* **1975**, *31*, 1-101.

(78) Stillinger, F. H., Water Revisited. *Science* **1980**, *209*, 451-457.

(79) Luzar, A.; Chandler, D., Hydrogen-Bond Kinetics in Liquid Water. *Nature* **1996**, *379*, 55-57.

(80) Luzar, A., Resolving The Hydrogen Bond Dynamics Conundrum. *J. Chem. Phys.* **2000**, *113*, 10663-10675.

(81) Luzar, A., Extent of Inter-Hydrogen Bond Correlations in Water. Temperature Effect. *Chem. Phys.* **2000**, *258*, 267-276.

(82) Luzar, A.; Chandler, D., Effect of Environment on Hydrogen Bond Dynamics in Liquid Water. *Phys. Rev. Lett.* **1996**, *76*, 928-931.

(83) Stillinger, F. H.; Rahman, A., Improved Simulation of Liquid Water by Molecular Dynamics. *J. Chem. Phys.* **1974**, *60*, 1545-1557.

(84) Mezei, M.; Beveridge, D. L., Theoretical Studies of Hydrogen Bonding in Liquid Water and Dilute Aqueous Solutions. *J. Chem. Phys.* **1981**, *74*, 622-632.

(85) Luzar, A.; Chandler, D., Structure and Hydrogen Bond Dynamics of Water-Dimethyl Sulfoxide Mixtures by Computer Simulations. *J. Chem. Phys.* **1993**, *98*, 8160-8173

(86) Rahman, A.; Stillinger, F. H., Molecular Dynamics Study of Liquid Water. *J. Chem. Phys.* **1971**, *55*, 3336-3359.

(87) Rapaport, D. C., Hydrogen Bonds in Water. *Mol. Phys.***1983**, *50*, 1151-1162.

(88) Sarupria, S.; Garde, S., Quantifying Water Density Fluctuations and Compressibility of Hydration Shells of Hydrophobic Solutes and Proteins. *Phys. Rev. Lett.* **2009**, *103*, 037803.

(89) Patel, A.; Varilly, P.; Chandler, D.; Garde, S., Quantifying Density Fluctuations in Volumes of All Shapes and Sizes Using Indirect Umbrella Sampling. *J. Stat. Phys.* **2011**, *145*, 265-275.

(90) Patel, A. J.; Varilly, P.; Jamadagni, S. N.; Hagan, M. F.; Chandler, D.; Garde, S., Sitting at the Edge: How Biomolecules Use Hydrophobicity to Tune Their Interactions and Function. *J. Phys. Chem. B* **2012**, *116*, 2498-2503.

(91) Chong, S.-H.; Ham, S., Atomic-Level Investigations on the Amyloid-β Dimerization Process and its Driving Forces in Water. *Phys. Chem. Chem. Phys.* **2012,** *14*, 1573-1575.

(92) Chong, S.-H.; Ham, S., Atomic Decomposition of the Protein Solvation Free Energy and its Application to Amyloid-Beta Protein in Water. *J. Chem. Phys.* **2011,** *135* , 034506.

Chapter 5

Spontaneous Association of the Amyloid-β and the αSynuclein Proteins in Fully Aqueous Environment

"The task is...not so much to see what no one has yet seen;

but to think what nobody has yet thought,

about that which everybody sees."

-Erwin Schrödinger

Abstract

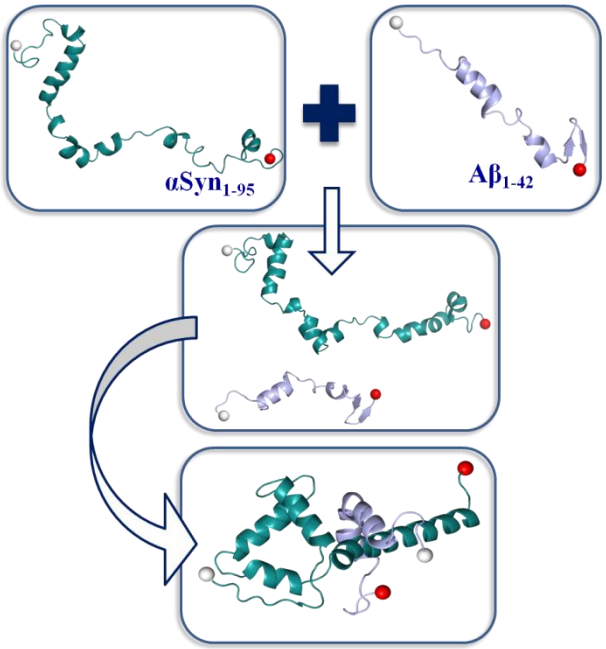

We have used atomistic molecular dynamics simulations to probe the possibility of cross dimerization between αSyn$_{1\text{-}95}$ and A$\beta_{1\text{-}42}$, and thereby gain insights into their plausible early assembly pathways in aqueous environment. Our analyses indicate a strong probability of association between the two sequences, with inter-protein attractive electrostatic interactions playing dominant roles. Principal component analysis revealed significant heterogeneity in the strength and nature of the associations in the key interaction modes. In most, the interactions of repeating Lys residues, mainly in the imperfect repeats 'KTKEGV' present in αSyn were found to be essential for cross interactions and formation of inter-protein salt bridges. Additionally, a hydrophobicity driven interaction mode devoid of salt bridges, where the non-amyloid component (NAC) region of αSyn came in contact with the hydrophobic core of A$\beta_{1\text{-}42}$ was observed. The existence of such hetero assembly pathways may lead to polymorphic aggregates with variations in pathological attributes. Our results provide a perspective on development of therapeutic strategies for preventing pathogenic interactions between these proteins.

5.1 Introduction

Misfolding and aggregation of amyloidogenic proteins in the intra- or extra-cellular regions of the human brain are associated with multiple neurodegenerative diseases (ND) [1-6]. Although these diseases differ in their pathological attributes, the toxic transformations of the proteins are associated with similar pathways characterized initially by the formation of soluble oligomers, followed progressively by the emergence and elongation of protofibrillar and fibrillar aggregates[7-11]. Interestingly, recent clinical studies indicate that the symptoms associated with different ND can occur synergistically, leading to the worsening of overall prognosis [12, 13]. Recent experimental and theoretical studies have found that the abnormal cross interactions between different misfolded proteins could lead to such mixed pathologies [14-16].

Among different NDs, Alzheimers Disease (AD), Lewy Body Disease (LBD), and Parkinson's Disease (PD) are the leading cause of dementia and moving disorders in the elderly. While oligomerisation and fibrillisation of Aβ has been identified as a toxic event in AD [2], progressive accumulation of αSyn has been linked to PD [3]. Recent studies suggest that αSyn may also have a crucial role to play in pathology of AD [3]. A large fraction of AD patients exhibit αSyn positive Lewy bodies associated with LBD in their brains [5, 17]. Evidences suggest that Aβ and αSyn interact directly *in vivo* and *in vitro* [14, 15, 18]. Transgenic mouse models demonstrate Aβ enhances αSyn accumulation and neuronal deficit [15]. Multi-dimentional NMR studies in membrane mimicking environment reported that the molecular interaction of αSyn with Aβ_{40} and Aβ_{42} are site-specific, and that membrane bound αSyn induced structural alterations that are more profound in Aβ_{42} compared to those in Aβ_{40} [14]. The same study also suggests that the oligomerization pathways for αSyn with Aβ_{42} and Aβ_{40} in the vicinity of cellular membranes are different [14]. Short MD simulations showed that Aβ and αSyn localized on a lipid bilayer surface are capable of forming ring-like hybrid structures that can porate the membrane [18]. Interestingly, recent kinetic study suggest that the fibrils and oligomers of Aβ_{40}, Aβ_{42} and αSyn can function as seeds for promoting each other's aggregation pathways [19].

Both Aβ and αSyn are intrinsically disordered proteins (IDPs) whose pathological transformations are fundamentally dependent on their primary sequences. Although Aβ_{1-42} is an amphiphilic peptide, it has distinctive hydrophobic patches, particularly the central hydrophobic core $L^{17}VFFA^{21}$ and the C-terminal hydrophobic region A^{30}-A^{42}.

The intra- and intermolecular interactions in these regions are known to lead to the compactification of this peptide in its monomeric state followed by its aggregation to form toxic species [8, 20-23]. In addition, the charged residues E^{22}, D^{23}, K^{28} of the Aβ peptide, that can form intra- and intermolecular salt bridges in the N-terminal fragment and at the central region play important roles in the peptide's the pathological transformations [17, 24-27]. αSyn is composed of three distinct regions; an N- terminal lipid binding domain (residues 1-60), a continuous hydrophobic domain (residues 61-95) and a highly acidic C terminal region. Among these, the hydrophobic segment is the non amyloid component (NAC) of the amyloid plaques found in AD [3]. The first two regions of αSyn is composed of six imperfect repeat sequence motifs KTKEGV, but the role of these repeats in the toxicity of the protein has not yet been understood.

We note that despite increasing evidences of overlapping pathologies of AD and PD and accelerated neurodegeneration arising from cross influences of Aβ and αSyn, there are relatively few molecular level studies that directly probe the interactions between these two dissimilar IDPs. To the best of our knowledge, molecular details of their spontaneous associations in regimes that resemble the aqueous cytoplasmic conditions remain uncharacterized. In this study, we have used microsecond scale unbiased molecular dynamics (MD) simulations to discern the early inter-molecular associations between the monomeric forms of Aβ and αSyn in aqueous environment. We mention here that interactions with surfaces can hinder the translation diffusion of proteins and affect the rates of their assembly and aggregation [28-30]. The initial diffusive regime has been noted to play important roles in self-assembly of amyloidogenic peptides [31]. Our simulations are performed such that restrictions on the initial diffusive regime due to surface tethering or adsorption are avoided. Our results indicate a high probability of cross-dimerization between the two sequentially dissimilar proteins leading to the formation of metastable complexes that may have the potential to further co-fibrillize. Principal component analysis revealed distinct association modes with variations in the strength and nature of inter-protein interactions, salt bridge propensities and extents of conformational disorder. The majority of cross-interactions were found to be driven electrostatically, with the Lys repeats of αSyn playing important roles in enhancing stability via inter-protein salt bridge formation. Remarkably, however, we also found the existence of an interaction mode that was predominantly stabilized via hydrophobic interactions. Our study provides evidence of marked heterogeneity in the cross

interactions responsible for primary association of the two disease-associated IDPs. The data strongly suggest the existence of multiple pathways of cross-fibrillization between Aβ and αSyn, and therefore high degrees of polymorphism in the resultant cross aggregates.

5.2 Methods

5.2.1 Generation of Initial Monomer Conformations

We generated putative monomeric conformations of Aβ and αSyn monomers in aqueous environment by employing the accelerated molecular dynamics simulations (AMD) method with torsional boost [32] to suitably alter the predominantly helical, solution-state NMR structures of Aβ (1Z0Q) [33] and αSyn (2KWW) [34], available in the PDB database. The Aβ structure was experimentally reported via solution NMR studies in a 3:7 mixture of hexafluoro-2-propanol and water, while the αSyn structure was reported in the micellar environment.

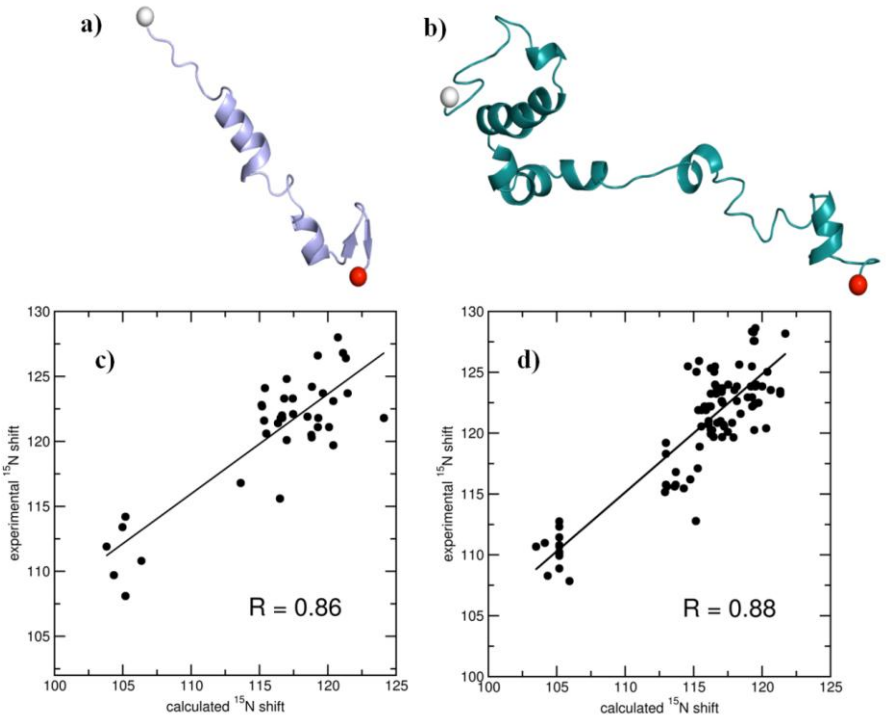

Figure 5.1.. Snapshots of starting monomeric structures of a) Aβ and b) αSyn used in the unbiased simulations in the study. Correlation of average theoretical ^{15}N chemical shifts with experimentally determined ^{15}N chemical shifts for c) Aβ and d) αSyn. The linear regressions (straight lines) and the corresponding Pearson Correlation Coefficients (R) are provided.

AMD as implemented in the NAMD2.8 package [35] was used with the CHARMM all atom force field with CMAP correction [36, 37]. The theoretical details of the AMD method can be found in Chapter 2 (section 2.7.1). The acidic tail region 96-140 of αSyn was excluded as the C-terminal truncated αSyn has been shown to have higher propensity for aggregation [38-40]. Aβ and αSyn are intrinsically disordered proteins with wide conformational ensembles [41-43]. However, the Aβ conformation obtained towards the end of our 17 ns long AMD simulations had marked similarities with important conformational members reported before, in terms of the emergence of anti-parallel C-terminal beta sheets and reduced N-terminal helicities [42, 44]. We generated an ensemble of the free peptide monomers with the conformations thus obtained, and calculated the average ^{15}N chemical shift values using the SHIFTS program, [45] and compared them with the experimentally determined values for Aβ [46] and αSyn [47]. The mean chemical shift values were positively correlated with the experimental values. The Pearson Correlation Coefficients (PCC) for Aβ and αSyn were 0.86 and 0.88, respectively. The selected conformations, and the corresponding chemical shift correlation plots are shown in Figure 5.1.

5.2.2 System Setup and Simulation Protocols

Spontaneous association of the Aβ and αSyn conformations obtained as described above were probed with unbiased simulations, also performed with the NAMD2.8 [35] package and the CHARMM force field [36, 37]. Ten independent trajectories, with the Aβ and αSyn placed at varying distances and relative orientations, were generated. The initial complexes were first solvated with TIP3P [48] water molecules followed by the addition of one chloride counter ion in order to neutralize the systems. We constructed large enough simulation boxes with sides extended at least 14 Å from the extremities of the proteins so that the monomers are free to interact or diffuse away. After 10,000 steps of conjugate gradient energy minimization, simulations were carried out in the isothermal-isobaric (NPT) ensemble with orthorhombic periodic boundary conditions. Constant temperature of 310 K was maintained with Langevin dynamics with a collision frequency of 1 ps^{-1}, and the Langevin piston Nosé-Hoover method, was used to maintain a constant pressure of 1 atm [49, 50]. The cutoff radius for Lennard Jones interaction was set to 12 Å. SHAKE [51] was used for constraining bonds involving hydrogen atoms. Electrostatic interactions were calculated with particle-mesh Ewald method [52]. A time step of 2 fs was used. A total of 1.3 μs of unbiased simulations were generated. Pymol [53] and the VMD [54] tools were used for the generation of snapshots and visualization of the trajectories.

5.2.3 Principal Component Analysis

In order to capture the most significant modes of cross-monomer interactions, clustering based on Cartesian Principal component analysis (PCA) was conducted on combined snapshots of the interacting trajectories using the program Carma [55]. PCA has been widely recognized as a reliable starting point to identify important modes of interacting systems produced by MD simulations [42, 56-58]. The heavily populated clusters are identified by analysing the distribution of first three principal components using an rmsd cutoff of 2.4 Å. The probability density of the distribution of first two principal components corresponding to the fluctuations of the C_α atoms in the bound system is calculated and converted into a free energy function using the following equation,

$$\Delta G = -k_B T \ln (p/p_{max}) \qquad (5.1)$$

where, k_B is Boltzmann's constant, T is the temperature in absolute units, p is probability obtained from the distribution of the first two principal components, and p_{max} is the corresponding maximum probability

5.2.3 Configurational Entropy

We have calculated the configurational entropy per heavy atoms of Aβ and αSyn peptides in bound and unbound state using Schlitter's method[59] as implemented in Carma program [55]. This method has been widely used to calculate the degree of change in internal conformation of bio-systems using MD trajectories[60-62]. Here the initial structure of each peptide is used as reference, to remove the translations and rotations with respect to the center of mass of the systems. According to Schlitter's method the absolute entropy can be approximated as follows,

$$S_{abs} < S = \frac{1}{2} k_B \ln \det \left[1 + \frac{k_B T e^2}{\hbar^2} M^{\frac{1}{2}} \sigma M^{\frac{1}{2}} \right] \qquad (5.2)$$

Where k_B is the Boltzmann's constant, $\hbar$ is Planck's constant divided by 2, e is Euler's number, M is the mass matrix of $3N$ dimension containing N atomic masses of the system and σ is the covariance matrix. The elements in the covariance matrix can be expressed as

$$\sigma_{ij} = \langle (x_i - \langle x_i \rangle)(x_j - \langle x_j \rangle) \rangle \qquad (5.3)$$

where, x_i and x_j are the Cartesian coordinates of the selected atoms.

Results

5.5.1 Evaluation of Inter-Protein Association

The initial inter-peptide center of mass distance, as well as their distances and relative orientations at 10 ns are provided in Table 5.1.

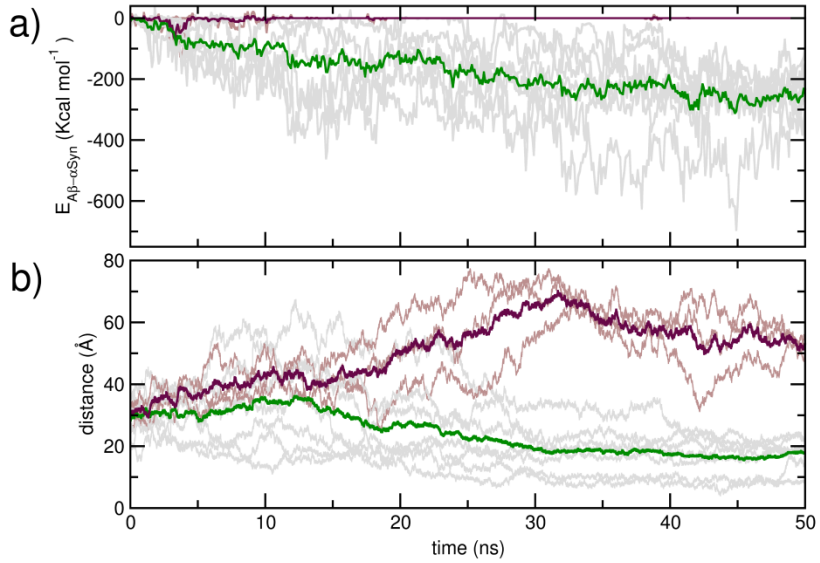

Figure 5.2. Evolution of the a) total inter-peptide interaction strength, and b) inter peptide distance over the first 50 ns of the unbiased simulation. Data for the dimerising trajectories are shown in *gray*, and averages shown in *green*; the data for non-dimerising trajectories are in *brown* and the averages shown in *maroon.*

In Figure 5.2 a), we present evolution of the peptide-peptide interaction strength over the first 50 ns of simulation for the trajectories. While three trajectories indicate no inter-protein interaction at the end of 50 ns, A*β* and αSyn in seven trajectories demonstrate strong interaction. The mean inter-protein interaction strength at the end of 50 ns is -172.96 (± 72.8) kcal mol^{-1}. We have shown corresponding evolution of the center of mass distances in Figure 5.2b. The mean inter-monomer center of mass distance at 50 ns of the seven trajectories where A*β* and αSyn interact are 17.5 Å, while the corresponding mean distance obtained from the non-interacting ones are 53.0 Å. The interaction energy, center of mass distances and relative orientations at 50 ns have also been provided in Table 5.1. The interacting trajectories were each further propagated for at least an additional 100 ns; evolutions of corresponding inter-peptide interaction strength and center of mass distances of these trajectories over 150 ns are provided in Appendix-III (Figure AIII-1).

We have further compared the residue-wise backbone mean squared fluctuation (MSF) in the Aβ and αSyn obtained at 0- 50 ns of the simulations, with that obtained over 100-150 ns, from the peptides in the interacting trajectories (Figure 5.3). An overall sharp reduction in the MSF is noted upon the formation of complexes from the two dissimilar peptides, with comparatively greater decrease in the middle regions. The interaction of Aβ and αSyn is thus commensurate with a decrease in the structural disorder.

Traj. No.	d_0	d_{10}	θ_{10}	d_{50}	θ_{50}	E_{int}
1	33.2	31.8	79.6	12.8	101.8	-177.3
2	33.2	53.0	27.5	19.7	65.6	-173.2
3	33.2	56.8	29.8	19.1	136.3	-213.1
4	33.2	23.0	134.2	19.1	99.1	-275.0
5	33.2	38.7	135.9	55.9	60.9	0.0
6	33.2	51.7	157.8	53.2	68.5	0.0
7	18.9	13.7	162.1	21.6	109.4	-94.6
8	18.3	43.2	133.3	22.0	76.0	-403.3
9	24.3	39.4	116.9	50.1	97.4	0.0
10	24.3	26.7	119.1	8.3	158.2	-297.5

Table5.1. The inter-protein center of mass distances (in Å) at the start of the unbiased simulations is denoted as d_0, at 10 ns is denoted as d_{10}, and at 50 ns is denoted as d_{50}. The relative orientations of the proteins are specified by the angle (in degrees) between the vectors joining the N- and C-terminii of each protein, at 10 ns (θ_{10}) and at 50 ns (θ_{50}). E_{int} denotes the total inter-protein interaction at 50 ns (in kcal mol^{-1}).

The discussion above shows that despite the early diffusive regime, Aβ and αSyn have a marked, enthalpy driven propensity to interact and form dimeric complexes in aqueous solution. In Figure 5.4, we provide a residue-wise breakdown of the total inter-peptide interaction. Interestingly, we found that the charged residues of each peptide exhibit significantly stronger interactions compared to the hydrophobic and polar residues. This was manifestly clear when we considered the strongest interaction arising from each residue (Figure 5.4 b and d). Interestingly, interactions arising from the repeating Lys residues of the repeating units in the N- and C-termini of αSyn give rise to distinctly strong interactions.

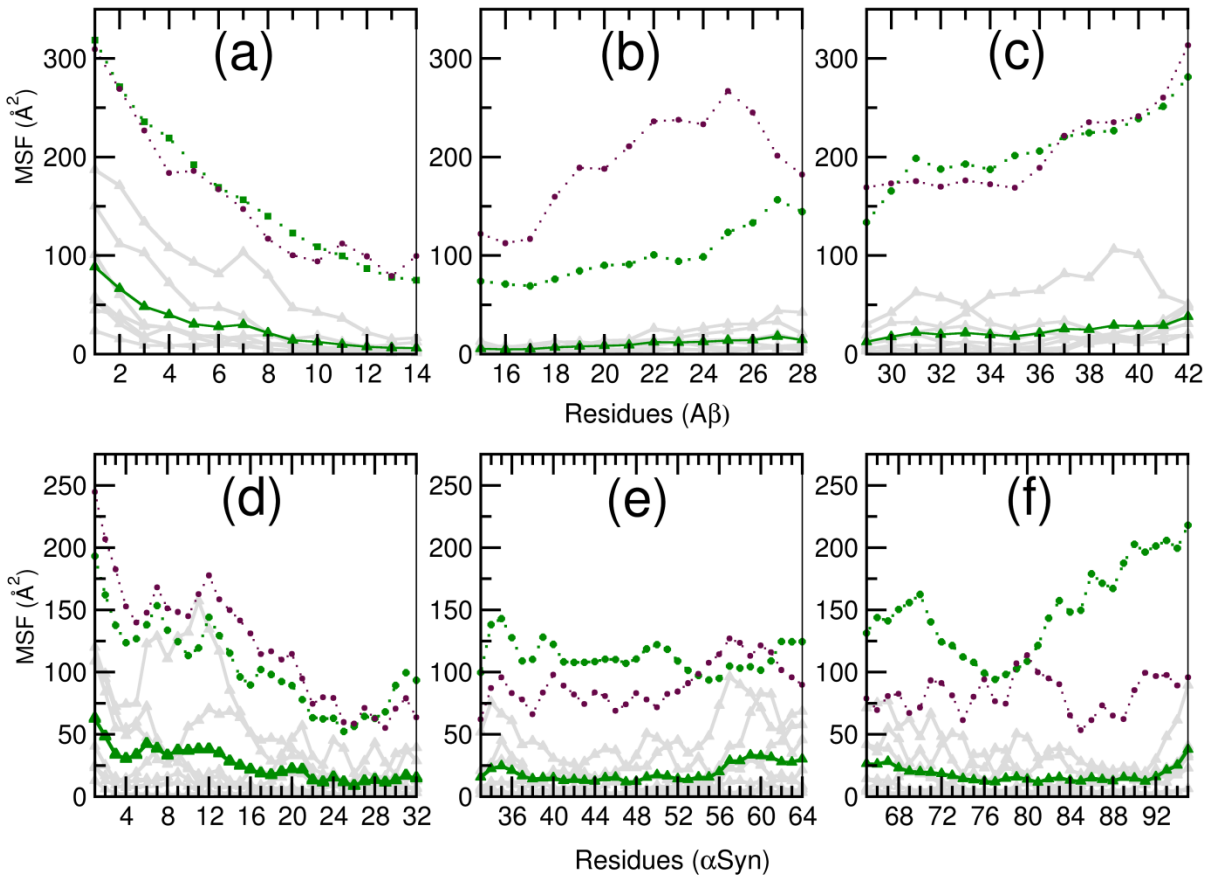

Figure 5.3. The backbone mean square fluctuation (MSF) for the a) N-terminal residues, b) middle regions, and c) C-terminal residues of A$\beta_{1\text{-}42,}$ and the d) N-terminal residues, e) middle regions, and f) C-terminal residues of αSyn$_{1\text{-}95}$. The data for the last 50 ns of the dimerising trajectories are shown in *gray*, with the averages in *green* (solid line). Corresponding average data for the same systems for the initial 50 ns is provided in green (broken line). Average data for the non-dimerising systems is shown in *maroon* (broken line) for comparison.

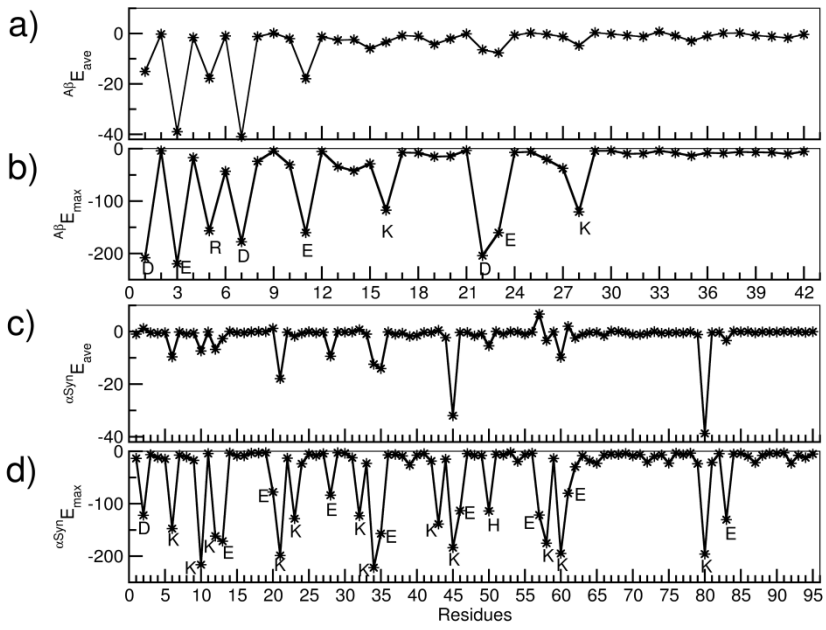

Figure 5.4. Non bonded interaction energies in kcal mol^{-1}. Residue wise: average interaction energy of A$\beta_{1\text{-}42}$ with $\alpha Syn_{1\text{-}95}$ (a), maximum interaction energy of A$\beta_{1\text{-}42}$ with $\alpha Syn_{1\text{-}95}$ (b), average interaction of $\alpha Syn_{1\text{-}95}$ with A$\beta_{1\text{-}42}$ (c), and maximum interaction energy of $\alpha Syn_{1\text{-}95}$ with A$\beta_{1\text{-}42}$ (D). The residues with strong interactions are labeled with one letter code of the respective amino acids.

5.3.2 Interaction Heterogeneity

Principal component analysis as described in *Methods* was performed with snapshots of the dimerized complexes where the proteins' centers of mass were closer than 30 Å. In Figure 5.5, we present the free energy landscape as a function of the first (PC1) and the second (PC2) principal components. Five distinct clusters were obtained from the PCA and named C1, C2, C3, C4 and C5 in order of decreasing cluster population. Snapshots corresponding to structures residing at the cluster centers have been shown in Figure 5.5. In order to decipher distinguishing traits of the individual complexes in each cluster, these representative structures were individually simulated for 4 ns under the same conditions as the original simulations.

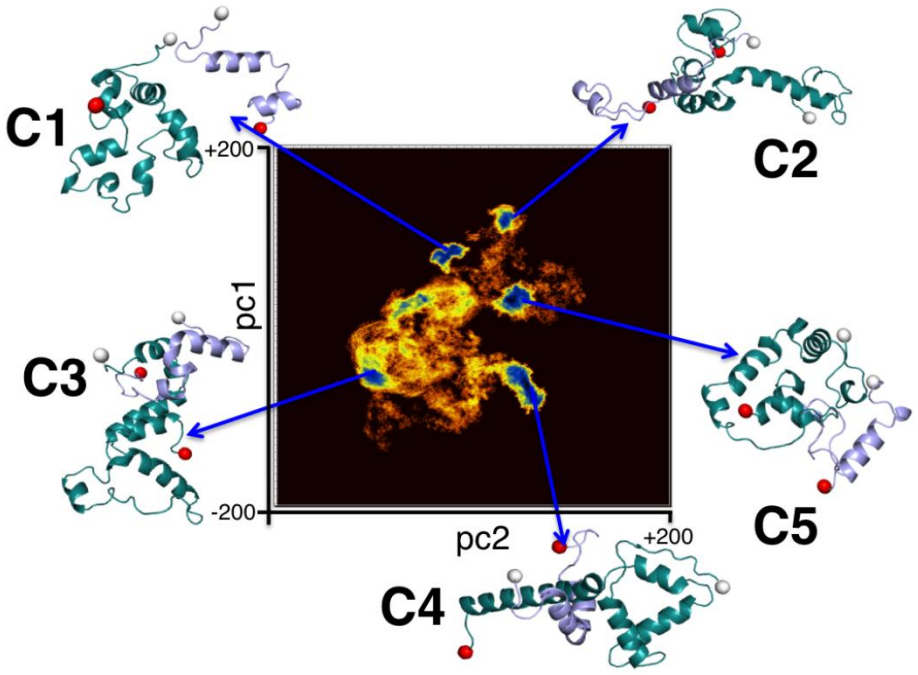

Figure 5.5. The clusters evolved during Cartesian principal component analysis (PCA) of A$\beta_{1\text{-}42}$ and αSyn$_{1\text{-}95}$ cross dimer system. The two dimentional representation of the distribution of density function Δ*G*, corresponding to the fluctuations of the Cα atoms on the plane of the top two principal components, pc1 and pc2 is shown. The Δ*G* values spread in the range of 0 to 4.2 kcal mol $^{-1}$. The representative structures from five distinct clusters are shown.

In Table 5.2, we have reported mean values of the number of inter-protein contacts; the radii of gyration (R_g) of the dimeric complexes; and electrostatic and van der Waals components of the Aβ-αSyn interaction strengths of all five clusters. As in a previously reported study [20], two residues are taken to form a contact if the centers of mass of their sidechains approach within a distance of 7 Å. The five clusters are found to have significant variation in the number of inter-protein contacts, the level of compactness of the complexes as well as of the individual protein units (reported in Table 5.3), and the strength of the inter-protein interactions. C5 has the highest average number of inter-protein residue contacts commensurate with the strongest inter-protein interaction ($E_{p\text{-}p}$) of -485.2 kcal/mol. C2 and C4 have a comparable number of inter-protein contacts, which are marginally lower than the contacts in C5. Interestingly, however, while the inter-protein interaction strength in C2 is comparable to that of C5, the interaction strength in C4 is significantly weaker, being only -82.7 kcal/mol in its mean value.

Clusters C3 and C1 have markedly lower mean inter-protein contacts, with values of only 23 and 14.6, respectively. However, the inter-protein interactions in C3 and C1 are stronger than that in C4.

Cluster	N_{cont}	R_g	E_{tot}	E_{Coul}	E_{vdW}
C1	14.6 (4.5)	17.6 (0.4)	-146.7 (47.0)	-124.1 (48.4)	-22.6 (8.4)
C2	41.0 (3.6)	18.8 (0.6)	-361.4 (97.0)	-297.7 (96.9)	-63.8 (7.1)
C3	23.0 (4.8)	16.3 (0.3)	-158.7 (57.3)	-131.2 (55.0)	-27.6 (6.6)
C4	43.4 (3.5)	22.5 (0.7)	-82.7 (17.4)	-23.5 (16.0)	-59.2 (4.7)
C5	49.1 (5.6)	18.6 (0.5)	-485.2 (54.7)	-428.3 (55.3)	-56.9 (9.2)

Table 5.2. The number of inter-protein contacts (N_{cont}), radius of gyration of the dimer complex (R_g), total interaction strength (E_{tot}), and the electrostatic (E_{coul}) and the van der Waals components (E_{vdW}) of the total interaction. The units for distances and energies are Å and kcal mol^{-1}, respectively.

Interestingly, we note that in C1, C2, C3 and C5, the inter-protein interaction is dominated by electrostatic energy. In contrast, in the cluster C4, the dominant non-bonded contribution arises from van der Waals interactions. However, despite the weaker inter-protein interaction, the number of residue-residue contacts in C4 is comparable to that of C5 and C2. We have compared the inter-protein side-chain contact probability maps for all five clusters in Figure 5.6. The contact maps reveal high degrees of contact heterogeneity amongst the various clusters. In C1, contacts were predominantly formed between the N-terminii of Aβ and αSyn. Relatively weaker contacts were noted between residues 35 to 50 of αSyn with the Aβ hydrophobic domain comprising of residues 30 to 35. In C2, the N-terminal residues of Aβ made contacts with two distinct domains of αSyn, namely the segments 32 to 53, and 63 to 85, while the Aβ C-terminal residues I^{41} and A^{42} made weaker contacts with the region A^{50} – E^{63} of αSyn. C3 was predominantly characterized by N-N and C-C terminal contacts between two peptides. It is very interesting to notice that in system C4, the hydrophobic NAC region of αSyn came in close proximity of the segment 10-42 of Aβ containing hydrophobic regions 17-21, 30-35 and 39-42. In system C5, we could observe high contact probability at the terminus of both the peptides. Residues from 1-35 region of αSyn were seen to make contact with

segments 1-5, 15-24 and 27-42 of Aβ. Similarly, the C-terminal residues 80-91 of αSyn made contact with the C-terminal segment 25-35 of Aβ.

Clusters	<Nint.$^{A\beta}$ >	<Nint.$^{\alpha S}$ >	$R_g^{A\beta}$	R_g^{aS}
C1	141.4 (7.4)	485.0 (18.0)	12.0 (0.5)	14.6 (0.2)
C2	141.5 (9.1)	414.6 (12.9)	14.67 (0.7)	16.7 (0.5)
C3	153.1 (7.6)	467.1 (12.9)	10.9 (0.2)	14.4 (0.2)
C4	126.0 (5.7)	361.9 (9.3)	14.2 (0.4)	23.8 (0.7)
C5	141.1 (7.8)	454.2 (13.2)	12.9 (0.3)	16.9 (0.3)

Table 5.3: Mean values of the total number of internal contacts formed in the Aβ ($N_{int}^{A\beta}$) and αSyn ($N_{int}^{\alpha S}$) proteins in the five clusters. The corresponding radii of gyration (in Å) have been denoted as $R_g^{A\beta}$ and $R_g^{\alpha S}$.

We have provided inter-protein residue-residue contact energy maps corresponding to the maximum interaction strength in Figure 5.7. This has been done separately for the electrostatic and the van der Waals interaction energies. We note that the strong inter-residue contact probabilities in C1, C2, C3 and C5 (as observed in Figure 5.6) are reflected sharply in the maximum electrostatic interactions. In contrast, the maximum contact probabilities in cluster C4 are reflected clearly in the van der Waals interactions, distinguishing this cluster from the others in the nature of interactions responsible for the dimeric complex. We note here that in every cluster except C4, the contact points were non-contiguous, and the repeating Lys residues in the αSyn sequence made significant contributions to the interaction strength.

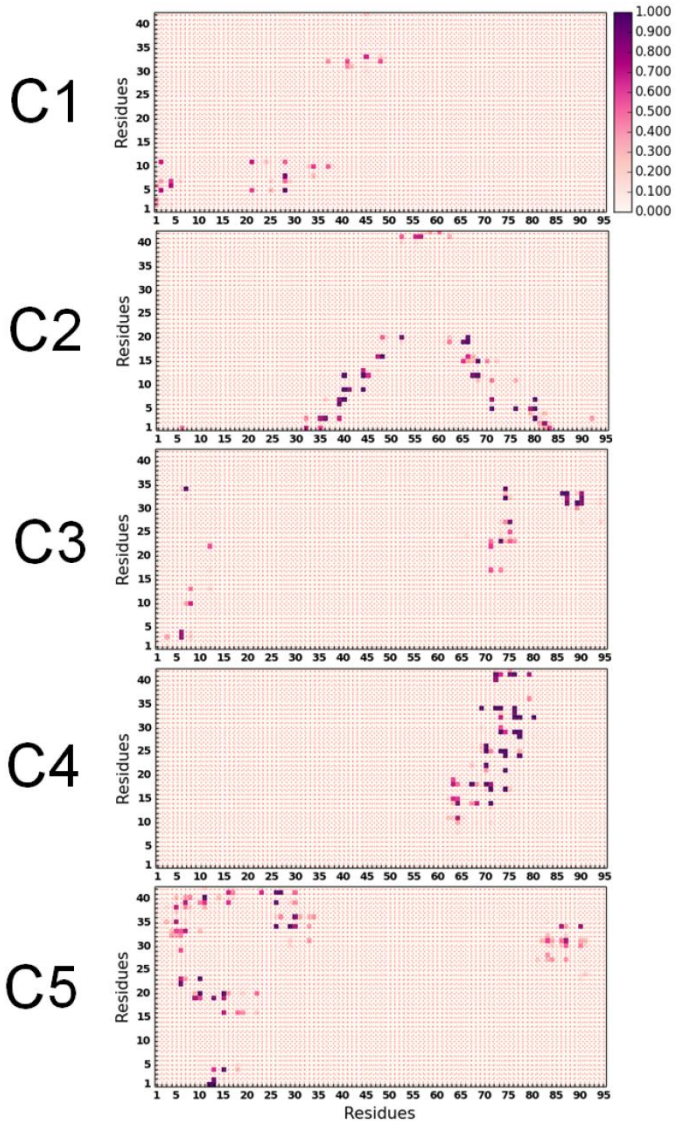

Figure 5.6. Residue specific side chain contact probability of αSyn$_{1\text{-}95}$ with A$\beta_{1\text{-}42}$ in different interaction sub modes.

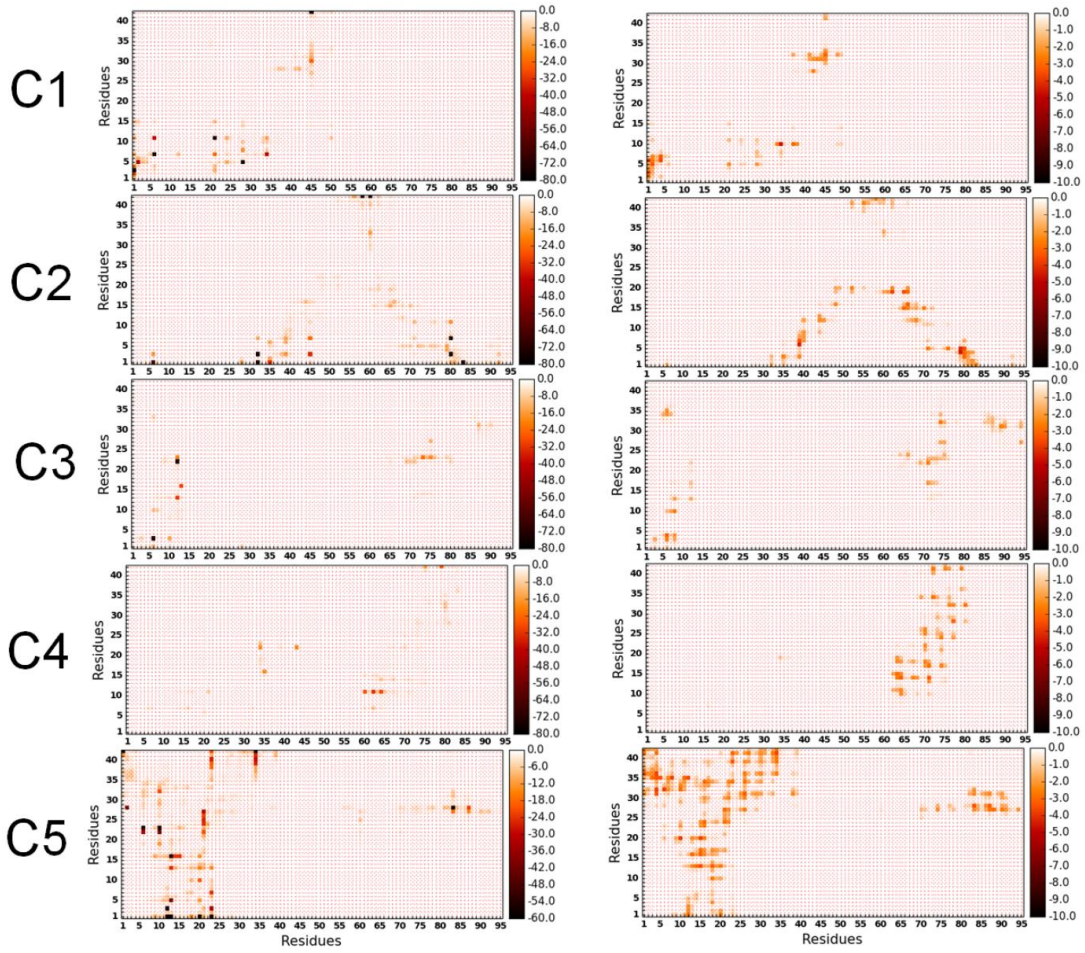

Figure 5.7. Residue wise maximum electrostatic (left column) and van der Waal (right column) interaction energies (in kcal mol^{-1}) of $\alpha Syn_{1\text{-}95}$ with $A\beta_{1\text{-}42}$ for clusters C1, C2, C3, C4 and C5.

5.3.3 Interfacial Salt Bridge Propensities

The significant electrostatic contribution to the inter-peptide interaction in the majority of clusters leads us to investigate the possible role of salt bridges in stabilizing the hybrid Aβ-αSyn complexes. We point out that inter-protein salt bridges are known to play important roles in intra- and inter-protein interactions [11, 24-27, 58, 63-66]. We utilized the VMD software for analyzing salt bridge propensities. While VMD reported no inter-peptide salt bridges in the cluster C4, multiple salt bridges were detected in clusters C1, C2, C3 and C5.

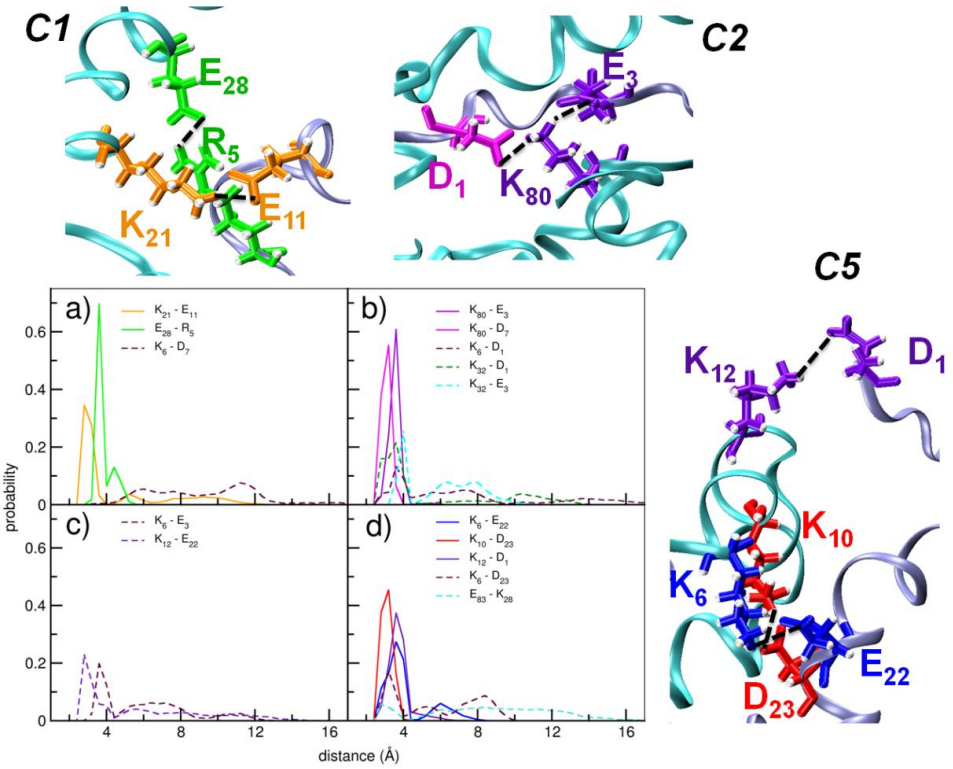

Figure 5.8. Distributions of the inter-residue distances between the residues that form inter-protein salt bridges, in clusters a) C1, b) C2, c) C3, d) C5. Distributions corresponding to the stable and the transient salt bridges are indicated in solid and broken lines, respectively. The first residue belongs to $\alpha Syn_{1\text{-}95}$, and the second to $A\beta_{1\text{-}42}$. Snapshots with the stable salt bridges are shown for clusters C1, C2 and C5.

In Figure 5.8, we present distributions of the inter-residue distances between the salt bridging pairs in C1, C2, C3 and C5. In each of these clusters, we found that the repeating Lys units of αSyn participated in all or a majority of the observed salt bridges. In C1, two salt bridges of high stability are formed between residues $\alpha SynK^{21}$-$A\beta E^{11}$, and between $\alpha SynE^{28}$-$A\beta R^{5}$, while a transient salt bridge is noted between $\alpha SynK^{6}$-$A\beta D^{7}$. Five salt bridges were noted in C2, out of which two ($\alpha SynK^{80}$-$A\beta E^{3}$ and $\alpha SynE^{80}$-$A\beta D^{7}$) were highly stable, while three ($\alpha SynK^{6}$-$A\beta D^{1}$, $\alpha SynK^{32}$-$A\beta D^{1}$ and $\alpha SynK^{32}$-$A\beta E^{3}$) were relatively more transient. The cluster C3 was found to have just two transient salt bridges, between $\alpha SynK^{6}$-$A\beta E^{3}$ and $\alpha SynK^{12}$-$A\beta E^{22}$. Five salt bridges were observed in cluster C5, of which the $\alpha SynK^{6}$-$A\beta E^{22}$, $\alpha SynK^{10}$-$A\beta D^{23}$ and $\alpha SynK^{12}$-$A\beta D^{1}$ were stable and the rest ($\alpha SynK^{6}$-$A\beta E^{23}$ and $\alpha SynE^{83}$-$A\beta K^{28}$) transient. In Appendix III (Table A3.1), we have reported the mean and standard deviations of the inter-residue center of mass

distance between the salt bridging pairs. In clusters C2 and C5, we note the propensity to form salt bridges involving more than two charged residues. Several previous studies have highlighted important roles of such 'complex' salt bridges in influencing protein stabilities [67-69]. In C2, K32 of αSyn transiently forms salt bridges with D1 and E3 of A*β*, while K80 of αSyn forms stable salt bridges with D7 and E3 of A*β*. In C5, both K6 and K10 of αSyn are found to form salt bridges with D23 of A*β*; while the former is transient, the latter is stable. The K6 of αSyn is also noted to form a transient salt bridge with E22 of A*β*.

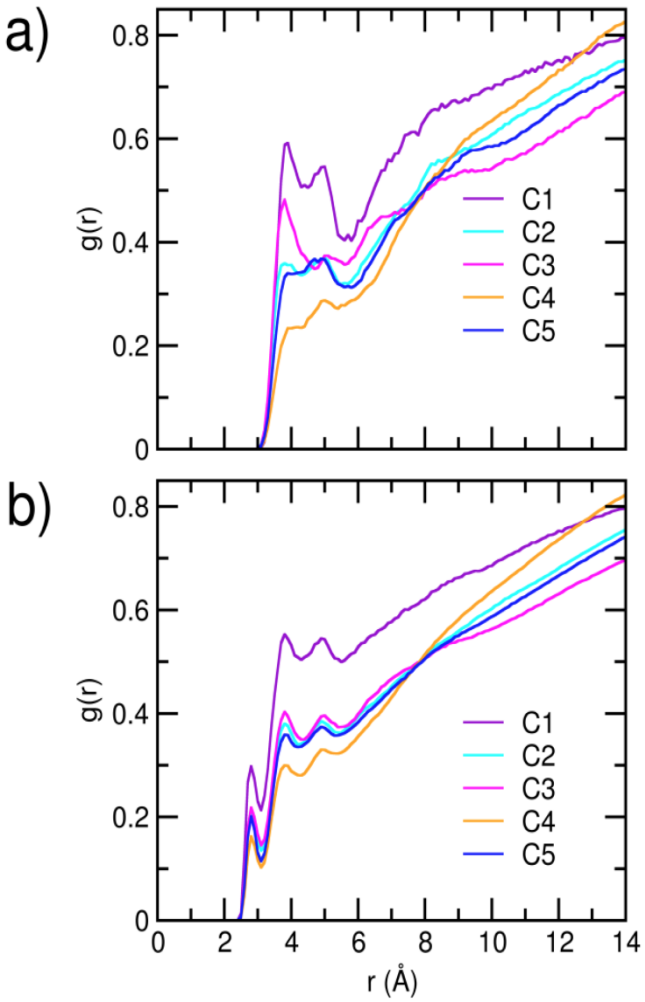

Figure 5.9. Radial distribution functions of water oxygens, around a) backbone C_α atoms, b) all heavy atoms of residues that make inter-protein contacts. A minimum contact probability of 0.7 has been considered.

In Figure 5.9, we report, for each cluster, the radial distribution functions (RDFs) calculated between oxygens of the solvent water molecules, and the C_α as well as the heavy atoms of residues that take display inter-residue contact. The first solvation shell of water oxygens is located at a distance of about 3.9 Å for C_α, and at about 2.8 Å when all protein heavy atoms are considered for all clusters. For each cluster, we first note a sharp reduction in the first solvation shell of the interfacial residues compared to the full complex. Interestingly, however, the interfacial RDFs describe significant variation in the extent of hydration at the inter-protein contacts. Both C_α as well as the heavy atom RDFs show that the interface corresponding to cluster C4 has the least hydration, reiterating the hydrophobicity driven stability of this particular protein-protein interaction mode. Amongst the remaining clusters, we find the inter-protein interfaces of C1 and C3 to be relatively more hydrated than those of C2 and C5. It is to be noted here that salt bridge formation is often associated with a desolvation barrier [70-72]. Thus, the observation of a relatively drier interface in C2 and C5, compared to C1 and C3, is consistent with the observation of a greater number of interfacial salt bridges in the former clusters.

5.3.4 Conformational Disorder

To compare the relative extents of disorder in each cluster, we estimated the cumulative configurational entropy per heavy atom in the individual protein units using Schlitter's method described earlier. For comparison, we also obtained the corresponding cumulative entropies in the unbound states of the proteins. The results are plotted in Figure 5.10. Individual protein units in each dimerizing cluster displayed marked decrease in the net configurational entropies over the corresponding unbound state. The configurational entropies of the Aβ units had greater overlap between the clusters compared to αSyn units.

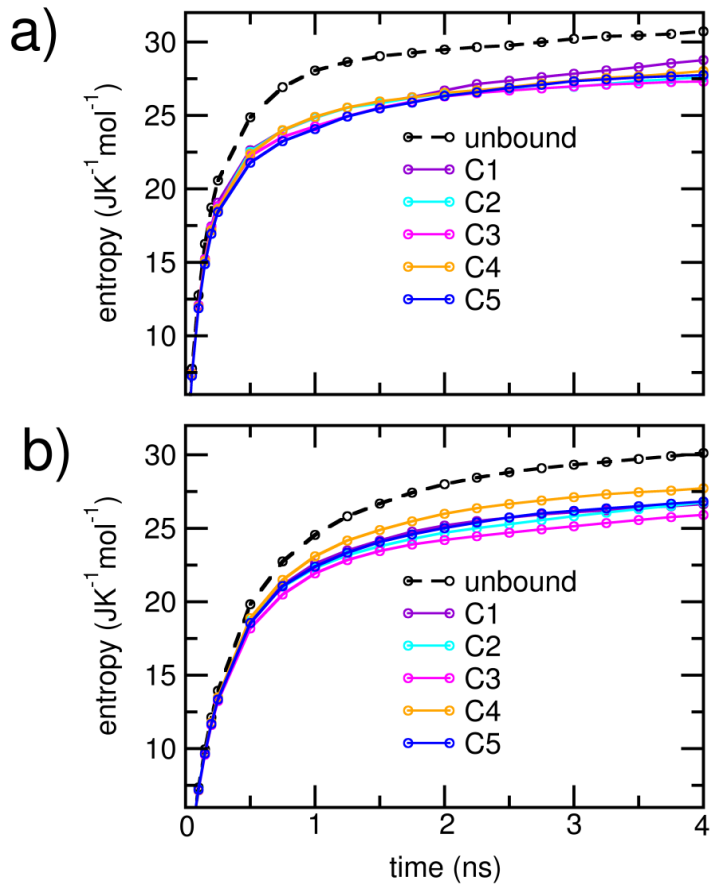

Figure 5.10. Cumulative configuration entropy per heavy atom for a) Aβ protein and b) αSyn protein. The entropy of the unbound states are denoted in black broken lines, while the entropies corresponding to the five clusters are denoted in solid, colored lines.

Systems	S_1	S_2	$S_{1(unbound)}$–S_1	$S_{2(unbound)}$–S_2	$S_1 - S_2$
Unbound	30.7	30.1	-	-	0.6
C1	28.8	26.6	1.9	3.5	2.2
C2	27.6	26.8	3.1	3.3	0.8
C3	27.3	25.9	3.4	4.2	1.4
C4	28.0	27.7	2.7	2.4	0.3
C5	27.7	26.8	3.0	3.3	0.9

Table 5.4. Configurational entropy per heavy atoms (in J K^{-1} mol^{-1}) for Aβ (S_1) and the αSyn (S_2) proteins in the unbound states and in the clusters C1, C2, C3, C4 and C5. The entropy differences between the unbound and bound states, as well as the difference between the entropies of Aβ and αSyn are also provided.

In Table 5.4, we have listed the saturation values of the entropies and the entropy loss upon dimerization for each cluster. The configurational entropy per atom was higher for Aβ, both in the free as well as in the dimerized states. However, for a given cluster, entropy losses on the average were greater for atoms belonging to the αSyn unit. The entropy per heavy atom for αSyn and Aβ was closest in the C4 cluster, indicating the closest level of conformational disorder in the two peptides. Further, C4 was also characterized by the least overall entropy loss. However, for the clusters with stronger electrostatic interactions, we noted the absence of clear correlations between the strength of inter-protein interaction and the extent of entropy loss upon dimerization. Particularly the cluster C3, which displayed largest entropy loss, ranked third in the strength of inter-protein interactions. However, it is observed that the cluster C3 has a relatively high number of internal atom-atom contacts, particularly in the αSyn protein; this is reflected in the smaller R_g values (Table 5.3). In comparison, the strongly associated clusters C2 and C5 had fewer internal contacts, and marginally higher configurational entropy than C3. These data suggest that the internal compactness of the protein units, particularly of αSyn, can be a contributing factor to the overall rigidity of the associated complexes.

5.4 Discussions and Conclusions

Recent *in vitro* and *in vivo* studies report that cross interactions between dissimilar IDPs can play significant roles in clinically observed mixed pathological traits in ND patients [14-19, 73-77]. Notably, significant experimental evidence exists to suggest that Aβ, whose assembly can trigger AD, and αSyn, whose assembly is responsible for PD, can co-associate in biological milieu [14, 15, 17, 18, 73, 75, 76]. However, to the best of our knowledge, there exist no molecular level studies probing their unrestricted associations in aqueous environments. In this study, we reported the heterogeneous interactions of A$\beta_{1\text{-}42}$ and $\alpha Syn_{1\text{-}95}$ from a large ensemble of the dimeric complex obtained from unbiased MD simulations of the protein sequences in explicit water.

In four of the five hybrid interaction modes discerned with Principal component analysis, electrostatic forces are seen to dominate over van der Waals interactions. Residue specific investigations revealed the importance of the Lys residues, especially those in the imperfect repeating units of αSyn, during cross dimerisation. We note here that Lys specific molecular tweezers have been reported to be capable of inhibiting the aggregation of various amyloidogenic peptides [78-81]. 1,4-napthoquinone based inhibitors

were also found to interact with Lys residues and efficiently reduced the fibrilisation propensity of αSyn [82]. Thus, our observation of the importance of the Lys repeats in the cross dimerization may be used for designing drugs targeted at inhibiting Aβ-αSyn co-assembly.

Clusters with dominant electrostatic interactions were characterized by the presence of multiple inter-protein salt bridges. Interestingly, the majority of salt bridges were formed between Lys residues of αSyn and Asp or Glu of A$\beta_{1\text{-}42}$. Studies suggest that the disruption of salt bridges is likely to affect the structure, toxicity and oligomerisation of αSyn [11]. Similarly, in Aβ aggregates, the salt bridge between D23 and K28 is crucial for stability of the hairpin form and formation of fibrillar aggregates[17, 24-27]. Further studies would reveal if the inter-protein salt bridges have any disruptive effects on the ones crucial for self-assembly, and the extent to which this may result in structural dissimilarities between the self-aggregates and the co-aggregates.

Importantly, hydrophobic interactions were also found to play crucial roles in the hetero dimerisation process. In a single interaction mode devoid of inter-protein salt bridges, the van der Waals interactions dominated over the average electrostatic interactions. In this particular system, the hydrophobic core regions comprising of 17-21, 30-35 and 39-42 of Aβ were found to be in contact with the NAC of αSyn. Additionally, we observed inter peptide contact of Aβ with residues of the NAC in all the electrostatically stabilized clusters except C1. We point out that the hydrophobic core regions in Aβ play crucial roles in its early dynamics, oligomerization and fibril formation [8, 20-22, 83, 84]. Similarly, in αSyn the central hydrophobic NAC region is necessary for its aggregation and this fragment is clinically observed in amyloid plaques found in patients with LBD[3, 5, 14, 85-88]. Earlier solid phase binding studies as well as NMR studies indicate that the NAC interacts with Aβ, particularly with residues G67, G73 and V74 and proposed a mechanism for the overlapping pathogenesis that the cleavage of NAC is catalyzed by Aβ oligomer [14]. It is worthwhile to mention here that a major strategy in the drug design against for amyloidogenic peptides is to target regions that drive hydrophobic interactions [83, 88-90]. Thus, the results of our analyses demonstrating NAC interaction with Aβ hydrophobic regions, along with the experimental reports, indicate that these regions could represent other plausible therapeutic targets.

Before concluding, we note that it is important to study secondary structural details of the peptide monomers during hetero assembly, and this requires careful comparison of results obtained from multiple force fields with experimental data. The clear evidence of complex formation without the emergence of strand motifs indicates that the complexes are metastable and prone to further assembly. Longer, millisecond timescale simulations may reveal more modes of Aβ-αSyn associations. Nevertheless, the evidence of significant heterogeneity in the nature of interactions leading to cross dimerization revealed by our microsecond simulations is strongly suggestive of heterogeneity during the seeding phase and along the early assembly pathways. This may result in the emergence of hetero oligomers and thus significant levels of polymorphism in higher ordered aggregates. In further studies, the interactions of preformed hybrid systems with lipid bilayers would greatly facilitate identification of the level of toxicity of each species. This information, along with the specific inter-residue interactions, could significantly aid the development of therapeutics against synergistic ND.

5.5 References

1. Grundke-Iqbal, I.; Iqbal, K.; Quinlan, M.; Tung, Y. C.; Zaidi, M. S.; Wisniewski, H. M., Microtubule-Associated Protein tau. A Component of Alzheimer Paired Helical Filaments. *J. Biol. Chem.* **1986,** 261, 6084-6089.

2. Hardy, J.; Selkoe, D. J., The Amyloid Hypothesis of Alzheimer's Disease: Progress and Problems on the Road to Therapeutics. *Science* **2002,** 297, 353-357.

3. Iwai, A.; Masliah, E.; Yoshimoto, M.; Ge, N.; Flanagan, L.; Rohan de Silva, H. A.; Kittel, A.; Saitoh, T., The Precursor Protein of Non-A Beta Component of Alzheimer's Disease Amyloid is a Presynaptic Protein of the Central Nervous System. *Neuron* **1995,** 14, 467-475.

4. Prusiner, S. B., Prions. *Proc. Natl. Acad. Sci. USA* **1998,** 95, 13363-13383.

5. Spillantini, M. G.; Schmidt, M. L.; Lee, V. M.-Y.; Trojanowski, J. Q.; Jakes, R.; Goedert, M., α-Synuclein in Lewy Bodies. *Nature* **1997,** 388, 839-840.

6. Hu, X.; Crick, S. L.; Bu, G.; Frieden, C.; Pappu, R. V.; Lee, J.-M., Amyloid Seeds Formed by Cellular Uptake, Concentration, and Aggregation of the Amyloid-Beta Peptide. *Proc. Natl. Acad. Sci. USA* **2009,** 106, 20324-20329.

7. Dobson, C. M., Protein Folding and Misfolding. *Nature* **2003,** 426, 884-890.

8. Bernstein, S. L.; Wyttenbach, T.; Baumketner, A.; Shea, J.-E.; Bitan, G.; Teplow, D. B.; Bowers, M. T., Amyloid β-Protein: Monomer Structure and Early Aggregation States of Aβ42 and Its Pro19 Alloform. *J. Am. Chem. Soc.* **2005,** 127, 2075-2084.

9. Cappai, R.; Barnham, K., Delineating the Mechanism of Alzheimer's Disease Aβ Peptide Neurotoxicity. *Neurochem. Res.* **2008,** 33, 526-532.

10. Liao, M. Q.; Tzeng, Y. J.; Chang, L. Y. X.; Huang, H. B.; Lin, T. H.; Chyan, C. L.; Chen, Y. C., The Correlation between Neurotoxicity, Aggregative Ability and Secondary Structure Studied by Sequence Truncated Aβ Peptides. *FEBS lett.* **2007,** 581, 1161-1165.

11. Winner, B.; Jappelli, R.; Maji, S. K.; Desplats, P. A.; Boyer, L.; Aigner, S.; Hetzer, C.; Loher, T.; Vilar, M.; Campioni, S.; Tzitzilonis, C.; Soragni, A.; Jessberger, S.; Mira, H.; Consiglio, A.; Pham, E.; Masliah, E.; Gage, F. H.; Riek, R., In Vivo Demonstration that α-Synuclein Oligomers are Toxic. *Proc. Natl. Acad. Sci. USA* **2011,** 108, 4194-4199.

12. Jellinger, K. A., Interaction between Alpha-Synuclein and Other Proteins in Neurodegenerative Disorders. *ScientificWorldJournal* **2011,** 11, 1893-1907.

13. Irwin, D. J.; Lee, V. M. Y.; Trojanowski, J. Q., Parkinson's Disease Dementia: Convergence of α-Synuclein, tau and Amyloid-β Pathologies. *Nat. Rev. Neurosci.* **2013,** 14, 626-636.

14. Mandal, P.; Pettegrew, J.; Masliah, E.; Hamilton, R.; Mandal, R., Interaction between Aβ Peptide and α Synuclein: Molecular Mechanisms in Overlapping Pathology of Alzheimer's and Parkinson's in Dementia with Lewy Body Disease. *Neurochem. Res.* **2006,** 31, 1153-1162.

15. Masliah, E.; Rockenstein, E.; Veinbergs, I.; Sagara, Y.; Mallory, M.; Hashimoto, M.; Mucke, L., β-Amyloid Peptides Enhance α-Synuclein Accumulation and Neuronal Deficits in a Transgenic Mouse Model Linking Alzheimer's Disease and Parkinson's Disease. *Proc. Natl. Acad. Sci. USA* **2001,** 98, 12245-12250.

16. Morales, R.; Moreno-Gonzalez, I.; Soto, C., Cross-Seeding of Misfolded Proteins: Implications for Etiology and Pathogenesis of Protein Misfolding Diseases. *PLOS Pathog* **2013,** 9, e1003537.

17. Resende, R.; Marques, S. F.; Ferreiro, E.; Simões, I.; Oliveira, C.; Pereira, C. u. M. F., Effect of α-Synuclein on Amyloid β Induced Toxicity: Relevance to Lewy Body Variant of Alzheimer Disease. *Neurochem Res.* **2013,** 38, 797-806.

18. Tsigelny, I. F.; Crews, L.; Desplats, P.; Shaked, G. M.; Sharikov, Y.; Mizuno, H.; Spencer, B.; Rockenstein, E.; Trejo, M.; Platoshyn, O.; Yuan, J. X. J.; Masliah, E., Mechanisms of Hybrid Oligomer Formation in the Pathogenesis of Combined Alzheimer's and Parkinson's Diseases. *PLOS ONE* **2008,** 3, e3135.

19. Ono, K.; Takahashi, R.; Ikeda, T.; Yamada, M., Cross-Seeding Effects of Amyloid β-Protein and α-Synuclein. *J. Neurochem.* **2012,** 122, 883-890.

20. Lee, C.; Ham, S., Characterizing Amyloid-Beta Protein Misfolding from Molecular Dynamics Simulations with Explicit Water. *J. Comput. Chem.* **2010**, 349-355.

21. Jana, A. K.; Jose, J. C.; Sengupta, N., Critical Roles of Key Domains in Complete Adsorption of Aβ Peptide on Single-Walled Carbon Nanotubes: Insights with Point Mutations and MD Simulations. *Phys. Chem. Chem. Phys.* **2012,** 15, 837-844.

22. Jana, A. K.; Sengupta, N., Adsorption Mechanism and Collapse Propensities of the Full-Length, Monomeric Aβ1-42 on the Surface of a Single-Walled Carbon Nanotube: A Molecular Dynamics Simulation Study. *Biophys J.* **2012,** 102, 1889-1896.

23. Zhang, S.; Iwata, K.; Lachenmann, M. J.; Peng, J. W.; Li, S.; Stimson, E. R.; Lu, Y. a.; Felix, A. M.; Maggio, J. E.; Lee, J. P., The Alzheimer's Peptide Aβ Adopts a Collapsed Coil Structure in Water. *J. Struct. Biol.* **2000,** 130, 130-141.

24. Anand, P.; Nandel, F. S.; Hansmann, U. H. E., The Alzheimer β-Amyloid (Aβ-39) Dimer in an Implicit Solvent. *J. Chem. Phys.* **2008,** 129, 1-7.

25. Ma, B.; Nussinov, R., Stabilities and Conformations of Alzheimer's β-Amyloid Peptide Oligomers (Aβ16–22, Aβ16–35, and Aβ10–35): Sequence Effects. *Proc. Natl. Acad. Sci. USA* **2002,** 99, 14126-14131.

26. Reddy, G.; Straub, J. E.; Thirumalai, D., Influence of Preformed Asp23-Lys28 Salt Bridge on the Conformational Fluctuations of Monomers and Dimers of Aβ Peptides with Implications for Rates of Fibril Formation. *J. Phys. Chem. B* **2009,** 113, 1162-1172.

27. Tarus, B.; Straub, J. E.; Thirumalai, D., Dynamics of Asp23-Lys28 Salt-Bridge Formation in Aβ10-35 Monomers. *J. Am. Chem. Soc.* **2006,** 128, 16159-16168.

28. Chatelier, R. C.; Minton, A. P., Adsorption of Globular Proteins on Locally Planar Surfaces: Models for the Effect of Excluded Surface Area and Aggregation of Adsorbed Protein on Adsorption Equilibria. *Biophys J.* **1996,** 71, 2367-2374.

29. Minton, A. P., Adsorption of Globular Proteins on Locally Planar Surfaces. II. Models for the Effect of Multiple Adsorbate Conformations on Adsorption Equilibria and Kinetics. *Biophys J.* **1999,** 76, 176-187.

30. Minton, A. P., The Influence of Macromolecular Crowding and Macromolecular Confinement on Biochemical Reactions in Physiological Media. *J. Biol. Chem.* **2001,** 276, 10577-10580.

31. Chong, S.-H.; Ham, S., Impact of Chemical Heterogeneity on Protein Self-Assembly in Water. *Proc. Natl. Acad. Sci. U.S.A.* **2012,** 109, 7636-7641.

32. Hamelberg, D.; Mongan, J.; McCammon, J. A., Accelerated Molecular Dynamics: A Promising and Efficient Simulation Method for Biomolecules. *J. Chem. Phys.* **2004,** 120, 11919-11929.

33. Simona, T.; Veronica, E.; Paolo, V.; Nico, A. J. v. N.; Alexandre, M. J. J. B.; Remo, G.; Teodorico, T.; Piero, A. T.; Delia, P., The alpha-to-beta Conformational Transition of Alzheimer's Abeta-(1-42) Peptide in Aqueous Media is Reversible: A Step by Step Conformational Analysis Suggests the Location of Beta Conformation Seeding. *ChemBioChem* **2006,** 7, 257-267.

34. Rao, J. N.; Jao, C. C.; Hegde, B. G.; Langen, R.; Ulmer, T. S., A Combinatorial NMR and EPR Approach for Evaluating the Structural Ensemble of Partially Folded Proteins. *J. Am. Chem. Soc.* **2010,** 132, 8657-8668.

35. Kale, L.; Skeel, R.; Bhandarkar, M.; Brunner, R.; Gursoy, A.; Krawetz, N.; Phillips, J.; Shinozaki, A.; Varadarajan, K.; Schulten, K., NAMD2: Greater Scalability for Parallel Molecular Dynamics. *J. Comp. Phys.* **1999,** 151, 283-312.

36. Mackerell, A. D.; Feig, M.; Brooks, C. L., Extending the Treatment of Backbone Energetics in Protein Force Fields: Limitations of Gas-phase Quantum Mechanics in Reproducing Protein Conformational Distributions in Molecular Dynamics Simulations. *J. Comp. Chem.* **2004,** 25, 1400-1415.

37. MacKerell, A. D.; Bashford, D.; Bellott; Dunbrack, R. L.; Evanseck, J. D.; Field, M. J.; Fischer, S.; Gao, J.; Guo, H.; Ha, S.; Joseph-McCarthy, D.; Kuchnir, L.; Kuczera, K.; Lau, F. T. K.; Mattos, C.; Michnick, S.; Ngo, T.; Nguyen, D. T.; Prodhom, B.; Reiher, W. E.; Roux, B.; Schlenkrich, M.; Smith, J. C.; Stote, R.; Straub, J.; Watanabe, M.; Wiorkiewicz-Kuczera, J.; Yin, D.; Karplus, M., All-Atom Empirical Potential for Molecular Modeling and Dynamics Studies of Proteins. *J. Phys. Chem. B* **1998,** 102, 3586-3616.

38. Games, D.; Seubert, P.; Rockenstein, E.; Patrick, C.; Trejo, M.; Ubhi, K.; Ettle, B.; Ghassemiam, M.; Barbour, R.; Schenk, D.; Nuber, S.; Masliah, E., Axonopathy in an α-Synuclein Transgenic Model of Lewy Body Disease Is Associated with Extensive Accumulation of C-Terminal-Truncated α-Synuclein. *Am. J. Pathol.* **2013,** 182, 940-953.

39. Kanda, S.; Bishop, J. F.; Eglitis, M. A.; Yang, Y.; Mouradian, M. M., Enhanced Vulnerability to Oxidative Stress by α-Synuclein Mutations and C-Terminal Truncation. *Neurosci.* **2000,** 97, 279-284.

40. Li, W.; West, N.; Colla, E.; Pletnikova, O.; Troncoso, J. C.; Marsh, L.; Dawson, T. M.; JÃ¤kÃ¤lÃ¤, P.; Hartmann, T.; Price, D. L.; Lee, M. K., Aggregation Promoting C-Terminal Truncation of α-Synuclein is a Normal Cellular Process and is Enhanced by the Familial Parkinson's Disease-Linked Mutations. *Proc. Natl. Acad. Sci. USA* **2005,** 102, 2162-2167.

41. Sgourakis, N. G.; Yan, Y.; McCallum, S. A.; Wang, C.; Garcia, A. E., The Alzheimer's Peptides Aβ40 and 42 Adopt Distinct Conformations in Water: A Combined MD / NMR Study. *J. Mol. Biol.* **2007,** 368, 1448-1457.

42. Lin, Y.-S.; Bowman, Gregory, R.; Beauchamp, Kyle, A.; Pande, Vijay, S., Investigating How Peptide Length and a Pathogenic Mutation Modify the Structural Ensemble of Amyloid Beta Monomer. *Biophys J.* **2012,** 102, 315-324.

43. Rosenman, D. J.; Connors, C. R.; Chen, W.; Wang, C.; GarcÃa, A. E., Aβ Monomers Transiently Sample Oligomer and Fibril-Like Configurations: Ensemble Characterization Using a Combined MD/NMR Approach. *J. Mol. Biol.* **2013,** 425, 3338-3359.

44. Ball, K. A.; Phillips, A. H.; Nerenberg, P. S.; Fawzi, N. L.; Wemmer, D. E.; Head-Gordon, T., Homogeneous and Heterogeneous Tertiary Structure Ensembles of Amyloid-β Peptides. *Biochemistry* **2011,** 50, 7612-7628.

45. Osapay, K.; Case, D. A., A New Analysis of Proton Chemical Shifts in Proteins. *J. Am. Chem. Soc.***1991,** 113, 9436-9444.

46. Hou, L.; Shao, H.; Zhang, Y.; Li, H.; Menon, N. K.; Neuhaus, E. B.; Brewer, J. M.; Byeon, I.-J. L.; Ray, D. G.; Vitek, M. P.; Iwashita, T.; Makula, R. A.; Przybyla, A. B.; Zagorski, M. G., Solution NMR Studies of the Aβ(1-40) and Aβ(1-42) Peptides Establish that the Met35 Oxidation State Affects the Mechanism of Amyloid Formation. *J. Am. Chem. Soc.* **2004,** 126, 1992-2005.

47. Eliezer, D.; Kutluay, E.; Bussell Jr, R.; Browne, G., Conformational Properties of α-Synuclein in its Free and Lipid-Associated States. *J. Mol. Biol.* **2001,** 307, 1061-1073.

48. Jorgensen, W. L.; Chandrasekhar, J.; Madura, J. D.; Impey, R. W.; Klein, M. L., Comparison of Simple Potential Functions for Simulating Liquid Water. *J. Chem. Phys.* **1983,** 79, 926-935.

49. Feller, S. E.; Zhang, Y.; Pastor, R. W.; Brooks, B. R., Constant Pressure Molecular Dynamics Simulation: The Langevin Piston Method. *J. Chem. Phys.* **1995,** 103, 4613-4621.

50. Martyna, G. J.; Tobias, D. J.; Klein, M. L., Constant Pressure Molecular Dynamics Algorithms. *J. Chem. Phys.* **1994,** 101, 4177-4189.

51. Ryckaert, J.-P.; Ciccotti, G.; Berendsen, H. J. C., Numerical Integration of the Cartesian Equations of Motion of a System with Constraints: Molecular Dynamics of n-Alkanes. *J. Comp. Phys.* **1977,** 23, 327-341.

52. Essmann, U.; Perera, L.; Berkowitz, M. L.; Darden, T.; Lee, H.; Pedersen, L. G., A Smooth Particle Mesh Ewald Method. *J. Chem. Phys.* **1995,** 103, 8577-8593.

53. WL, D., PyMOL: an Open-source Molecular Graphics Tool. *Ccp4 Newslett. Protein Crystallogr.* **2002,** 40,.

54. Humphrey, W.; Dalke, A.; Schulten, K., VMD: Visual Molecular Dynamics. *J. Mol. Graph.* **1996,** 14, 33-38.

55. Glykos, N. M., Software News and Updates Carma: A Molecular Dynamics Analysis Program. *J. Comp. Chem.* **2006,** 27, 1765-1768.

56. Fadouloglou, V. E.; Stavrakoudis, A.; Bouriotis, V.; Kokkinidis, M.; Glykos, N. M., Molecular Dynamics Simulations of BcZBP, A Deacetylase from Bacillus cereus: Active Site Loops Determine Substrate Accessibility and Specificity. *J. Chem. Theory Comput.* **2009,** 5, 3299-3311.

57. Wan, H.; Hu, J.-p.; Li, K.-s.; Tian, X.-h.; Chang, S., Molecular Dynamics Simulations of DNA-Free and DNA-Bound TAL Effectors. *PLOS ONE* **2013,** 8, e76045.

58. Nguyen, P. H.; Li, M. S.; Derreumaux, P., Amyloid Dligomer Structure Characterization from Simulations: A General Method. *J. Chem. Phys.* **2014,** 140, 094105-1-9.

59. Schlitter, J., Estimation of Absolute and Relative Entropies of Macromolecules Using the Covariance Matrix. *Chem. Phys. Lett.* **1993,** 215, 617-621.

60. Schäfer, H.; Daura, X.; Mark, A. E.; van Gunsteren, W. F., Entropy Calculations on a Reversibly Folding Peptide: Changes in Solute Free Energy cannot Explain Folding Behavior. *Proteins: Struct. Funct. Bioinf.* **2001,** 43, 45-56.

61. Sinha, S. K.; Chakraborty, S.; Bandyopadhyay, S., Secondary Structure Specific Entropy Change of a Partially Unfolded Protein Molecule. *Langmuir* **2010,** 26, 9911-9916.

62. Furini, S.; Barbini, P.; Domene, C., DNA-Recognition Process Described by MD Simulations of the Lactose Repressor Protein on a Specific and a Non-Specific DNA Sequence. *Nucleic Acids Research* **2013,** 41, 3963-3972.

63. Barz, B.; Urbanc, B., Dimer Formation Enhances Structural Differences between Amyloid β-Protein (1-40) and (1-42): An Explicit-Solvent Molecular Dynamics Study. *PLOS ONE* **2012,** 7, e34345.

64. Petkova, A. T.; Ishii, Y.; Balbach, J. J.; Antzutkin, O. N.; Leapman, R. D.; Delaglio, F.; Tycko, R., A structural Model for Alzheimer's β-Amyloid Fibrils Based on Experimental Constraints from Solid State NMR. *Proc. Natl. Acad. Sci. USA* **2002,** 99, 16742-16747.

65. Rezaei-Ghaleh, N.; Amininasab, M.; Giller, K.; Kumar, S.; Stündl, A.; Schneider, A.; Becker, S.; Walter, J.; Zweckstetter, M., Turn Plasticity Distinguishes Different Modes of Amyloid-β Aggregation. *J. Am. Chem. Soc.* **2014,** 136, 4913-4919.

66. Wise-Scira, O.; Xu, L.; Kitahara, T.; Perry, G.; Coskuner, O., Amyloid-β peptide Structure in Aqueous Solution Varies with Fragment size. *J. Chem. Phys.* **2011,** 135, 2051011-2051013.

67. Donald, J. E.; Kulp, D. W.; DeGrado, W. F., Salt Bridges: Geometrically Specific, Designable Interactions. *Proteins: Struct. Funct. Bioinf.* **2011,** 79, 898-915.

68. Gvritishvili, A. G.; Gribenko, A. V.; Makhatadze, G. I., Cooperativity of Complex Salt Bridges. *Protein Sci.* **2008,** 17, 1285-1290.

69. Musafia, B.; Buchner, V.; Arad, D., Complex Salt Bridges in Proteins: Statistical Analysis of Structure and Function. *J. Mol. Biol.* **1995,** 254, 761-770.

70. Meuzelaar, H.; Tros, M.; Huerta-Viga, A.; van Dijk, C. N.; Vreede, J.; Woutersen, S., Solvent-Exposed Salt Bridges Influence the Kinetics of α-Helix Folding and Unfolding. *J. Phys. Chem. Lett.* **2014,** 5, 900-904.

71. Salari, R.; Chong, L. T., Desolvation Costs of Salt Bridges across Protein Binding Interfaces: Similarities and Differences between Implicit and Explicit Solvent Models. *J. Phys. Chem. Lett.* **2010,** 1, 2844-2848.

72. Salari, R.; Chong, L. T., Effects of High Temperature on Desolvation Costs of Salt Bridges Across Protein Binding Interfaces: Similarities and Differences between Implicit and Explicit Solvent Models. *J. Phys. Chem. B* **2014,** 116, 2561-2567.

73. Bate, C.; Gentleman, S.; Williams, A., Alpha-Synuclein Induced Synapse Damage is Enhanced by Amyloid-beta1-42. *Molecular Neurodegeneration* **2010,** 5, 55.

74. Berhanu, W. M.; Yaşar, F.; Hansmann, U. H. E., In Silico Cross Seeding of Aβ and Amylin Fibril-like Oligomers. *ACS Chem. Neurosci.* **2013,** 4, 1488-1500.

75. Crews, L.; Tsigelny, I.; Hashimoto, M.; Masliah, E., Role of Synucleins in Alzheimer's Disease. *Neurotox. Res.* **2009,** 16, 306-317.

76. Hashimoto, M.; Masliah, E., Alpha-synuclein in Lewy Body Disease and Alzheimer's Disease. *Brain Pathol.* **1999,** 9, 707-720.

77. Lajtha, A.; Banik, N.; Ray, S.; Crews, L.; Spencer, B.; Masliah, E., Immunotherapy Strategies for Lewy Body and Parkinson's Diseases. In *Handbook of Neurochemistry and Molecular Neurobiology*, Springer US: 2009; pp 599-613.

78. Acharya, S.; Safaie, B. M.; Wongkongkathep, P.; Ivanova, M. I.; Attar, A.; Klärner, F.-G.; Schrader, T.; Loo, J. A.; Bitan, G.; Lapidus, L. J., Molecular Basis for Preventing α-Synuclein Aggregation by a Molecular Tweezer. *J. Biol. Chem.* **2014,** M113.524520.

79. Dutt, S.; Wilch, C.; Gersthagen, T.; Talbiersky, P.; Bravo-Rodriguez, K.; Hanni, M.; Sánchez-García , E.; Ochsenfeld, C.; Klärner, F.-G.; Schrader, T., Molecular Tweezers with Varying Anions: A Comparative Study. *J. Org. Chem.* **2013,** 78, 6721-6734.

80. Prabhudesai, S.; Sinha, S.; Attar, A.; Kotagiri, A.; Fitzmaurice, A.; Lakshmanan, R.; Ivanova, M.; Loo, J.; Klärner, F.-G.; Schrader, T.; Stahl, M.; Bitan, G.; Bronstein, J., A Novel "Molecular Tweezer" Inhibitor of α-Synuclein Neurotoxicity in Vitro and in Vivo. *Neurotherapeutics* **2012,** 9, 464-476.

81. Sinha, S.; Lopes, D. H. J.; Du, Z.; Pang, E. S.; Shanmugam, A.; Lomakin, A.; Talbiersky, P.; Tennstaedt, A.; McDaniel, K.; Bakshi, R.; Kuo, P.-Y.; Ehrmann, M.; Benedek, G. B.; Loo, J. A.; Klärner, F.-G.; Schrader, T.; Wang, C.; Bitan, G., Lysine-

Specific Molecular Tweezers are Broad-Spectrum Inhibitors of Assembly and Toxicity of Amyloid Proteins. *J. Am. Chem. Soc.* **2011,** 133, 16958-16969.

82. da Silva, F. L.; Coelho Cerqueira, E.; de Freitas, M. S.; Gonçalves, D. L.; Costa, L. T.; Follmer, C., Vitamins K Interact with N-Terminus α-Synuclein and Modulate the Protein Fibrillization in vitro. Exploring the Interaction between Quinones and α-Synuclein. *Neurochem. Int.* **2013,** 62, 103-112.

83. Li, J.; Liu, R.; Lam, K. S.; Jin, L.-W.; Duan, Y., Alzheimer's Disease Drug Candidates Stabilize A-β Protein Native Structure by Interacting with the Hydrophobic Core. *Biophys. J.* **2011,** 100, 1076-1082.

84. Luhrs, T.; Ritter, C.; Adrian, M.; Riek-Loher, D.; Bohrmann, B.; Dobeli, H.; Schubert, D.; Riek, R., 3D Structure of Alzheimer's Amyloid-β(1-42) fibrils. *Proc. Natl. Acad. Sci. USA* **2005,** 102, 17342-17347.

85. Kim, H.-Y.; Heise, H.; Fernandez, C. O.; Baldus, M.; Zweckstetter, M., Correlation of Amyloid Fibril β-Structure with the Unfolded State of α-Synuclein. *ChemBioChem* **2007,** 8, 1671-1674.

86. Ullman, O.; Fisher, C. K.; Stultz, C. M., Explaining the Structural Plasticity of α-Synuclein. *J. Am. Chem. Soc.* **2011,** 133, 19536-19546.

87. Hashimoto, M.; Hsu, L. J.; Xia, Y.; Takeda, A.; Sisk, A.; Sundsmo, M.; Masliah, E., Oxidative Stress Induces Amyloid-Like Aggregate Formation of NACP/α-Synuclein in vitro. *NeuroReport* **1999,** 10, 717-721.

88. Giasson, B. I.; Murray, I. V. J.; Trojanowski, J. Q.; Lee, V. M. Y., A Hydrophobic Stretch of 12 Amino Acid Residues in the Middle of α-Synuclein Is Essential for Filament Assembly. *J. Biol. Chem.* **2001,** 276, 2380-2386.

89. Cheng, P.-N.; Liu, C.; Zhao, M.; Eisenberg, D.; Nowick, J. S., Amyloid β-Sheet Mimics that Antagonize Protein Aggregation and Reduce Amyloid Toxicity. *Nat. Chem.* **2012,** 4, 927-933.

90. Viet, M. H.; Ngo, S. T.; Lam, N. S.; Li, M. S., Inhibition of Aggregation of Amyloid Peptides by Beta-Sheet Breaker Peptides and Their Binding Affinity. *J. Phys. Chem. B* **2011,** 115, 7433-7446.

Chapter 6

Conclusions and Future Perspectives

"Learn from yesterday, live for today, hope for tomorrow.
The important thing is not to stop questioning."
- Albert Einstein

This thesis describes computational work aimed at unraveling the mechanism of conformational dynamics and interactions of a representative intrinsically disordered amyloidogenic peptide, Aβ. The MD simulation studies conducted in different biologically relevant environments are performed keeping in mind the existing limitations associated with experimental techniques for probing molecular level details of the early dynamics of the monomeric peptide and its hydration properties at physiological conditions. The conformational preferences of the peptide in the vicinity of a model hydrophilic nano surface and the peptide's interactions with another intrinsically disordered amyloidogenic peptide, αSyn, addressed in this thesis give insights into the mechanism of possible toxic aggregation pathways of this peptide in the extracellular space. The key findings in this body of work and the future directions they lead to is briefly summarized in this chapter.

The understandings about the substantial role that hydrophobicity of CHC plays in the early structural collapse of Aβ peptide monomer provide basis for subsequent studies on the adsorption mechanism of the CHC on nano surfaces[1-5] The observed heterogeneity in the hydration dynamics as well as in the effective hydrophobicity of selected Aβ conformers necessitate a detailed investigation of solvent dynamics around different hydrophobic and hydrophilic regions of the peptide. A systematic investigation is essential to decouple the complex protein-water dynamic correlations. To make more generalizations regarding the observed differences in the hydration properties of globular proteins and IDPs, further comparative studies by selecting different proteins from these two classes are also ineluctable. Extended investigations on solvent dynamics at the interfaces of the reported cross amyloids can provide more mechanistic insights about the pathological interactions and transformations of the peptide in biological environments. It is also essential to study the interactions of the preformed cross amyloid dimers with model lipid bilayer to distinguish toxic interaction modes. The findings reported in this thesis and its proposed extensions can provide enhanced understanding about the complexities of intrinsically disordered amyloidogenic proteins to design efficient measures to block the toxic transformations.

6.1 Future Perpectives

6.1.1 Decoupling the Influence of Local and Global Dynamics of Protein on Hydration Shell Water Molecules

Recently, with the help of computational simulations it has been theoretically proven that the aggregation of amyloidogenic IDPs is greatly influenced by solvent energetics[6, 7]. An exhaustive understanding of the nature of dynamic correlation of the protein and its hydration shell water molecules is thus inevitable. We have studied the solvent dynamics around conformationally flexible IDP systems in comparison with that of a globular protein. The enhanced flexibility of proteins had significant influence on the dynamics of water around it. As explained in Chapter 4, substantial dynamic slow down of hydration shell water molecules around a representative IDP, Aβ_{42} as well as a globular protein, UBQ was observed when we had frozen the dynamics of these proteins.

Dynamics of biological molecules determine its function in the body. The 'jiggling and wiggling of atoms' in a biological molecule and its impact on the environment is require to be studied to understand any biological process[8]. Hence, we have extended the investigation to understand the influence of local and global dynamics of proteins on the hydration shell water molecules. Two representative IDPs, Aβ_{42} and αSynuclein (PDB ID: 2KKW[9]) as well as two representative globular proteins, ubiquitin (UBQ) (PDB ID: 1UBQ[10]) and Lyzosime (LYZ) (PDB ID:2LYM[11]) were chosen for this study. Among different conformations of Aβ_{42} used for the study reported in Chapter 4, AB4 conformation is selected for this study because its hydration waters exhibited the fastest translational motions.

We have generated three atomistic MD trajectories for each of these proteins. The first one is an unbiased system, we labeled this system 'flexible'; in the second system we have restrained the RMSD of the protein heavy atoms. It has been done by applying required external force using the colvar module implemented with NAMD package and we use the term 'rigid' for representing this system, here our intension is to freeze the local vibrations but not the rotational or translational motion of the proteins. The third trajectory, we represent as 'frozen' is generated by restraining the movement of all heavy atoms of the proteins and in this case both local as well as global dynamics of the protein get arrested.

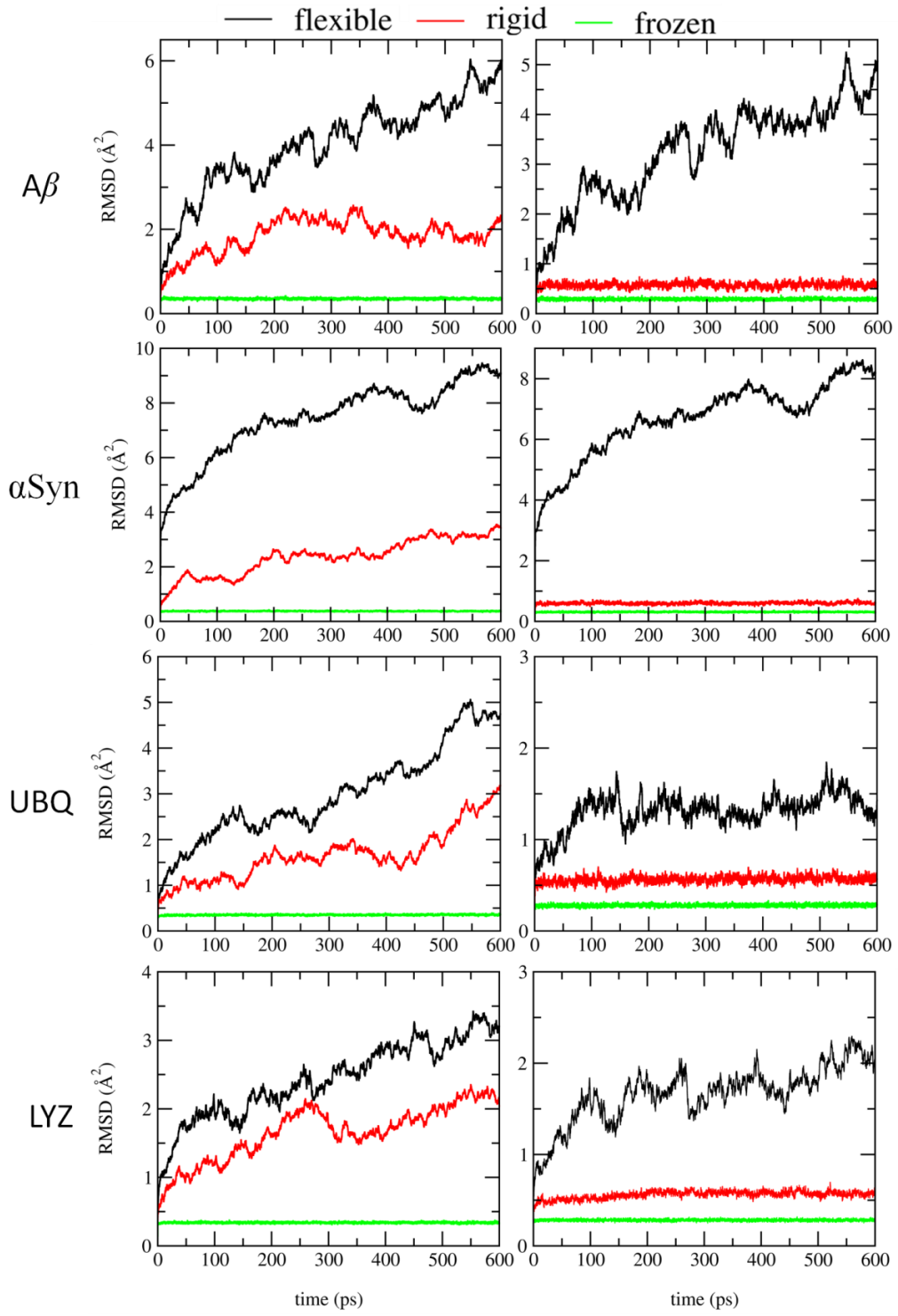

Figure 6.1. The Root Mean Squared Deviations (RMSD) of Aβ, αSyn, UBQ and LYZ for flexible, rigid and frozen systems. RMSDs of heavy atoms are presented in the left column and RMSDs of back bone atoms are in the right column.

In Figure 6.1 we have plotted the RMSD of all heavy atoms (left column) and back bone atoms (right column) for all the three trajectories of the selected proteins. RMSD is increasing in the unbiased flexible trajectories of all the four proteins but the

change in RMSD is completely restrained in the frozen trajectories. In the case of rigid systems, back bone atoms are significantly restrained so that the RMSD is very low in comparison with the flexible system. We couldn't completely restrain all heavy atoms because of methodological limitations hence, the local vibrations are not completely restrained. However, the RMSD is found to be reduced noticeably in case of all the proteins and therefore these systems can be considered as less flexible with reduced vibrational freedom.

The translational dynamics of hydration shell water molecules were investigated by calculating van Hove autocorrelation function. We have done this analysis as explained in Chapter 4. In Figure 6.2, the van Hove function, $4\pi r^2 G_s(r, t)$ or P(r; t), for the hydration shell water molecules of flexible, rigid and frozen trajectories of all the four selected proteins is presented. The probability of a water molecule residing in the hydration layer at time $t = 0$, to have moved a distance r in time t at 5, 20, 50 and 100 ps was calculated.

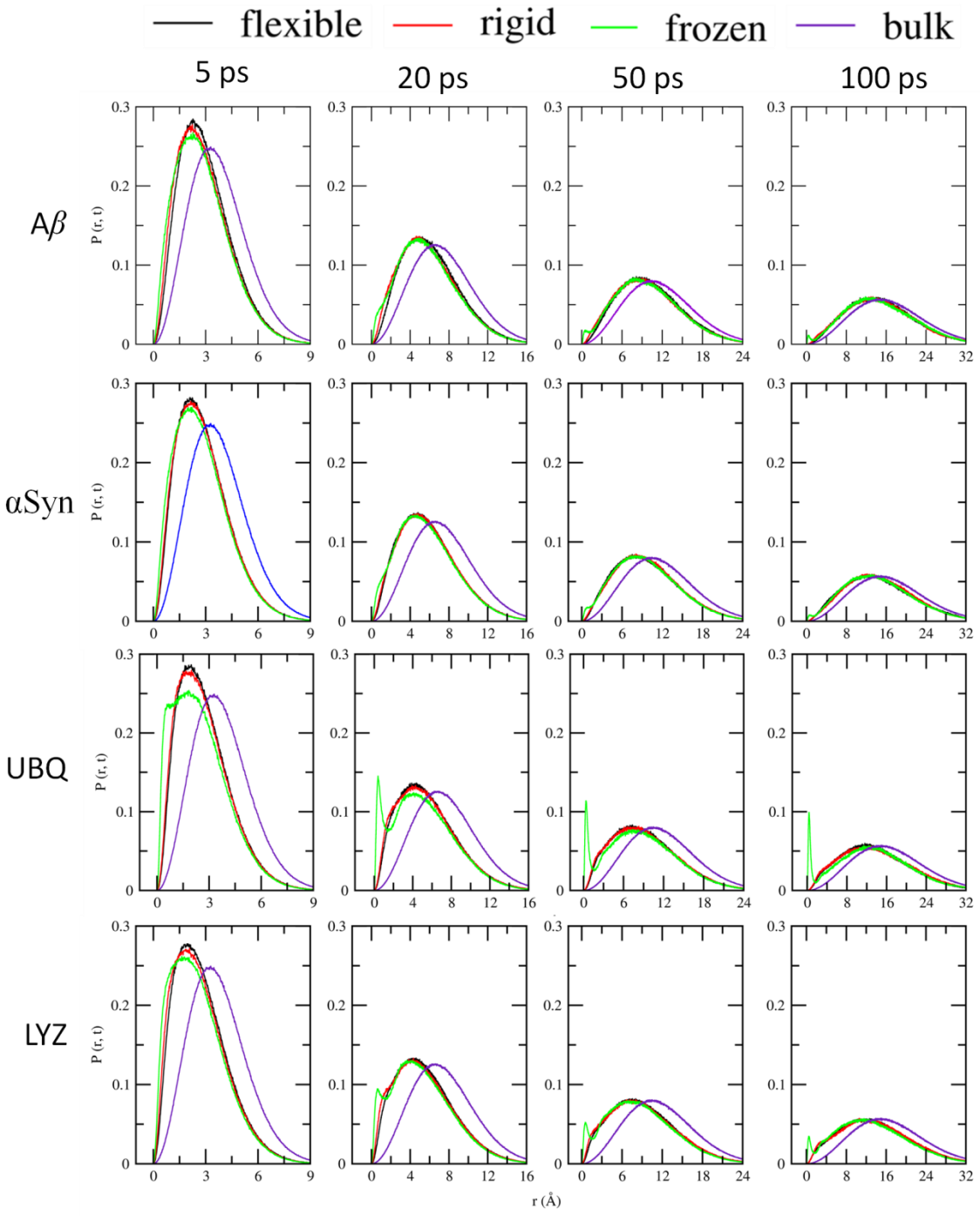

Figure 6.2. *P*(*r*; *t*) as a function of *r* for the first hydration layer water molecules around A*β*, αSyn, UBQ and LYZ. The corresponding functions for pure bulk water are included.

The corresponding data for pure bulk water is also included in the figure. Compared to bulk water the hydration shell water molecules show slower dynamics. The water molecules were found to be more sluggish on restraining the dynamics of protein molecules. An inhomogeneous distribution of the van Hove function was observed for the rigid and frozen trajectories. The inhomogeneity in the translational motion of waters was

found to be more prominent for globular proteins in comparison with the amyloidogenic systems on completely restraining all degrees of freedoms of the proteins. Hydration shell around UBQ exhibited the inhomogeneity in the distribution in a profound manner. It seems a group of water molecules tend to confine around the protein surface when there is no dynamics on the protein surface and this trend reduces with increase in the dynamic freedom of the protein.

The degree of freedom has influence on the diffusion of protein surface waters is evidenced from van Hove correlation function. To get a clear understanding about the translational motion of water molecules hydrating the selected proteins in the flexible, rigid and frozen systems we have calculated the mean square displacements (MSD), as a function of time. The MSD of bulk water is also included here for comparison. The methodological details are given in Chapter 4. As discussed earlier, compared to the bulk water hydration shell water molecules showed slower dynamics around all the selected proteins in its unbiased trajectories. We have observed the slowest dynamics of hydration shell water molecules in the frozen trajectories. This is in conjunction with what we observed in the van Hove calculation. Dynamic slow down of protein hydration waters observed in comparison with the flexible system was observed in Aβ, αSyn and LYZ for the rigid trajectories while in case of UBQ the water molecules undergo faster dynamics compared to the flexible system.

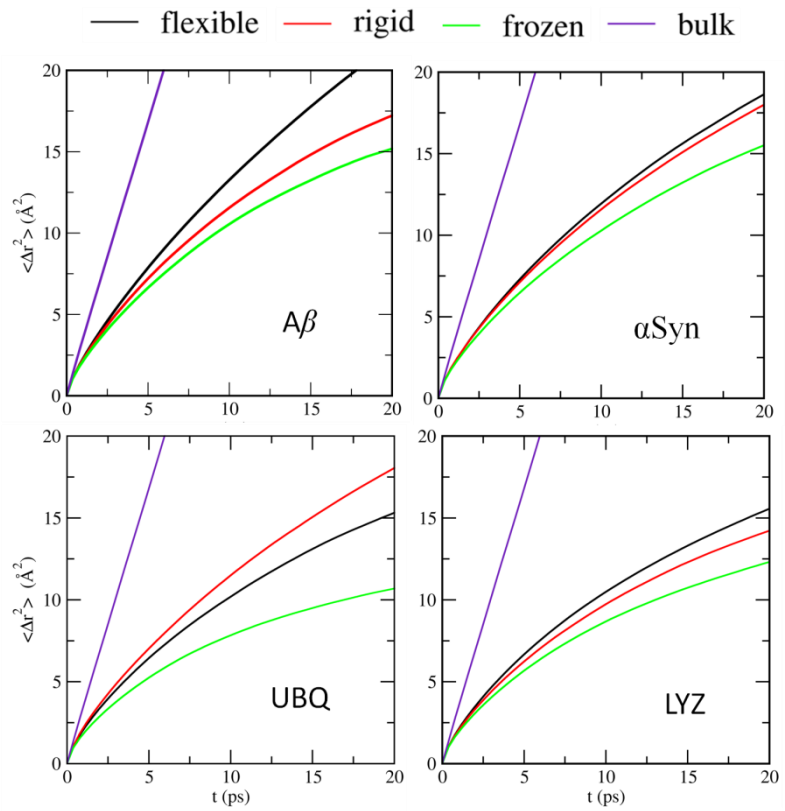

Figure 6.3. Mean square displacement (MSD) of water molecules present in the first hydration layers of different proteins. The MSD of water in pure bulk state is shown for comparison.

These preliminary studies and observations are inadequate to make any generalization about the influence of global and local dynamics of protein on the solvent dynamic. We have to study this problem using more proteins from both the classes with varying sizes. More sophisticated methodologies should be adopted to generate trajectories with decoupled degrees of freedom.

6.2.2 Heterogeneous dynamics of the interfacial water molecules in the stabilization of amyloid assemblies

We have identified different cross interaction modes of IDPs A$\beta_{1\text{-}42}$ and αSynulein$_{1\text{-}95}$. The detailed investigation of these different interaction modes gave a molecular level understanding about the early pathological cross aggregation of these peptides in water. It was interesting to observe that the interfaces in the studied cross dimers were highly heterogeneous. Four out of five interaction modes were dominated by hydrophilic interactions while we could observe a minor mode with very stable hydrophobic interface. All the hydrophilic interfaces were characterized by permanent or

transient salt bridge formation while the hydrophobic interface was the most dried without any salt bridges.

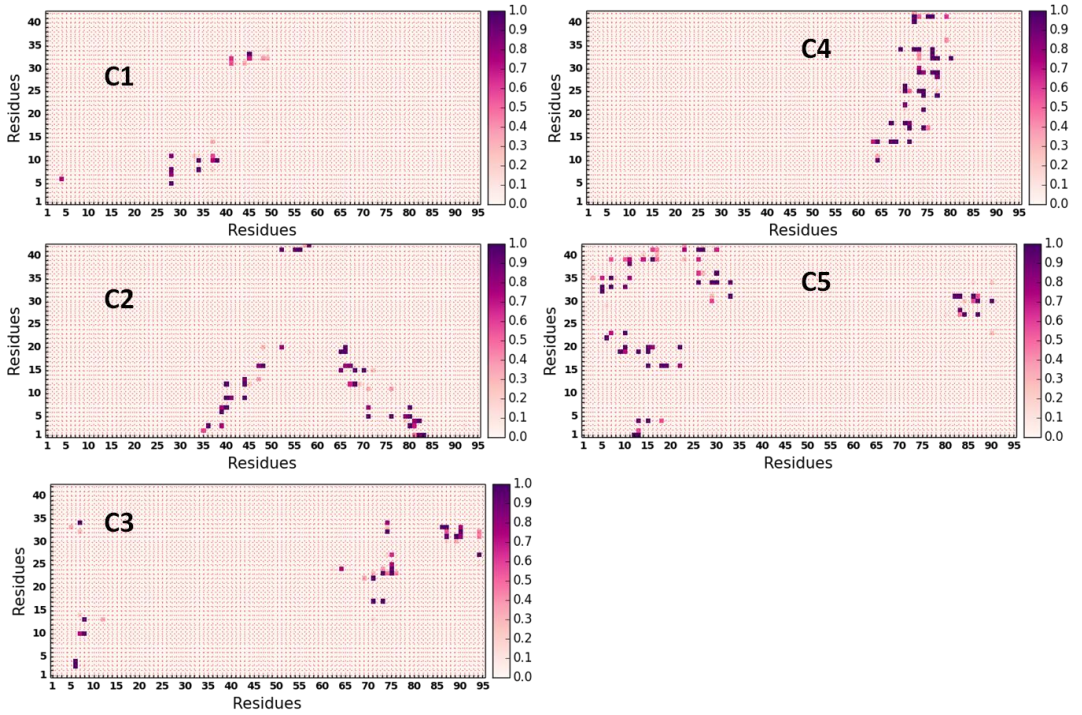

Figure 6.4 Residue specific side chain contact probability of αSyn$_{1\text{-}95}$ with A$\beta_{1\text{-}42}$ in different interaction sub modes.

The role of repeating LYS residues present in Asyn in the stabilization of the interfaces and saltbridge formation was prominent. 'Complex' salt bridge formation and enhanced dryness was observed in two among the four hydrophilic interfaces of the dimeric systems with highest contact area and strongest inter peptide interactions. It has been reported in literature that the salt bridge formation is often associated with a desolvation barrier[12-14]. Hence, further investigation of these heterogeneous interfaces will be useful to explore the role of water in the stabilization of different amyloidogenic assemblies.

To get a preliminary idea about the behavior of water molecules at the inter peptide interfaces, we have generated 100 ps of high frequency (8 fs) trajectory in NVT ensemble after 4 ns of equilibration in NPT ensemble from the representative structure taken for the study reported in Chapter 5.

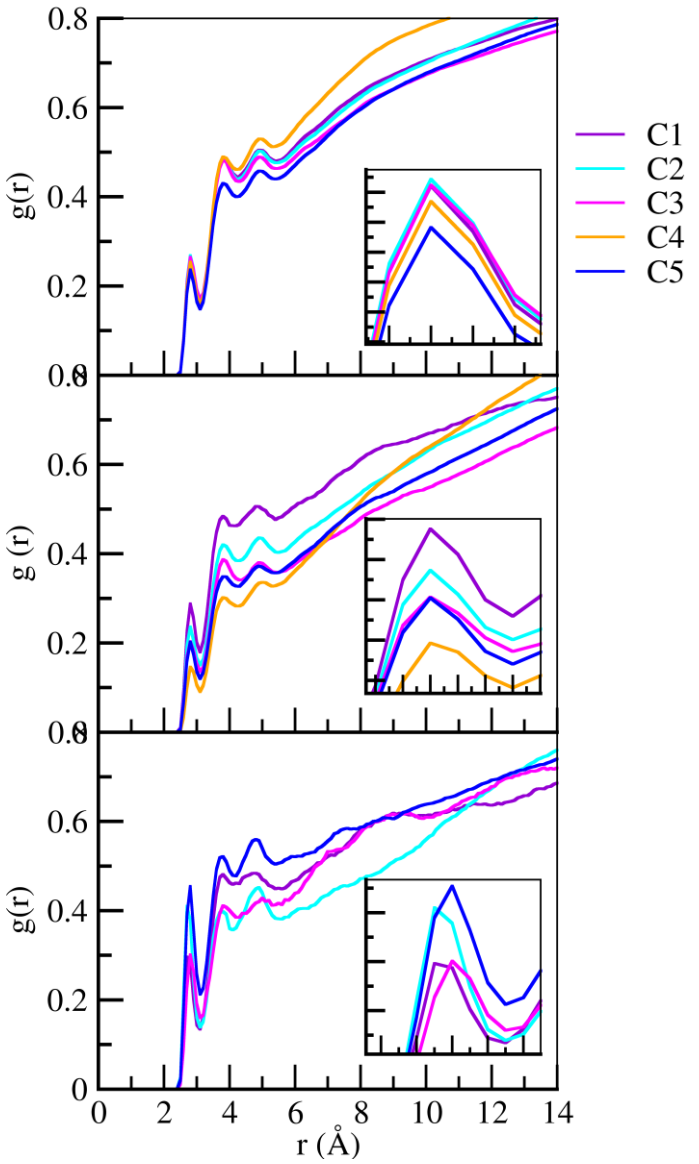

Figure 6.5. The radial distribution function (g (r)) calculated between oxygens of the solvent water molecules and the heavy atoms of (1) the peptide dimer; (2) all the residues in the contact region (residues exhibit a contact probability of more than 0.7 in figure 1); (3) all the residues forming salt bridge.

We have given the same names for the respective systems as C1, C2, C3, C4 and C5. Eventhough, the contact pattern and the nature of the interfaces are maintained as in the previously reported study (Figure 6.4**.** inter peptide distance based contact probability map) we have noticed slight variations in the salt bridge formation in the newly generated systems. As observed earlier the hydrophobic interface C4 is exceptional with the absence of salt bridge and predominance in van der Waals interaction. A single but persistent salt

bridge was formed between Asyn^{28}Glu and Ab^{5}Arg in C1. Complex salt bridge was formed by Asyn^{80}Lys with Ab^{3}Asp and Ab^{7}Asp in system C2. In system C3 only one transient salt bridge was formed between Asyn^{6}Lys and Ab^{3}Glu. However in system C5 three salt bridges were observed between Asyn^{12}Lys and Ab^{7}Asp; Asyn^{10}Lys and Ab^{23}Asp; Asyn^{6}Lys and Ab^{22}Glu among which the last one was transient.

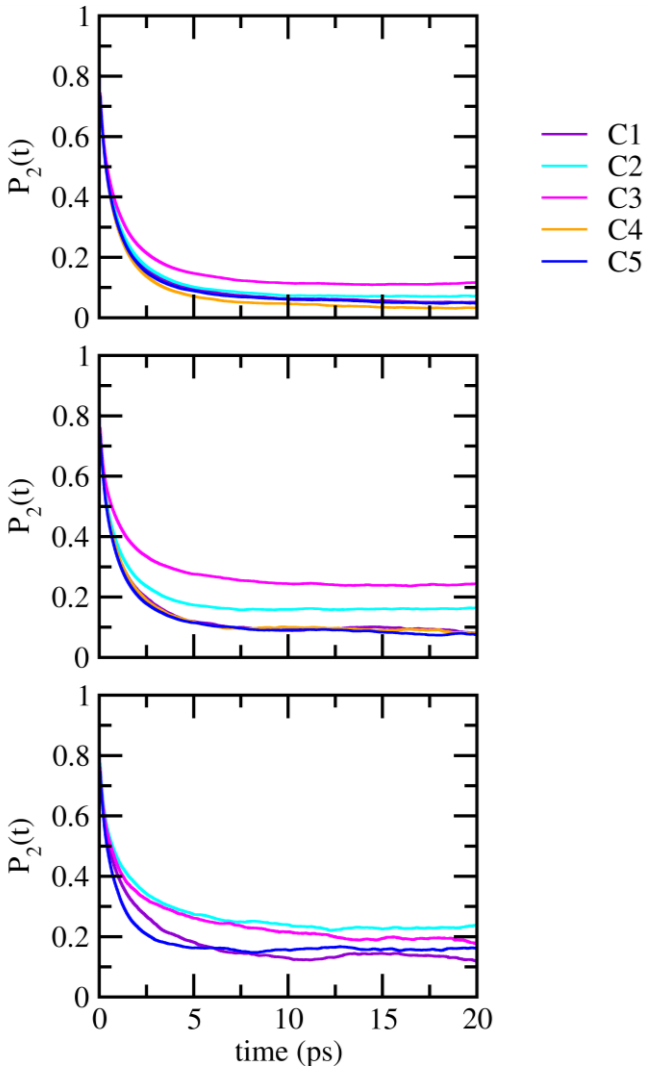

Figure 6.6. The rotational reorientation time correlation function of hydration layer water molecules around the heavy atoms of (1) the peptide dimer; (2) all the residues in the contact region (residues exhibit a contact probability of more than 0.7 in Figure 6.4); (3) all the residues forming salt bridge.

Here, in this study we have probed the comparative distribution, interaction and rotational dynamics of water molecules around the peptide dimer complex; at the interfaces and at close proximity of the salt bridges. Figure 6.5 is the radial distribution function (g (r)) calculated between oxygens of the solvent water molecules and the heavy

atoms of (1) the peptide dimer; (2) all the residues in the contact region (residues exhibit a contact probability of more than 0.7 in Figure 6.4); (3) all the residues forming salt bridge.The heterogeneity in the surface hydration is more prominent in the contact region compared to the peptide dimer complex. The solvation heterogeneity is observed also around the salt bridge forming residues in clusters C1, C2, C3, and C5.

The rotational reorientation time correlation function (P_2t) of hydration layer (5Å) water molecules near the surface of the above three selections are represented in Figure 6. 6. It shows slowest solvent rotational dynamics for system C3 around the dimeric system and also in the contact region followed by system C2. The fastest rotational dynamics around the hetero dimer was observed in C4 but the rotational relaxation pattern is almost similar at the interface for systems C3, C4, and C5. The rotational dynamics of solvation waters on the surface of the heavy atoms of salt bridge forming residues shows slowest dynamics around C2, where we have observed the complex salt bridge formation. To get mechanistic insights regarding the role of solvent in stabilizing the observed heterogenic amyloid interfaces further sampling and analyses are required.

6.2.3 Toxicity of the Heterogeneous Cross Amyloids

It has been already reported that the cross oligomers of Aβ and αSyn interact with lipid bilayer and these oligomeric species can induce toxicity in vivo[15-17]. The identification of dimers with heterologic interaction patterns invokes us to investigate the toxicity of these species. The hetero dimerisation pathways perhaps lead to polymorphic oligomeric as well as fibrilar assemblies. It can be hypothesis that the interactions of these polymorphic species with a lipid bilayer will be heterogeneous. Hence, it is necessary to identify the molecular level interaction mechanism of these hetero dimers with the lipid bilayer. Such a study with representative dimeric species and model biological surface by utilizing the MD simulation technique will be helpful to distinguish the toxic cross amyloids.

6.3 References

1. Jana, A. K.; Sengupta, N., Adsorption Mechanism and Collapse Propensities of the Full-Length, Monomeric Aβ1-42 on the Surface of a Single-Walled Carbon Nanotube: A Molecular Dynamics Simulation Study. *Biophys. J.* **2012,** 102, 1889-1896.
2. Jana, A. K.; Jose, J. C.; Sengupta, N., Critical Roles of Key Domains in Complete Adsorption of Aβ Peptide on Single-Walled Carbon Nanotubes: Insights with Point Mutations and MD Simulations. *Phys. Chem. Chem. Phys.* **2012,** 15, 837-844.

3. Jana, A. K.; Sengupta, N., Surface Induced Collapse of Aβ1-42 with the F19A Replacement Following Adsorption on a Single Walled Carbon Nanotube. *Biophys. Chem.* **2013,** 184, 108-115.
4. Xie, L.; Lin, D.; Luo, Y.; Li, H.; Yang, X.; Wei, G., Effects of Hydroxylated Carbon Nanotubes on the Aggregation of Aβ16-22 Peptides: A Combined Simulation and Experimental Study. *Biophys. J.* **2014,** 107, 1930-1938.
5. Xie, L.; Luo, Y.; Lin, D.; Xi, W.; Yang, X.; Wei, G., The Molecular Mechanism of Fullerene-Inhibited Aggregation of Alzheimer's β-Amyloid Peptide Fragment. *Nanoscale* **2014,** 6, 9752-9762.
6. Chong, S.-H.; Ham, S., Atomic-Level Investigations on the Amyloid-β Dimerization Process and its Driving Forces in Water. *Phys. Chem. Chem. Phys.* **2012,** 14, 1573-1575.
7. Chong, S.-H.; Ham, S., Atomic Decomposition of the Protein Solvation Free Energy and its Application to Amyloid-β Protein in Water. *J. Chem. Phys.* **2011,** 135, 034506.
8. Feynman, R. P., Robert B. Leighton, Matthew Sands, Lectures on Physics. **1963,** vol. 1, p. 3-6
9. Rao, J. N.; Jao, C. C.; Hegde, B. G.; Langen, R.; Ulmer, T. S., A Combinatorial NMR and EPR Approach for Evaluating the Structural Ensemble of Partially Folded Proteins. *J. Am. Chem. Soc.* **2010,** 132, 8657-8668.
10. Vijay-Kumar, S.; Bugg, C. E.; Cook, W. J., Structure of ubiquitin refined at 1.8Å resolution. *J. Mol. Biol.* **1987,** 194, 531-544.
11. Kundrot, C. E.; Richards, F. M., Crystal Structure of Hen Egg-White Lysozyme at a Hydrostatic Pressure of 1000 Atmospheres. *J. Mol. Biol.* **1987,** 193, 157-170.
12. Meuzelaar, H.; Tros, M.; Huerta-Viga, A.; van Dijk, C. N.; Vreede, J.; Woutersen, S., Solvent-Exposed Salt Bridges Influence the Kinetics of α-Helix Folding and Unfolding. *J. Phys. Chem. Lett.* **2014,** 5, 900-904.
13. Salari, R.; Chong, L. T., Desolvation Costs of Salt Bridges across Protein Binding Interfaces: Similarities and Differences between Implicit and Explicit Solvent Models. *J. Phys. Chem. Lett.* **2010,** 1, 2844-2848.
14. Salari, R.; Chong, L. T., Effects of High Temperature on Desolvation Costs of Salt Bridges Across Protein Binding Interfaces: Similarities and Differences between Implicit and Explicit Solvent Models. *J. Phys. Chem. B* **2014,** 116, 2561-2567.
15. Mandal, P.; Pettegrew, J.; Masliah, E.; Hamilton, R.; Mandal, R., Interaction between Aβ Peptide and α Synuclein: Molecular Mechanisms in Overlapping Pathology of

Alzheimer's and Parkinson's in Dementia with Lewy Body Disease. *Neurochem. Res.* **2006,** 31, 1153-1162.

16. Masliah, E.; Rockenstein, E.; Veinbergs, I.; Sagara, Y.; Mallory, M.; Hashimoto, M.; Mucke, L., β-Amyloid Peptides Enhance α-Synuclein Accumulation and Neuronal Deficits in a Transgenic Mouse Model Linking Alzheimer's Disease and Parkinson's Disease. *Proc. Natl. Acad Sci. USA* **2001,** 98, 12245-12250.
17. Tsigelny, I. F.; Crews, L.; Desplats, P.; Shaked, G. M.; Sharikov, Y.; Mizuno, H.; Spencer, B.; Rockenstein, E.; Trejo, M.; Platoshyn, O.; Yuan, J. X. J.; Masliah, E., Mechanisms of Hybrid Oligomer Formation in the Pathogenesis of Combined Alzheimer's and Parkinson's Diseases. *PLOS ONE* **2008,** 3, e3135.

Appendix I

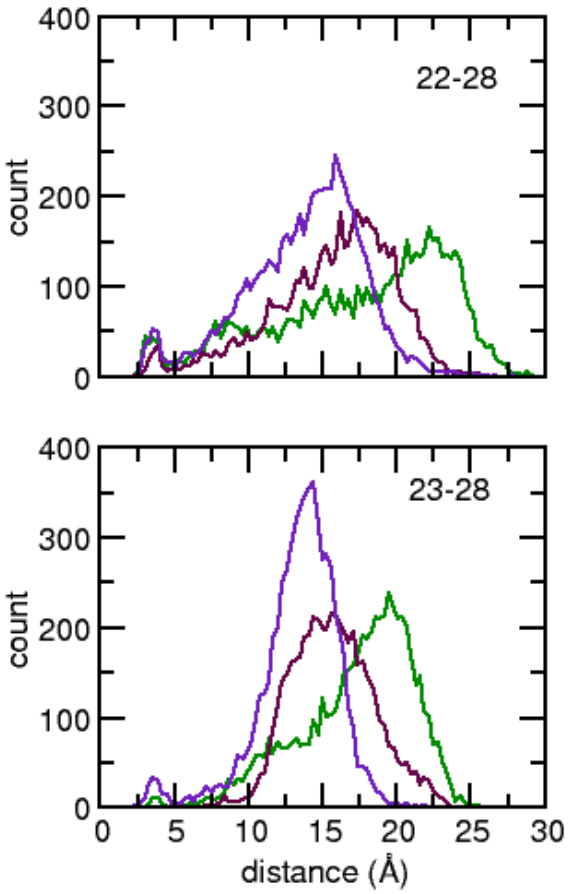

Figure AI-1. Population distribution of the distance between atoms which can form salt bridge in E22-K28 (top) and D23-K28 (bottom). Data for systems A, B and C are depicted in green, maroon and indigo, respectively.

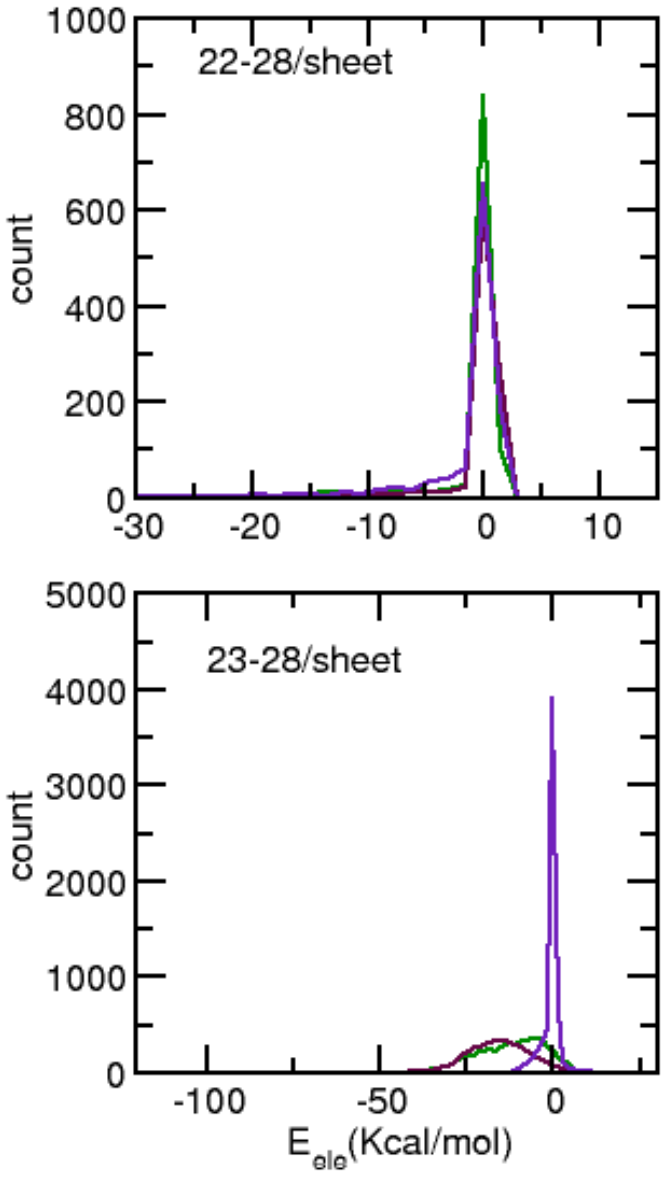

Figure AI-2. Population distribution of the electrostatic interaction of the TiO_2 surface with the sidechains of residue pairs which can form saltbridges. Data for systems A, B and C are depicted in green, maroon and indigo, respectively.

Appendix II

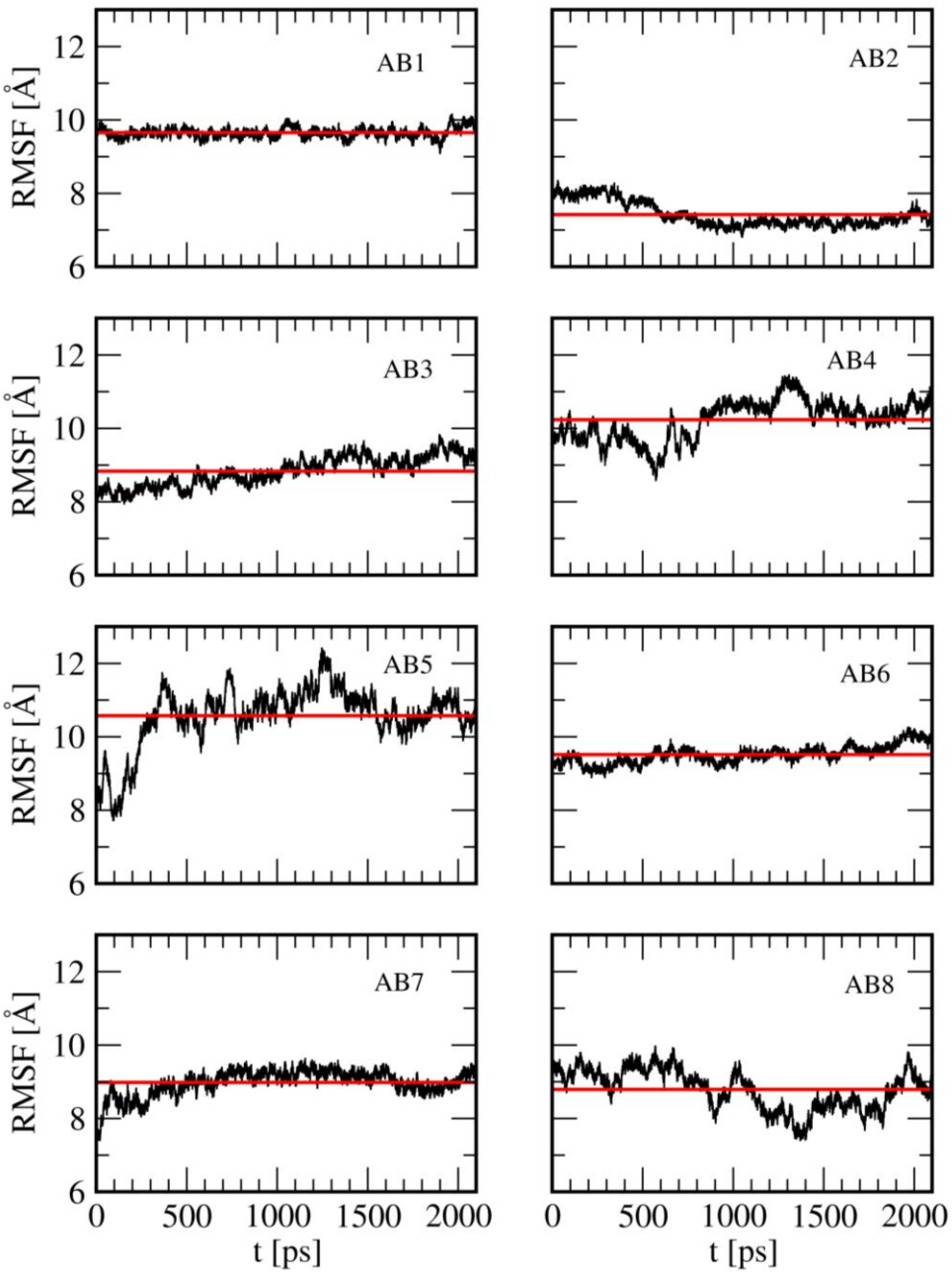

Figure AII-1. Root mean squared fluctuations (RMSF) of all the non-hydrogen atoms during the 2 ns analysis run for the eight AB conformations. The straight lines indicate the corresponding average values.

Systems	*Q*
AB1	0.88 (0.01)
AB2	0.86 (0.03)
AB3	0.79 (0.02)
AB4	0.79 (0.03)
AB5	0.76 (0.03)
AB6	0.82 (0.02)
AB7	0.75 (0.03)
AB8	0.80 (0.01)

Table AII-1. Structural persistence, *Q*, averaged over the 2 ns analysis run for each Aβ conformation. Standard deviations are provided in the parentheses.

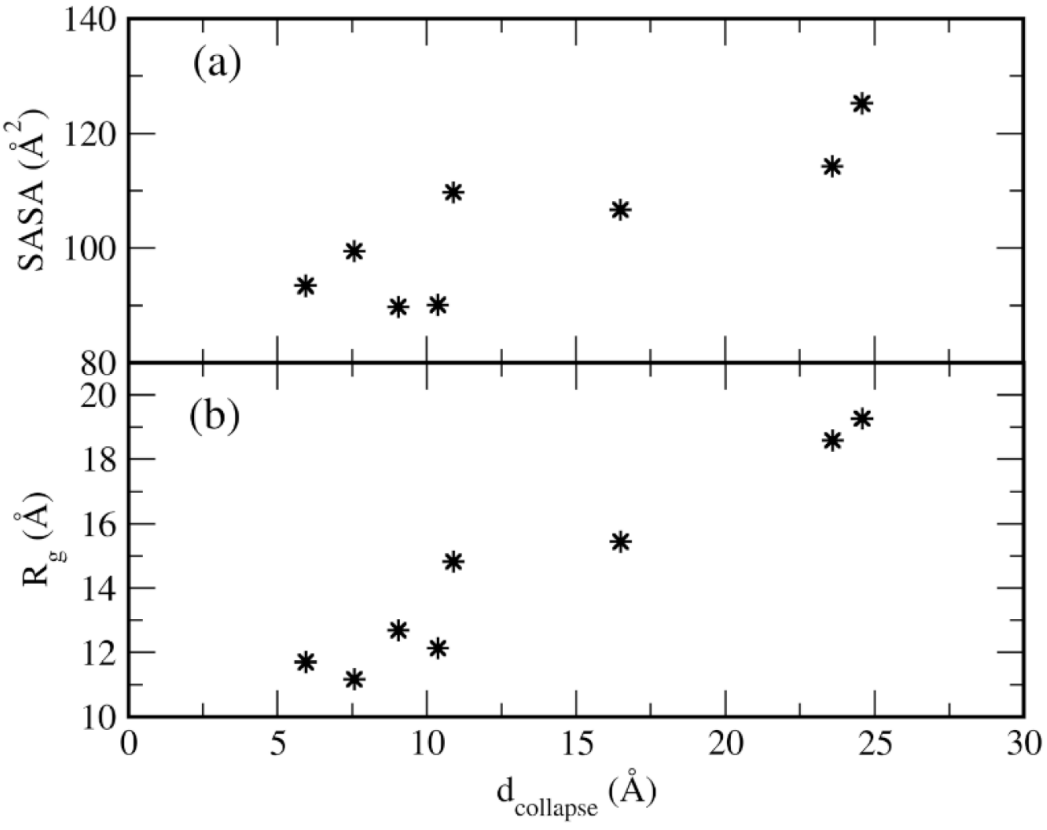

Figure AII-2. (a) Average $d_{collapse}$ vs average SASA, and (b) average $d_{collapse}$ vs average R_g of different Aβ peptide conformations.

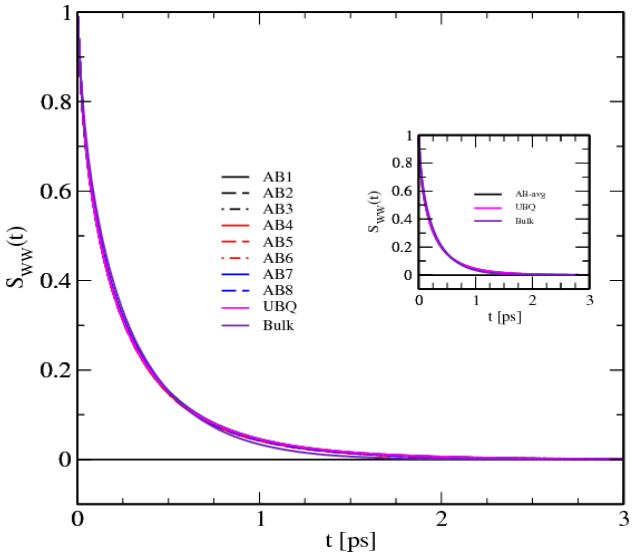

Figure AII-3. Continuous time correlation function, $S_{WW}(t)$, as calculated using the energy-based criterion to define WW hydrogen bonds formed by the first hydration layer water molecules around different Aβ peptide conformations and UBQ. $S_{WW}(t)$ for water in pure bulk state is shown for comparison. The results for UBQ, pure bulk water, and that averaged over the Aβ monomers are also included in the inset.

conf.	$<\tau_S^{WW}>$ (ps)
AB1	0.25
AB2	0.25
AB3	0.25
AB4	0.25
AB5	0.25
AB6	0.25
AB7	0.25
AB8	0.25
AB-avg	0.25
UBQ	0.25
bulk water	0.25

Table AII-2. Average relaxation times as obtained from the continuous WW ($<\tau_s^{WW}>$) hydrogen bond TCFs (calculated using the energy-based criterion) for the water molecules present in the first hydration layers around different Aβ peptide conformations and UBQ. The corresponding data averaged over the Aβ monomers (AB-avg) and that for pure bulk water are listed for comparison.

Appendix III

Cluster	Salt Bridge	d^{SB}
C1	K6 – D7	9.1 (2.9)
	K21 – E11	4.5 (2.7)
	E28 – R5	3.6 (0.5)
C2	K6 – D1	7.4 (4.3)
	K32 – D1	5.5 (3.4)
	K32 – E3	5.9 (1.9)
	K80 – D7	2.9 (0.2)
	K80 – E3	3.3 (0.3)
C3	K6 – E3	5.9 (2.4)
	K12 – E22	5.7 (3.2)
C5	K6 – E22	4.0 (1.3)
	K6 – D23	5.6 (2.2)
	K10 – D23	2.9 (0.3)
	K12 – D1	3.5 (0.6)
	E83 – K28	8.5 (3.4)

Table AIII-1. Mean value of the inter-residue sidechain distances (d^{SB}, in Å) between the residues that form salt bridges in the clusters a) C1, b) C2, c) C3, d) C5. Standard deviations are provided in braces. The first residue belongs to αSyn; the second residue belongs to A*β*.

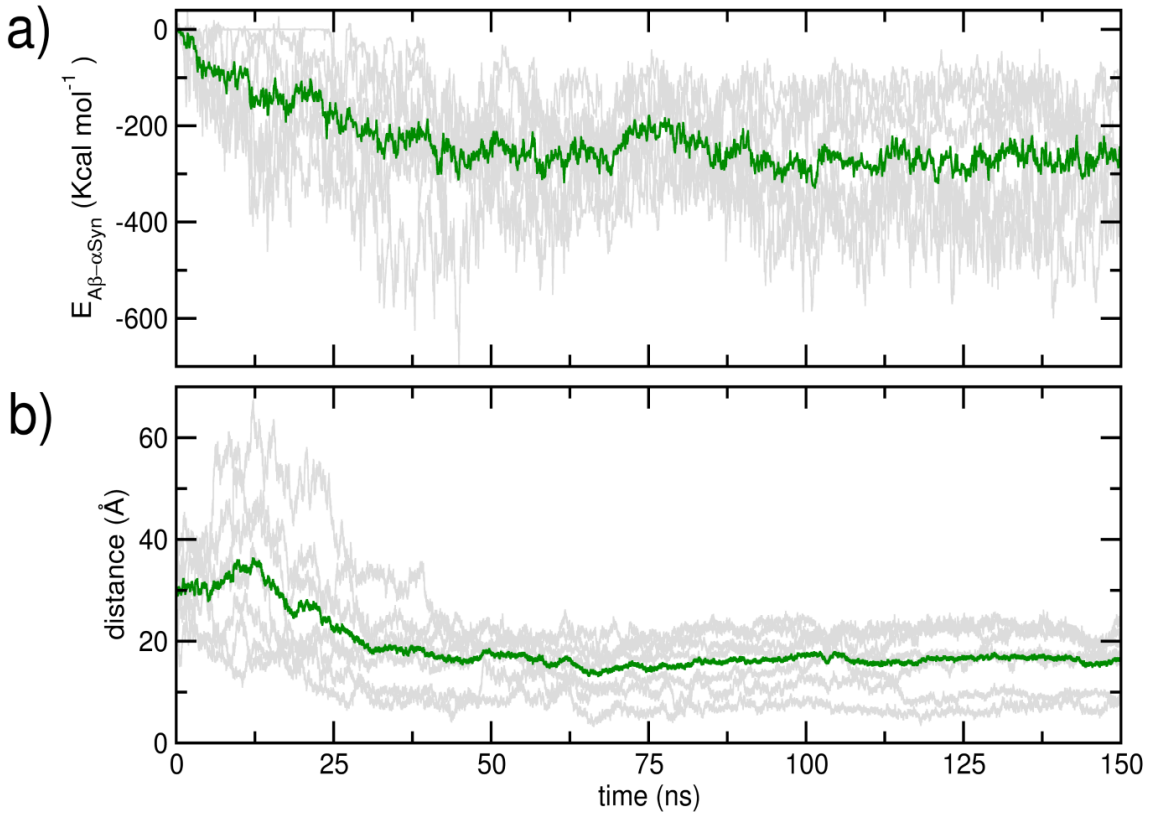

Figure AIII-1. Evolution of the a) total inter-peptide interaction strength, and b) inter peptide distance over 150 ns for the dimerising trajectories.

Research Publications

1. Cross Dimerization of Amyloid-β and αSynuclein Proteins in Aqueous Environment: A Molecular Dynamics Simulations Study. **Jose, J. C.**, Chatterjee, P., Sengupta, N. *PLOS ONE* **2014,** *9*: e106883

2. Microscopic Hydration Properties of the Aβ_{1-42} Peptide Monomer and the Globular Protein Ubiquitin: A Comparative Molecular Dynamics Study. **Jose, J. C.**, Khatua P, Bansal N, Sengupta N, Bandyopadhyay S. *J. Phys. Chem. B.* **2014**, *118*, 11591-11604.

3. Molecular dynamics simulation studies of the structural response of an isolated Aβ_{42} monomer localized in the vicinity of the hydrophilic TiO_2 surface. **Jose, J. C.**, Sengupta, N. *Eur. Biophys. J.* **2013**, *42*, 487-494.

4. The basic structural motif and major biophysical properties of Amyloid-β are encoded in the fragment. Chandrakesan, M., B. Sarkar, V. S. Mithu, R. Abhyankar, D. Bhowmik, S. Nag, B. Sahoo, R. Shah, S. Gurav, R. Banerjee, S. Dandekar, **Jose, J. C**, Sengupta N, P. K. Madhu, and S. Maiti. *Chem. Phys.* **2013**, *422*, 80-87

5. Critical roles of key domains in complete adsorption of Aβ peptide on single-walled carbon nanotubes: insights with point mutations and MD simulations. Jana, A. K., **Jose, J. C.**, Sengupta, N. *Phys. Chem. Chem. Phys.* **2013**, *15*, 837.